The Aerodynamics of Low Sweep Delta Wings

Jose M. Rullan

Dissertation submitted to the faculty of the Virginia Polytechnic Institute and State University in partial fulfillment of the requirements for the degree of

Doctor of Philosophy

In

Engineering Mechanics

Dr. Demetri P. Telionis, Chair

Dr. Scott Hendricks

Dr. Ronald Kriz

Dr. Saad Ragab

Dr. Pavlos Vlachos

April 21, 2008

Blacksburg, Virginia

Keywords: low sweep delta wings, streamwise vortex, vortex breakdown, flow control, three-dimensional actuation

The Aerodynamics of Low Sweep Delta Wings

Jose M. Rullan

Abstract

The aerodynamics of wings with moderately swept wings continues to be a challenging and important problem due to the current and future use in military aircraft. And yet, there is very little work devoted to the understanding of the aerodynamics of such wings. The problem is that such wings may be able to sustain attached flow next to broken-down delta-wing vortices, or stall like two-dimensional wings, while shedding vortices with generators parallel to their leading edge. To address this situation we studied the flow field over diamond-shaped planforms and sharp-edged finite wings. Possible mechanisms for flow control were identified and tested. We explored the aerodynamics of swept leading edges with no control. We presented velocity and vorticity distributions along planes normal and parallel to the free stream for wings with diamond shaped planform and sharp leading edges. We also presented pressure distributions over the suction side of the wing. Results indicated that in the inboard part of the wing, an attached vortex can be sustained, reminiscent of delta-wing type of a tip vortex, but further in the outboard region 2-D stall dominated even at 13° AOA and total stall at 21° AOA. To explore the unsteady flow field and the effectiveness of leading-edge control of the flow over a diamond-planform wing at 13° AOA, we employed Particle Image Velocimetry (PIV) at a Reynolds number of 43,000 in a water tunnel. Our results indicated that two-D-like vortices were periodically generated and shed. At the same time, an underline feature of the flow, a leading edge vortex was periodically activated, penetrating the separated flow, eventually emerging downstream of the trailing edge of the wing. To study the motion and its control at higher Reynolds numbers, namely 1.3×10^6 we conducted experiments in a wind tunnel. Three control mechanisms were employed, an oscillating mini-flap, a pulsed jet and spanwise continuous blowing. A finite wing with parallel leading and trailing edges and a rectangular tip was swept by 0°, 20°, and 40° and the pulsed jet employed as is control mechanism. A wing with a diamond-shaped-planform, with a leading edge sweep of 42°, was tested with the mini-

flap. Surface pressure distributions were obtained and the control flow results were contrasted with the no-control cases. Our results indicated flow control was very effective at 20° sweep, but less so at 40° or 42°. It was found that steady spanwise blowing is much more effective at the higher sweep angle.

Dedication

To the two people that trust me more than I trust myself, my wife Mari and my son Miguel Antonio. The sacrifice was worth doing.

Acknowledgements

I would like to express my most sincere appreciation to my advisor, Dr. Demetri Telionis. Your support, encouragement and dedication to this job and to my wellbeing were unmatched. I would not be completing these requirements if it were not for you. For all these I am extremely grateful.

I need to express my appreciations to my other committee members. Dr. Pavlos Vlachos, your advice and comments are welcomed. Dr. Saad Ragab, thanks for being always there when any question arises. A visit to your office is another class session. Dr. Hendricks and Kriz, thank you for accepting and submitting yourself to my performances.

To all my friends in the Fluids Lab, you made spending the days in the lab easier. I need to recognize Jason Gibbs who found the time to be spent when he did not needed to. Ali Etebari for always being helpful and at hand whenever work had to be done. Thanks to Dr. Matt Zeiger for all his ideas, input, and advice in this research. I also appreciate the efforts and advice put on by the ESM Shop personnel. Both David Simmons and Darrel Link are extremely diligent.

Last, to my family, whose encouregment and unconditional love made possible all the years spent here.

Table of Content

List of Figures

List of Tables

1. Introduction

Sharp-edged wings such as highly swept delta wings have been studied and used in combat and supersonic aircraft for several decades. Recently there have been interest in low and moderate-sweep angle delta wings ($\lambda \cong 35°$ to $60°$) for use in combat aircraft, such as the new fighters going into service in the next years and also in unmanned combat aircraft vehicles (UCAV). Considering that limited research that has been devoted to wings with low aspect ratios, a thorough understanding of the corresponding aerodynamics is essential. In fact, it is important not only to investigate and fully develop their potential, but to also address any adverse effects, such as flow separation and vortex breakdown, that are inherent in the flow.

For delta wings, it has been shown that the lift coefficient decreases as the sweep angle decreases[1]. For highly swept delta wings, the flow is dominated by two large counter-rotating leading-edge vortices (LEV) that are critical to the wing's performance. In the case of sharp-edged wings, LEV form by the rolling of free-shear layers that separate along the sharp leading edge. Previous studies have shown that as the angle of attack increased the LEV's undergo a flow disruption or breakdown also known as vortex burst that result in a sudden flow stagnation in the core and an expansion of core size by a factor of about three[2-3]. Vortex breakdown has negative effects such as a decrease in lift, a resulting pitching moment, and the onset of stalling. Moreover, the position of the vortex breakdown is not stationary but instead indicates unsteady oscillations over some mean position[4].

For non-slender delta wings, there is a similar formation of LEV's at angles of attacks (AOA) as low as 2.5 although at these low angles the flow field behaves as wake-like flow[5]. There is also the peculiarity that a second vortex forms downstream[6-8], at very low angles of attack, with vorticity of the same sign as the primary, albeit weaker and smaller originating from the interaction of the secondary flow due to the leading edge vortex and the shear layer. As the angle of attack is increased, the primary vortex becomes stronger and eventually this dual vortex structure looks similar to the structures over higher-swept wings.

In recent years there has been an increased interest in flow control, and in particular aircraft aerodynamics, with the purpose of increasing lift and decreasing drag of airfoils and wings. Wings suffer from flow separation at high angles of attack due to viscous effects, which in turn causes a major decrease in lift and increase in drag. This occurs to all types of airfoils, but sharp-edged wings are particularly vulnerable to such detrimental effects. These types of wings are used on supersonic transports as well as in stealth technology due to the fact that flat surfaces and sharp edges help reduce the radar signature of the airplane by reflecting the radar signals away from the radar, while also reducing the wave drag due to the shock wave that otherwise would be detached if round edge airfoils were used. The problems with these types of wing geometries are that they need long runways and require a lot of power for takeoff and landing since at subsonic flight the lift characteristics of these airfoils are poor. They also require advanced control systems and highly-skilled pilots to maintain a safe degree of maneuverability.

Sharp edge airfoils suffer from separation even at low angles of attack such as 8°, because the flow cannot negotiate the sharp turn at the leading edge. As the flow separates, the airfoil behaves as a bluff body. Due to this separation, a reduction in lift is experienced by the airfoil and vortex shedding starts. The interest in this study is to try to control separated flow, not flow separation. With the implementation of flow control techniques, improvements in the lift coefficient can be obtained in a time-averaged sense. This is achieved by controlling the vortex-shedding phenomenon that in turn will improve a mixing enhancement of high momentum flow from the free stream with low momentum flow in the separated region. This mechanism is known as vortex lift.

1.1 Separated flow and Vortex breakdown

As stated earlier, the purpose of this research is to control separated flow and not flow separation. It is important to make this distinction, since the former refers to effort to manage a flow field that has already separated, while the latter tries to prevent or delay separation, or reattach the flow on the wing walls. Flow separation and possible techniques to address their situation has been classified[9] as shown in Figure 1-1.

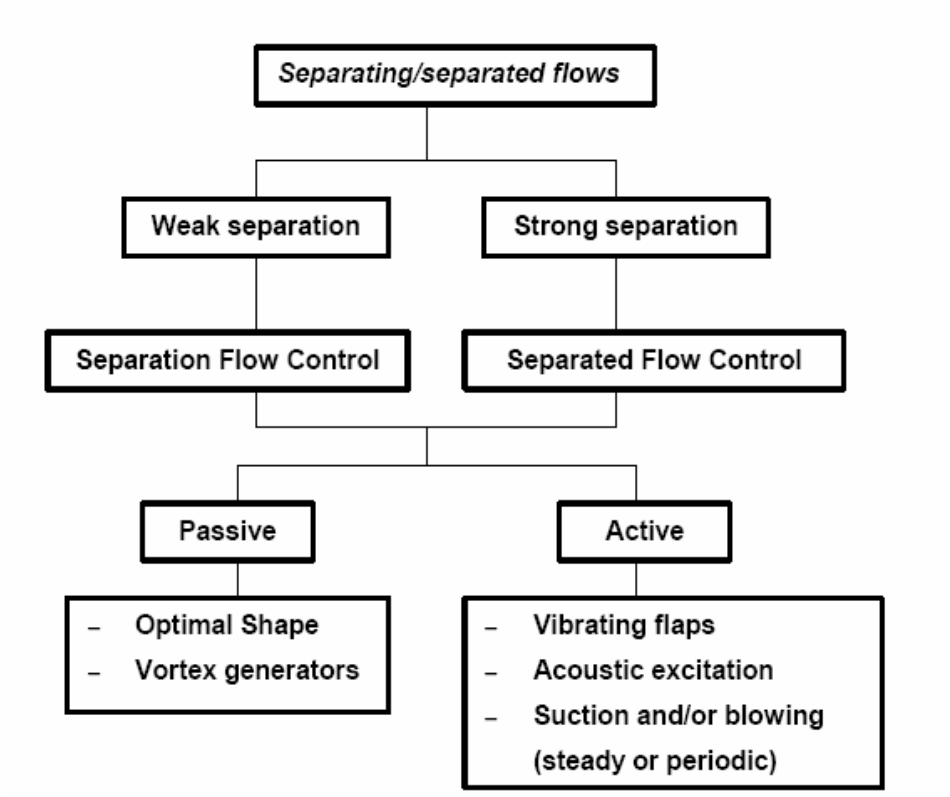

Figure 1-1: Classification of flow field separation and flow management techniques

Viscous flow theory indicates that flow will separate in the presence of an adverse pressure gradient. Separation over rounded leading edges and smooth airfoil surfaces is dictated by a combination of viscous and inviscid effects. For sharp edge airfoils, separation is always fixed at the sharp leading edge. Sharp edge airfoils will suffer from massive separation for angle of attack higher than about 8 degrees. .

When the flow separates from the wall, the boundary layer theory no longer holds. Vortices will be formed and they will be shed from the separation points located at the leading and trailing edges. These vortices are energized by the interaction of each other. The ones that are shed from the leading edge are in a disadvantage since these leading edge vortices are very weak to accomplish roll-up formation[10]. As a result, they may not form until they reach the wake. This research will try to accomplish the enhancement of the leading edge vortices to promote their roll over the suction side surface, and thus induce a lower pressure and increase in lift. We need to lay out the physical mechanism of the production, shedding, capture and enhancement of these vortices at post-stall angles of attack.

For high–sweep delta wings vortex breakdown occurs at much lower AOA's than for low-sweep wings. Also, vortex breakdown has been reported to occur further upstream along the chord. Experimental and computational measurements report that an elongated separated region exists very close to the upper surface[6-7]. Although many studies have provided some information on the flow topology over some planes[11] there has not been any comprehensive study performed over the surface of the wing. Most studies have been performed at low Reynolds numbers (less than 40,000) with little attention devoted to see how this parameter affects the flow. Experimental data on the structures of subsonic flow over delta wings have been carried out in both water and wind tunnels. Previous work[12-15] indeed indicates Reynolds number dependence to leading edge vortex formation and breakdown. For low Reynolds numbers, weak vortex formation was observed but no vortex breakdown[6]. It was presumed that the shear layer was not able to roll-up into a concentrated core. As the Reynolds number increased, though, the vortex core was more compact, the onset of vortex breakdown was more clearly evident, and the breakdown occurred farther upstream. Moreover, as the Reynolds number increased, it has also been observed that the leading edge vortex core shifted from being close to the centerline to a location closer to the leading edge[17-18].

1.2 Flow control

Flow control has been defined[16] as the ability to actively or passively manipulate a flow field to effect a desired change. The challenge is to achieve that change with a simple device that is inexpensive to build and to operate, and has minimum side effects. Control of separated flow is possible by both passive and active means as presented in Figure 1-2. Passive control refers to the ones that require no auxiliary power and no control loop, and sometimes are referred as flow management rather than control. Examples include changing the geometry of the aircraft to increase its aerodynamic properties such as wings equipped with leading edge flaps. These are heavy, require extra hydraulic control and introduce serious problems to sustain the stealth integrity of the aircraft. This type of control is unacceptable in the present case, due to stealth geometry and speed constraints.

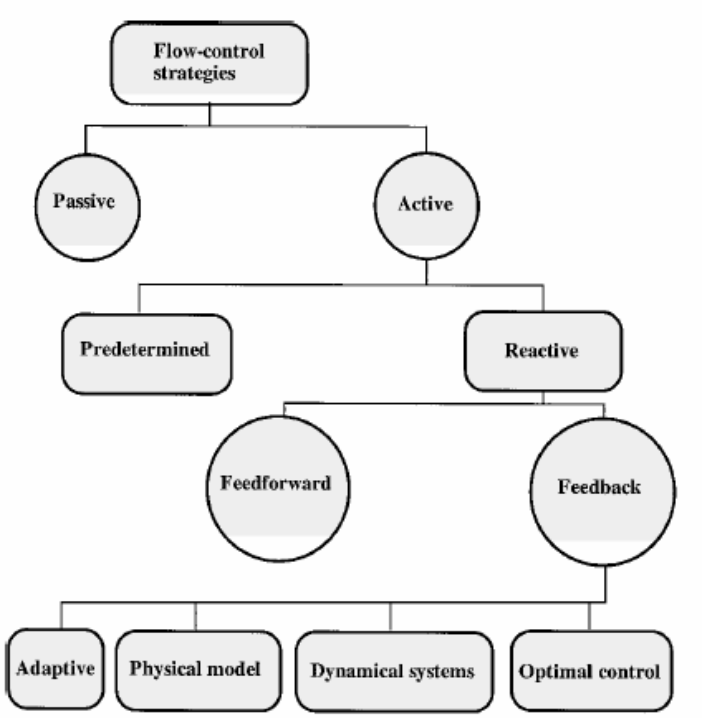

Figure 1-2: Classification of flow control methods.

On the other hand, active flow control refers to the ones where a control loop is used and energy expenditure is required. They are also further divided into predetermined and reactive. Predetermined control loops refer to the application of steady or unsteady activation, without regard to the particular state of the flow, so no sensors are required. This is the difference with the reactive ones, since these employ a sensor to continuously adjust the controller. These reactive ones in turn could be either feed-forward or feed-back controlled. In the present research, we employ a predetermined loop control.

The majority of contributions on airfoil flow control are based on the control of separation. There is another area of airfoil and wing flow control that has received little attention although it has greater potential in defense applications[19]. This is the management and control of separated flow, which is the only approach appropriate for flows over sharp-edged wings. Impressive advancements have been made in controlling the flow over wings with rounded leading edges, but very little work has been devoted to the control of the flow over sharp-edged wings and low sweep trapezoidal wings. Some of the approaches have been with passive flow control such as flexible wings[20] while others have used active flow control such as mechanical flaps including leading edge

flaps[21] and apex flaps[22], and pneumatic systems including spanwise blowing[23], continuous leading edge blowing and periodic leading edge suction and blowing[24].

1.2.1 Mechanical Flaps

Among the research conducted one examined the use of leading edge flaps for delta wings with 60° and 70° degrees sweep[21]. By implementing various flap geometries he demonstrated the importance of flap size. It also demonstrated that leading edge flaps forced the vortex to form on a protruding surface rather than on the wing's surface.

Others have looked into the influence of an apex flap[22]. They used a standard flap and also drooping or negative-angle apex flaps. Both produced considerable delays in vortex breakdown location. A maximum delay was observed for an apex deflected to a negative 15°.

One of the first to try to control the flow over a sharp edge airfoil[25] used a rounded edge airfoil placed backwards in a wind tunnel, so the sharp trailing edge faced the oncoming flow. Their test was only at 27° angle of attack but their results indicated that an increase in lift could be achieved.

Other research has tried[26] a pulsed micro-flap on the leading edge of a wing to control separated flow. They focused on the position, amplitude, and frequency of the flap motion necessary to improve the aerodynamics characteristics of the flow over an airfoil at high angles of attack. It was found that periodic perturbations can organize and enhance the average strength of the shedding vortices and can increase in a time-average sense the lift by as much as 50%. Later[27], with some modifications to their previous design, it was found that the most effective excitation corresponds to a flap motion with the vortex shedding frequency. They also found that larger amplitudes of excitation motion produced a larger lift coefficient.

In order to create the necessary flow disturbance, some have used a small oscillating flap placed on the leading edge of a circular-arc, sharp-edged airfoil[28]. This pulsing flap creates an unsteady excitation at the leading edge, which is affecting the flow in the desired way. They showed an increased in lift of up to 70%. Previous work has demonstrated that the maximum effect on separated flow can be achieved when the actuation frequency is near the vortex shedding frequency. But the flap must penetrate the

separated region in order to have any effect on the formation of vortices. This is the reason suggested, since the effect was greatly reduced as the angle of attack was increased. They also found that oscillating flaps are not limited in their frequency domain. Indeed, they demonstrated that an oscillating flap could generate a wide range of effective frequencies for the control of separated flow over a sharp-edged airfoil. But such devices may not be attractive to the aircraft designer.

1.2.2 Periodic blowing

A blowing technique has also been tested to control separated flow. Small jet slots are placed near the leading edge of airfoils for the purpose of developing periodic perturbations into the boundary layer. The idea is to produce streamwise vortices using transverse, steady and oscillating flow jets to increase the cross-stream mixing and lead to stall suppression in adverse pressure gradients. Several studies have been conducted on the use of oscillating blowing. One of these studied the separation control in incompressible and compressible flow using pulsed jets[29]. They tested a NACA-4412 airfoil section with a leading-edge flap. The leading-edge flap was fitted with flow control actuators, each actuator consisted of a cross flow jet with pitch and screw angles of 90 and 45 degrees respectively. High-speed flow control valves were used to control the pulsed flow to each jet individually. The leading edge contained three jet nozzles; however only two were used. The valve open-and-close cycle was manipulated using a computer function generator driving a solenoid valve power supply. The valve controller allowed pulse rates up to 500 Hz and volume flow rates in excess of 20 slugs/min for each jet. A constant average mass flow of air was supplied to the jet using a closed-loop servo valve. Their data indicated that maximum lift enhancements occur with a jet pulse Strouhal number of approximately 0.6. McManus and Magill found the pulsed jets caused an increase in lift of up to 50 percent over a base line case for $\alpha \leq 10$ degrees. They also found that the effectiveness decreased with the increase in Mach number. The best results were found when the angle of attack was equal to the angle corresponding to the maximum lift coefficient, Cl_{max}.

Another research conducted examined oscillatory blowing on the trailing edge flap of a NACA-0015 airfoil[30]. They activated jets mounted in a 2-D slot located on the upper surface above the hinge of the flap. The airfoil was placed at an angle of attack of 20

degrees. They concluded that steady blowing had no effect on lift or drag. However, modulating blowing generated an increase in lift and cut the drag in half.

Synthetic-jet actuators can be used effectively to achieve dynamic blowing and suction. Synthetic-jet actuators based on piezoelectric devices are most efficient at the resonance frequency of the device and limited by the natural frequency of the cavity. Such actuators have proven very useful in the laboratory but may not be as effective in practice including an actuator, which was essentially a small positive-displacement machine[31]. The same group later designed a similar device and tested a NACA0015 airfoil with rounded leading edges containing six reciprocating compressors, which were driven by two DC motors. These compressors/pistons created a synthetic jet (zero mean flux) at the leading edge of the airfoil. They found that flow separation control was achieved at angles of attack and free stream velocities as high as 25° and 45 m/s, respectively. These actuators may have overcome some of the problems faced by other designs but they are complex machines, requiring high-speed linear oscillatory motions and complex mechanical components.

1.2.3 Other actuations

There are other devices tried for active flow control and could be applied to post-stall flow control. Among some recent technology, one of the most talked about in general is piezoresistors where one of the actuators consisted of a piezoelectrically-driven cantilever mounted flush with the flow wall and could be used in large arrays for actively controlling transitional and turbulent boundary layers[32]. When driven, the resulting flow disturbance over the actuator is a quasi-steady pair of counter-rotating streamwise vortices with strengths controlled by the amplitude of the actuator drive signal. These vortices decayed rapidly downstream of the actuator but they produce a set of high- and low-speed streaks that persist far downstream. Piezoelectric actuators used are also mechanical[33] where one sheet of piezoceramic was attached to the underside of a shime. Here the actuator works as a flap and is able to produce significant velocity fluctuations even in relatively thick boundary layers.

Another type of actuators considered are called electrohydrodynamic,[34] introduced by Artana et al (2002) where flush-mounted electrodes in a flat plate with a DC power supply are used to create a plasma sheet. This plasma sheet seems to induce acceleration

in the flow close to surface, thereby increasing its momentum and inducing a faster reattachment as seen in flow visualizations.

1.3 Methodology

So far, efforts have been reported to control the flow separation over airfoils with rounded leading edges, while here we report on the control of separated flow over sharp-edged airfoils. These techniques are equally applicable for the control of separated flows over rounded airfoils. But there are two important differences between the actuator requirements for the two cases. First, the location of the actuators for the control of separation over rounded airfoils is not critical since separation is gradual, and the flow is still receptive to an external disturbance, whereas for the control of separated flow the actuation must interact with the free-shear layer. This fact dictates that the actuator of a sharp-edged wing must be as close as possible to the sharp edge, which leads to the second important difference. The direction of the actuation disturbance must be adjusted to lead the disturbance as much as possible in the direction of the free shear layer. Two important parameters are the momentum coefficient, C_μ and the frequency of the actuation. Different angles of attack and free-stream velocities require a wide variety of possible combinations. Being able to independently control both is a great challenge. These requirements may appear too stringent for the sharp-edged airfoils, but on the other hand, they may provide some opportunities for robust control with minimal energy input. It is possible that free shear layers would be more receptive to disturbances right at their initiation, that is, as close as possible to the sharp leading edge. Another similar situation is the control of asymmetric wakes over pointed bodies of revolution at incidence. In this case, minute disturbances very close to the apex can feed into the global instability of the flow and lead to very large wake asymmetries[35-36].

It is important to note that periodic blowing is more effective than a steady jet due to resonance. For blowing, the momentum coefficient is defined[37] as

$$C_\mu = \frac{(u^2 H\rho)_{jet}}{(U^2 C\sin(\alpha)\rho)_\infty}$$

where ρ is the density of air and cancels out, h is the slot height, c is the chord of the airfoil and u and U are the respective velocities of the jet and the free stream. This is the

ratio of the input momentum to the momentum of the free stream and is suggested in Wu et al (1997) that it should to be at least 1%.

The disturbance frequency likely to be amplify the most is given, using linear stability theory, by the Strouhal number $St = \frac{f_{shedding} C \sin(\alpha)}{U_\infty}$ where $f_{shedding}$ is the shedding frequency, C is the airfoil chord, α is the angle of attack and U_∞ is the free stream velocity. We are going to assume a value of St=0.2 for this research as is widely accepted in literature. Some[39] give the actuation frequency, related to the shedding frequency, the reduced non-dimensional frequency $F^+ = \frac{f_{actuation}}{f_{shedding}}$. They suggests that this reduced frequency to be $0.4 < F^+ < 2$ since it seems that harmonics play a role in the dynamic process.

1.4 Dissertation Structure

This dissertation has been structured in the manuscript format. Each chapter represents a stand-alone contribution prepared in a format required for archival publication. In the present case most chapters have been presented at AIAA conferences, with the author of this PhD dissertation as the first author. For these reasons, some of the material presented in the first introductory chapters of the dissertation, like some review of literature or description of the facilities is repeated at the beginning of each chapter.

In Chapter 3 (AIAA 2005-0059) we discuss the aerodynamics of low-sweep wings. Wings swept by 30 to 40 degrees are today very common in fighter aircraft. And yet there is very little work devoted to the understanding of the aerodynamics of such wings. The problem is that such wings may be able to sustain attached although broken down delta wing vortices, but stall like two-dimensional wings, shedding vortices with generators parallel to their leading edge. In this chapter, we explore the aerodynamics of such wings. We present velocity and vorticity distributions along planes normal and parallel to the free stream for a wing with a trapezoidal planform and sharp leading edges. We also present pressure distributions over both the pressure and the suction side of the wing.

In the fourth chapter we describe flow control methods for flows over diamond-shaped wings with sharp edges (AIAA 2006-0857). We explore the effectiveness of leading-edge control of the flow over such wings. The work described in this chapter was carried out with Particle-Image Velocimetry (PIV). Our results indicate that two-D-like vortices are periodically generated and shed. At the same time, an underline feature of the flow, a leading edge vortex is periodically activated, penetrating the separated flow, and eventually emerging downstream of the trailing edge of the wing.

In Chapter 5, we discuss the control of the flow over wings swept by different angles. (AIAA 2007-0879). There are three basic elements that distinguish the flow control problems discussed here from other such problems. The first is the effect of sharp leading edges. The second is the effect of sweeping the wing at moderate angles, namely 30° to 40°. And the third element is controlling and organizing the resulting separated flow, instead of attempting to mitigate separation. These problems are basic in character that will improve our fundamental understanding of the dynamics of unsteady/actuated separated turbulent flows. But they also have significant relevance to current and future air platforms. Our research on a four-foot span wing at a Reynolds number of over a million has revealed that in this range of parameters, the flow may stall like the flow over an unswept wing, or it could stall like a delta wing, sustaining a leading-edge vortex that breaks down, and that the two stalling modes can coexist. Our data now indicate for the first time that we can manage the development of vortices over the separated suction side of a diamond planform wing to reduce the pressure and thus increase lift. We have evidence that streamwise vortices parallel to the tip vortices are generated inboard of the tip that form an underlying feature of the flow. In this paper we demonstrate that using local actuation we can excite and reinforce these vortices, favorably modifying the character of the flow.

Finally in the last chapter we discuss the significance of our findings and the relationship between the findings presented in each of the previous chapters.

1.5 References

1. Earnshaw, P.B., Lawford, J.A., "*Low-speed wind tunnel experiments on a series of sharp-edged delta wings"*. ARC Reports and Memoranda No. 3424, March 1964

2. Delery, J., "*Aspects of vortex breakdown"*, Progress in Aerospace, Vol 30, Issue 1, 1994, p. 1-59
3. Kumar, A., *"On the structure of vortex breakdown on a delta wing"*, Proceedings of the Royal Society A: Mathematical, Physical and Engineering Sciences, Volume 454, Issue 1968, 08 Jan 1998, Page 89-110
4. Menke, M., Yang, H., Gursul, I., "*Experiments on the steady nature of vortex breakdown over delta wings",* Experiments of Fluids, 1999, 27, 262-272
5. Ol, M., Gharib, M., *"Leading edge vortex structures of non-slender delta wings at low Reynolds numbers".* AIAA Journal, Vol.41, No. 1 January 2003, p. 16-26.
6. Gordnier, R. E. and Visbal, M. R., "*Higher-Order Compact Difference Scheme Applied to the Simulation of a Low Sweep Delta Wing Flow*," 41st AIAA Aerospace Sciences Meeting and Exhibit, Paper No. AIAA-2003-0620, AIAA, Reno, NV, January 6-9, 2003.
7. Yaniktepe B., and Rockwell, D.,*"Flow structure on a delta wing of low sweep"*, AIAA Journal, Vol.42, No. 3, March 2004, p. 513-523.
8. Taylor, G. S., Schnorbus, T., and Gursul, I., *"An Investigation of Vortex Flows over Low Sweep Delta Wings"* AIAA Fluid Dynamics Conference, Paper No. AIAA-2003-4021, Orlando, FL, June 23-26, 2003.
9. Fiedler, H. E., (1998). "Control of Free Turbulent Shear Flows". In *Flow Control: Fundamentals and Practices* (ed. Gad-el-Hak, M., Pollard, A., Bonnet, J. P.), pp. 335-429
10. Roshko, A., (1967), "A review of concepts in separated flow", Proceedings of Canadian Congress of Applied Mechanics, Vol. 1, 3-81 to 3-115
11. Yavuz, M.M., Elkhoury, M., and Rockwell, *"Near Surface Topology and Flow Structure on a Delta Wing"*, AIAA Journal, Vol.42, No. 2, February 2004, p. 332-340.
12. Fritzelas, A., Platzer, M., Hebbar, S., *"Effects of Reynolds Number of the High Incidence Flow over Double Delta Wings"*, 43rd AIAA Aerospace Sciences Meeting and Exhibit,, Paper No. AIAA-1997-0046, Reno, NV, January 6-9, 1997.
13. Ghee, T., Taylor, N.*, "Low-Speed Wind tunnel tests on a diamond wing high lift configuration"*, AIAA Applied Aerodynamics Conference, 18th, Denver, CO, Aug. 14-17, 2000, Collection of Technical Papers. Vol. 2, p 772-782.
14. Luckring, J., Taylor, N.*, "Subsonic Reynolds number effects on a diamond wing configuration"*, 39th AIAA Aerospace Sciences Meeting and Exhibit, Paper No. AIAA-2001-0907, Reno, NV, Jan. 8-11, 2001
15. Elkhoury, M., Rockwell, D., *"Visualized Vortices on Unmanned Combat Air Vehicle Planform: Effect of Reynolds Number"*, Journal of Aircraft 2004, Vol.41, No.5, p.1244-1247
16. Gad-el-Hak, M., (2001). "Flow Control: the Future," J. of Aircraft. Vol. 38, No. 3, pp. 402-418
17. Traub,L., Galls, S. & Rediniotis, O., *"Reynolds number effects on Vortex Breakdown of a Blunt-edged Delta"*, Journal of Aircraft, Vol. 33. No. 4, p. 835-837.
18. Moore, D. W., and Pullin, D.I., *"Inviscid Separated Flow Over a Non-Slender Delta Wing"*, Journal of Fluid Mechanics, Vol. 305, p. 307-345.

19. Wood, R, *A Discussion of Aerodynamic Control Effectors (ACEs) for Unmanned Air Vehicles (UAVs)*, AIAA 1st UAV Conference, AIAA 2002-3494, Portsmouth, Virginia, May 20-23, 2002
20. Taylor, G. S., Krokeas, A., and Gursul, I., *"Passive Flow Control over Flexible Non-Slender Delta Wings"* 43rd AIAA Aerospace Sciences Meeting and Exhibit, Paper No. AIAA-2005-865, Reno, NV, January 10-13, 2005.
21. Marchman, J.F., "*Effectiveness of Leading-Edge Vortex Flaps over 60 and 70 Degree Delta Wings*", AIAA Journal, Vol.18, No. 4 April 1981, p. 280-286.
22. Klute, S., Rediniotis, O., and Telionis, D., "*Flow Control over Delta Wings at High Angles of Attack*", AIAA Applied Aerodynamics Conference, Paper No. AIAA-1993-3494, August 1993.
23. Campbell, J, *"Augmentation of Vortex Lift by Spanwise Blowing"*, AIAA Journal, Vol.13, No. 9 September 1976, p. 727-732.
24. Gad-El-Hak, M., Blackwelder, R.F., "*Control of the Discrete Vortices from a Delta Wing*", AIAA Journal, Vol.25, No. 8 August 1987, p. 1042-1049.
25. Zhou, M. D., Fernholz, H. H., Ma, H. Y., Wu, J. Z., Wu, J. M., (1993). "Vortex Capture by a Two-Dimensional Airfoil with a Small Oscillating Leading-Edge Flap". AIAA Paper 93-3266.
26. Hsiao, F. –B., Wang, T.-Z., Zohar, Y., (1993). "Flow separation Control of a 2-D Airfoil by a Leading-Edge Oscillating Flap," Intl. Conf. Aerospace Sci. Tech., Dec. 6-9, 1993, Tainan, Taiwan.
27. Hsiao, F. B., Liang, P. F., Huang, C. Y., (1998). "High-Incidence Airfoil Aerodynamics Improvement by Leading-edge Oscillating Flap". J. of Aircraft. Vol. 35, No. 3, pp. 508-510.
28. Miranda, S., Telionis, D., Zeiger, M., (2001). "Flow Control of a Sharp-Edged Airfoil", AIAA Paper No. 2001-0119, Jan. 2001
29. McManus, K., Magill, J., (1996). "Separation Control in Incompressible and Compressible Flows using Pulsed Jets". AIAA Paper 96-1948.
30. Seifert, A., Bachar, T., Wygnanski, "*Oscillatory Blowing, a Tool to Delay Boundary Layer Separation"*, 31st AIAA Aerospace Sciences Meeting and Exhibit, Paper No. AIAA-1993-0440, Reno, NV, Jan. 11-14, 1993
31. Rao, P. Gilarranz, J.L., Ko, J. Strgnac, T. and Rediniotis, O.K., (2000). "Flow Separation Control Via Synthetic Jet Actuation", AIAA Paper 2000-0407
32. Jacobson, S.A, Reynolds, W.C., (1998), "Active Control of Streamwise Vortices and Streaks in Boundary Layers", J. of Fluid Mechanics. Vol. 360, pp. 179-211.
33. Cattafesta, L.N, Garg, S., Shukla, D., (2001). "Development of Piezoelectric Actuators for Active Flow Control". AIAA Journal Vol. 39, pp. 1562-1568
34. Artana, G., D'Adamo, J., Léger, L., Moreau, E., Touchard, G., (2002). "Flow Control with Electrohydrodynamic Actuators" AIAA Journal Vol. 40, pp. 1773-1779
35. Zilliac, G.G., Degani, D. and Tobak, M. (1990). "Asymmetric Vortices on a Slender Body of Revolution". AIAA Journal, pp 667-675
36. Zeiger, M.D. and Telionis, D.P. (1997). "Effect of Coning Motion and Blowing on the Asymmetric Side Forces on a Slender Forbody". AIAA Paper No 97-0549
37. McCormick, D. (2000), "Boundary Layer Separation Control with synthetic jets", AIAA Paper 2000-0519

38. Seifert, A., Pack, L.G., (1999). “Active Control of Separated Flows on Generic Configurations at High Reynolds Numbers”. AIAA Paper 1999-3403
39. Wu, J.M., Lu, X., Denny, A.G.,Fan, M. Wu, J.Z., (1997). “Post Stall Flow Control on an Airfoil by Local Unsteady Forcing”. Prog. AIAA Paper No 97-2063

2. Experimental Setup And Equipment

2.1 Introduction

Experimental investigations were carried out in two wind tunnels and a water tunnel. The water tunnel and one of the wind tunnels, the small one, are located in the ESM fluids laboratory in Norris Hall. The other wind tunnel is the Stability Wind Tunnel located in Randolph Hall. Two different types of models were constructed: one for air pressure measurements in the wind tunnels and another for flow visualization and velocity measurements in the water tunnel. The facilities and the models are here briefly described.

2.2 Wind tunnels

2.2.1 ESM wind tunnel

The ESM wind tunnel is an open-circuit, low-speed tunnel constructed in 1983. To reduce the turbulence level, one honeycomb and four nylon-conditioning screens are included in the settling chamber. A five-to-one contraction follows the settling chamber. The test section dimensions are 51 cm x 51 cm x 125 cm (20 in x 20 in x 50 in) and include a removable Plexiglass wall for easy access as well as visualization. The tunnel is powered by a 15 hp motor. Adjusting the relative diameters of the drive pulleys sets the tunnel speed. It can achieve free-stream velocities from 4 m/s to 35 m/s. The turbulence level does not exceed 0.51% at a free-stream velocity of 10 m/s, except for regions very near the tunnel walls. The flow across the test section has a velocity variation of less than 2.5%. Figure 2-1 shows a schematic of the wind tunnel.

The tunnel free-stream velocity is obtained by a Pitot tube mounted on one of the side walls, which is connected to the data acquisition system, described in section 2.3.3, and also to an Edwards-Datametrics Barocel precision transducer model 590D-100T-3Q8-H5X-4D and this in turn was connected to a 1450 Electronic Manometer that would provide a readout of the dynamic pressure. The Barocel has a range of 0-100 Torr with an accuracy of 0.05% of the pressure reading and a full-scale resolution of 0.001% .

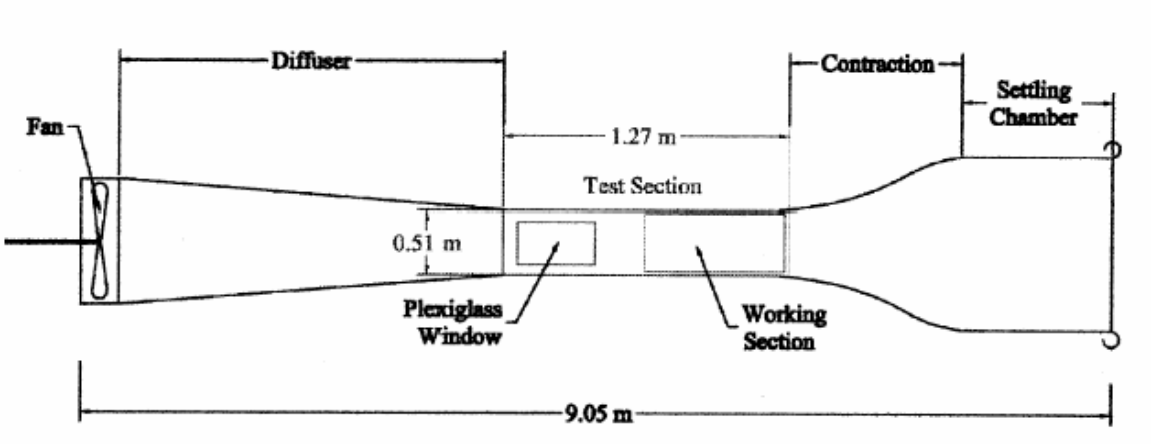

Figure 2-1: ESM Wind Tunnel Schematic

2.2.2 Virginia Tech Stability wind tunnel

The Virginia Tech Stability wind tunnel is a continuous, closed-loop subsonic wind tunnel. The maximum achievable flow speed is 275 ft/s (83.8 m/s) in a 6-foot by 6-foot by 25-foot (1.83m x 1.83m x 7.62m) test section. This facility was constructed in 1940 at the present site of NASA Langley Research Center by NASA's forerunner, NACA. Use of the tunnel at Langley in the determination of aerodynamic stability derivatives lead to its current name. In 1959, the tunnel was moved to Virginia Tech where it has been located outside of Randolph Hall.

The settling chamber has a contraction ratio of 9 to 1 and is equipped with seven anti-turbulence screens. This combination provides an extremely smooth flow in the test section. The turbulence levels vary from 0.018% to 0.5% and flow angularities are limited to 2° maximum. The settling chamber is 3m long and the diffuser has an angle of 3°. The ambient temperature and pressure in the test section is nearly equal to the ambient outdoor conditions due to the presence of a heat exchanger. During testing the control room is maintained at the same static pressure as the test section. The tunnel fan has a 14-foot (4.27m) diameter and is driven by a 600 hp motor that provides a maximum speed of 230 ft/sec and a Reynolds number per foot up to 1.4 x 10^6 in a normal 6' x 6' configuration. Figure 4 shows a schematic of the Stability tunnel.

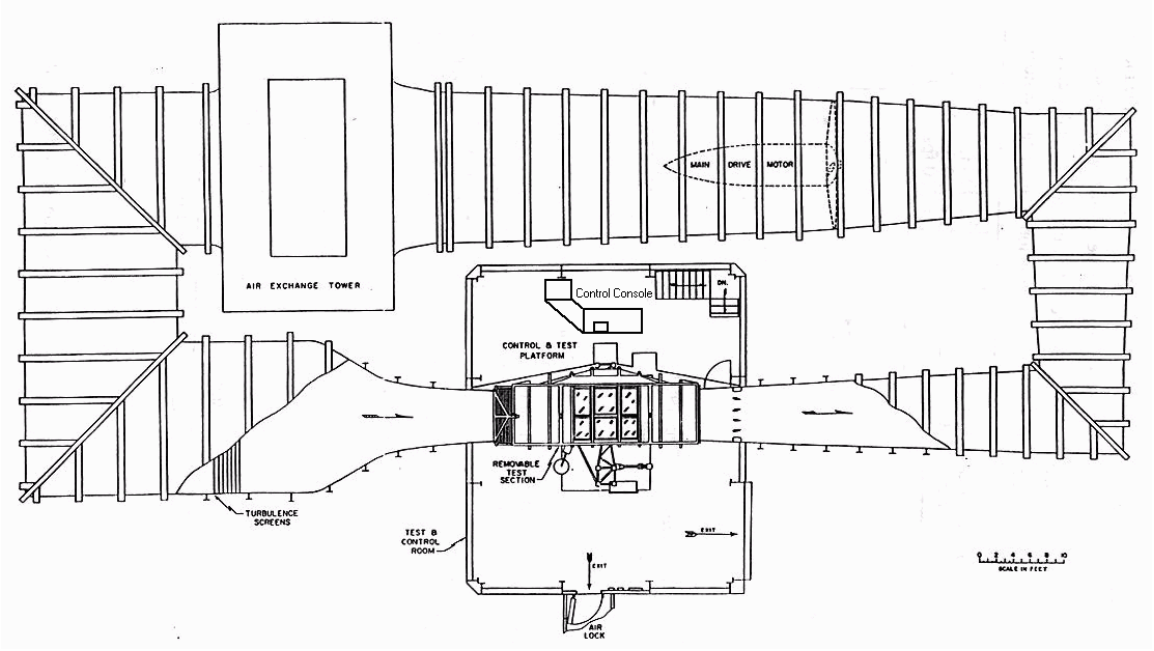

Figure 2-2: Stability tunnel schematic

2.3 Wind tunnel models

2.3.1 Model A

Model A shown in Figure 3 is a rectangular circular-arc wing that can be mounted at different sweep angles, and angles of attack. We have tested two such wings in the past at low and high Reynolds numbers, with both oscillating mini-flaps and unsteady leading-edge blowing[1,2]. The present model, Model A has a smaller thickness ratio (10%) and a larger aspect ratio that improves the delivery of pulsed jets. This model was mounted on the floor of the tunnel via a mechanism that allowed the setting of the angle of attack at any desired value and the sweep angle at the values of 0°, 20° and 40°. The model tip reached only close to the middle of the tunnel, and thus the mounting allowed the study of three-dimensional effects. This model is equipped with an unsteady jet actuator, which is described later. Pressure taps were placed along four chordwise lines on both the pressure and the suction side, as indicated in Figure 2-3. The spacing of the taps was smaller on the front part of the model. The four stations are labeled with Roman numerals as shown in the Figure.

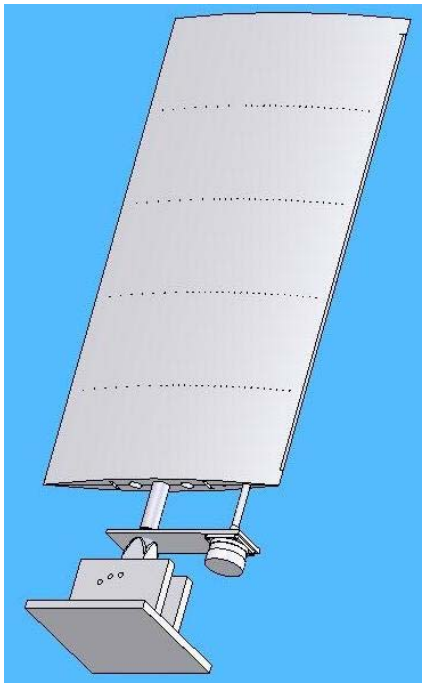

Figure 2-3: Model A

The design of the jet mechanism took into account the need of having it as close as possible to the leading edge of the airfoil. The leading edge part of the wing is essentially a wedge prism as shown in Figure 2-4. The actuation mechanism consists of two concentric cylindrical surfaces as seen in Figure 2-4. The inner cylinder is a 7/16"-diameter inner brass tube that contains twelve 1/16" wide slots and 1 ½ "long with 1/16 separation between them. The inner cylinder rotates about a fixed axis inside a fixed outer cylindrical surface machined on the wing body and free to rotate on three bushings. One bushing was machined to fit snugly between the brass tubing and the machined leading edge at mid-span. This was done to eliminate possible warping of the tube during rotation. The inner cylinder was fixed to a motor drive shaft so that it can be driven by a small DC motor as shown in Figure 2-3. The DC motor employed is a Pittman brushless DC servo motor that operates at 24 VDC. It features 3 Hall sensors for feedback control so as to obtain linear torque. It is operated with an Allmotion EZSV23 servo motor controller which in turn is connected to a PC by a serial port. This provides a direct frequency control of the motor. A wire was connected from the output of one of the Hall sensors to obtain a read-out and to record the actual driving frequency.

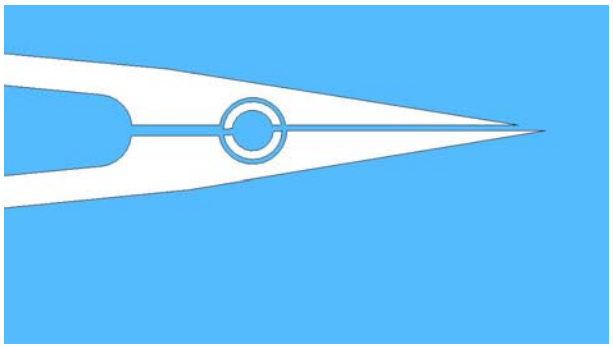

Figure 2-4: Model A actuator with cylinder slots aligned

Each station has 29 pressure taps on the suction side and 25 pressure taps on the pressure side aligned and located at 177.8 mm (7 in) from starboard side as can be seen in Figure 2-3. The taps start at 63.5 mm (2 ½ “) from the leading edge and are spaced at 10.16 mm (0.4 in) along the arc. Stainless steel tubing of 1.27 mm (0.05 in) o.d., and 0.8382 mm (0.033 in) i.d. was inserted in each tap and ran to quick disconnect connections outside the body next to the root and these connections in turn to the pressure transducers.

To evaluate the capabilities of the actuator, the assembled wing was mounted along with a rake of high-frequency-response Pitot tubes were mounted, similar to the assembly in Figure 2-5. Endevco model 8510 pressure transducers were used as sensing elements inside the rake. The output of the pressure transducers was connected to a HP digital signal analyzer, which was used to measure jet frequencies. In addition, these were also connected to the data acquisition system used in Wind Tunnel Testing and discussed in section 2.3.3. Their signals were connected to the external channels, first during calibration and later during acquisition. The rake was mounted on traversing scales so it could easily be displaced to obtain data at different locations relative to the slotted nozzle.

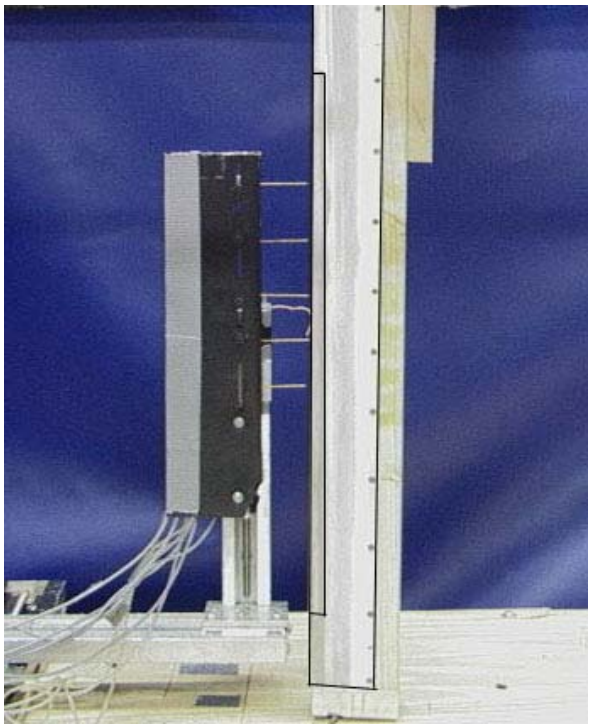

Figure 2-5: Leading Edge Aligned with Pitot Rake

2.3.2 Model B

Model B, seen in Figure 2-6, is a pair of wings in the form of a diamond-planform wing with a leading-edge sweep of 40°. This model is a stainless-steel model on loan by Lockheed Martin, and has a root chord of 25.8" and a half span of 19.8". It has 155 pressure ports on each wing. The pressure ports on the starboard wing are located in the lower surface to obtain the pressure side, and the pressure ports on the port wing are located on the top surface for suction-side measurements. The flow over this model is controlled by an oscillating mini-flap device, similar to the one already tested on circular-arc wing sections[1]. The spanwise stations are numbered with numerals starting from the root side of the wing. We have also designed, constructed and tested a similar but smaller diamond-planform wing that was tested in our water tunnel described in a later section.

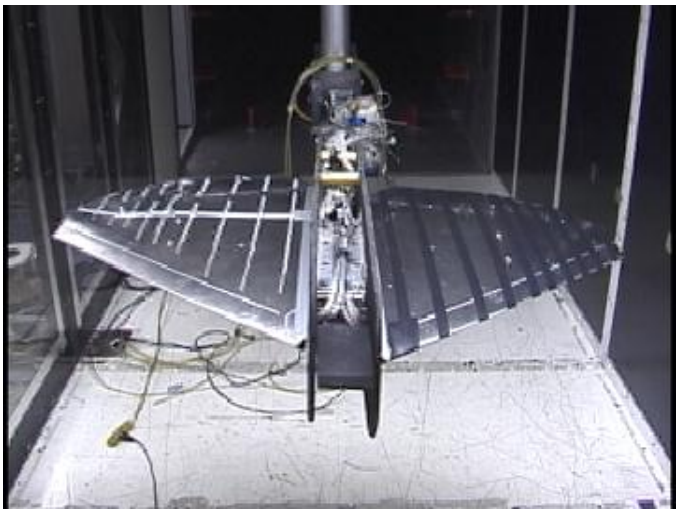

Figure 2-6: Model B

2.3.3 Data Acquisition system

Pressure data were acquired using PSI's ESP pressure scanners that were mounted inside the model, or at its root. The ESPs were connected to dedicated boards for digital addressing as well as voltage regulation. Since the ESPs have a maximum frequency response of 50 Hz, they were sampled at 256 Hz and the sampling was performed by a data acquisition board by Computer Boards model CIO-DAS16 12-bit A-D converter installed on a 800 MHz Pentium III processor installed computer. The Endevco pressure transducers were connected to the same setup system although their inputs are acquired as external sources. They were calibrated properly.

ESP pressure scanners are small, high-density packages containing multiple differential sensors. Two 32-channel scanners were used here, one with 10" of water range and the other with 20" of water range. Each channel is a mini piezoresistive pressure transducer and its output is internally amplified to ±5V full scale. These transducers have an accuracy of 0.10% of full scale after full calibration and a frequency response of 50 Hz. The transducers are differential and the reference pressure taken was the free stream static pressure. The last port in the second ESP was set aside for the tunnel total pressure to obtain the free stream velocity from the dynamic pressure. This system was developed in house but also employs Aeroprobe Corp. proprietary software as well as physical setup.

2.4 Water Tunnel

The ESM Water Tunnel was designed and built by Engineering Laboratory Design (ELD). The system is a closed loop design with the flow arranged in a vertical configuration with an approximate capacity of 9463 liters (2500 gallons) of water. A schematic is provided in Figure 2-7. Among the tunnel components are the flow section that includes a return plenum, 14 inches return PVC pipe, an inlet plenum, a flow straightener and a three-way contraction convergence. The test section is a 61 cm x 61 cm x 183 cm (24" x 24" x 72") made out of a 1 ¼ inch clear acrylic plexiglass and a removable top that was not used during the present work. The final components of interest are a 17000 liters/min (4500 gpm) single stage pump and a variable speed drive assembly that consist of a 15 kW (20 hp) AC motor and a variable frequency controller that allows for a range of flow velocities in the test section from 3 cm/s (0.1 ft/s) to 91 cm/s (1.5 ft/s).

A return plenum with a turning vane system divides and directs the flow after the test section. A 0.3 m x 0.61 m Plexyglass window at the end of the return plenum allows for visual access to the test section directly downstream. A perforated cylinder feeds the flow to the inlet plenum. Stainless steel perforated plates placed in the plenum act as head loss baffles. Round-cell polycarbonate honeycombs and two 60% porosity stainless steel screens work as flow straighteners upstream of the contraction.

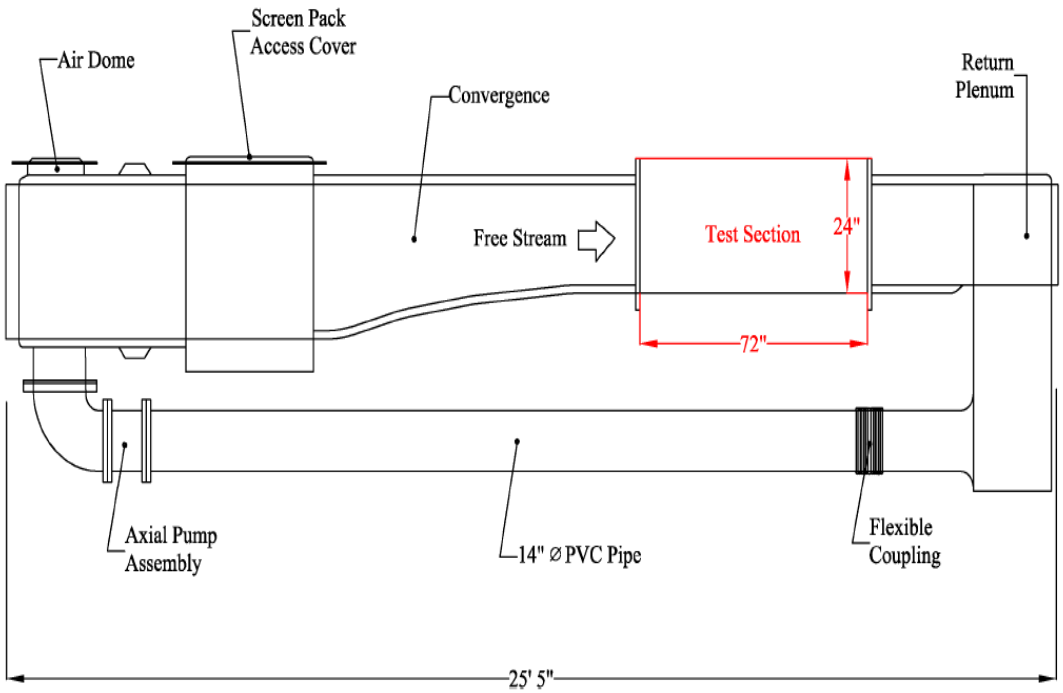

Figure 2-7: ESM Water tunnel Schematic

2.5 Water Tunnel Model

A first-generation, trapezoidal, sharp-edge wing model was designed and fabricated out of ABS plastic using a rapid-prototyping facility. This model is shown

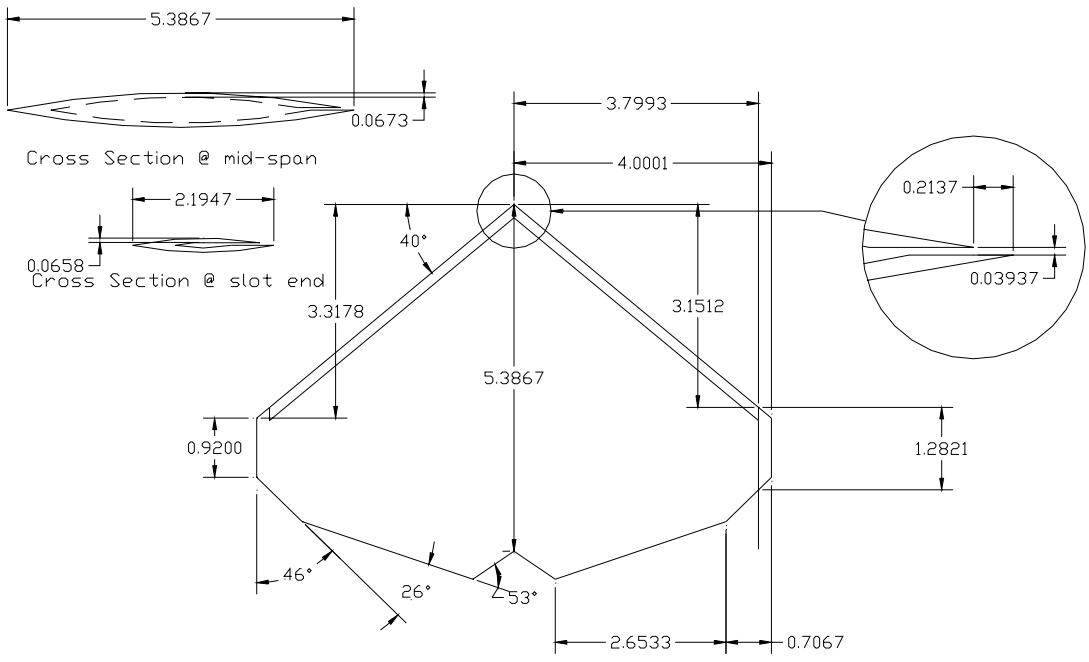

in

Figure 2-8. The airfoil section is geometrically similar to the one fabricated for the wind-tunnel tests. The root chord was 136.8 mm and the maximum thickness was approximately 10% of the chord. The mid-span of the model was 101.4 mm while a uniform jet-exit slot with 1 mm width was placed within 5% from the leading edge. Its internal chamber is connected through two 1/4" brass tubings located at the trailing edge to two high precision, computer-controlled gear pumps via the water supply connector shown in the same figure. These tubes also work as the model's support. The pumps allow the generation of pulsing jets with non-zero mean flow.

For the experimental results presented here, the Reynolds number based on the root chord was Re = 42,566. The wing planform was placed at an AOA=13 deg in order to generate a massively separated flow. Based on a Strouhal number of 0.2 the natural shedding frequency was estimated to be around 1 Hz. The latter was chosen as the actuator frequency yielding $F^{+}=1$. The actuator pulsed as a positive net-mass flow actuator with zero offset and an amplitude of $u_{jet}=0.15$ m/s with 50% duty cycle. The above numbers result in a $C_{\mu}=0.006$. Three cases will be presented here. First the flow of the pulsing jet alone, second the flow over the airfoil with no control and finally the flow with the control. These cases were investigated using two different magnifications, first with the field of view covering the whole airfoil with 1 mm spatial resolution, and then, with fine resolution of 0.5 mm, zooming near the actuator jet.

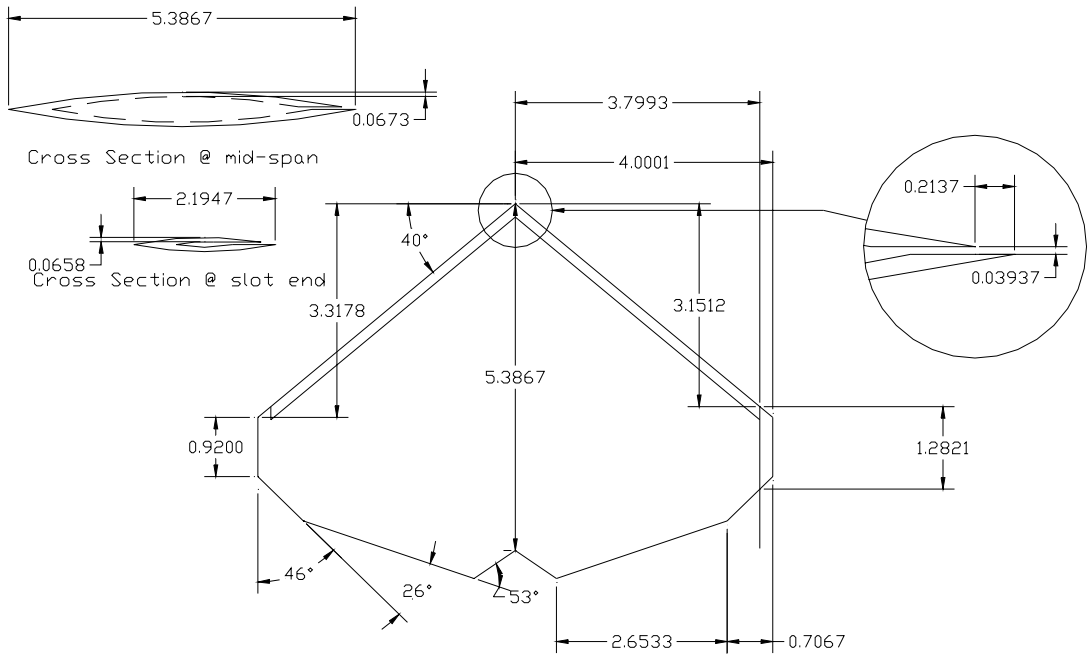

Figure 2-8: Water tunnel model

2.6 Particle Image Velocimetry System

The ESM Water Tunnel is a facility equipped with state of the art, in-house developed Time Resolved Digital Particle Image Velocimetry (TRDPIV). This PIV system is based on an a 50 W 0-30 kHz 2-25 mJ/pulse Nd:Yag laser, which is guided through a series of special mirrors and lenses to the area of interest and is opened up to a laser sheet directed across the field as shown in Figure 2-9. For the research conducted here, the laser sheet was placed in the mid-span of the airfoil aligned parallel to the free-stream. The free-stream velocity was 0.25 m/s with corresponding water tunnel free stream turbulence intensity approximately 1%. A traversing system allows adjusting the distance from the model to the laser sheet. The flow is seeded with neutrally-buoyant fluorescent particles from Boston Scientific which serve as flow tracers. The mean diameter of the particles is on the order of 12 microns, such that the particles accurately follow the flow with no response lag to any turbulent fluctuations. A CMOS IDT v. 4.0 camera with 1280 x 1024 pixels resolution and 1-10 kHz sampling rate kHz frame-straddling (double-pulsing) is employed to capture the instantaneous positions of the particles. The laser and the camera are synchronized to operate in dual frame single exposure DPIV mode. This mode of

operation allows very detailed temporal resolution, sufficient for resolving the turbulent flow fluctuations present in the wake[5].

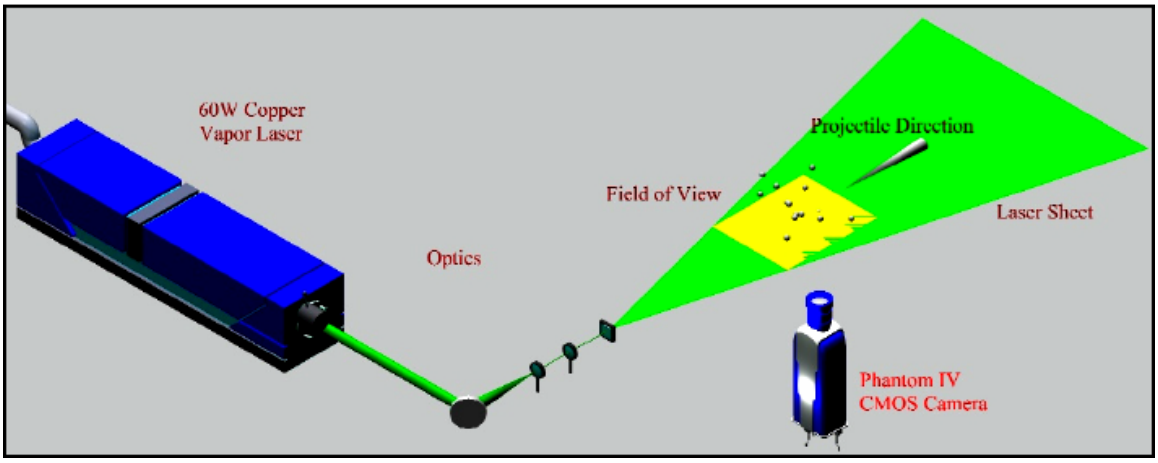

Figure 2-9: Schematic of experimental setup, which includes a 55-Watt Cu-Vapor pulsing laser, a high speed CMOS camera, optical lenses, and the flow field.

The velocity evaluation is carried out using multi-grid iterative DPIV analysis. The algorithm is based on the work by Scarano and Rieuthmuller[3]. In addition to their method, we incorporated a second-order Discrete Window Offset (DWO) as proposed by Wereley and Meinhart[4]. This is a simple but essential component. Time-resolved DPIV systems are limited by the fact that the time separation between consecutive frames is the reciprocal of the frame rate, thus on the order of milliseconds. This value is relatively large compared with microsecond time-intervals employed by conventional DPIV systems. By employing a second order DWO we provide an improved predictor for the particle pattern matching between the subsequent iterations. Moreover, the algorithm employed performs a localized cross-correlation which, based on previous work[6] conducted by this group, when compared to standard multi-grid schemes for resolving strong vortical flows was proven to be superior.

For the needs of the present study, the multigrid scheme was employed with a window hierarchy of (64 x 32)-(32 x 32) pixel^2 and a space resolution of 8 pixel/vector. A three-point Gaussian peak estimator for the correlation peak is used, achieving sub-pixel accuracy of 0.1 pixel for the peak detection process. The overall performance of the method yield time resolution 1 milliseconds with sampling time up to 2 sec and average uncertainty of the velocity measurement on the order of 10^{-3} m/s independently

of the velocity magnitude. The vorticity distribution in the wake is calculated from the measured velocities using 4th order, compact, finite-difference schemes.

2.7 Uncertainty analysis for data taken during this effort

2.7.1 Uncertainty analysis for the pressure coefficients

The differential pressures applied at the pressure ports on the planform surfaces are measured by the ESP's and subsequently converted into dimensionless pressure coefficients. The pressure coefficient is defined as

$$C_p = \frac{P - P_\infty}{\frac{1}{2}\rho U_\infty^2} = \frac{\Delta P}{P_{dyn}} \qquad (2.1)$$

where P_∞ is the free stream static pressure, the reference pressure for the measurements considered, ΔP is the differential port pressure measured by the ESP, and P_{dyn} is the free stream dynamic pressure. The dynamic pressure is measured by employing a Pitot-static tube and measuring the differential pressure between the total and static ports, that is $P_o - P_\infty$, assuming incompressible flow. The ESP are used to measure both the local surface pressure and the dynamic pressure in equation 2.1, and thus both ΔP and P_{dyn} are subject to the measurement errors of the ESP.

Applying the method of Kline & McKlintock[7] for error propagation to the definition of the pressure coefficient in equation 2.1, we find

$$\delta C_P = \left\{ \left[\left(\frac{\partial C_P}{\partial (\Delta P)} \right) \delta(\Delta P) \right]^2 + \left[\left(\frac{\partial C_P}{\partial P_{dyn}} \right) \delta P_{dyn} \right]^2 \right\}^{\frac{1}{2}} = \left\{ \left[\frac{\delta(\Delta P)}{P_{dyn}} \right]^2 + \left[-\frac{\delta P_{dyn} \cdot \Delta P}{P_{dyn}^{\,2}} \right]^2 \right\}^{\frac{1}{2}} \qquad (2.2)$$

But since the measurement of P_{dyn} and P are made by the same instrument and in the same manner, they are subject to the same uncertainties, so $\delta P_{dyn} = \delta(\Delta P) = \delta P$. Substituting for the error quantities, expanding and rearranging equation 2.2 results in

$$\delta C_P = \left\{ \frac{([\delta P]^2 [P_{dyn}^{\,2} + (\Delta P)^2]}{P_{dyn}^{\,4}} \right\}^{\frac{1}{2}} \qquad (2.3)$$

We observe that the largest value of δC_P for a given P_{dyn} would result when ΔP is a maximum. The relation of P_{dyn} and ΔP is such that $(\Delta P)_{Max}$ is no greater than $3P_{dyn}$. Using $\Delta P = 3\ P_{dyn}$ as a worst-case scenario, equation 2.3 becomes

$$\delta C_P = \left\{ \frac{([\delta P]^2 \cdot 9 P_{dyn}^{\ 2}}{P_{dyn}^{\ 4}} \right\}^{\frac{1}{2}} = \left\{ \frac{(9[\delta P]^2}{P_{dyn}^{\ 2}} \right\}^{\frac{1}{2}} = \frac{3 \cdot \delta P}{P_{dyn}} \qquad (2.4)$$

which gives the uncertainty in the measured pressure coeffcient as a function of the uncertainty in the measured pressures and the dynamic pressure of the test.

$\delta P = 0.001 * 4981.8 = 4.981 Pa$

$P_{dyn} = 499.85 Pa$

$\delta C_P = 0.03$

There are three distinct ESP uncertainty cases to be treated: a ±10" H_2O ESP operating in the ESM Wind Tunnel, a ±10" H_2O ESP operating in the Virginia Tech Stability Tunnel, and a ±20" H_2O ESP operating in the Virginia Tech Stability Tunnel. There are three contributions to the uncertainty in the pressure measurement: (1) The static uncertainty of the ESP – δP_1 (2) The bit error associated with the analog-to-digital conversion of the presure by the data acquisition board has an associated pressure uncertainty – δP_2 (3) The uncertainty in the measurement of the calibration pressures by the Barocel pressure transducer - δP_3.

The static error associated with the ESP units is ±0.1% of the full scale, which corresponds to $\delta P_1 = \pm$ 0.01" H_2O for the ±10" H_2O ESP, and $\delta P_1 = \pm 0.02$" H2O for the ±20" H_2O ESP. These were the static uncertainties regardless of the facility in which the units were used.

2.7.2 Uncertainty Analysis for Velocities Measured with PIV

In PIV systems is important to consider the spatial resolution and the accuracy of the velocity estimations. The spatial resolution is defined as the maximum displacement of a particle Δx_{max} over the measurement time Δt. For the work presented here the free stream velocity was in the order of U_∞=0.25 m/s and the Δt=0.001 for a spatial resolution of Δx_{max}=0.25mm or about 0.24% of the model chord. The uncertainty of the velocity estimation can be quantified as:

$$\left(\frac{\sigma_u}{u^2}\right)^2 = \left(\frac{\sigma_{\Delta X}}{\Delta X^2}\right)^2 + \left(\frac{\sigma_{\Delta t}}{\Delta t^2}\right)^2 \qquad (2.5)$$

where σ_u is the uncertainty in the velocity, $\sigma_{\Delta X}$ is the uncertainty in the displacement and $\sigma_{\Delta t}$ is the uncertainty in the time interval of the displacement. Since the laser has very little jitter in the pulses timing and by using a digital interrogation procedure the uncertainty $\sigma_{\Delta t}$ is negligible. Thus the primary error source will be introduced by the displacement estimation. Assuming a typical particle image diameter of 2 pixels in order to optimize the correlation peak detection algorithm, the uncertainty of the velocity estimation is on the order of 1% of the maximum resolvable velocity.

The uncertainty in the average fluctuations in the velocity components can be determined by using the fact that the statistical uncertainty of the estimation of a fluctuating quantity is inversely proportional to the square root of the number of samples used. Therefore, for a typical experiment with 3000 time records, the uncertainty of the estimation of U_{rms} or V_{rms} is on the order of 2% of the mean value.

2.8 References

1. Miranda, S., Vlachos, P. P., Telionis, D. P. and Zeiger, M. P., "Flow Control of a Sharp-Edged Airfoil," Paper No. AIAA-2001-0119, 2001, also *AIAA Journal*, vol. 43, pp 716-726, 2005.
2. Rullan, J.G., Vlachos, P.P. and Telionis, D.P., "Post-Stall Flow Control of Sharp-Edged Wings via Unsteady Blowing" *41st Aerospace Sciences Meeting and Exhibit, 6-9 January 2003, Reno, Nevada,* Paper No AIAA-2003-0062, also Journal of Aircraft, Vol. 43, No 6, November 2006, pp. 1738-1746.
3. Scarano, F. and Rieuthmuller, M. L. (1999). "Iterative multigrid approach in PIV image processing with discrete window offset". Experiments in Fluids, 26, 513-523
4. Wereley S.T., Meinhart C.D. (2001). "Second-order accurate particle image velocimetry". Experiments in Fluids, 31, pp. 258-268.
5. Abiven, C., Vlachos, P. P., (2002). "Super spatio-temporal resolution, digital PIV system for multi-phase flows with phase differentiation and simultaneous

shape and size quantification", Int. Mech. Eng. Congress, Nov. 17-22, 2002, New Orleans, LA

6. Abiven, C., Vlachos P. P., Papadopoulos, G., (2002). "Comparative study of established DPIV algorithms for planar velocity measurements", Int. Mech. Eng. Congress, Nov. 17-22, 2002, New Orleans, LA
7. Kline, S.J., and McClintok, F.A., Describing Uncertainties in Single-Sample Experiments, The American Society of Mechanical Engineers, Vol. 75, Number 1, Easton, PA, January 1953

3. The Aerodynamics of Diamond-Shaped-Planform Wings

Wings swept by 30 to 40 degrees are today very common in fighter aircraft. And yet, there is very little work devoted to the understanding of the aerodynamics of such wings. The problem is that such wings may be able to sustain attached flow next to broken-down delta-wing vortices, or stall like two-dimensional wings while shedding vortices with generators parallel to their leading edge. In this chapter, we explore the aerodynamics of swept leading edges. We present velocity and vorticity distributions along planes normal and parallel to the free stream for a wing with a trapezoidal planform and sharp leading edges. We also present pressure distributions over the suction side of the wing. Vorticity distributions and out-of-plane velocities for the wake are also presented.

3.1 Introduction

At very low sweep angles, namely angles less than 20°, the flow over sharp-edged wings stalls like the flow over an unswept wing. Vortices are shed with their axis nearly normal to the free stream. Such vortices are often called “rollers”. At high sweep angles, that is, larger than 50°, the flow is similar to delta wing flows that are dominated by leading-edge vortices (LEV). We will refer to these vortices here as “streamers”. These wings stall due to vortex breakdown.

The effects of sweeping a wing at moderate angles, namely 30° to 40°, and moderate to high angles of attack are very little understood. And yet, such wings are today the norm for most fighter aircraft. The problem is that in this range of parameters, the flow may stall like the flow over an unswept wing, shedding large roller vortices in an unsteady fashion, or it could stall like a delta wing, sustaining a leading-edge vortex (LEV) that breaks down. The significant difference between the two modes is that delta wing vortices, or streamers, are attached to the leading edge of the wing and shed vorticity by directing it in the core of the vortex, and then telescoping it downstream, whereas rollers, grow and then shed by rolling over the wing and detaching from its surface similar to the Von Karman Vortex Street. This is essentially the phenomenon of unsteady stall.

It is imperative that we understand the basic aerodynamics of these phenomena, before we attempt to control them at high Reynolds numbers. To this end, we have been

conducting flow visualizations and PIV measurements at low Reynolds numbers. We found that both stalling modes are possible on a planform with a sweep angle of 40°. But even with what appears like two-dimensional stall, there is some recirculation in planes normal to the free stream that appears like LEV. We therefore conclude that there is indeed a hybrid mode of stalling. The exciting implication is that with flow control, we should be able to dictate the mode of stalling and therefore the effectiveness of flow control.

Research on delta wing flows for sweep angles as low as 50° indicate that delta-wing vortices are present, but break down very close to the leading edge[1-5]. In fact, even before break down, these vortices display wake-like flow, where the velocity is very low in the core of the vortex. In some cases[2] it was found that the low-aspect-ratio wing at medium angles of attack does not behave like a delta wing but rather like an unswept wing. A sweep angle of 50° is not low enough to demonstrate the transition from the vortex breakdown stall to the two-dimensional unsteady stall. More recently, Yaniktepe and Rockwell[6] studied the flow over a wing with a sweep angle of 38.7°. They provided evidence that up to an angle of attack, α, of 25° the flow appears to be dominated by delta wing tip vortices. At the highest angle of attack, the vortices seem to be displaced inboard.

In both the studies of Ol and Gharib[2] and Yaniktepe and Rockwell[6], the flow field was interrogated along planes normal to the free steam. In our studies we cut the fields with planes that are both normal and parallel to the free stream. We are interested in the possibility that control mechanisms could actually dictate the desired stall mechanism. We provide evidence that our wing stalls by shedding rollers.

Impressive advancements have been made in controlling the flow over wings with rounded leading edges, but very little work has been devoted to the control of the flow over sharp-edged wings. The present authors[7,8] have demonstrated that flows over sharp edges can be effectively controlled with lift increases as high as 70%. Control of delta wing flows has been successful but the efforts were focused so far for relatively high sweep angles[9-11]. The objective of this project is to capitalize on our experience and extend the work to moderately swept wings and wings with practical planforms.

Flow control is the ultimate goal of the present effort, and the aerodynamics of leading edges plays a vital role in lending itself to control mechanisms. The majority of contributions on airfoil flow control are based on separation control. Their aim is to delay separation and stall altogether. There is another area of airfoil and wing flow control, which so far has received little attention but which has greater potential in defense applications. This is the management and control of separated flow. Such flows are encountered over sharp-edged wings at low to moderate angles of attack or over wings in deep stall. The idea is to accept the fact that in some situations, the flow is fully separated, and periodic shedding of vortices is established. The aim then becomes to control the dynamic development of vortical structures in order to improve the performance of the lifting surface. These are the type of flows that develop over wings moderately swept and the focus of the present research.

We discuss in this paper the results of experiments conducted in a water tunnel and a wind tunnel with a trapezoidal planform wing model typical of wings used in industry. These models were tested at low and moderate Reynolds numbers, namely Re=42,000 and 1,200,000. In the water tunnel we employ Digital Particle Image Velocimetry (DPIV). For wind tunnel testing, we assembled the hardware that allows us to test large stainless steel models. We have also developed seven-hole probe measurement techniques that return sectional circulation values and vorticity distributions that will allow us to confirm the effectiveness of flow control.

3.2 Facilities, Models and Equipment

3.2.1 Facilities and Models

Experiments were carried out in the Engineering Science and Mechanics (ESM) water tunnel and in the VA Tech Stability Wind Tunnel. The ESM Water Tunnel was built by Engineering Laboratory Design (ELD) and operates in a closed loop, in a vertical plane, with up to 2,500 gallons of water. The settling chamber leads to the 24" x 24" x 72" Plexiglas test section via a three-way convergence. A 4500-gpm pump driven by a 20-hp motor provides flow which can attain a maximum speed of 1 m/s, corresponding to a maximum Reynolds number per unit length of 9900/cm. The free-stream turbulence level in the test section is less than 2%. The Virginia Tech Stability wind tunnel is a continuous, closed-loop subsonic wind tunnel. The tunnel fan is 14-foot (4.27m) in

diameter and is driven by a 600 hp motor. The maximum achievable flow speed is 275 ft/s (83.8 m/s) in a 6ft x 6ft x 25ft (1.83m×1.83m×7.62m) test section. The settling chamber has a contraction ratio of 9 to 1 and is equipped with anti-turbulence screens. This combination provides an extremely smooth flow in the test section. The turbulence level varies from 0.018% to 0.5% and flow angularities are limited to 2° maximum.

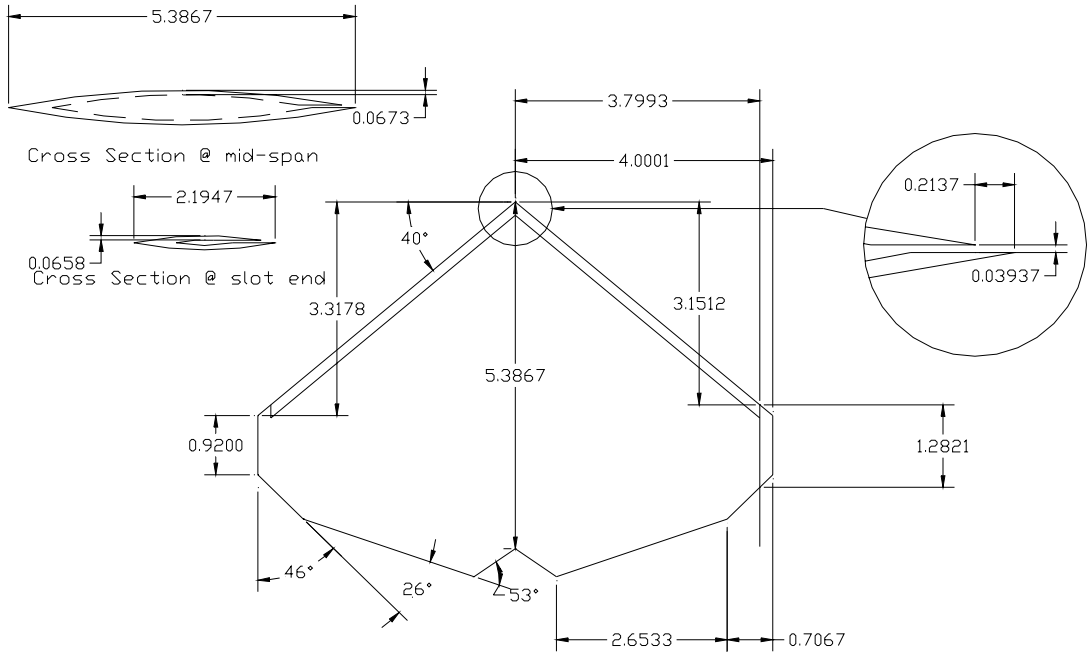

Figure 3-1: Engineering drawing of the trapezoidal planform model for water tunnel testing.

The model for this experimental investigation has a trapezoidal planform, also known as a diamond-shaped-planform wing or cropped delta wing shown in Figure 3-1. In this Figure the dimensions, in inches, correspond to a small model designed for testing in the water tunnel. This model is equipped with an internal compartment that can generate a pulsing jet in the leading edge for flow control. Lockheed Martin, a co-sponsor of this effort has availed to us a large, 2.5-feet-span, stainless steel model, equipped with pressure taps. This model is geometrically similar to the model shown in Figure 3-1. Pressure taps are distributed along lines parallel to the root of the wing at spanwise distances z/c= 0.063, 0.1508, 0.2424, 0.3339, 0.4061, 0.4588, 0.5115, 0.5641, 0.6238, and 0.6904. Along the axial direction the distribution of pressure ports varies with the span. There are 17 next to the root and nine near the tip. The model is mounted on a sting

that permits changes of the angle of attack while keeping the aerodynamic center of the wing at the same elevation in the test section. The wing mounted on the sting is shown in Fig. 2. Short splitter plates were mounted along the roots of the wings, to simulate the a plane of symmetry. This aerodynamic conditions are not the same with those imposed along the plane z=0 of the wing model shown in Fig. 1, nor are they equivalent to the conditions imposed by a fuselage model. We will estimate these effects by comparing with data obtained earlier with a full model that includes the fuselage.

Figure 3-2: Trapezoidal model for wind tunnel testing mounted on sting.

3.2.2 Particle Image Velocimetry

Particle-Image Velocimetry (PIV) is a powerful tool that we employ in this effort. The most common implementation of the method, (currently commercially available) focuses on a single-exposure double-frame digital cross correlation approach. A high-resolution (1Kx1K pixels) CCD camera that can sample up to 30 fps, results in a sampling frequency of the flow field of only 15Hz. Cameras are usually synchronized with a Nd:YAG pulsing laser that illuminates the interrogation area. The velocity field is traditionally treated as a linear transfer function that corresponds to a flow pattern displacement between two consecutive images. This transfer function is revealed in a statistical manner incorporating second-order statistical moments of the image patterns (Westerweel[13,14]).

A major disadvantage of this approach is the inability to provide sufficient frequency resolution, which is necessary, in order to investigate any high-frequency phenomena that

occur in turbulent, separated flows. A system developed at VA Tech has overcome the difficulty of low sampling frequency. This was accomplished with the integration of a high-power (50 W) pulsing laser with special type of optics and a unique CMOS camera, capable of acquiring up to 1000 frames per sec (fps) resulting to a DPIV system with 1 KHz maximum sampling frequency[15]. To our knowledge, there are no results published in the open literature that employ high-speed CMOS technology to perform DPIV measurements. Our ongoing research to integrate this technology with our existing PIV system demonstrated very high sensitivity, equivalent to 1000 ASA, and signal-to-noise ratio in the order to 100,000:1. The great advantage of this new technology is that each pixel is treated as an individual sensor and any cross-coupled interaction between neighborhood pixels is eliminated. The conditioning of the signal is performed on the sensor. Thus, the spatial and temporal resolution of our PIV system is increased by almost an order of magnitude in comparison with our previous configuration, and two orders of magnitude compared with systems that are commercially available.

Members of our group were able to perform dual-frame cross-correlation time-resolved DPIV by employing single and multiple exposures. The first example of single-exposure double frame cross-correlation time resolved DPIV was presented by Vlachos et al.[15]. However this implementation was limited to very low-speed liquid flows (U~10 cm/s). In a different approach, we performed multiple exposures per frame and we evaluated the vectors using standard cross-correlation. This approach was employed in the analysis of the characteristics of turbulent shear layers by Vlachos et al.[16] and in the investigation of the post-vortex-breakdown region characteristics of delta wings by Klute et al.[17].

One major drawback of conventional DPIV systems results from limitations inherited from the velocity evaluation methods. Our group recently launched an effort to integrate and combine some of the most effective and well established of these proposed methods[18]. The outcome is a dynamically-adaptive hybrid algorithm for the evaluation of the velocity vectors that overcomes these limitations to a great extent, thus increasing accuracy and space resolution. The overall performance of the method, if quantified, yields space resolution in the order of 0.5 mm average, time resolution in the order 1

milisec with sampling time up to 4 secs and uncertainty of the velocity measurement in the order of 0.1% of the reference velocity.

The advancements in this effort are employed in the global characterization of the separated flow over the sharp airfoil, providing insight on the interaction of the shear layers with the incident free stream and their roll up to coherent vortices. These data will be used to analyze the flow control mechanism, providing spatio-temporal correlations, information about the interaction of the various frequency modes in the flow field and the route to the formation of coherent structures in the separated flow region. Data were obtained along laser cuts as shown in Figure 3-3. Cuts A, B, C, D and E are parallel to the free stream, while cuts 1, 2 and 3 are normal to the free stream. These cuts are located along z/c= 0, 0.1, 0.38, 0.57 and 0.77 and x/c=0.1856, 0.3712 and 0.5568, respectively.

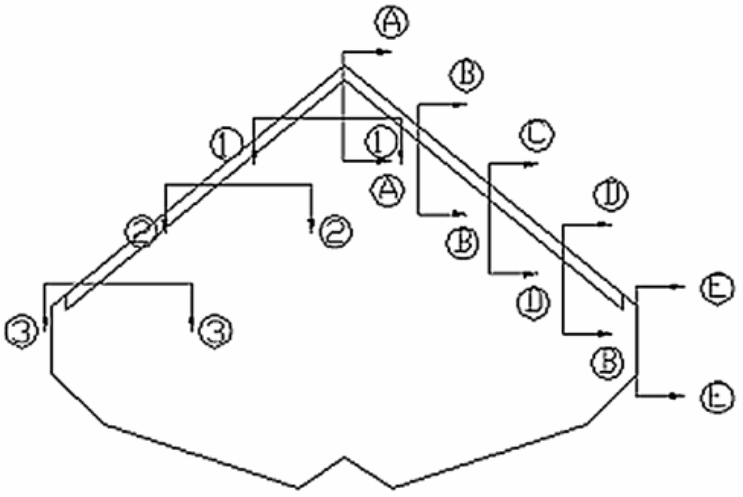

Figure 3-3: Laser cuts for the water tunnel flow visualization and PIV.

3.2.3 Sensors and Actuators

Pressure scanners are employed to monitor the pressure distribution over the wing. ESP scanners by Pressure Systems Inc. are used. Two 32-channel ESPs are employed to monitor the pressure distribution along ten spanwise stations of the wing over the suction side and seven stations over the pressure side. A calibrated 5-hole embedded sensor probe, produced by Aeroprobe Corporation was used to take velocity measurements in the wake of the wings. The probe can measure the three components of the velocity as well as static and dynamic pressure, but the frequency response is limited to about 50 Hz.

The probe was mounted to a two-axis motorized traversing system and placed at the model's trailing edge.

The ability to demonstrate vortex shedding lock-on control for a closed-loop, adaptive wing configuration will rely on robust sensing and actuation schemes which are realizable for a full-scale aircraft. An equally important consideration is the design and demonstration of feasible closed-loop control algorithms that can affix the shear layer excitation at the sensed vortex shedding frequency for constant and changing airspeeds.

3.3 Results and Discussion

3.3.1 Flow Visualization and PIV Results

The velocity field over the airfoil was explored in water tunnel tests using flow visualization and Time-Resolved DPIV. These data were processed using an in-house developed multi-grid iterative DPIV, with second-order, Discrete Window Offset (DWO). Time-resolved DPIV systems are limited by the fact that the time separation between consecutive frames is the reciprocal of the frame rate, thus on the order of milliseconds. This value is relatively large compared with microsecond time intervals employed by conventional DPIV systems. By employing a second-order DWO we provide an improved predictor for the particle pattern matching between subsequent iterations. Moreover, the algorithm employed performs a localized cross-correlation, which, when compared to standard multi-grid schemes for resolving strong vortical flows was proven to be superior.

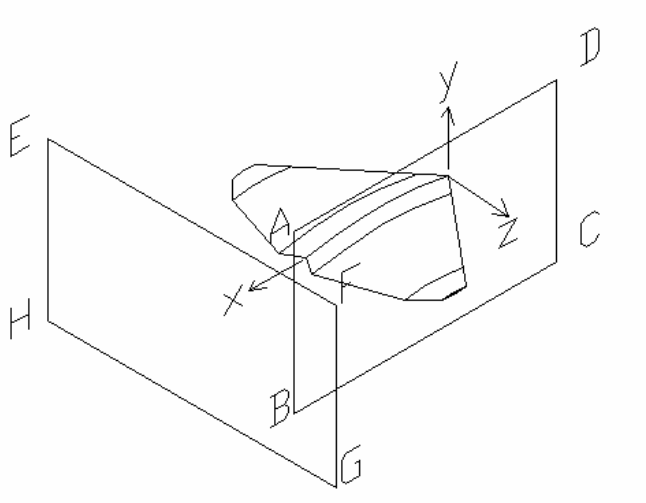

Figure 3-4: Schematic of planes of data acquisition.

For both flow visualizations and PIV measurements, we cut the field by laser sheets parallel and perpendicular to the free stream as shown schematically in Figure 3-3. We have data for four angles of attack along the eight planes marked in Figure 3-3. Our flow visualization, seen in Figure 3-5, on a Trefftz plane, namely plane EFGH shown in Figure 3-4 indicates results very similar to those of Yaniktepe and Rockwell[6], which imply that the flow develops leading edge vortices. We found that such visualizations could be deceiving. For the same configuration, cutting the flow by a plane parallel to the free stream essentially passes a section through a LEV. Leading edge vortices have a nearly circular cross-section if they are cut normal to their axis. But if cut by a plane inclined with respect to their axis, they should show vorticity of the same sign along a closed and nearly elliptical contour. Moreover, the velocity component along the axis of a LEV should be jet-like. The PIV data along a plane parallel to the flow shown in Figure 3-7 are void of such characteristics. Instead they indicate vorticity only on the upper side, which is compatible with two-D stall. The axial velocity distribution indicates wake-like behavior, which confirms the fact that we have two-D stall. A detail of this flow is shown in Figure 3-7.

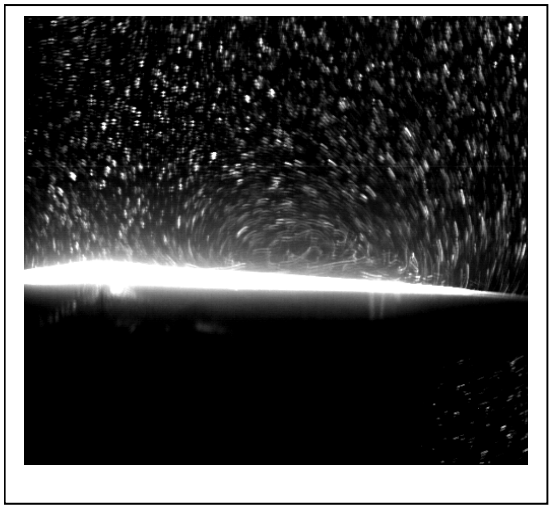

Figure 3-5: Flow visualization along a Trefftz plane.

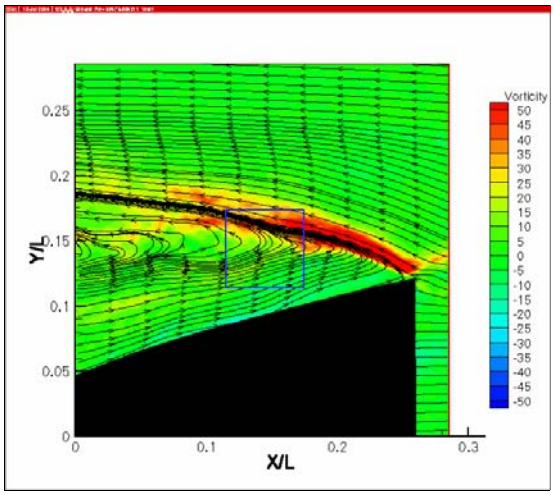

Figure 3-6: PIV data obtained along Plane C

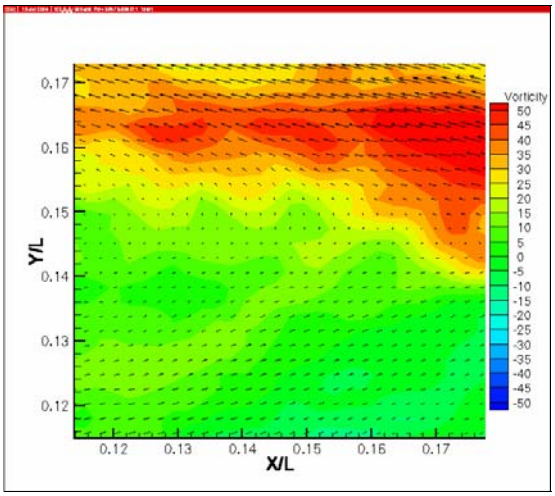

Figure 3-7: Field detail from Figure 3-6

In Figure 3-8 through Figure 3-10 we present data along planes parallel to the free stream at five different spanwise stations, as shown in Figure 3-3 and indicated in the caption of the frames. The planform of the wing was added in a perspective way to help visualizing the location of the planes of data. In this and the following figures we present a very small portion of the actual number of data, to avoid cluttering the images. But quantities like vorticity have been calculated using all data along the full grid. If a delta-wing vortex were present at these locations, then our planes would have cut across them and would have indicated a closed loop of vorticity. These data therefore indicate that the flow separates in the form of rollers, and what we captured are the averages over time of rollers displacing towards the trailing edge. Note that near the root of the wing, the separated region tends to close near the trailing edge, whereas further outboard, the wakes are open. It should be emphasized that these are averaged fields. Our instantaneous frames indicate that the flow field involves the rolling and shedding of rollers.

In Figure 3-11 through Figure 3-14 we present data obtained along planes normal to the oncoming stream, namely planes 1,2 and 3 which are positioned at x/c=0.1856, x/c=0.3712 and x/c=0.5568, respectively. These correspond to the flow visualization of Figure 3-3. The data indicate some recirculation that is reminiscent of delta wing vortices. However, vorticity distributions point to the opposite direction. The fact again that vorticity is present only on the top of the domain of recirculation, implies that these planes only cut free shear layers that delineate a separated region.

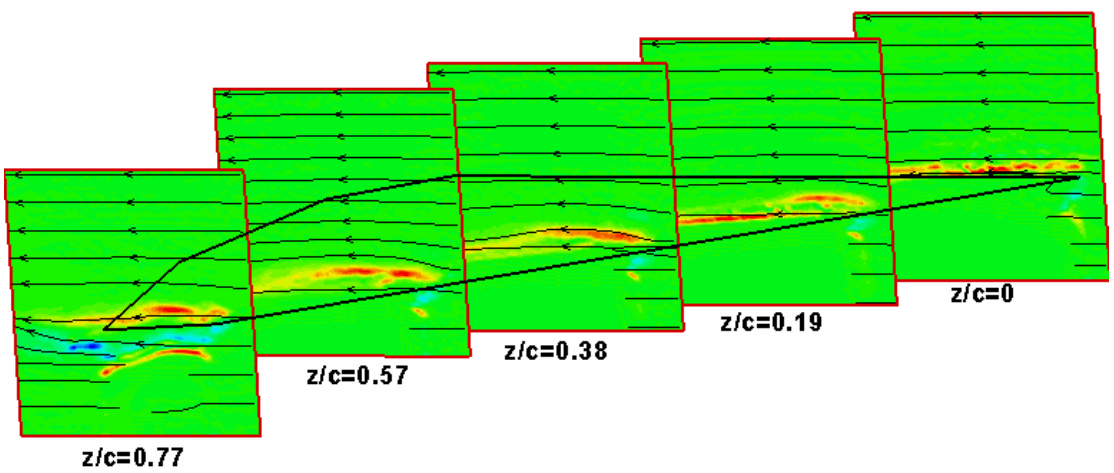

Figure 3-8: Streamlines and vorticity contours along spanwise planes for α= 7°.

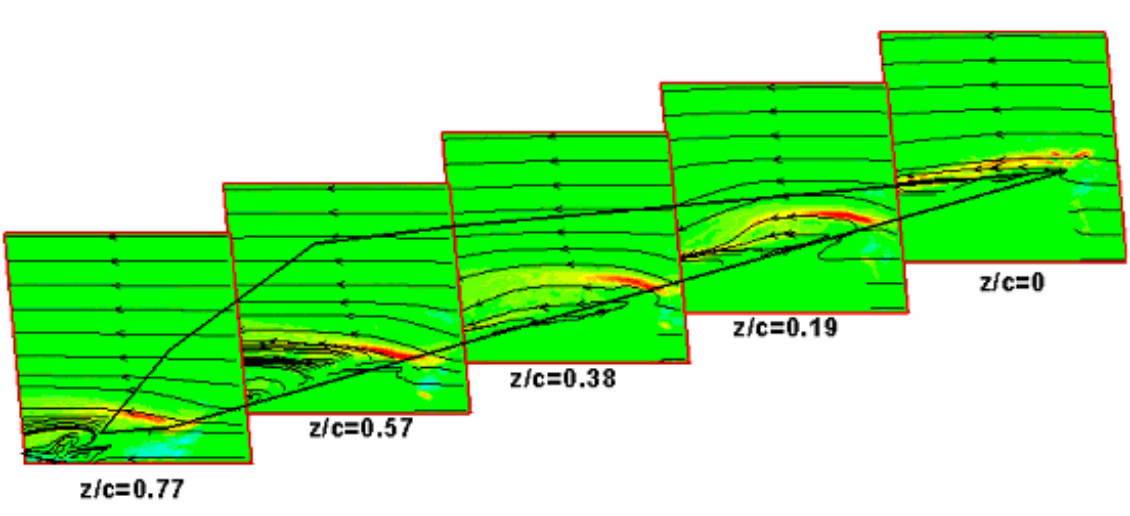

Figure 3-9: Streamlines and vorticity contours along spanwise planes for α= 13.

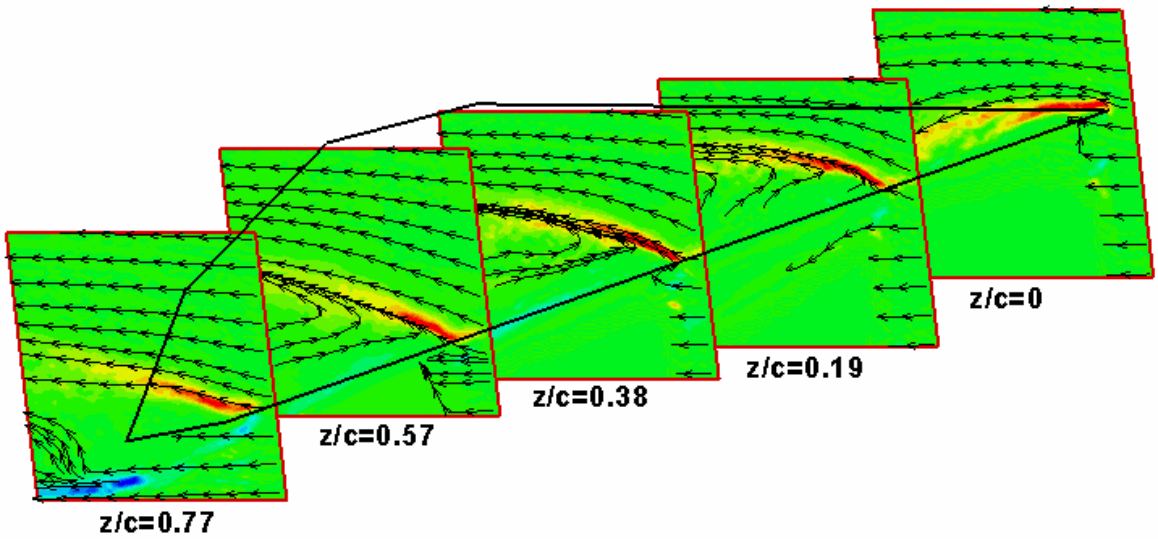

Figure 3-10: Streamlines and vorticity contours along spanwise planes for α= 25^0.

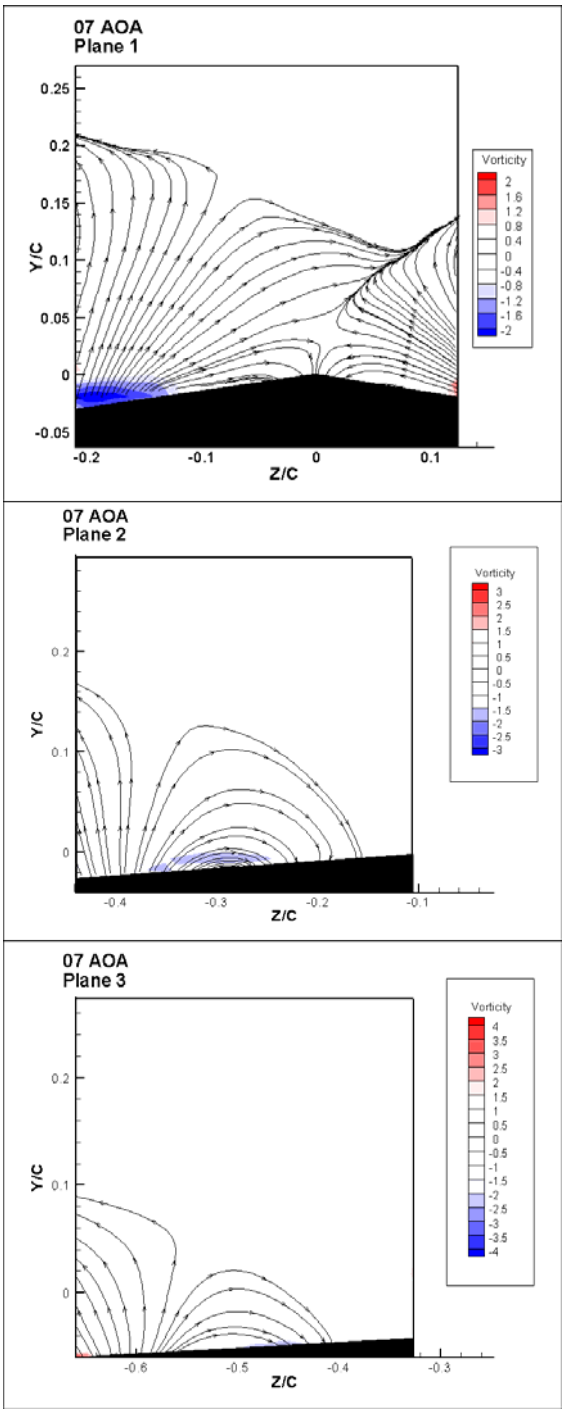

Figure 3-11: Streamlines and vorticity contours along Trefftz planes for α=7°

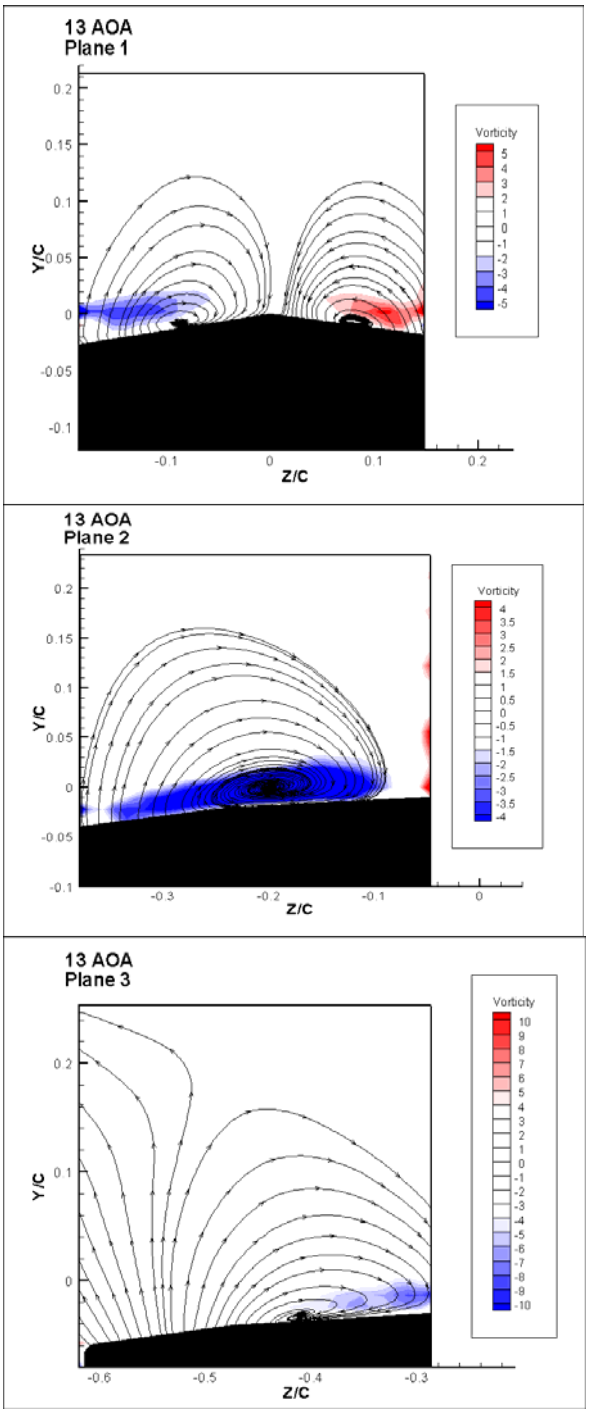

Figure 3-12: Streamlines and vorticity contours along Trefftz planes for α=13°

.

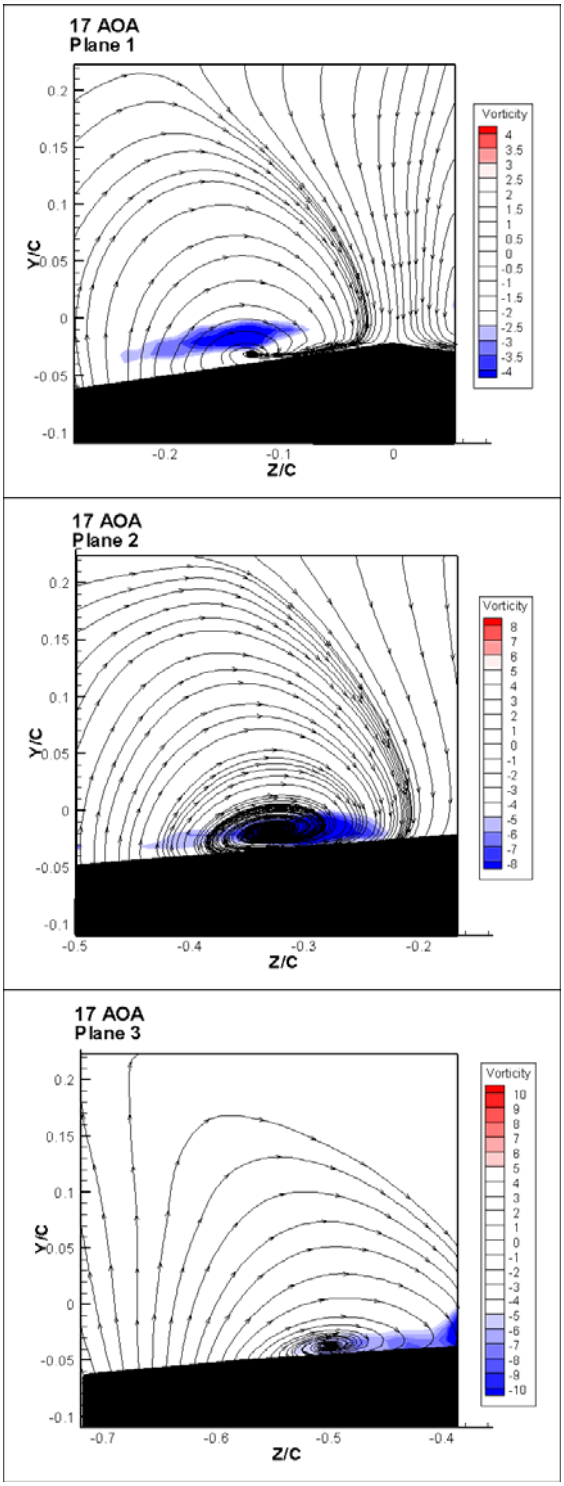

Figure 3-13: Streamlines and vorticity contours along Trefftz planes for α=17°

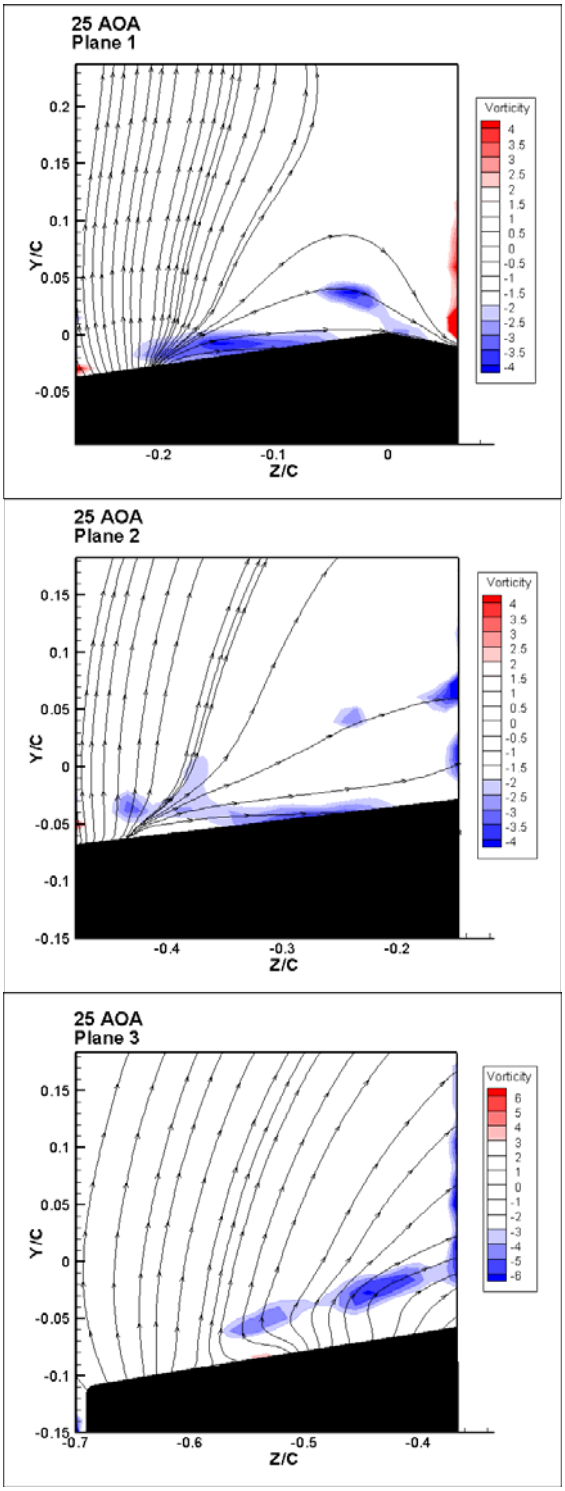

Figure 3-14: Streamlines and vorticity contours along Trefftz planes for α=25°

3.3.2 Pressure Distributions and Wake Trefftz Plane Results

Pressure distributions were obtained over the large model for a Reynolds number of 1,200,000, at angles of attack of 7°, 13°, 17° and 21°. In Figure 3-15 through Figure 3-18 we present data for four angles of attack, as indicated in the figure captions. In these figures the horizontal axis represents the distance along the chord. But the data are projected as if the wing is viewed from its tip in a direction normal to the root axis, or say the fuselage of the aircraft. Since the leading edge is swept, the pressure curves begin at higher values of the x coordinate as we move from the root to the tip.

All these pressure distributions may appear unfamiliar to researchers who study flows over wings with rounded edges. At high angles of attack, the flow is fully separated and thus, the suction side sustains a uniform pressure distribution. But at low angles of attack, there is a distinct region of very low pressure near the leading edge. This may be interpreted as a leading edge vortex, common on delta wings. This may well be the case, since the low pressure is fixed on the wing. But earlier experiments[7] indicate exactly this type of pressure variation over sharp-edged wings with no sweep. This vortex could therefore be captured on the wing regardless of the sweep angle. Our data indicate that the imprint of this vortex, is confined to the root area of the wing and it retreats closer to the wing as the angle of attack increases. The flow over the wing must be fully separated for $\alpha>12°$, in agreement with the data obtained at lower Reynolds numbers.

Areas of recirculation near the leading edge of a wing could also be due to a separated bubble. Such a phenomenon is common at Reynolds numbers below 100,000, and involves a free shear layer that transitions to turbulence, and them reattaches. But these bubbles cannot sustain very low pressures or considerable lengths, as indicated in Figure 3-16, Figure 3-17 and Figure 3-18.

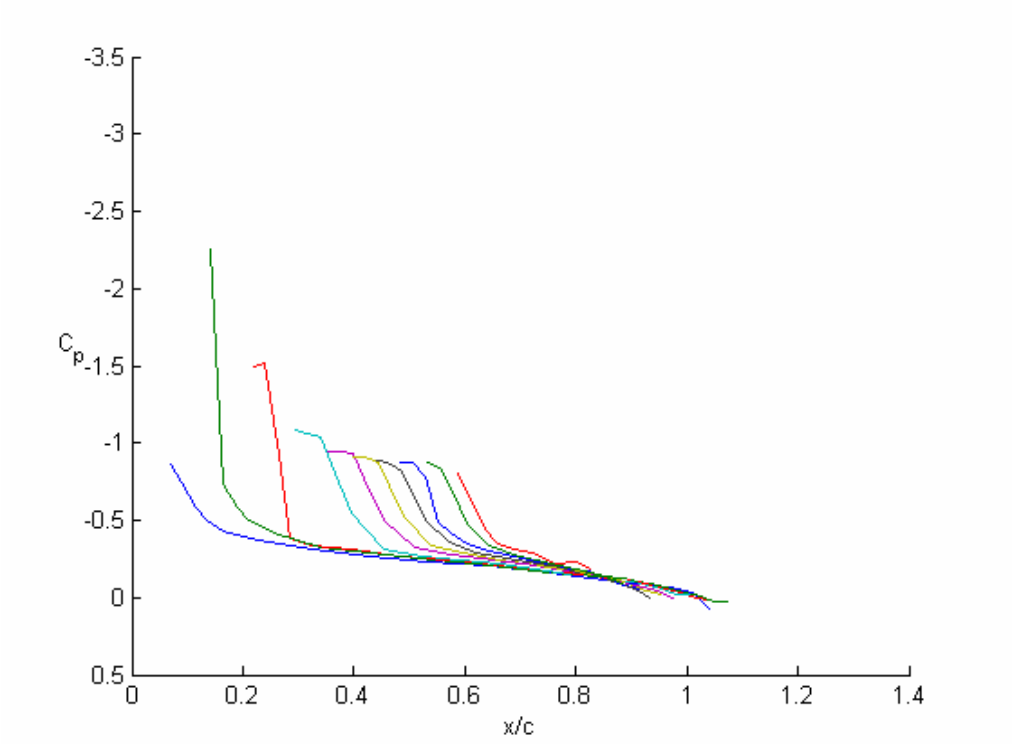

Figure 3-15: Pressure distribution for α=7°, at spanwise stations of z/c= 0.063, 0.1508, 0.2424, 0.3339, 0.4061, 0.4588, 0.5115, 0.5641, 0.6238, and 0.6904.

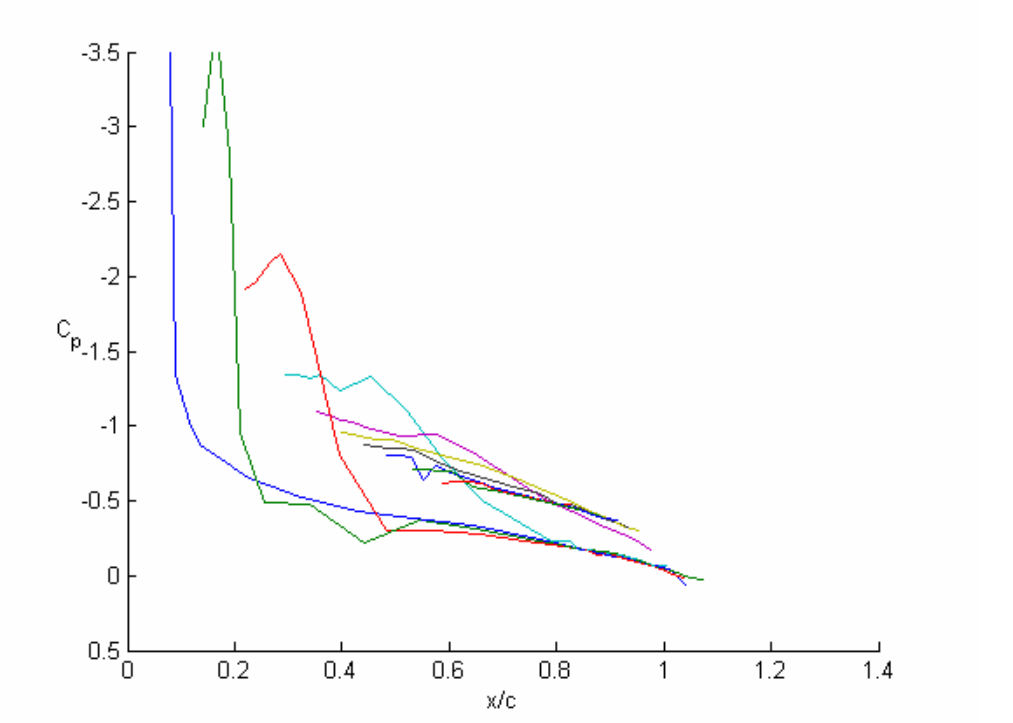

Figure 3-16: Pressure distribution for α=13°, at spanwise stations of z/c= 0.063, 0.1508, 0.2424, 0.3339, 0.4061, 0.4588, 0.5115, 0.5641, 0.6238, and 0.6904.

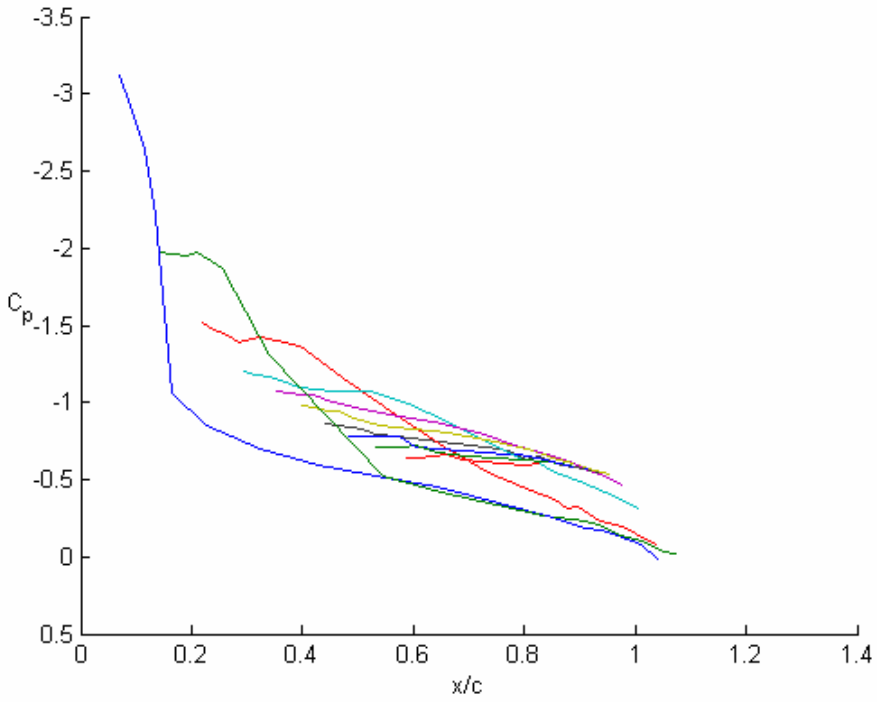

Figure 3-17: Pressure distribution for α=17°, at spanwise stations of z/c= 0.063, 0.1508, 0.2424, 0.3339, 0.4061, 0.4588, 0.5115, 0.5641, 0.6238, and 0.6904.

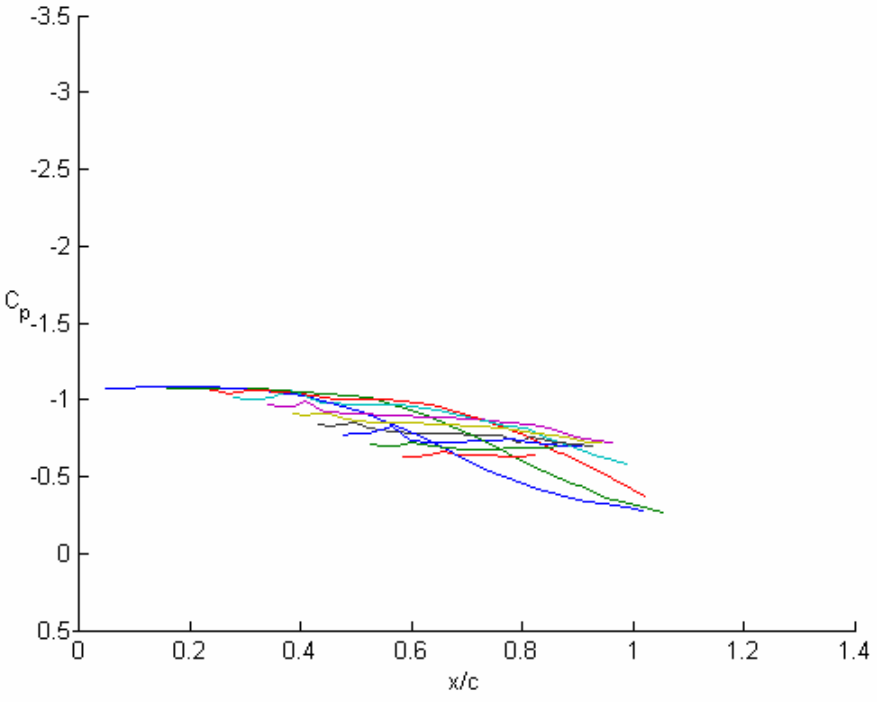

Figure 3-18: Pressure distribution for α=21°, at spanwise stations of z/c= 0.063, 0.1508, 0.2424, 0.3339, 0.4061, 0.4588, 0.5115, 0.5641, 0.6238, and 0.6904.

We turn now to data obtained on a Trefftz plane normal to the free stream and placed at x/C=1.09 (just behind the trailing edge), as indicated in Figure 3-3. The five-hole probe was traversed on a rectangular grid covering the domain -0.5<y/c<.1 and 0<z/c<1.0 domain. In Figure 3-19 through Figure 3-22 we present results for angles of attack of 13° and 21°. In these figures we display the in-plane velocity component in terms of arrows. In Figure 3-19 and Figure 3-21, the streamwise velocity component is displayed in terms of color/shade contours and in Figure 3-20 and Figure 3-22 the in-plane vorticity component is presented in the same way. The velocity vectors in Figure 3-19 and Figure 3-20 indicate the presence of a tip vortex for α=13°. We note that this vortex is broken down, as is clearly indicated by the wake-like character of the streamwise velocity component. Figure 3-19 indicates a much more dominant wake-like effect and very slow velocity downstream of the major portion of the wing. It should be noted here that the broken-down delta wing vortices retain their character and display a wake-like profile, which however is confined to the core of the vortex. This is not the case for the flow field of Fig. 20. For α=21°, the situation is clearer. Now we observe evidence of a massive separated region, with streamwise velocity magnitudes approaching zero and a few pockets of reversed flow. In the vorticity contours of Figure 3-22, there seems to be no vorticity present, except a weak amount very near the tip. Apparently the tip vortex will sustain its presence even at higher angles of attack.

Even though there is no evidence of delta wing vortices in planes normal to the free stream, it appears that there is a tendency for the velocity vectors in these planes to follow some pattern of recirculation, consistent with the direction induced on all finite wings. This is evident in Figure 3-19 through Figure 3-22 but also in Figure 3-11 to Figure 3-14. This is true even though the flow is fully separated.

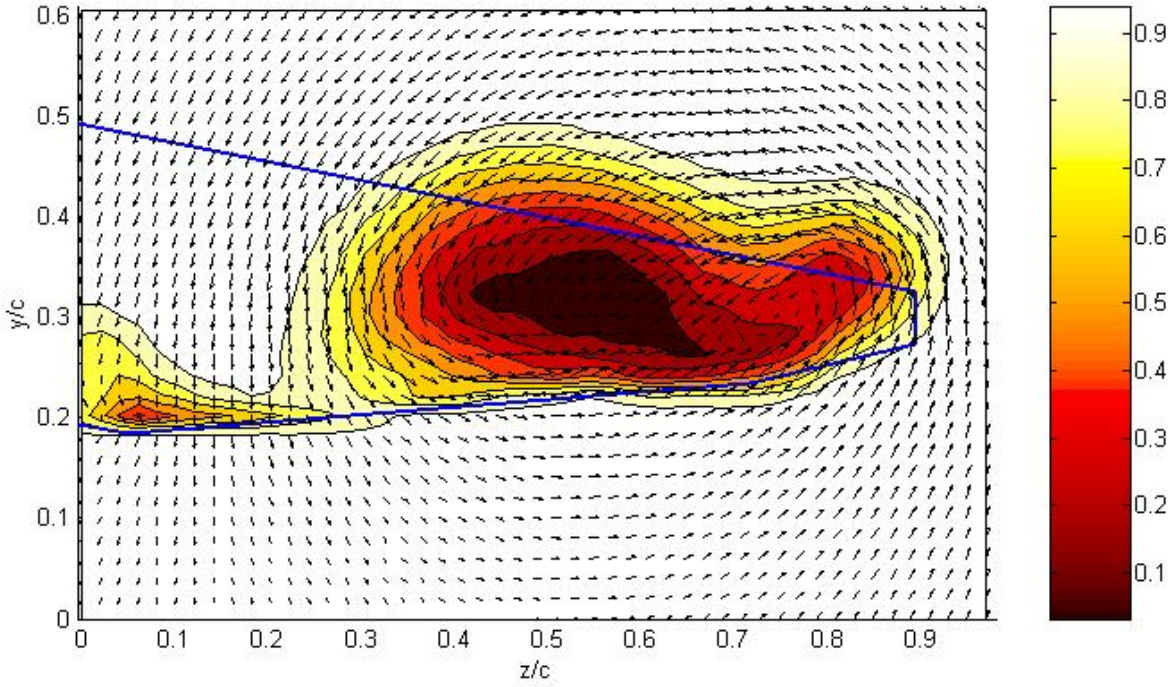

Figure 3-19: Axial velocity contours for α=13°

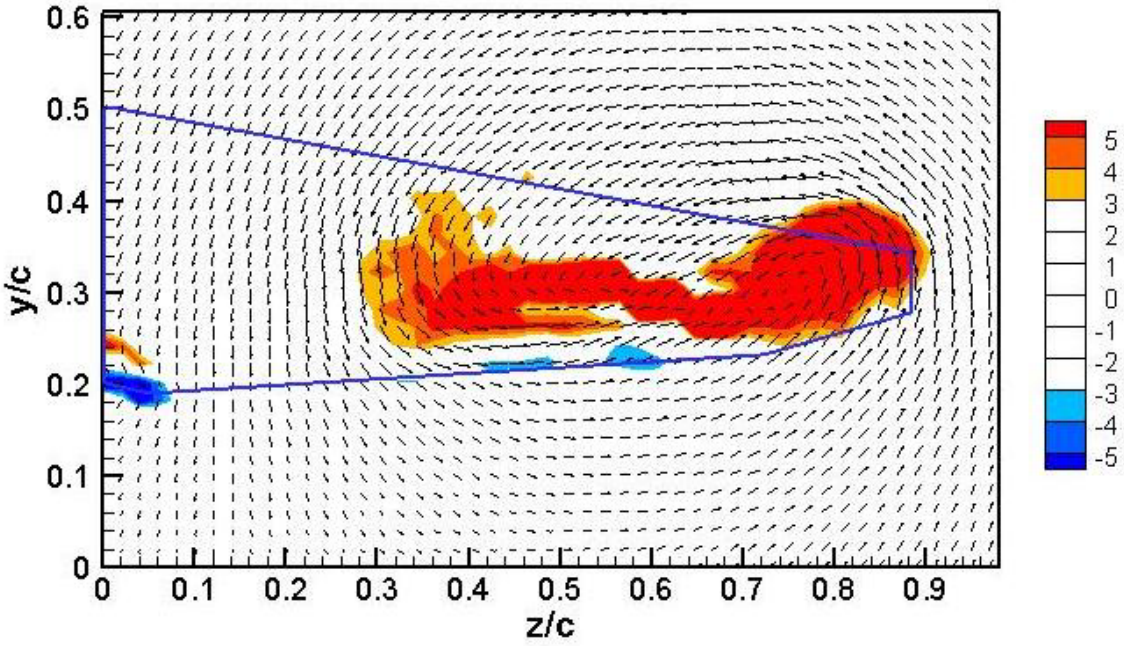

Figure 3-20: Vorticity contours for α=13°

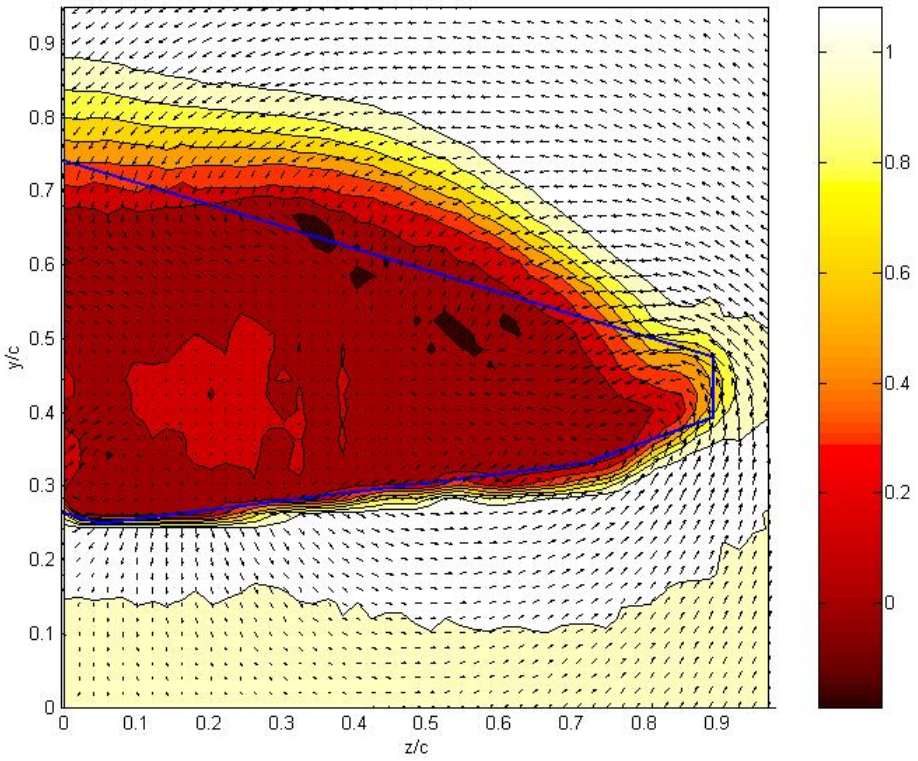

Figure 3-21: Axial velocity contours for α=21°

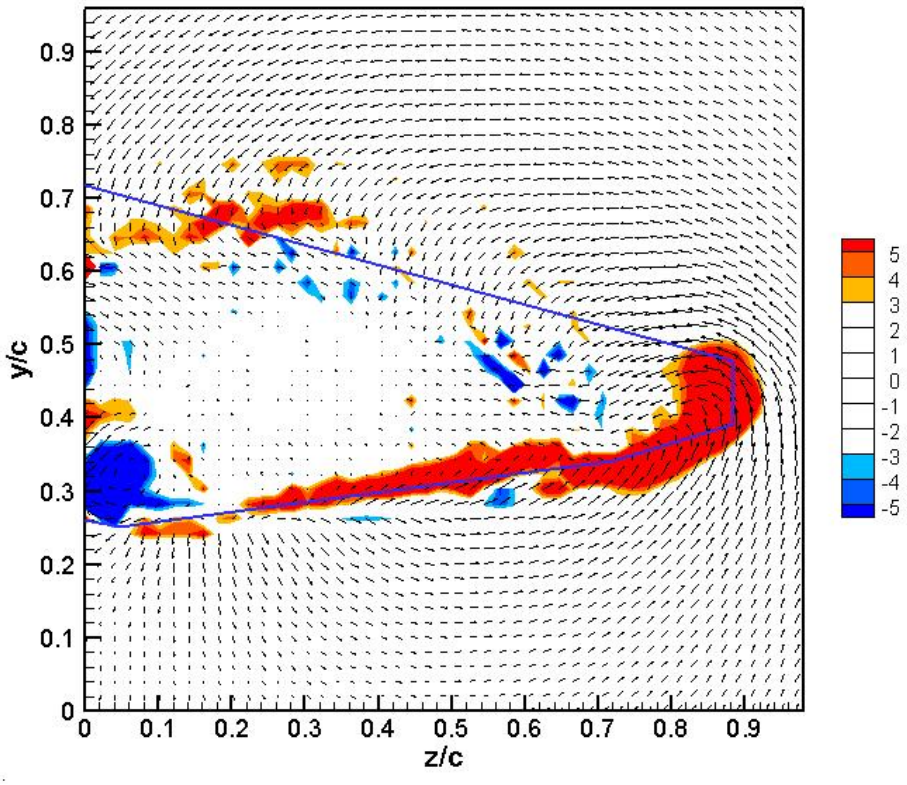

Figure 3-22: Vorticity contours for α=21°

3.4 Conclusions

There are two distinct modes of stall for wings with low sweep. The delta wing mode, whereby leading edge vortices break down but remain more or less in the same position over the wing and 2-D stall whereby vortices form, grow and then detach and shed in the wake. Both modes are possible over a planform with a 40° sweep, but our research indicates that the flow develops in the form of 2-D stall. We presented evidence that in the inboard part of the wing, an attached vortex can be sustained, reminiscent of delta-wing type of a tip vortex, but further in the outboard region 2-D stall dominates. The flow is unsteady and vortices are shed periodically. We anticipate and already generated preliminary evidence (not shown here) that unsteady blowing right at the leading edge of a sharp wing can reduce the size of the separated flow over the pressure side of a wing in 2-D mode of stall. This is the most effective means of increasing lift in the average, even if the flow remains fully separated. We also have evidence that our control method can actually dictate the character of the flow, and force wing section that sustains a delta wing vortex to stall in the 2-D mode.

3.5 References

8. Miau, J. J., Kuo, K. T., Liu, W. H., Hsieh, S. J., Chou, J. H., and Lin, C. K., "Flow Developments Above 50-Deg Sweep Delta Wings with Different Leading-Edge Profiles," *Journal of Aircraft*, Vol. 32, No. 4, July-August 1995, pp. 787-794.
9. Ol, M. V. and Gharib, M., "Leading-Edge Vortex Structure of Nonslender Delta Wings at Low Reynolds Number," *AIAA Journal*, Vol. 41, No. 1, January 2003, pp. 16-26.
10. Gursul, I., Taylor, G., and Wooding, C., "Vortex Flows over Fixed-Wing Micro Air Vehicles," *40th AIAA Aerospace Sciences Meeting & Exhibit*, Paper No. 2002-0698, AIAA, January 2003.
11. Taylor, G. S., Schnorbus, T., and Gursul, I., "An Investigation of Vortex Flows over Low Sweep Delta Wings," *AIAA Fluid Dynamics Conference*, Paper No. AIAA-2003-4021, Orlando, FL, June 23-26, 2003.
12. Gordnier, R. E. and Visbal, M. R., "Higher-Order Compact Difference Scheme Applied to the Simulation of a Low Sweep Delta Wing Flow," *41st AIAA*

Aerospace Sciences Meeting and Exhibit, Paper No. AIAA-2003-0620, AIAA, Reno, NV, January 6-9, 2003.

13. Yaniktepe, B. and Rockwell, D., "Flow Structure on a Delta Wing of Low Sweep Angle," *AIAA Journal*, Vol. 42, pp. 513-523.
14. Rullan, J., Vlachos, P. P., Telionis, D. P. and Zeiger, M. D., "Flow Control of Unswept and Swept, Sharp-Edged Wings via Unsteady Blowing," *42nd Aerospace Sciences Meeting*, Paper No. AIAA-2004-0226, January 2004.
15. Miranda, S., Vlachos, P. P., Telionis, D. P. and Zeiger, M. P., "Flow Control of a Sharp-Edged Airfoil," Paper No. AIAA-2001-0119, 2001, also *AIAA Journal*, 2005 (in press).
16. Guy, Yair, Morrow, Julie, A., McLaughlin, Thomas, E., "Velocity Measurements on a Delta Wing with Periodic Blowing and Suction," *38th Aerospace Sciences Meeting and Exhibit*, Paper No. AIAA-2000-0550, Reno, NV, January 10-13, 2000.
17. Guy, Y., Morton, S. A. and Morrow, J. A., "Numerical Investigation of the Flow Field on a Delta Wing with Periodic Blowing and Suction," *AIAA Fluids 2000*, Paper No. AIAA-2000-2321, Denver, CO, June 19-22, 2000.
18. Folk, C., and Ho, C.-M., "Micro-Actuators for Control of Delta Wing with Sharp Leading Edge," Paper No. AIAA-2001-0121.
19. Washburn, A. E., and Amitay, M., "Active Flow Control on the Stingray UAV: Physical Mechanisms," *42nd Aerospace Sciences Meeting & Exhibit*," Paper No. AIAA-2004-0745, Reno, NV, January 5-8 2004.
20. Westerweel, J., *Digital Particle Image Velocimetry, Theory and Application*, Delft University Press, 1993.
21. Westerweel, J., *Optical Diagnostics in Fluid and Thermal Flow*, SPIE 2005, pp. 624-635.
22. Vlachos, P. P., Donnelly, M. J. and Telionis, D. P., "On the Wake of a Circular Cylinder Piercing a Water Free Surface," *Proceedings of FEDS'98*, FEDS98-5177, 1998 ASME Fluids Engineering Division Summer Meeting.

23. Vlachos, P. P. and Telionis, D. P., "Turbulence Characteristics in the Wake of a Circular Cylinder Near the Free Surface," FEDSM2000-11320, Boston, MA, 2000.
24. Klute, S. M., Vlachos, P. P. and Telionis, D. P., "High-Speed DPIV Study of Vortex Breakdown," *Fluid Dynamics Symposium, Fluids 2000 Conference*, also *AIAA Journal* (in press).
25. Asimopoulos, N., Vlachos, P. P., Telionis, D. P., "A High Speed, High Particle Density Particle Tracking Method for Turbulent Flows," ASME FEDSM'99-7139.

4. Flow Control over Diamond-Shaped-Planform Wings with Sharp Edges. Velocity and Vorticity Fields

Wings swept by 30 to 40 degrees are today very common in fighter aircraft. And yet, there is very little work devoted to the understanding of the aerodynamics of such wings. The problem is that such wings may be able to sustain attached flow behind broken down delta wing vortices, or stall like two-dimensional wings while shedding vortices with generators parallel to their leading edge. In this chapter, we explore the effectiveness of leading-edge control of the flow over such wings. Our results indicate that two-D-like vortices are periodically generated and shed. At the same time, an underline feature of the flow, a leading edge vortex is periodically activated, penetrating the separated flow, eventually emerging downstream of the trailing edge of the wing.

Nomenclature

U_∞ = Characteristic velocity (free stream)
b=semis-span
c = root chord
C_μ = momentum coefficient
T= period of pulsing jet
x,y,z = coordinate system (see Figure 3)
α= Angle of attack

4.1 Introduction

In previous chapters we discussed the flow over a diamond-shaped wing planform at low and moderate angles of attack. We presented velocity fields and pressure distributions for steady flows at different Reynolds numbers. In this chapter we explore the effect of flow control over the same wing planform. Some of the introductory comments included in previous chapters are cited here again for completeness

The work described here is focused on wings with moderate sweep angles. At very low sweep angles, namely angles less than 20°, the flow over sharp-edged wings stalls like the flow over an unswept wing. Vortices are shed with their axis nearly normal to the free stream. Such vortices are often called “rollers”. At high sweep angles, that is, larger than 50°, the flow is similar to delta wing flows that are dominated by leading edge

vortices (LEV). We will refer to these vortices here as "streamers". These wings stall due to vortex breakdown.

The effects of sweeping a wing at moderate angles, namely 30° to 40°, and moderate to high angles of attack are very little understood. And yet, such wings are today the norm for most fighter aircrafts. The challenge is that in this range of parameters, the flow may stall like the flow over an unswept wing, shedding large vortices in an unsteady fashion, or it could stall like a delta wing, sustaining a leading-edge vortex (LEV) that breaks down. The significant difference between the two modes is that delta wing vortices, or streamers, are attached to the leading edge of the wing and shed vorticity by directing it in the core of the vortex and then telescoping it downstream, whereas rollers, grow and then shed by rolling over the wing and detaching from its surface. This is essentially the phenomenon of unsteady stall.

Research on delta-wing flows for sweep angles as low as 50° indicate that delta wing vortices are present, but break down very close to the leading edge[1-5]. In fact even before break down, these vortices display a wake-like flow character, where the velocity is very low in the core of the vortex. In some cases[2] it was found that the low-aspect- ratio wing at medium angles of attack does not behave like a delta wing but rather like an unswept wing. A sweep angle of 50° is not low enough to demonstrate the transition from the vortex breakdown stall to the two-dimensional unsteady stall. More recently, Yaniktepe and Rockwell[6] studied the flow over a wing with a sweep angle of 38.7°. They provided evidence that up to an angle of attack, α, of 25°, the flow appears to be dominated by delta wing tip vortices. At the highest angle of attack, the vortices seem to be displaced inboard.

In both the studies of Ol and Gharib[2] and Yaniktepe and Rockwell[6], the flow field was interrogated along planes normal to the free steam. In our studies we cut the fields with planes that are both normal and parallel to the free stream. We are interested in the possibility that the control mechanisms could actually dictate the desired stall mechanism.

Impressive advancements have been made in controlling the flow over wings with rounded leading edges, but very little work has been devoted to the control of the flow over sharp-edged wings. The present authors[7,8] have demonstrated that flows over sharp

edges can be effectively controlled with lift increases as high as 70%. Control of delta wing flows has been successful but the efforts were focused so far on relatively high sweep angles[9-11]. The objective of this project is to capitalize on our experience and extend the work to moderately swept wings and wings with practical planforms.

The majority of contributions on airfoil flow control are based on separation control. Their aim is to delay separation and stall altogether. There is another area of airfoil and wing flow control, which so far has received little attention, but which has greater potential in defense applications. This is the management and control of separated flow. Such flows are encountered over sharp-edged wings at low to moderate angles of attack or over wings in deep stall. The idea is to accept the fact that in some situations, the flow is fully separated, and periodic shedding of vortices is established. The aim then becomes to control the dynamic development of vortical structures in order to improve the performance of the lifting surface. These are the type of flows that develop over moderately swept wings. This is the focus of the present research.

We discuss in this chapter the results of experiments conducted in a water tunnel with a diamond-shaped-planform wing model typical of wings used in aeronautical industry. The model was tested[1] at a Reynolds numbers of Re=30,000. We employ Digital Particle Image Velocimetry (DPIV) along planes parallel and perpendicular to the stream. We report results obtained with a high-speed digital camera that provides instantaneous data.

4.2 Facilities, Models and Equipment

4.2.1 Facilities and Models

Experiments were carried out in the Engineering Science and Mechanics (ESM) water tunnel. This tunnel was built by Engineering Laboratory Design (ELD) and operates in closed loop in a vertical plane with up to 2,500 gallons of water. The settling chamber leads to the 24" x 24" x 72" Plexiglas test section via a three-way convergence. A 4500-gpm pump driven by a 20-hp motor provides flow which can attain a maximum speed of 1 m/s, corresponding to a maximum Reynolds number per unit length of 9900/cm. The free stream turbulence level in the test section is less than 2%.

The model for this experimental investigation has a diamond-shaped-planform wing shown in Figure 4-1. In this Figure the dimensions, in inches, correspond to a small model designed for testing in the water tunnel. This model is equipped with an internal

compartment that can generate a pulsing jet in the leading edge for flow control. It is geometrically similar to a stainless-steel model provided by Lockheed Martin, which we have tested earlier[1].

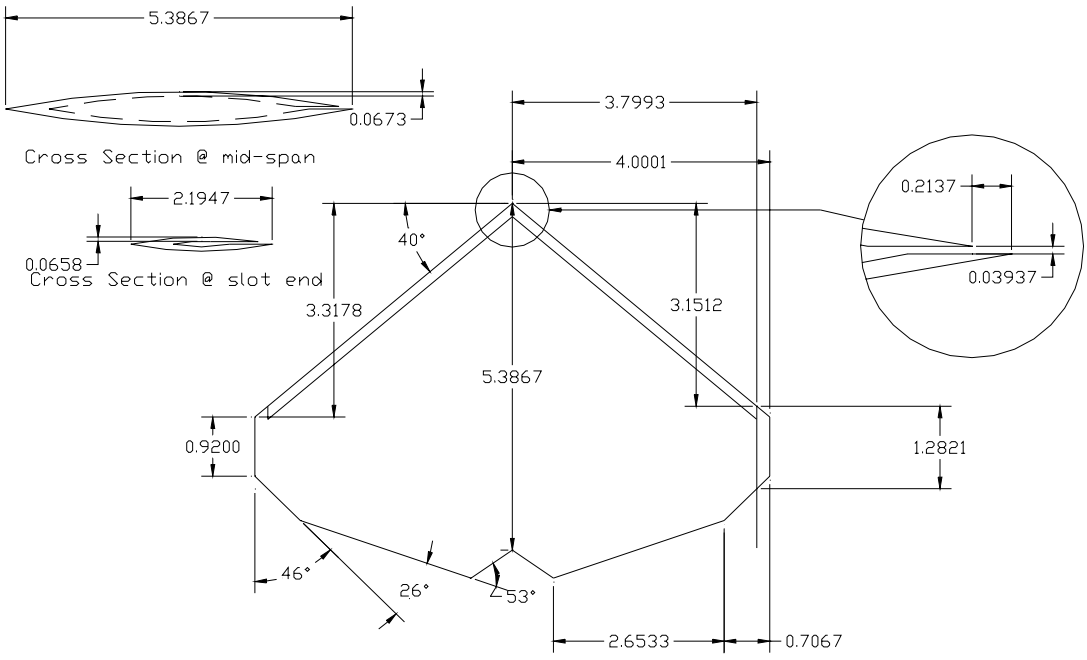

Figure 4-1: Engineering drawing of the diamond-shaped planform model for water tunnel testing.

4.2.2 Particle Image Velocimetry

Particle-Image Velocimetry (PIV) is a powerful tool that we employed in this project. The most common implementation of the method, (currently commercially available) focuses on a single-exposure double-frame digital cross correlation approach. A high-resolution (1Kx1K pixels) CCD camera that can sample up to 30 fps, results in a sampling frequency of the flow field of only 15Hz, is usually synchronized with a Nd:YAG pulsing laser that illuminates the interrogation area. The velocity field is traditionally treated as a linear transfer function that corresponds to a flow pattern displacement between two consecutive images. This transfer function is revealed in a statistical manner, incorporating second order statistical moments of the image patterns (Westerweel[13, 14]).

A major disadvantage of this approach is the inability to provide sufficient frequency resolution, which is necessary, in order to investigate any high-frequency phenomena that

occur in turbulent, separated flows. A system developed at VA Tech has overcome the difficulty of low sampling frequency. This was accomplished with the integration of a high-power (50 W) pulsing laser, with special type of optics and a unique CMOS camera, capable of acquiring up to 2000 frames per sec (fps), resulting to a DPIV system with 1 KHz maximum sampling frequency[15]. Our ongoing research to integrate this technology with our existing PIV system demonstrated very high sensitivity, equivalent to 1000 ASA, and signal-to-noise ratio in the order to 100,000:1. The great advantage of this new technology is that each pixel is treated as an individual sensor and any cross-coupled interaction between neighborhood pixels is eliminated. The conditioning of the signal is performed on the sensor. Thus, the spatial and temporal resolution of our PIV system is increased by almost an order of magnitude in comparison with our previous configuration, and two orders of magnitude compared with systems that are commercially available.

Members of our group were able to perform dual-frame, cross-correlation, time-resolved DPIV by employing single and multiple exposures. The first example of single-exposure double frame cross-correlation, time-resolved DPIV was presented by Vlachos et al.[15]. However this implementation was limited to very-low-speed liquid flows (U~10 cm/s). In a different approach, we performed multiple exposures per frame and we evaluated the vectors using standard cross-correlation. This approach was employed in the analysis of the characteristics of turbulent shear layers by Vlachos et al.[16] and in the investigation of the post-vortex-breakdown region characteristics of delta wings by Klute et al.17.

One major drawback of conventional DPIV systems results from limitations inherited from the velocity evaluation methods. Our group recently launched an effort to integrate and combine some of the most effective and well established of these proposed methods18. The outcome is a dynamically-adaptive hybrid algorithm for the evaluation of the velocity vectors that overcomes these limitations to a great extent, thus increasing accuracy and space resolution. The overall performance of the method, if quantified, yields space resolution in the order of 0.5 mm average, time resolution in the order of 1 milisecond, with sampling time up to 4 seconds and uncertainty of the velocity measurement in the order of 0.1% of the reference velocity.

Table 4-1: Laser Cut Locations

planes	Z/C	Z/b
1	0.068	0.092
2	0.156	0.209
3	0.249	0.334
4	0.340	0.456
5	0.417	0.559
6	0.467	0.626
7	0.531	0.711
8	0.581	0.778
9	0.644	0.863
10	0.694	0.930
planes	X/C	
A	0.28	
B	0.513	
C	0.746	
D	1.086	

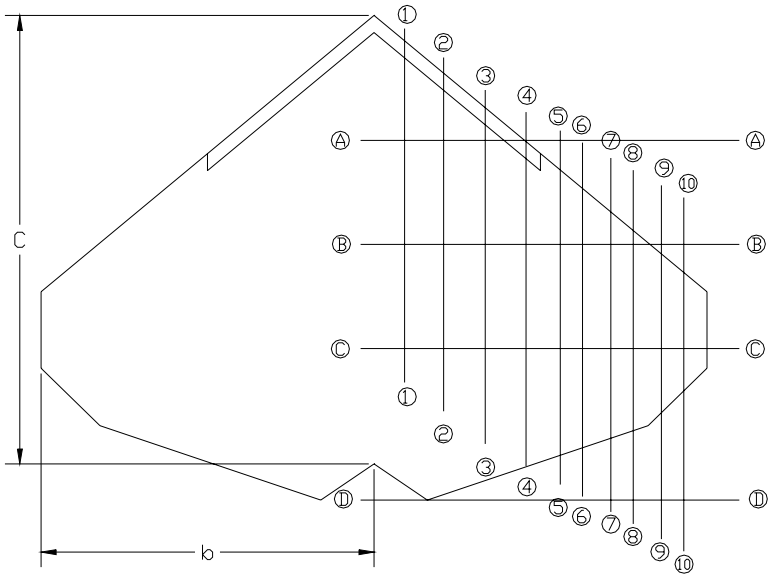

Figure 4-2: Laser cuts for the water tunnel flow visualization and PIV.

The advancements in DPIV are employed in the global characterization of the separated flow over the sharp airfoil, providing insight on the interaction of the shear layers with the incident free stream and their roll-up to coherent vortices. These data are used to analyze the flow control mechanism, providing information about the interaction of the various frequency modes in the flow field and the route to the formation of

coherent structures in the separated flow region. Data were obtained along laser cuts as shown in Figure 2. The coordinate system is shown in Figure 3. The laser cuts were along planes parallel to the yz plane, like plane EFGH in Figure 3 and parallel to the xy plane, like plane ABCD in Figure 3. Cuts 1 through 10 are parallel to the free stream, while cuts A, B, C and D are normal to the free stream. The locations of these planes are shown in Table 1.

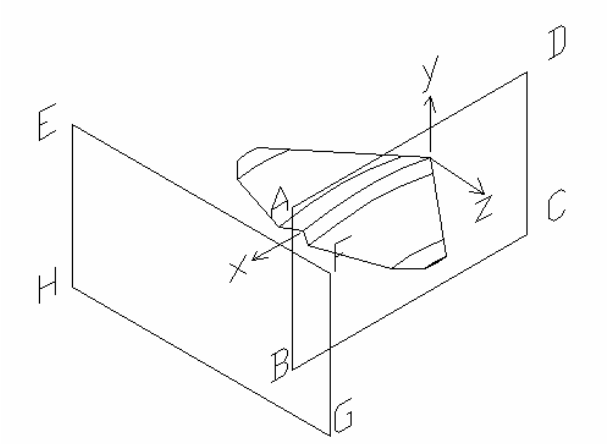

Figure 4-3: Schematic of planes of data acquisition.

4.2.3 Flow Control Mechanism

Pulsing jets were activated using two pumps connected to the wing cavity. The jet issues from a slot spanning only 50% of the leading edge, starting at the root of the wing. This control mechanism therefore activates only the inboard potion of the wing. The jet was activated at the natural shedding frequency that corresponds to the angle of attack of 13° and a free-stream velocity of 50 cm/sec, namely 1.71 Hz. This was calculated in terms of a Strouhal number which was measured earlier for this configuration. The corresponding period was therefore T=0.585 sec. The operation of the pumps was monitored with a flow meter. A specific point on the periodic signal of the flow meter was arbitrarily chosen as the origin of time. All instantaneous frames are labeled with time measured from the common origin. We obtained data at a rate of 1,000 frames per second and recorded 2700 frames for each plane. In this way, each sequence of instantaneous frames includes more than one period of the actuation disturbance. With interrogation windows of 64 x 32 pixels, we obtained vectors along grids with sizes of 93 x 61 to 93 x 77. Each instantaneous frame therefore contains over 5900 velocity vectors.

4.3 Results and Discussion

Time-Resolved DPIV data were processed using an in-house developed multi-grid iterative DPIV, with second-order, Discrete Window Offset (DWO). Time-resolved DPIV systems are limited by the fact that the time separation between consecutive frames is the reciprocal of the frame rate, thus on the order of milliseconds. This value is relatively large compared with microsecond time intervals employed by conventional DPIV systems. By employing a second-order DWO, we provide an improved predictor for the particle pattern matching between subsequent iterations. Moreover, the algorithm employed performs a localized cross-correlation, which, when compared to standard multi-grid schemes for resolving strong vortical flows was proven to be superior.

For both flow visualizations and PIV measurements, we cut the field by laser sheets parallel and perpendicular to the free stream as shown schematically in Figure 4-2 and Figure 4-3. All the data presented here were obtained with the wing at an angle of attack of 13°. Flow visualization on a Trefftz plane, namely plane EFGH indicates results very similar to those of Yaniktepe and Rockwell[6], which imply that the flow develops leading edge vortices. We found that such visualizations could be deceiving. For the same configuration, cutting the flow by a plane parallel to the free stream essentially passes a section through a LEV. Leading edge vortices have a nearly circular cross-section if they are cut normal to their axis. But if cut by a plane inclined with respect to their axis, they should show vorticity of the same sign along a closed and nearly elliptical contour. Moreover, the velocity component along the axis of a LEV should be jet-like. The PIV data along planes parallel to the free-stream flow direction are void of such characteristics. Instead they indicate vorticity only on the upper side, which is compatible with two-dimensional stall. The axial velocity distribution indicates wake-like behavior, which confirms the fact that we have two-dimensional stall.

In Figure 4-4, we present a preview of the phenomena we will discuss in this chapter. In this figure we display all the velocity vectors available in each frame in order to demonstrate the fine experimental grid of our data. But in the following figures we display only a very small portion of the actual number of data, to avoid cluttering the images. The three frames in this Figure present instantaneous data along Plane D-no-control, Plane D-with-control and Plane 5 with control. Quantities like vorticity have

been calculated using all data along the full grid. In this and all the following figures vorticity is displayed in the form of contours. The top frame in Figure 4-4 indicates the presence of a typical wing-tip vortex. Since there is very little vorticity near the center of the vortex, the core of the vortex must be broken down. This should be expected for a wing with low sweep angle and a moderate angle of attack, and has been reported earlier by Yaniktepe and Rockwell[6]. These authors experimented with a delta wing swept with almost the same angle as ours. The basic difference between the two models is that ours is cropped. In the second frame of Figure 5 we present one of the instantaneous frames for flow control. As we will discuss later, a second axial vortex, a streamer, develops upstream and penetrates all the way to Plane D. We chose one of the instantaneous frames that most clearly indicates the presence of this vortex. Finally, in the last frame of this Figure we present instantaneous data along Plane 5 when control is activated. Here we observe a stall vortex in the process of being swept downstream over the wing.

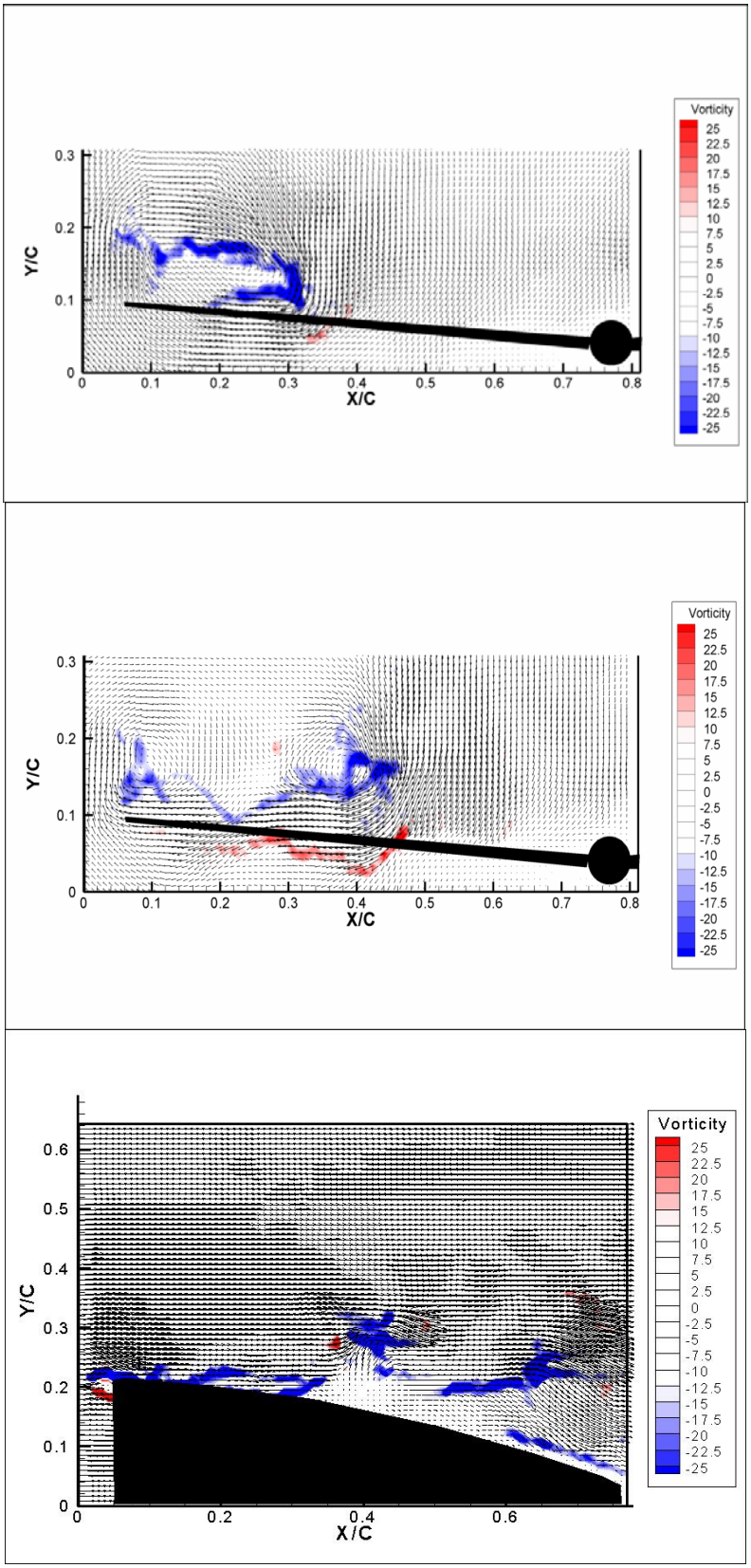

Figure 4-4: Velocity vectors and vorticity contours for top, Plane D –no control, middle, Plane D-control and bottom, Plane 5-control.

The next figures are instantaneous data along xy planes. Figure 4-5a-d correspond to Plane 2, Figure 4-6a-d to Plane 3 and Figure 4-7a-b to Plane 4, and each of the eight frames per plane correspond to one of eight equally spaced instances within one period. With the activation of the leading edge, a recirculation region is initiated at T=3T/8 almost simultaneously in Plane 2 and 3. And in subsequent times, the disturbance grows and displaces downstream. The vorticity associated with this vortex-like structure is mostly found along its periphery, the area where one would expect to find shear layers. This phenomenon therefore could be classified as a two-D stall vortex. But as we will see later, the other vorticity component, that is vorticity normal to Planes 2, 3 and 4, is actually larger. So this is a truly three-dimensional phenomenon.

In Figures 4-8a-d we present instantaneous data on Plane A, which cross the wing planform very close to the edge of the jet slot. When comparing Planes A and 3 we now see that the disturbance that so far appeared as a roller, resembling two-dimensional stall is actually the generation of an axial vortex. At first, the vortex appears as a tip vortex, or a delta wing vortex. But as it evolves, it moves in the inboard direction. We will later find that it moves a little further towards the wingtip direction from the current location of $Z/C \cong 0.25$, but remains in the inboard area over the wing.

Plane C and Plane 8 are shown in Figures 4-9a-d and 4-10a-d. Here Planes C and 8, like Plans A and 3, correspond to instantaneous data along two mutually perpendicular planes but being further outboard. We observe a sequence of very similar events. Yet it should be recalled that only the first half of the wing is activated. But the actuation is enough to trigger a roll up of vorticity that has moved to $Z/C \cong 0.5$. This time the vortex coexists with a weak tip vortex that can be seen at the end of the wing at $Z/C \cong 0.75$. Both these vortices penetrate the separated flow that dominates the entire suction surface of the wing and periodically reach Plane D, which is placed downstream of the trailing edge, as shown in Figure 4-11a-d. Comparing these frames with those of Figure 5a, where control has not been activated, we observe that the recirculation is more compact and forms closer to the wingtip.

Vorticity generated along the leading edge of a swept wing turns in the streamwise direction at the tip of a wing and forms the tip vortex. The results presented here indicate that when activated, the leading edge vortex may turn in the streamwise direction in the

midspan. To confirm this fact we calculated the overall circulation on planes parallel and perpendicular to the free stream, namely Planes 1 through 10 and Planes A through D. These circulations capture the instantaneous values of the vorticity flux through these planes. In Figure 4-12 and Figure 4-13 we plot the temporal variations of circulation along Planes A and B. These planes cut the leading edge ahead of the cropped tip, and therefore the tip vortex is left out of the integration. We observe in these figures that actuation gives rise to periodic increases of circulation, and that the magnitude increases with the flow control momentum coefficient. We next plot in Figure 4-14 and Figure 4-15 the circulation along Planes 4 and 5. In Plane 4 which is near the tip of the actuation slot, the effect of the pulsed jet generates some increases of circulation, and this is in magnitude close to the increases measured along Planes A and B. Apparently this vorticity is turned in the streamwise direction somewhere between Planes 4 and 5. Indeed, in Figure 4-15, which corresponds to Plane 5, we see that for C_μ=0.01 and 0.02, circulation decreases periodically. This implies that vorticity aligned with the leading edge in steady flow penetrated Plane 5 on its way to the tip of the wing. But with actuation, this vorticity is turned inboard of this Plane and thus circulation in this Plane decreases.

4.4 Conclusions

There are two distinct modes of stall for wings with low sweep. The delta wing mode, whereby leading edge vortices break down but remain more or less in the same position over the wing and 2-D stall whereby vortices form, grow and then detach and shed in the wake. Both modes are possible over a planform with a 40^0 sweep, but our research indicates that the flow develops in the form of 2-D stall. This is consistent with the findings of Yaniktepe and Rockwell[6] who present data in a plane similarly situated to our Plane D. They observe a broad area of cross-flow recirculation that contains weak and unorganized vorticity. For no-control flow, we presented evidence that in the inboard part of the wing, an attached vortex can be sustained, reminiscent of delta-wing type of a tip vortex, but further in the outboard region 2-D stall dominates. The flow is unsteady and vortices are shed periodically. The flow visualizations of Yaniktepe and Rockwell[6] and ours indicate that the leading edge vortex has the tendency to move inboard, but looses its coherence in the dead-air region of two-dimensional flow wake. We now present

experimental evidence that leading edge activation with a C_μ=0.02 activates this vortex, which periodically penetrates the separated region and reaches beyond the trailing edge of the wing. The leading edge vortex is periodically turned in the streamwise direction in the midspan of the wing. This finding is consistent with the results we presented in Ref. 1, which indicate that the pressure periodically drops in this region, resulting in increases of the lift in the average. Actuation on the inboard half of the leading edge has a strong effect on the outboard region as well. We find that the flow is much better organized, void of weak vortices that roll downstream. Instead the tip vortex is strengthened periodically. This must also contribute to the increase of lift in the average.

4.5 Acknowledgments

This work was supported by the Air Force Office of Scientific Research, under Grant No FA9550-04-1-0144, LtCol Rhett W Jefferies, monitor. Dr. Carl Tillman is our point of contact at Air Force Research Labs. We appreciate their interest in our work and their support.

4.6 References

1. Rullan, J.G., Vlachos, P.P. and Telionis, D.P., "The Aerodynamics of Low-Sweep Diamond-shaped Wings" presented at the 43rd Aerospace Sciences Meeting and Exhibit, 10-13 January 2005, Reno, Nevada, Paper No AIAA-2005-0059.
2. Ol, M. V. and Gharib, M., "Leading-Edge Vortex Structure of Nonslender Delta Wings at Low Reynolds Number," *AIAA Journal*, Vol. 41, No. 1, January 2003, pp. 16-26.
3. Gursul, I., Taylor, G., and Wooding, C., "Vortex Flows over Fixed-Wing Micro Air Vehicles," *40th AIAA Aerospace Sciences Meeting & Exhibit*, Paper No. 2002-0698, AIAA, January 2003.
4. Taylor, G. S., Schnorbus, T., and Gursul, I., "An Investigation of Vortex Flows over Low Sweep Delta Wings," *AIAA Fluid Dynamics Conference*, Paper No. AIAA-2003-4021, Orlando, FL, June 23-26, 2003.
5. Gordnier, R. E. and Visbal, M. R., "Higher-Order Compact Difference Scheme Applied to the Simulation of a Low Sweep Delta Wing Flow," *41st AIAA*

Aerospace Sciences Meeting and Exhibit, Paper No. AIAA-2003-0620, AIAA, Reno, NV, January 6-9, 2003.

6. Yaniktepe, B. and Rockwell, D., "Flow Structure on a Delta Wing of Low Sweep Angle," *AIAA Journal*, Vol. 42, pp. 513-523.
7. Rullan, J., Vlachos, P. P., Telionis, D. P. and Zeiger, M. D., "Flow Control of Unswept and Swept, Sharp-Edged Wings via Unsteady Blowing," *42nd Aerospace Sciences Meeting*, Paper No. AIAA-2004-0226, January 2004.
8. Miranda, S., Vlachos, P. P., Telionis, D. P. and Zeiger, M. P., "Flow Control of a Sharp-Edged Airfoil," Paper No. AIAA-2001-0119, 2001, also *AIAA Journal*, vol. 43, pp 716-726, 2005.
9. Guy, Yair, Morrow, Julie, A., McLaughlin, Thomas, E., "Velocity Measurements on a Delta Wing with Periodic Blowing and Suction," *38th Aerospace Sciences Meeting and Exhibit*, Paper No. AIAA-2000-0550, Reno, NV, January 10-13, 2000.
10. Guy, Y., Morton, S. A. and Morrow, J. A., "Numerical Investigation of the Flow Field on a Delta Wing with Periodic Blowing and Suction," *AIAA Fluids 2000*, Paper No. AIAA-2000-2321, Denver, CO, June 19-22, 2000.
11. Folk, C., and Ho, C.-M., "Micro-Actuators for Control of Delta Wing with Sharp Leading Edge," Paper No. AIAA-2001-0121.
12. Washburn, A. E., and Amitay, M., "Active Flow Control on the Stingray UAV: Physical Mechanisms," *42nd Aerospace Sciences Meeting & Exhibit*," Paper No. AIAA-2004-0745, Reno, NV, January 5-8 2004.
13. Westerweel, J., *Digital Particle Image Velocimetry, Theory and Application*, Delft University Press, 1993.
14. Westerweel, J., *Optical Diagnostics in Fluid and Thermal Flow*, SPIE 2005, pp. 624-635.
15. Vlachos, P. P., Donnelly, M. J. and Telionis, D. P., "On the Wake of a Circular Cylinder Piercing a Water Free Surface," *Proceedings of FEDS'98*, FEDS98-5177, 1998 ASME Fluids Engineering Division Summer Meeting.

16. Vlachos, P. P. and Telionis, D. P., "Turbulence Characteristics in the Wake of a Circular Cylinder Near the Free Surface," FEDSM2000-11320, Boston, MA, 2000.
17. Klute, S. M., Vlachos, P. P. and Telionis, D. P., "High-Speed DPIV Study of Vortex Breakdown," *Fluid Dynamics Symposium, Fluids 2000 Conference*, also *AIAA Journal* (in press).
18. Asimopoulos, N., Vlachos, P. P., Telionis, D. P., "A High Speed, High Particle Density Particle Tracking Method for Turbulent Flows," ASME FEDSM'99-7139.

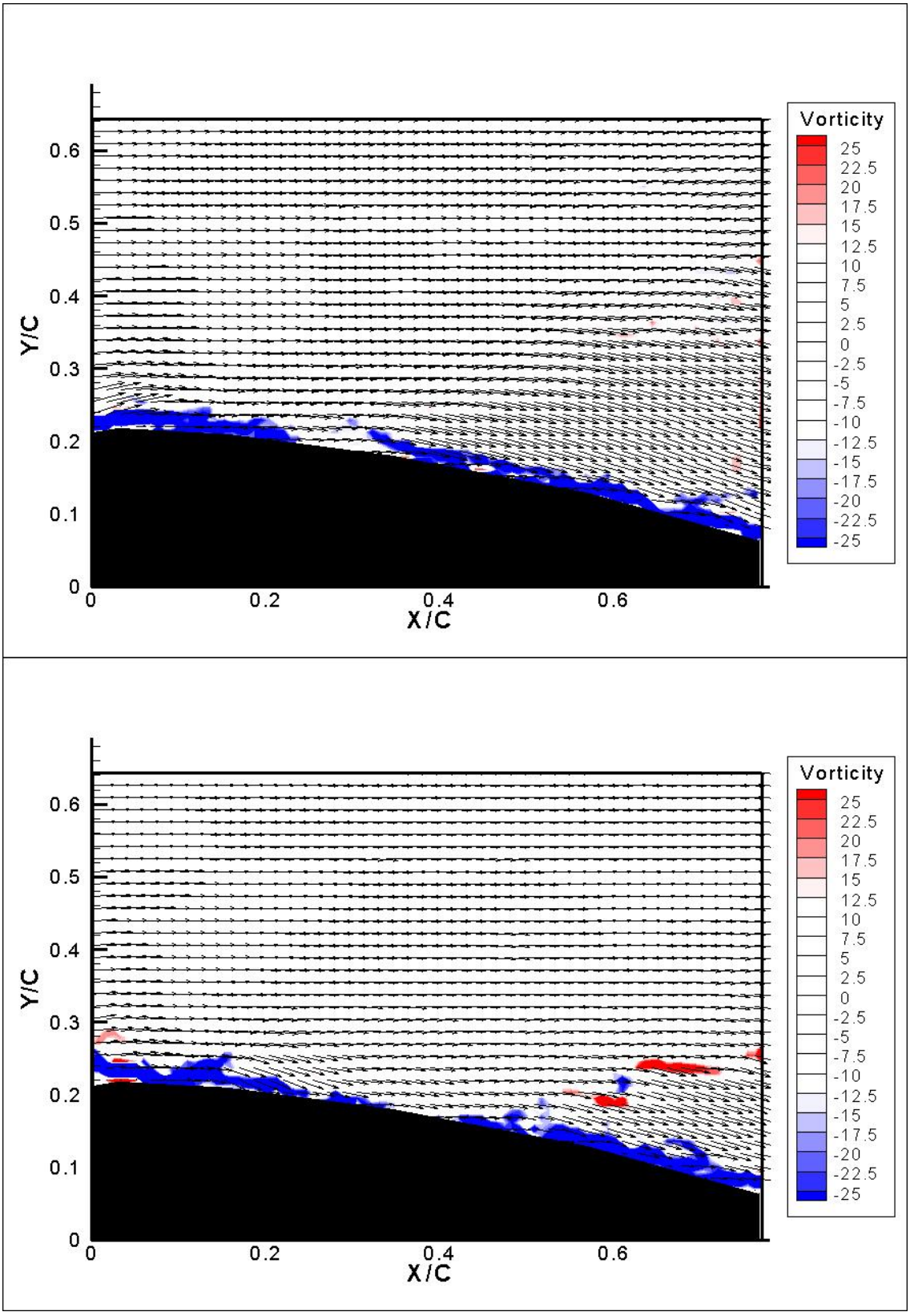

Figure 4-5a: Plane 2 with control at t=0 & t=1/8T.

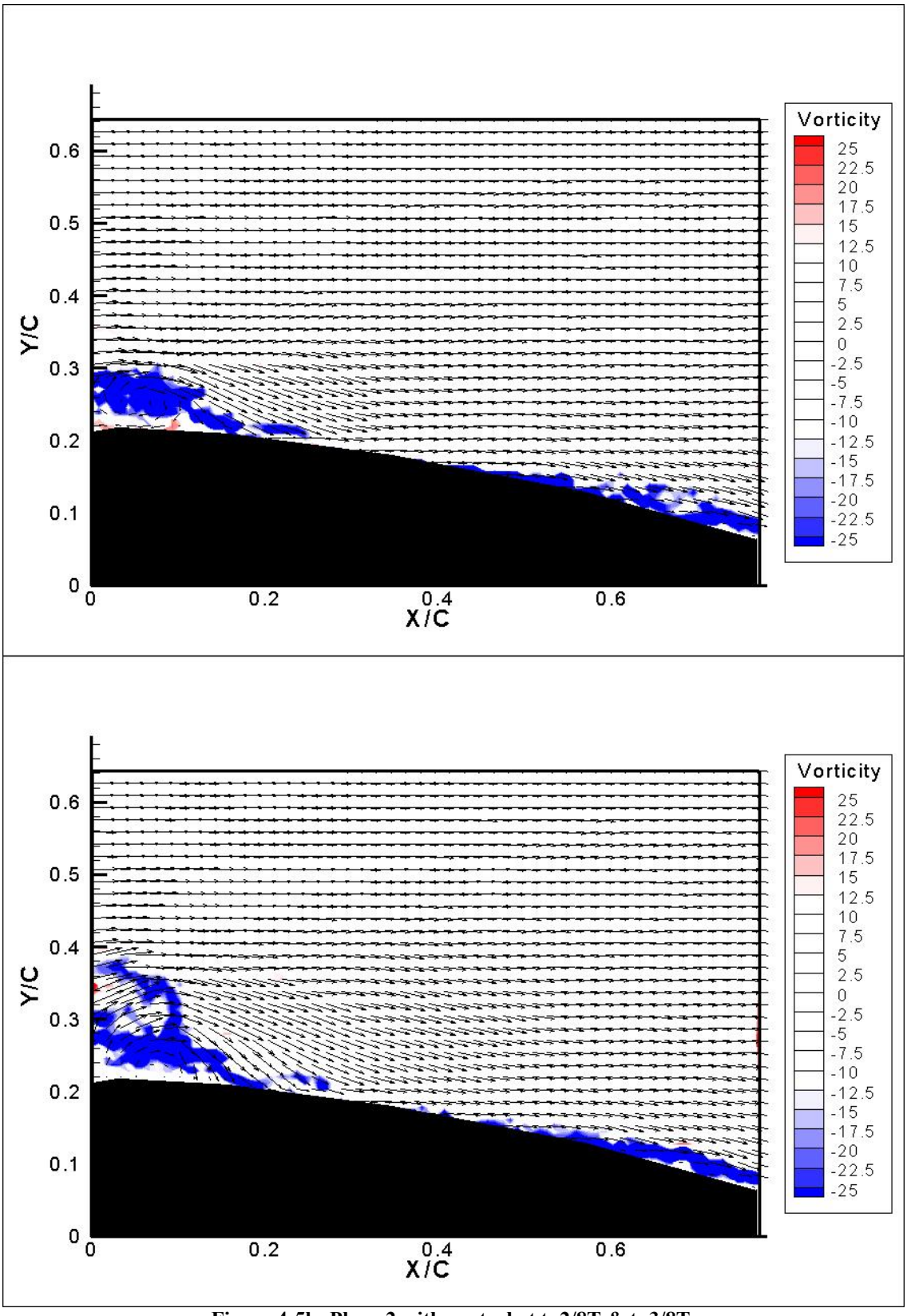

Figure 4-5b: Plane 2 with control at t=2/8T & t=3/8T.

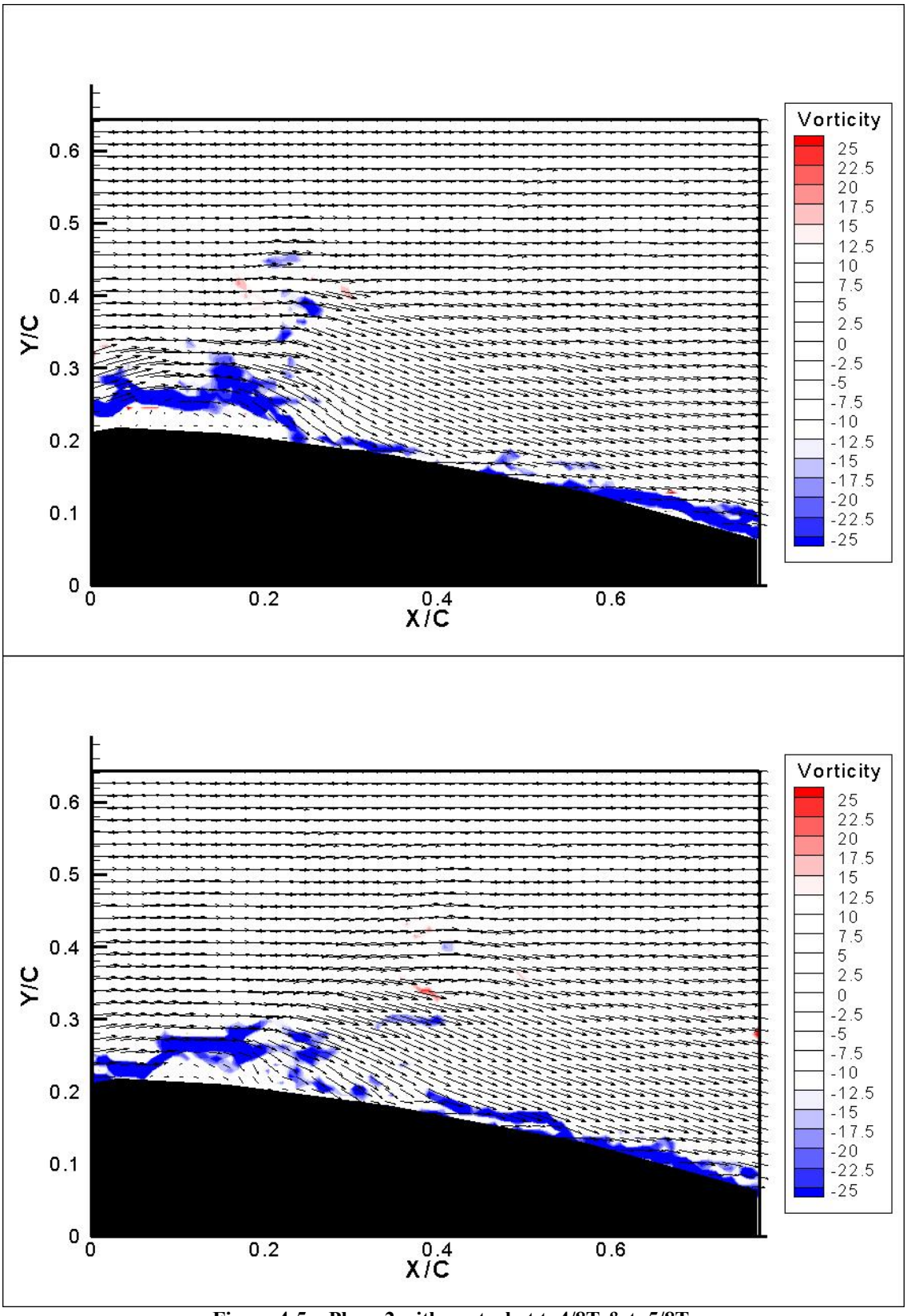

Figure 4-5c: Plane 2 with control at t=4/8T & t=5/8T.

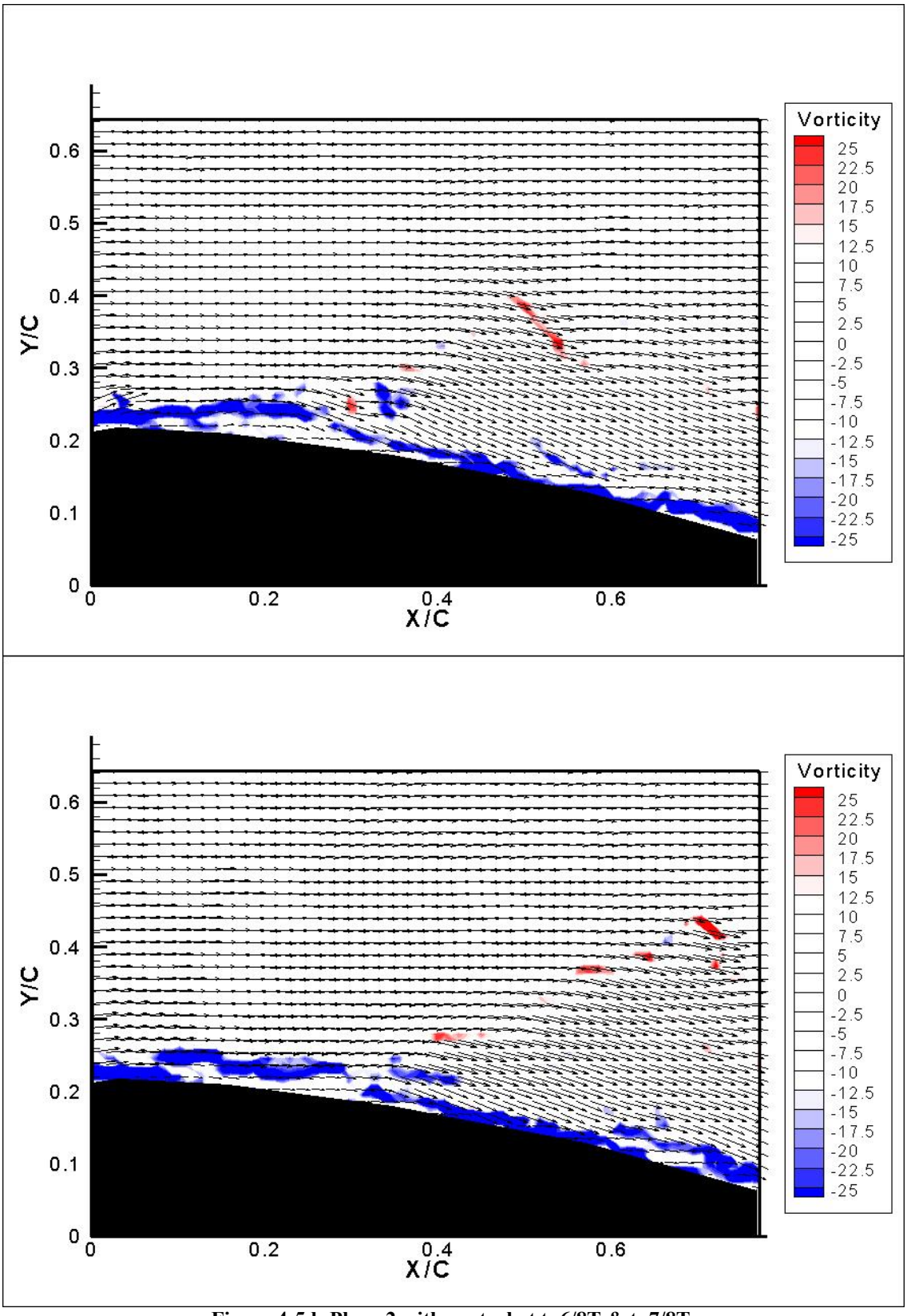

Figure 4-5d: Plane 2 with control at t=6/8T & t=7/8T.

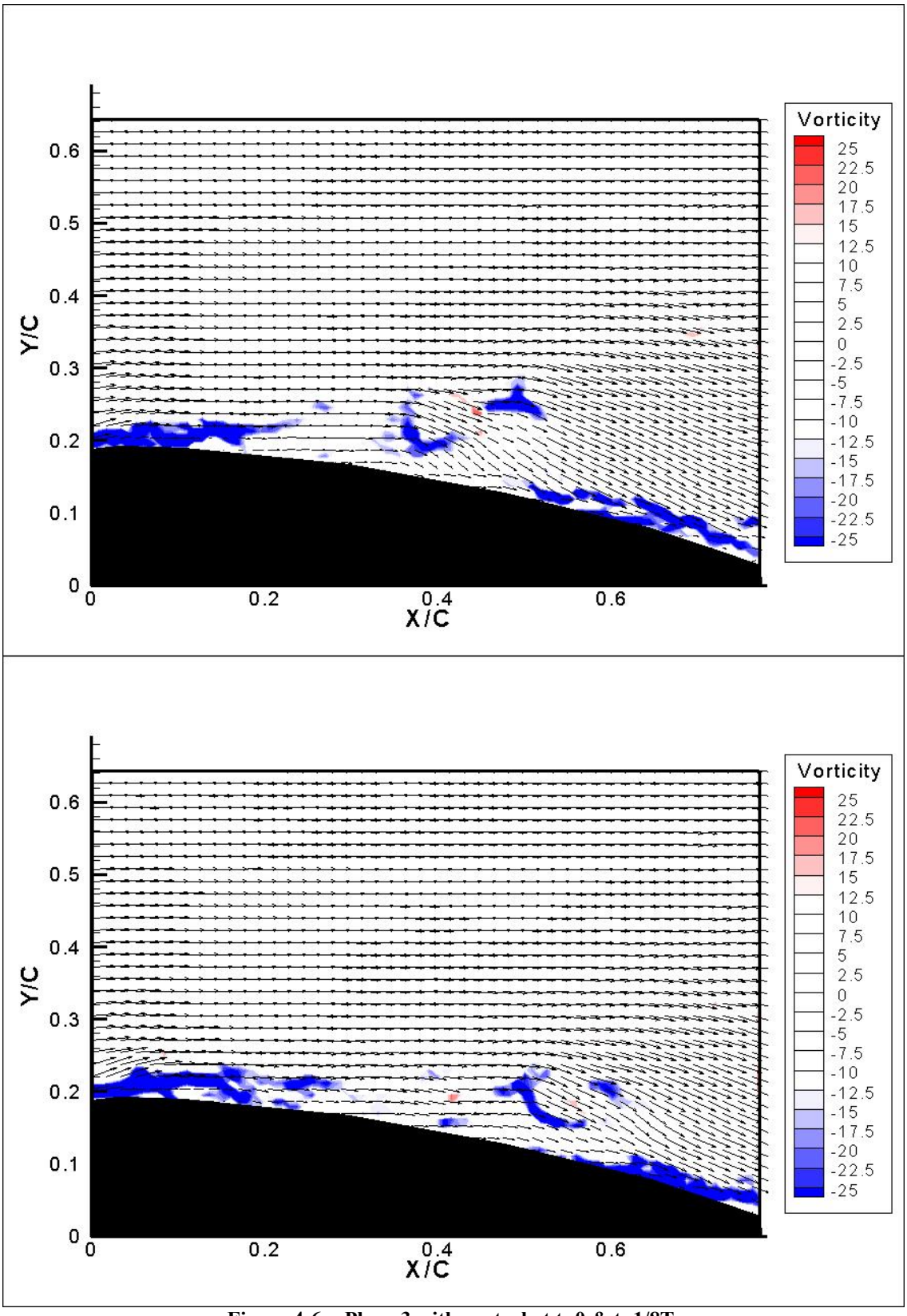

Figure 4-6a: Plane 3 with control at t=0 & t=1/8T.

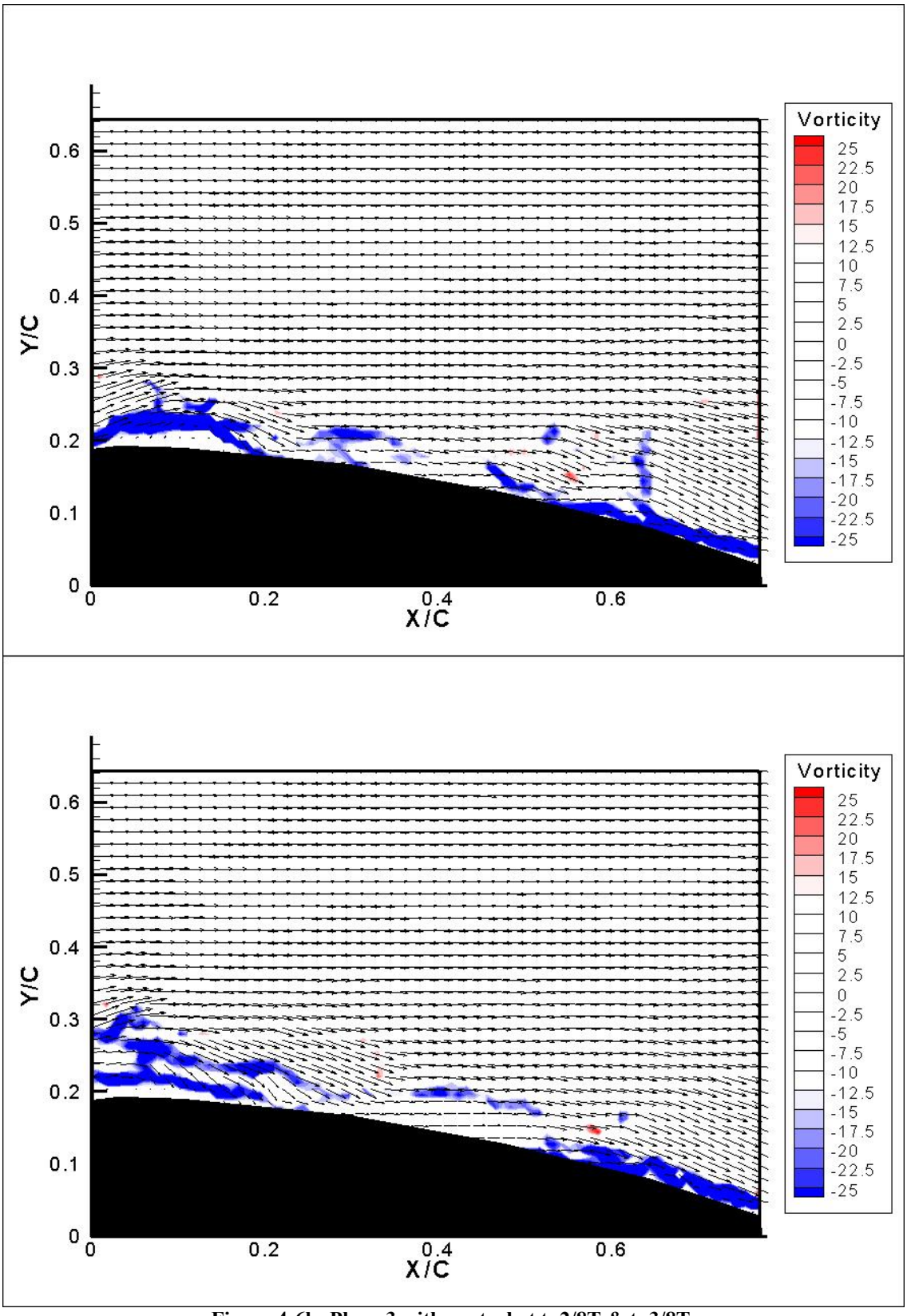

Figure 4-6b: Plane 3 with control at t=2/8T & t=3/8T.

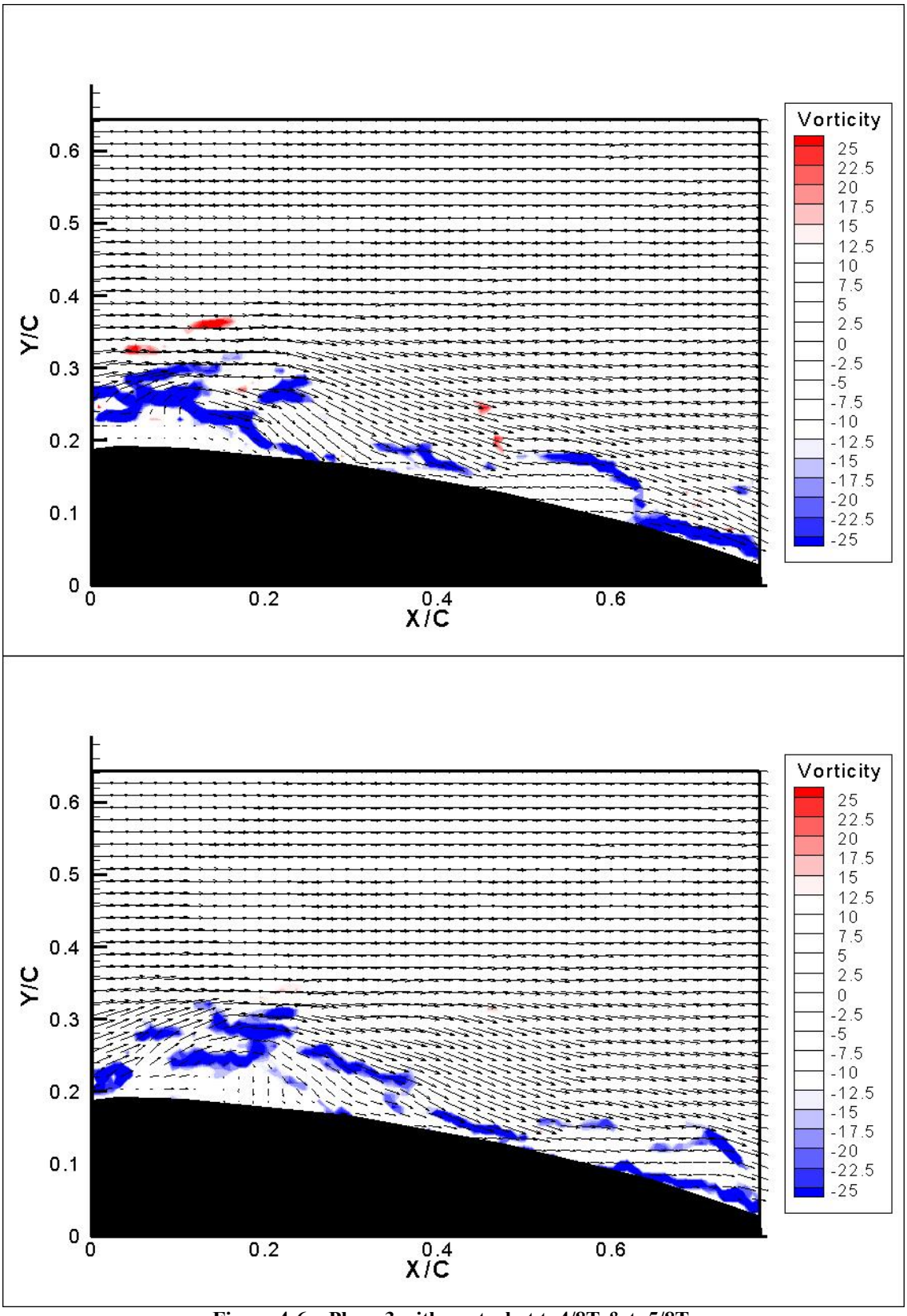

Figure 4-6c: Plane 3 with control at t=4/8T & t=5/8T.

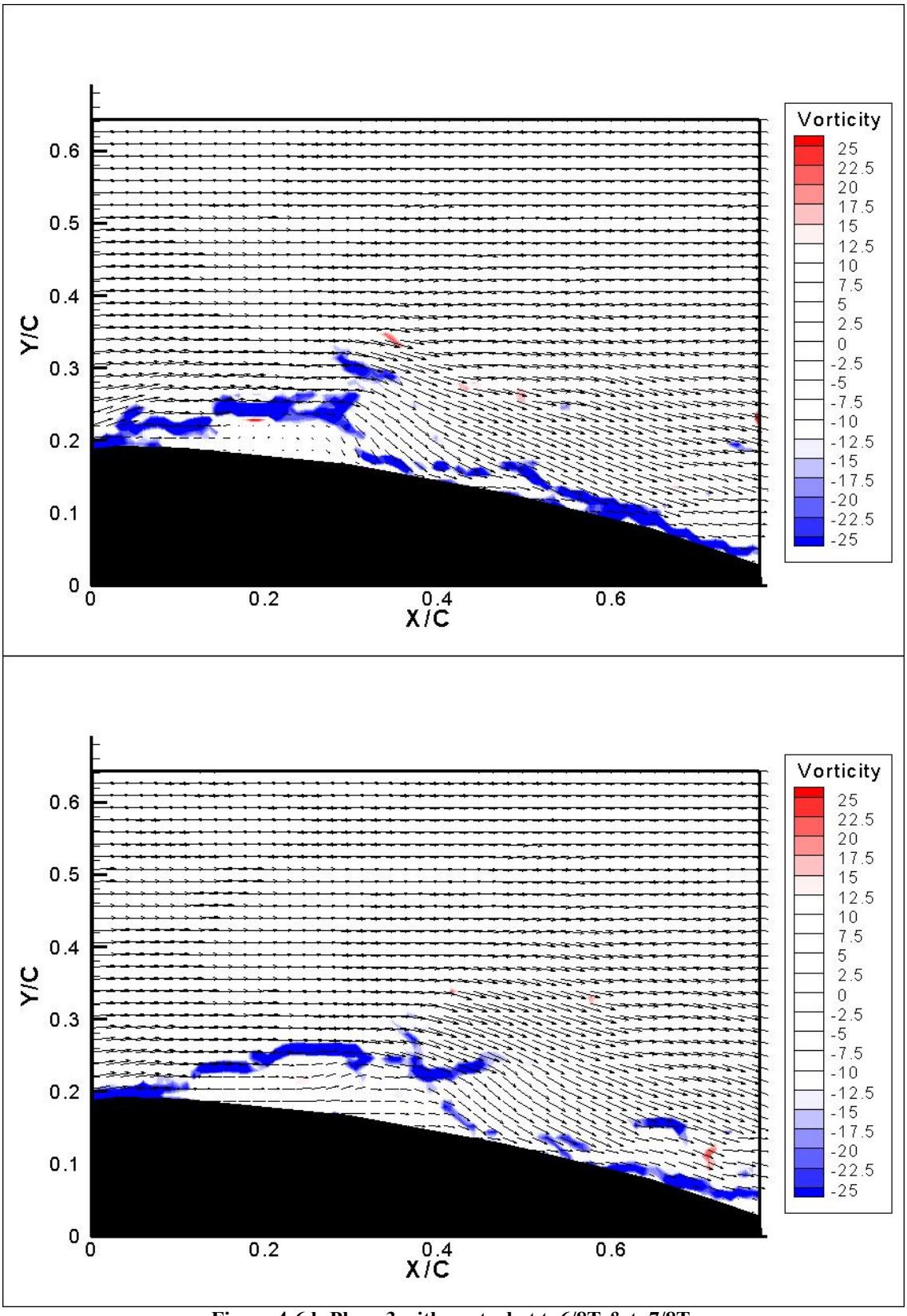

Figure 4-6d: Plane 3 with control at t=6/8T & t=7/8T.

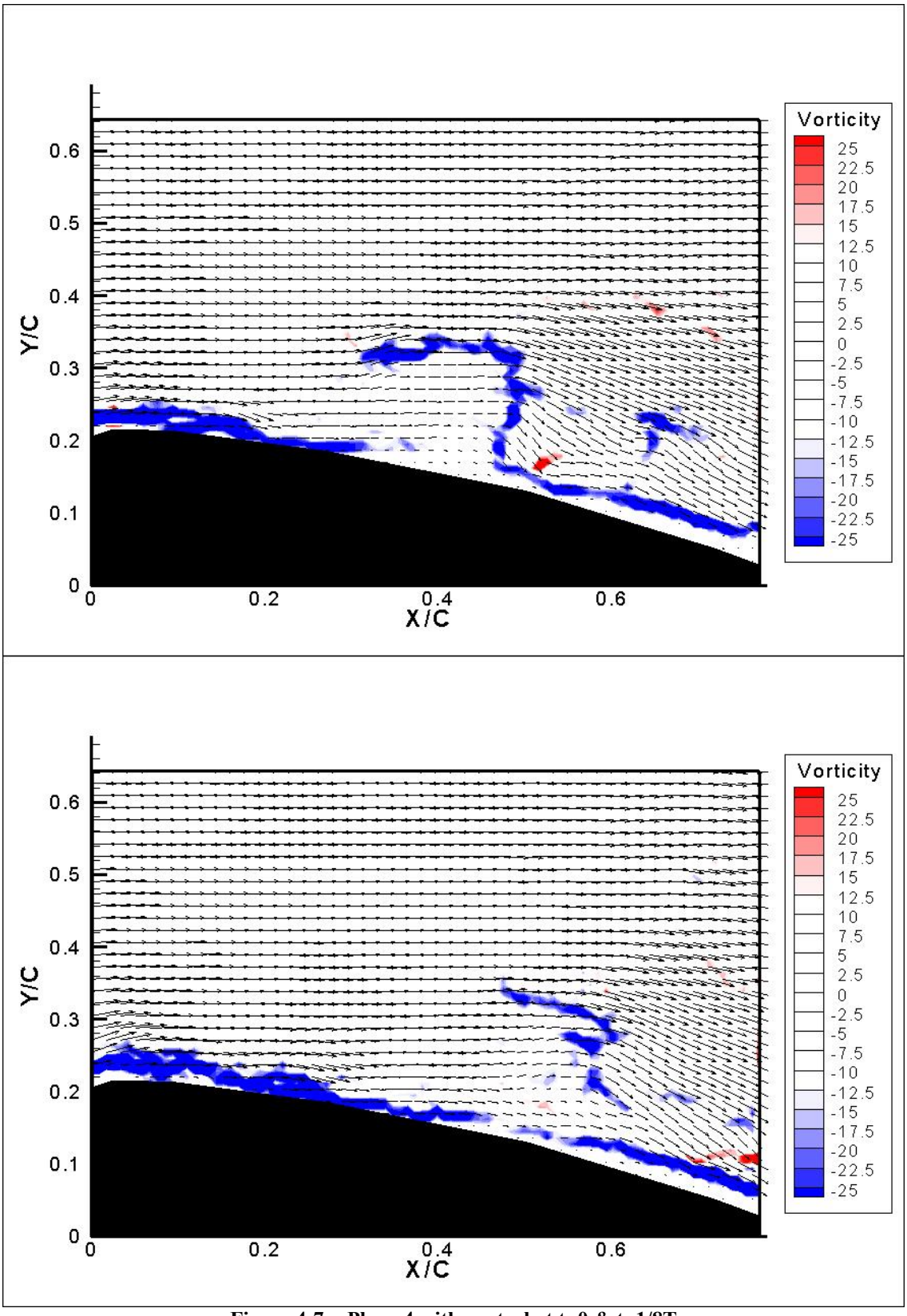

Figure 4-7a: Plane 4 with control at t=0 & t=1/8T

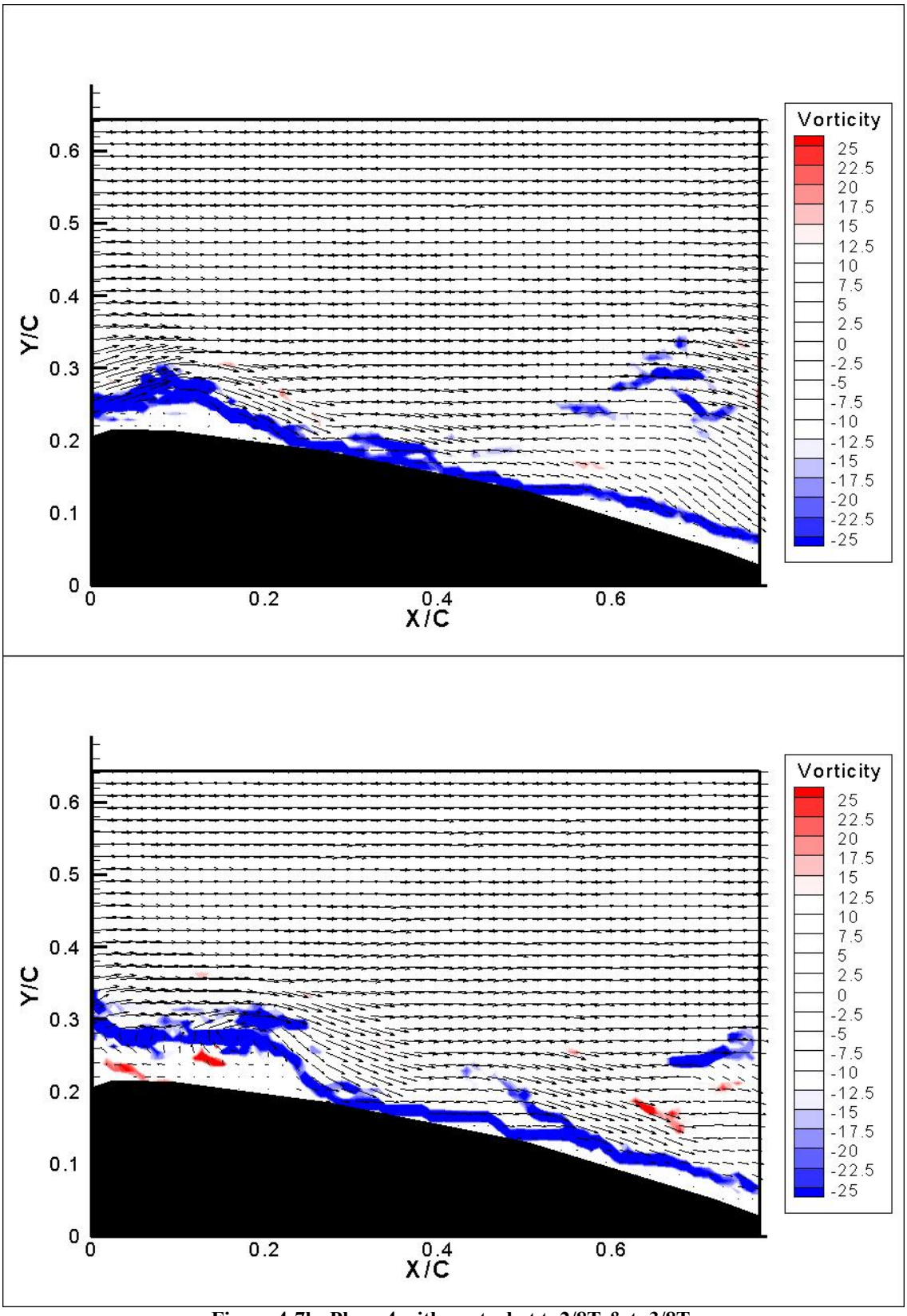

Figure 4-7b: Plane 4 with control at t=2/8T & t=3/8T.

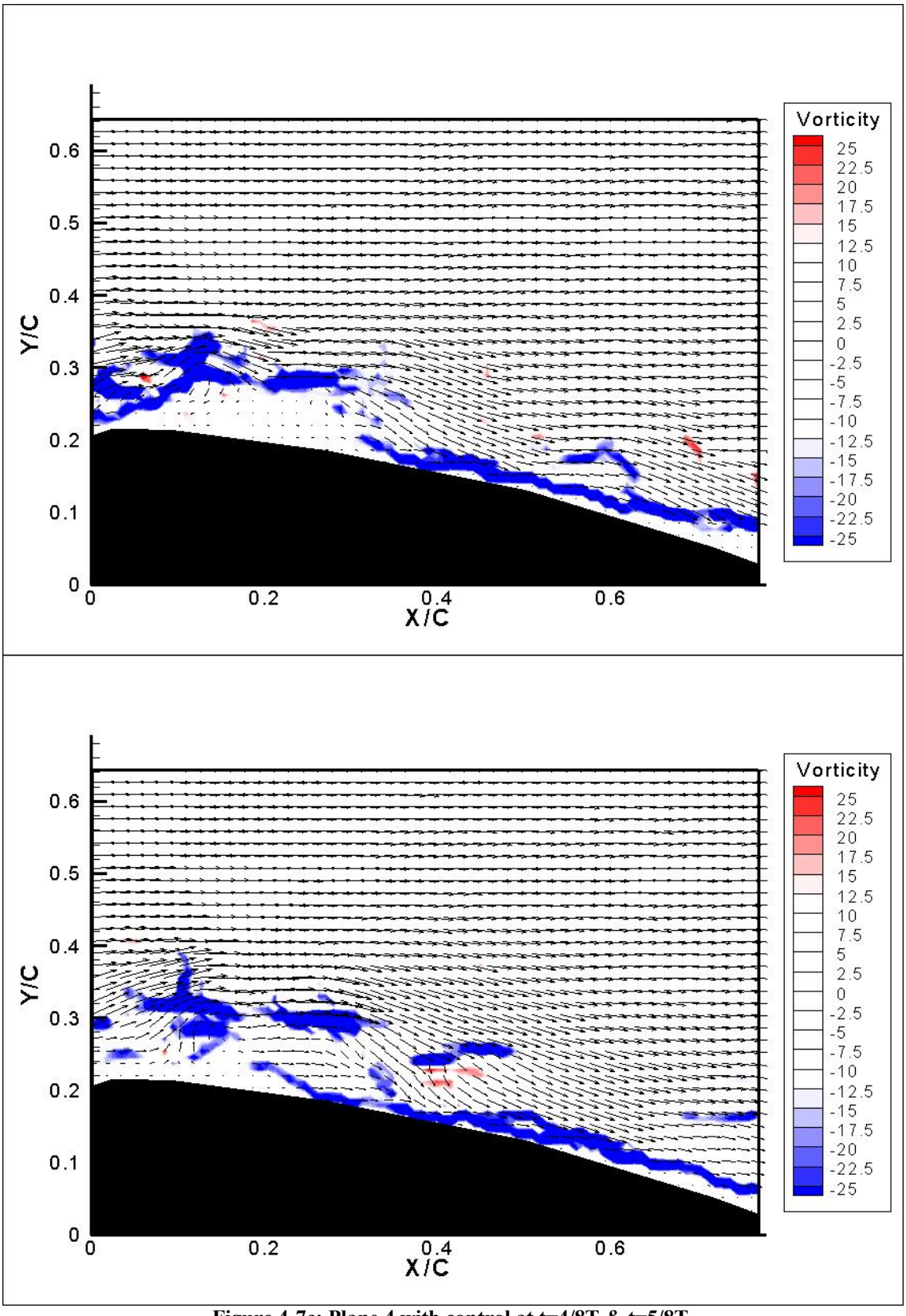

Figure 4-7c: Plane 4 with control at t=4/8T & t=5/8T.

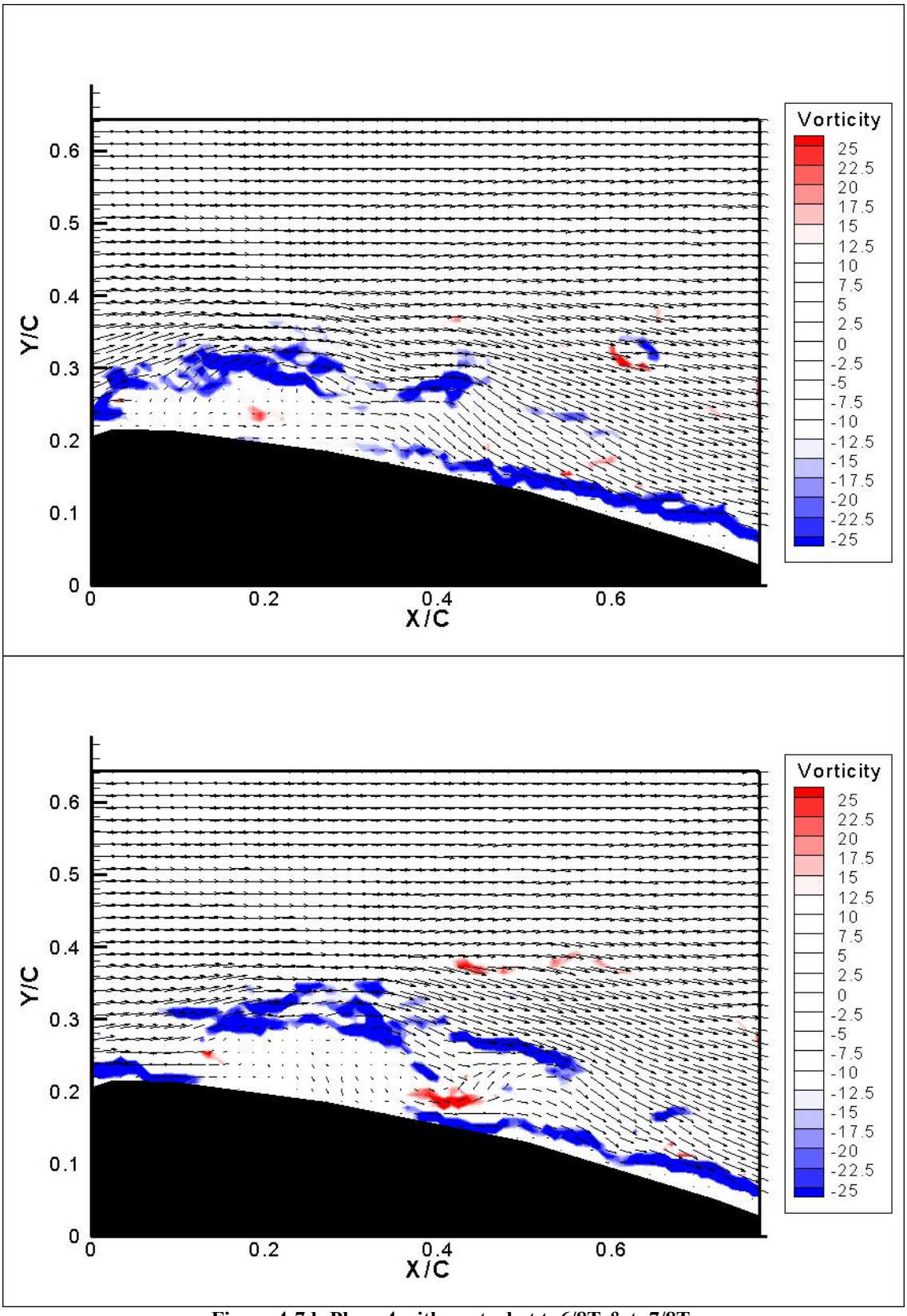

Figure 4-7d: Plane 4 with control at t=6/8T & t=7/8T.

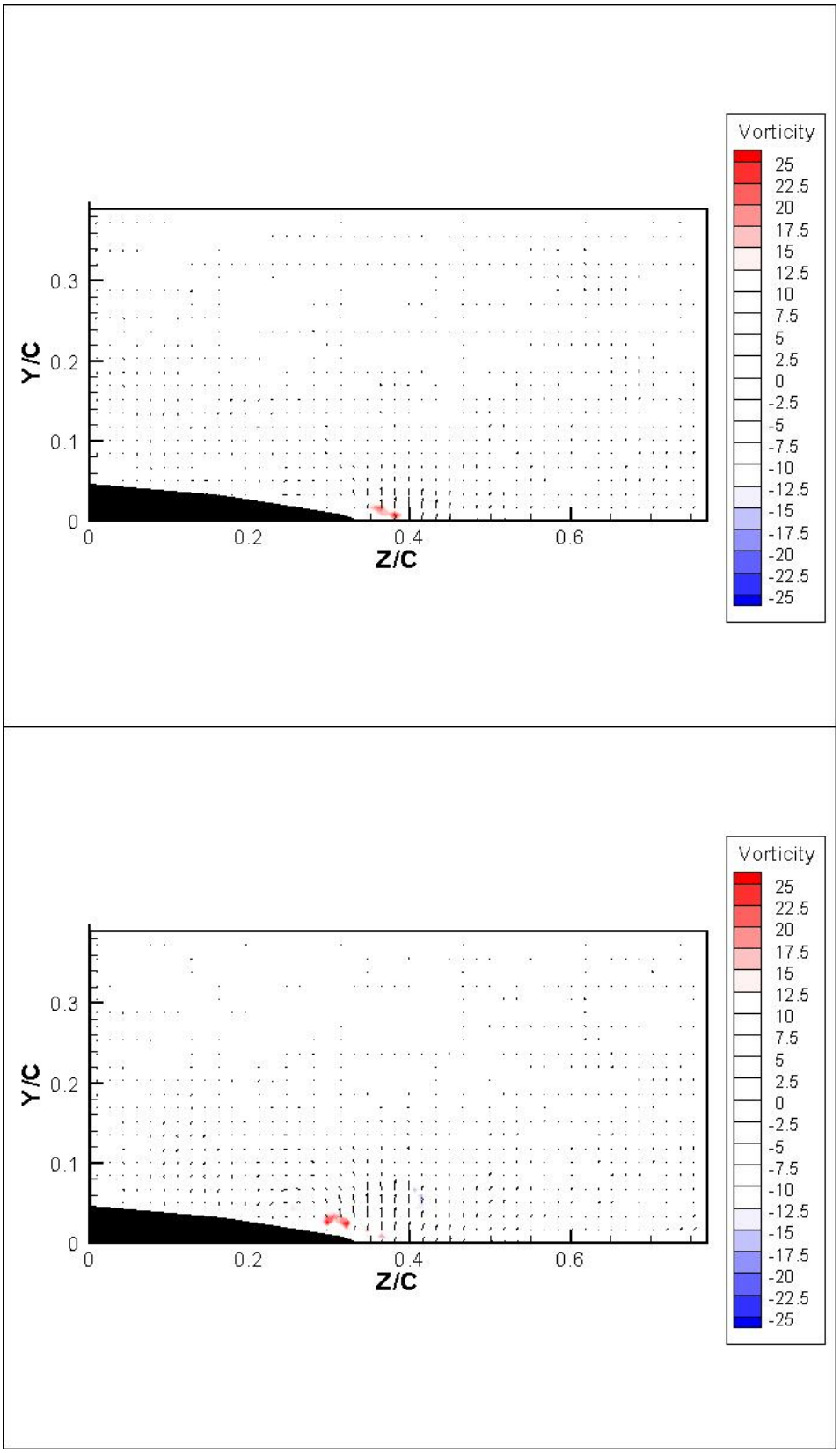

Figure 4-8a: Plane A with control at t=0 & t=1/8T

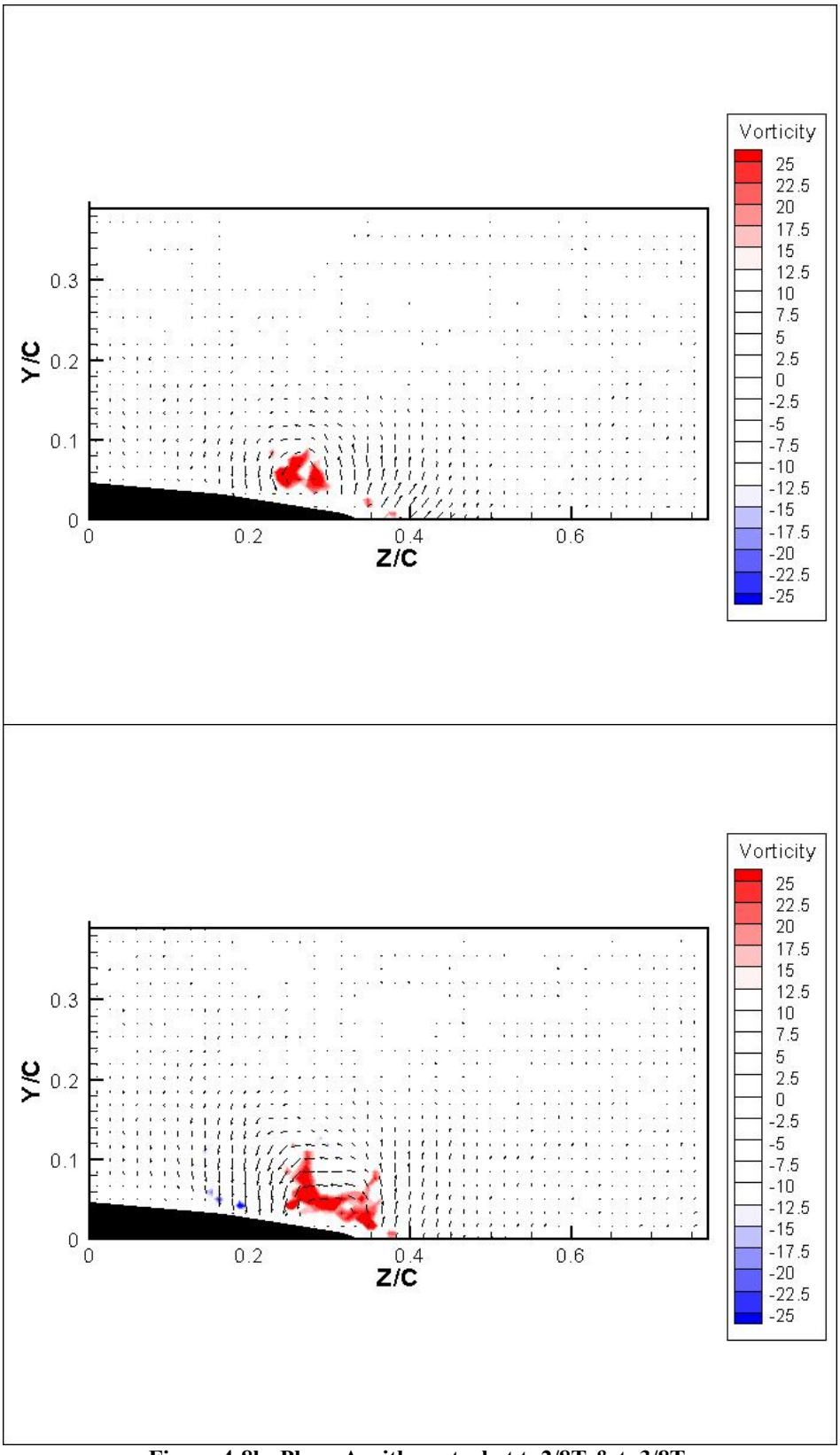

Figure 4-8b: Plane A with control at t=2/8T & t=3/8T.

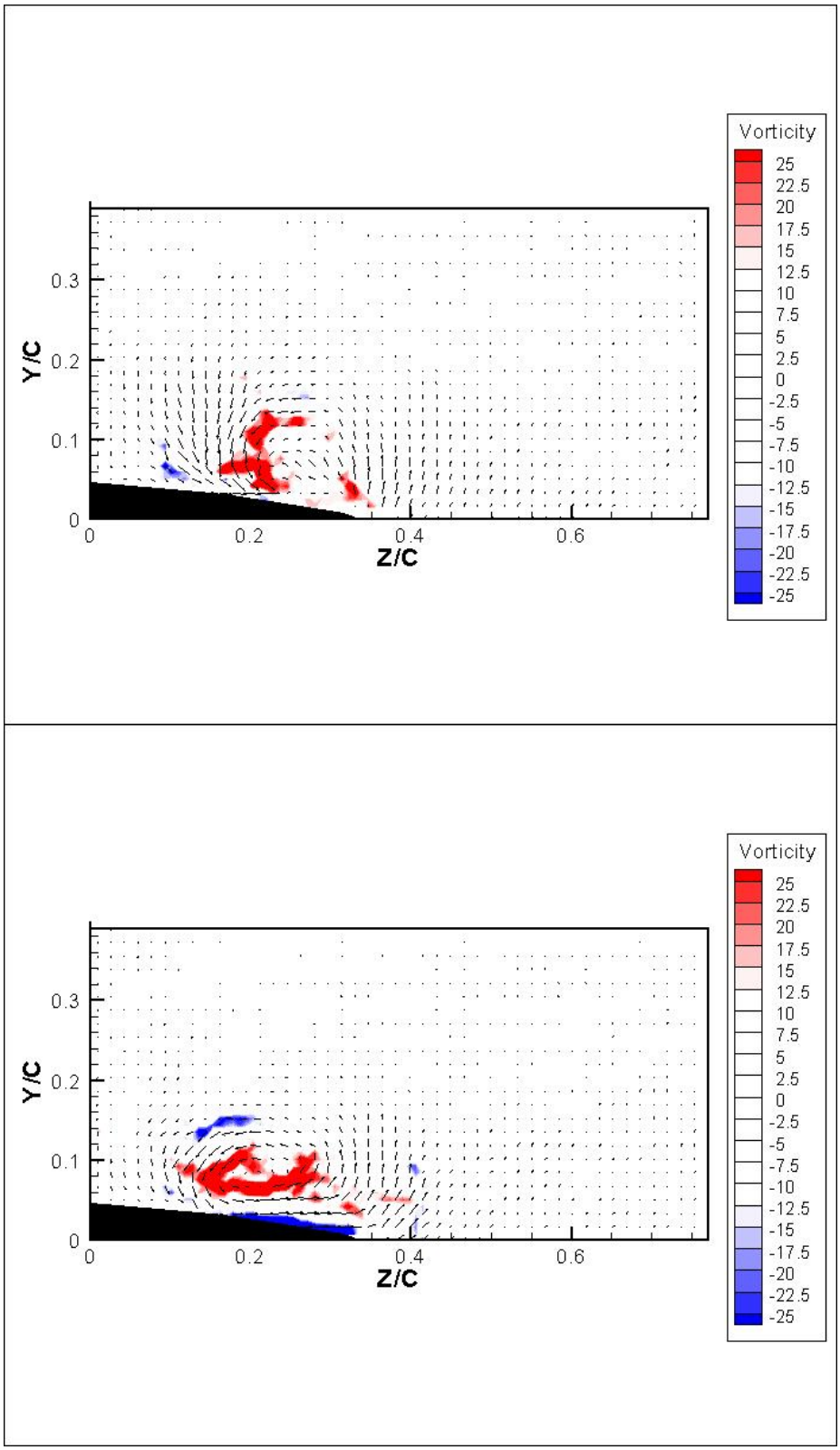

Figure 4-8c: Plane A with control at t=4/8T & t=5/8T.

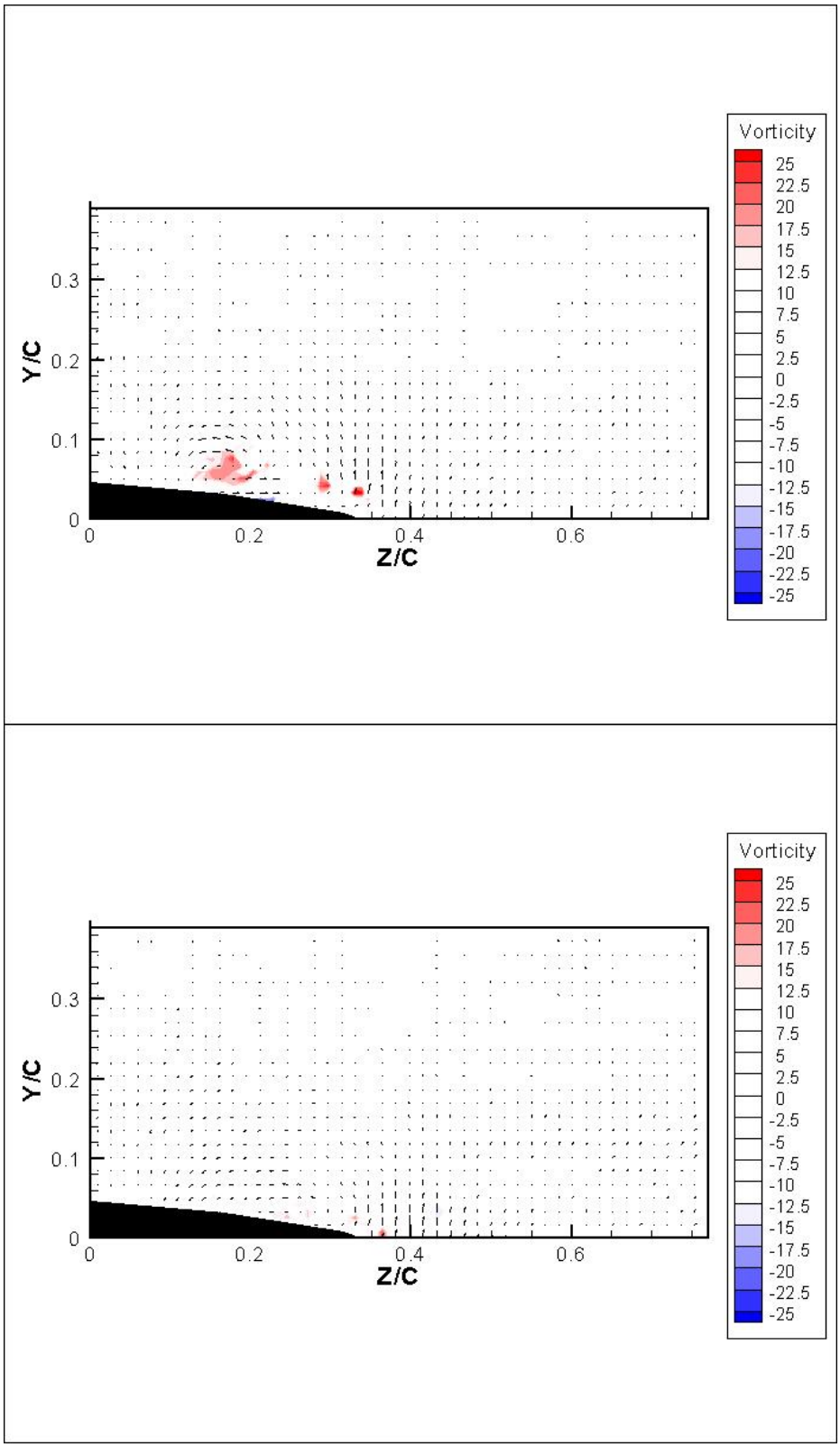

Figure 4-8d: Plane A with control at t=6/8T & t=7/8T.

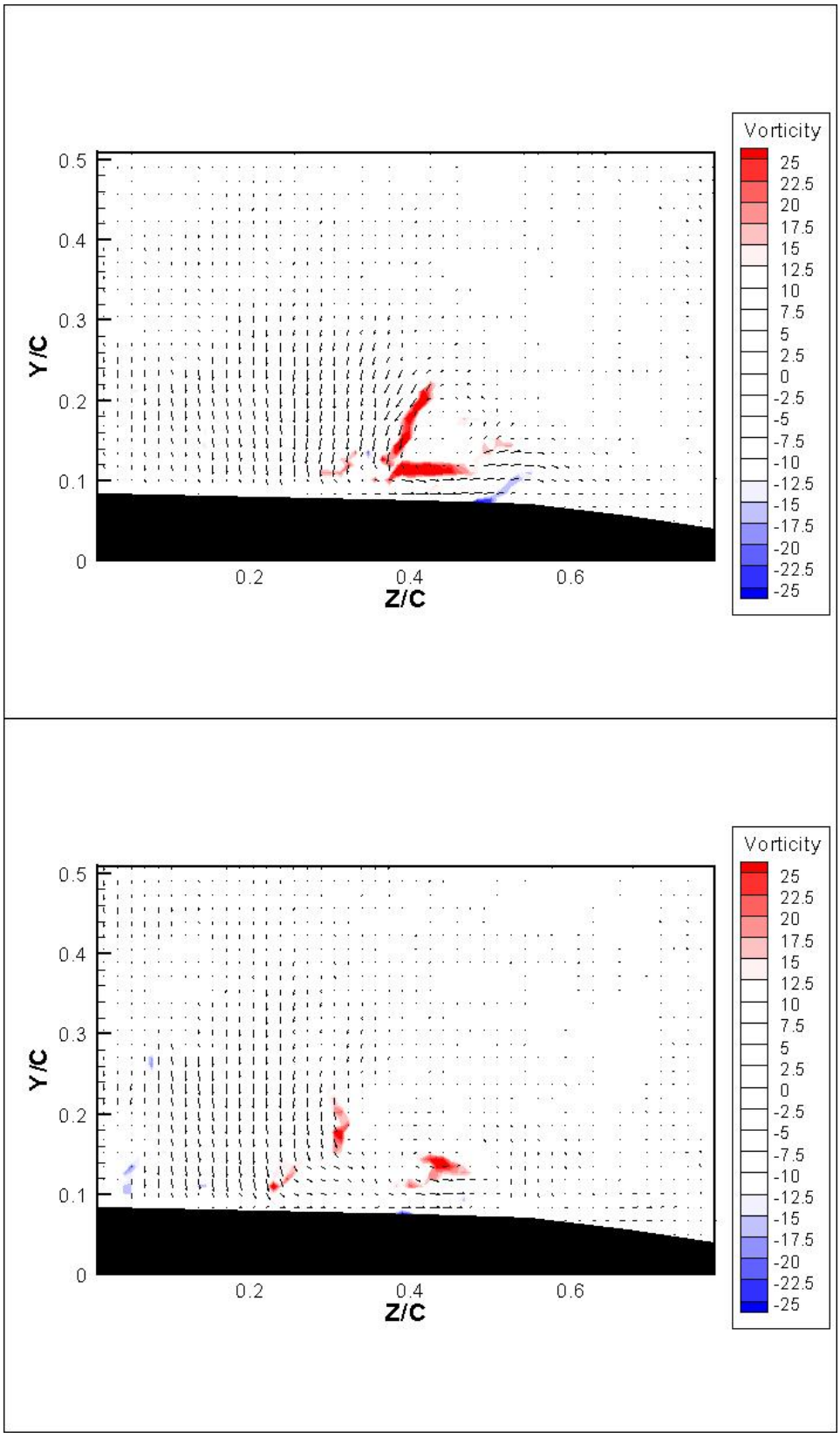

Figure 4-9a: Plane C with control at t=0 & t=1/8T.

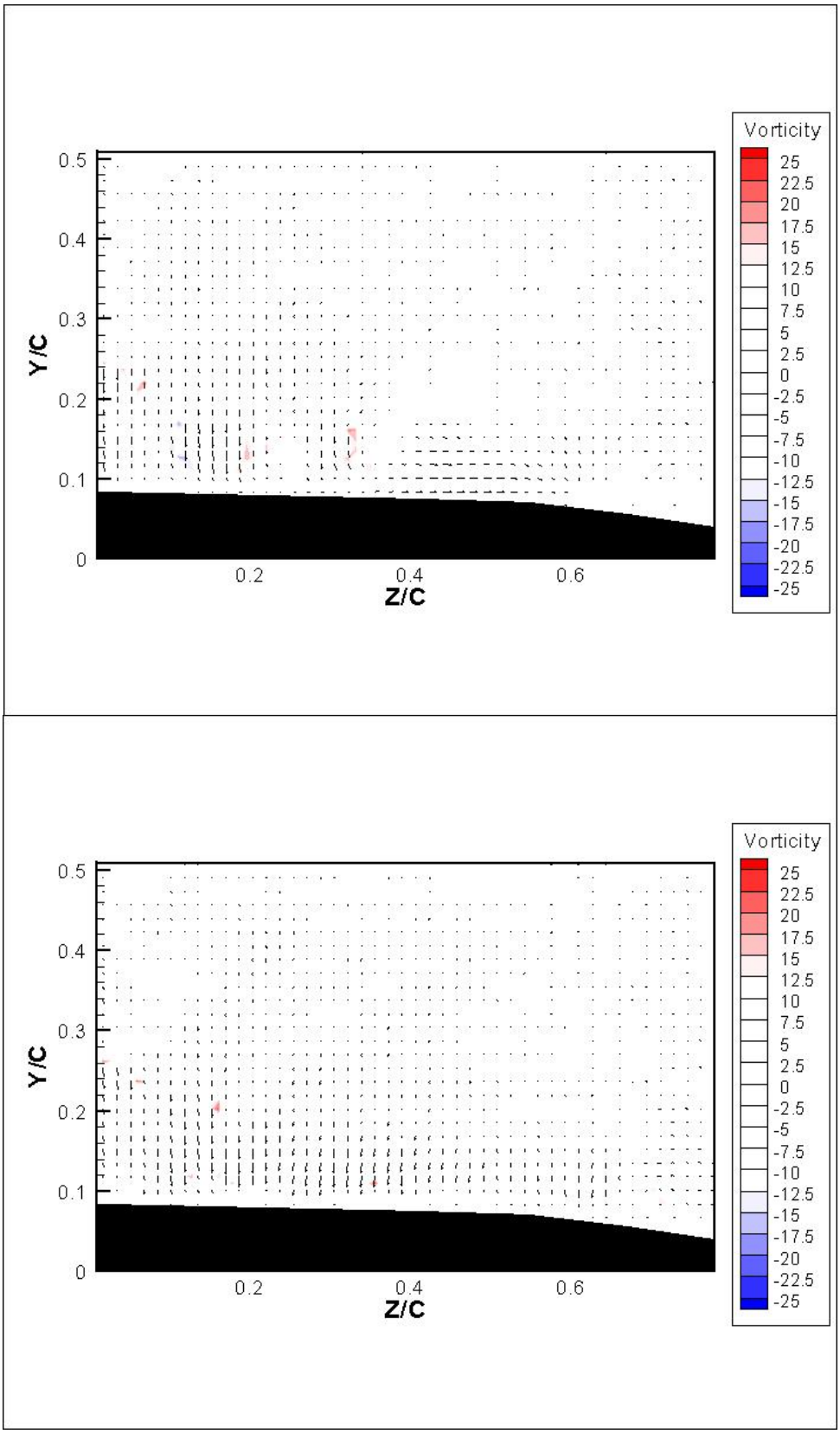

Figure 4-9b: Plane C with control at t=2/8T & t=3/8T.

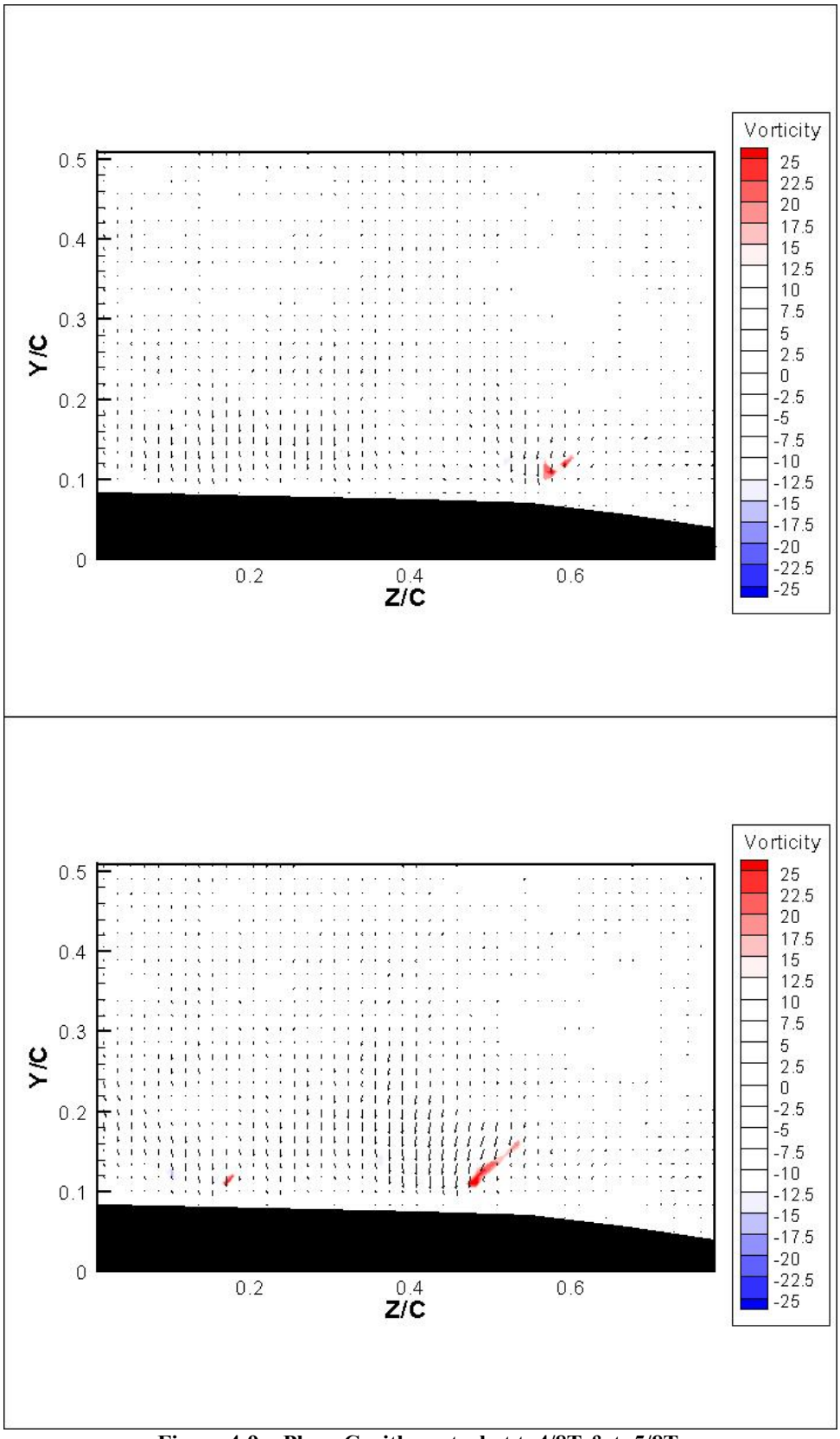

Figure 4-9c: Plane C with control at t=4/8T & t=5/8T.

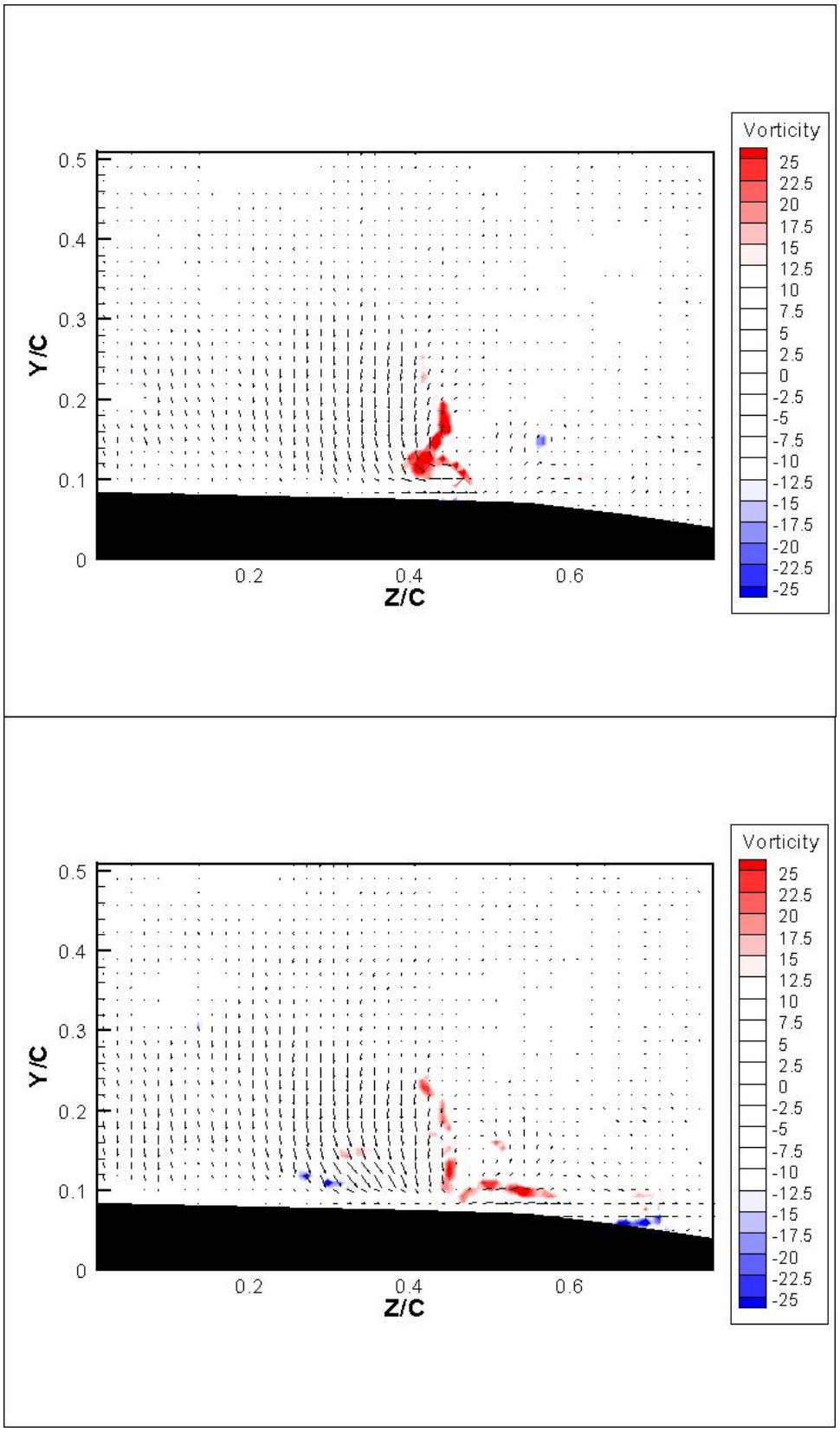

Figure 4-9d: Plane C with control at t=6/8T & t=7/8T.

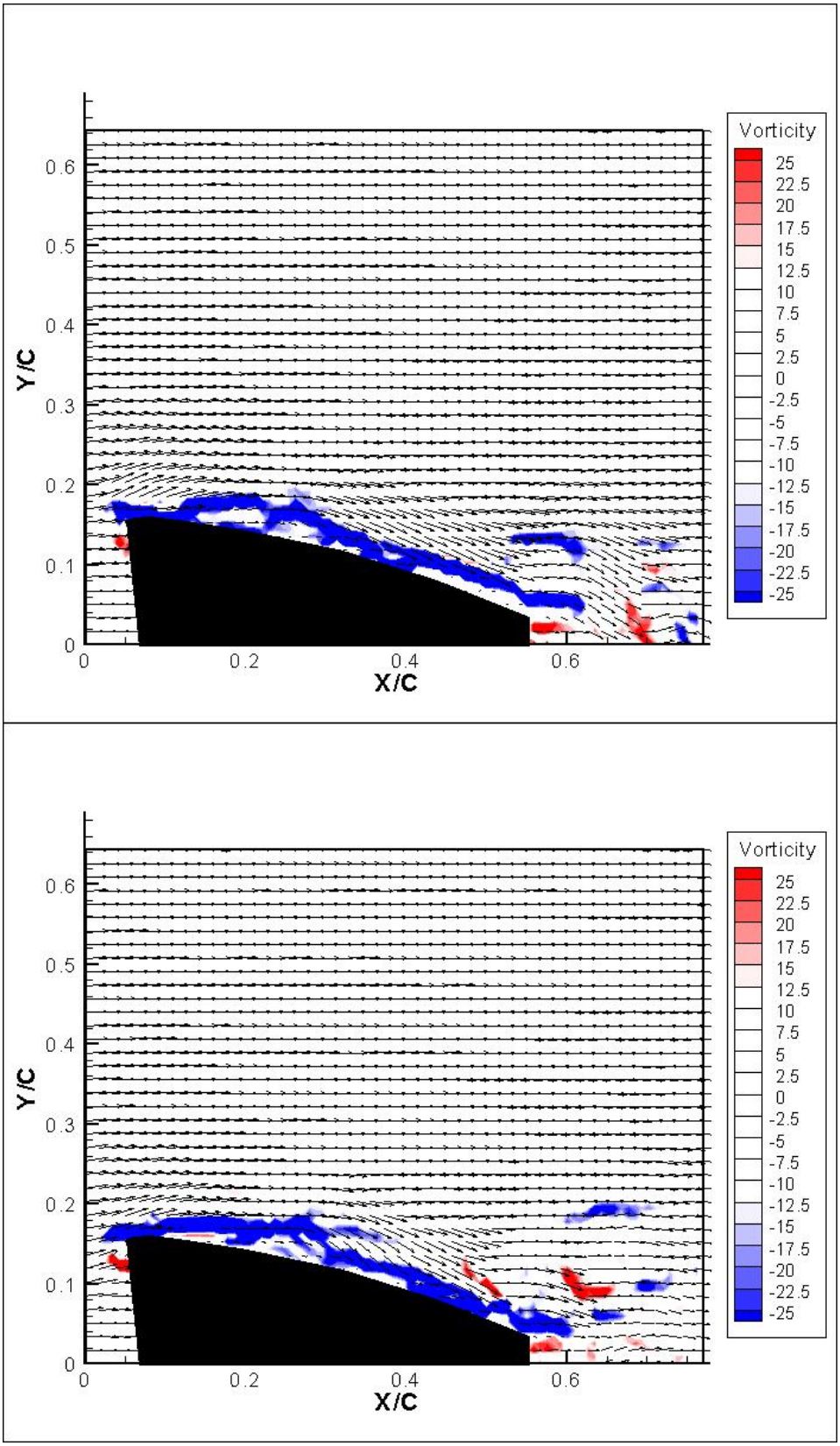

Figure 4-10a: Plane 8 with control at t=0 & t=1/8T.

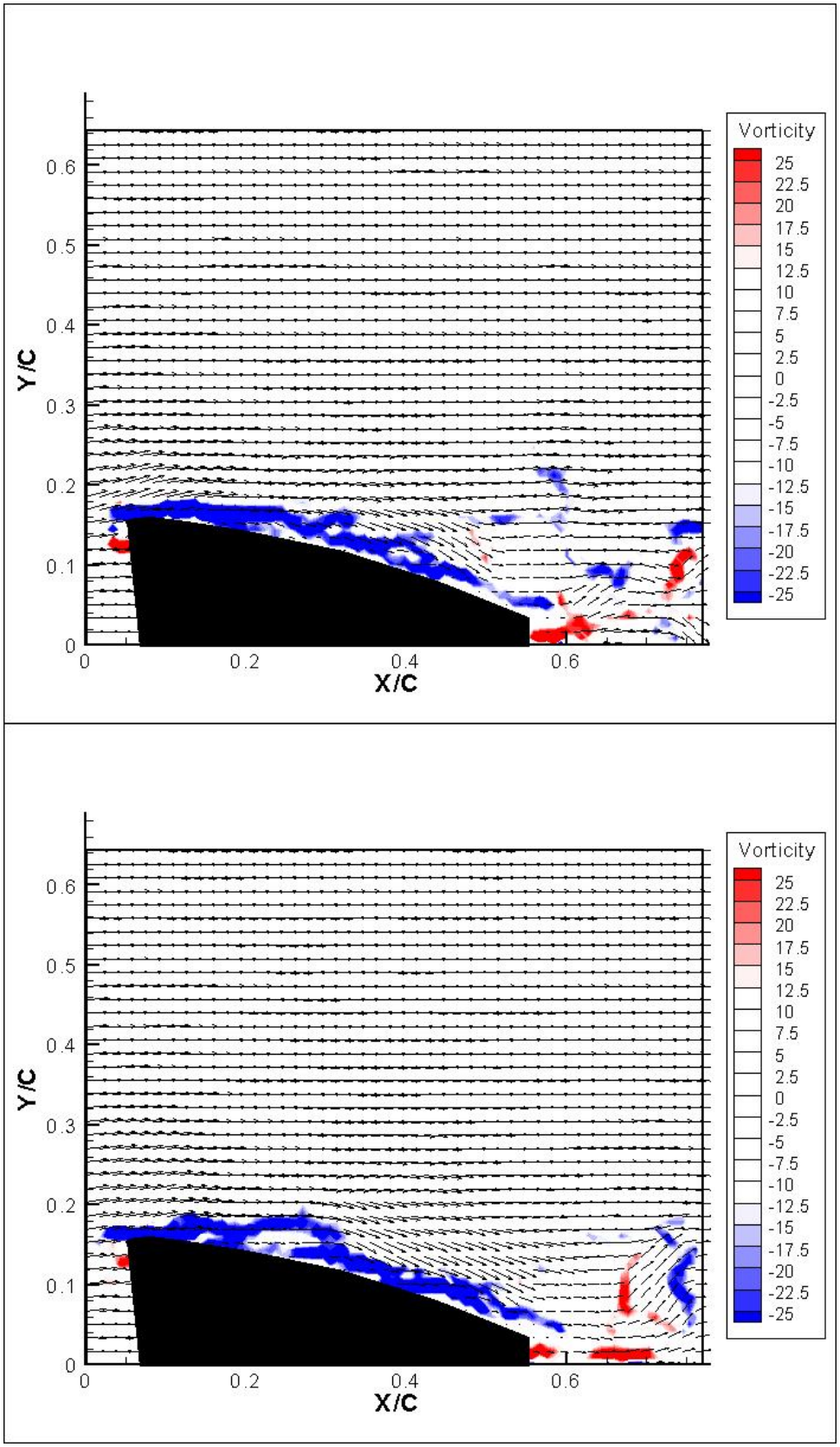

Figure 4-10b: Plane 8 with control at t=2/8T & t=3/8T.

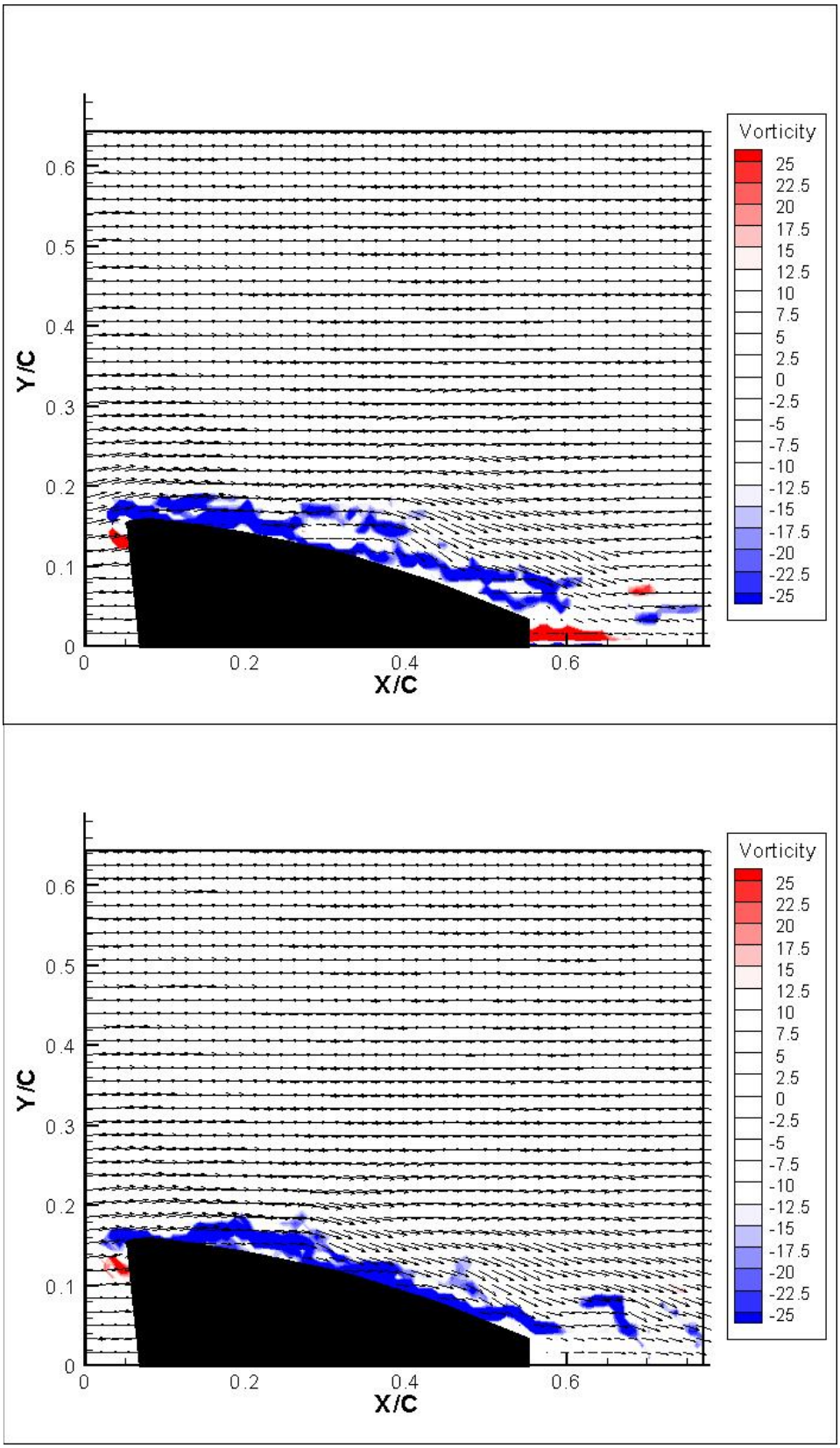

Figure 4-10c: Plane 8 with control at t=4/8T & t=5/8T.

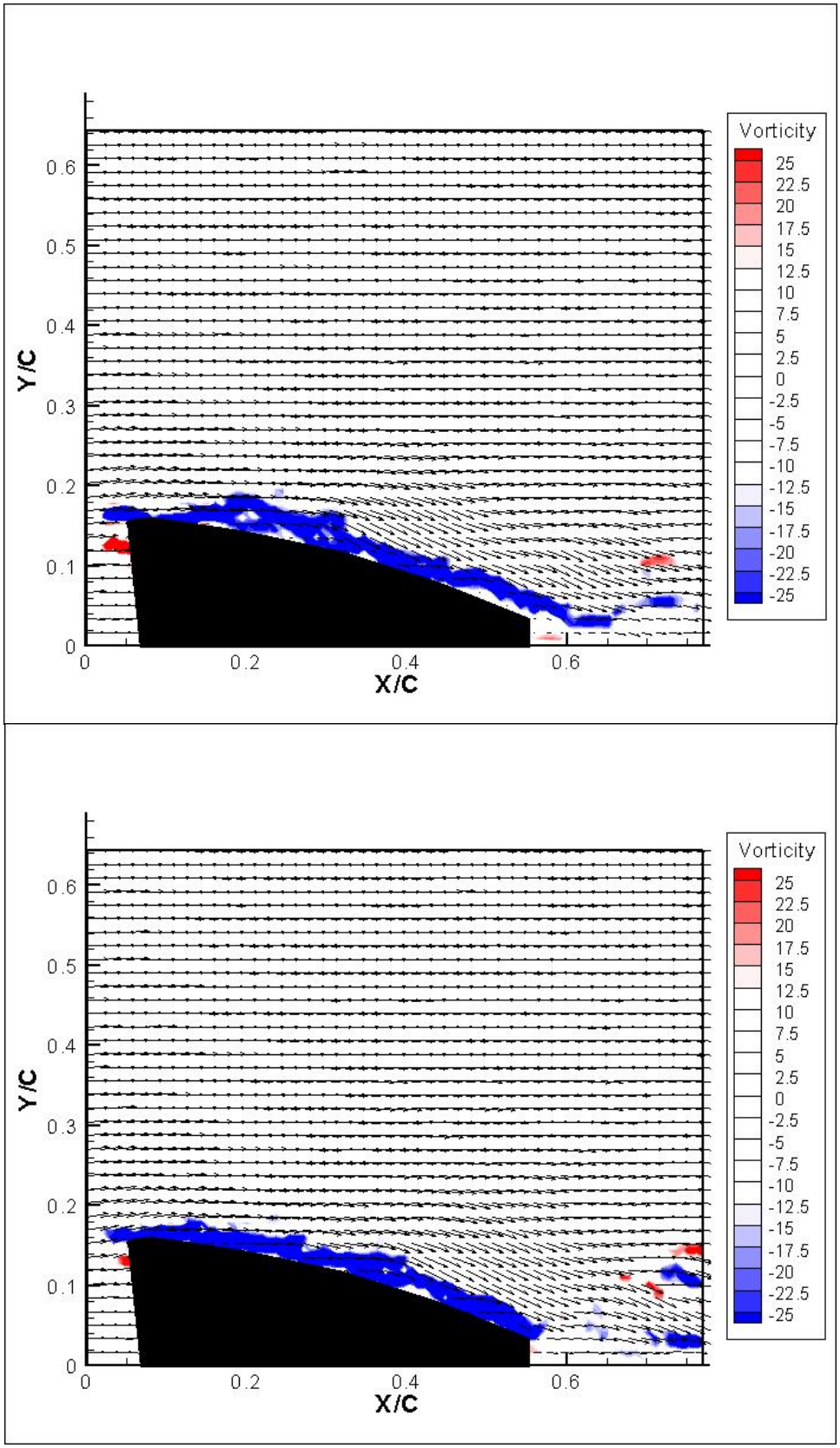

Figure 4-10d: Plane 8 with control at t=6/8T & t=7/8T.

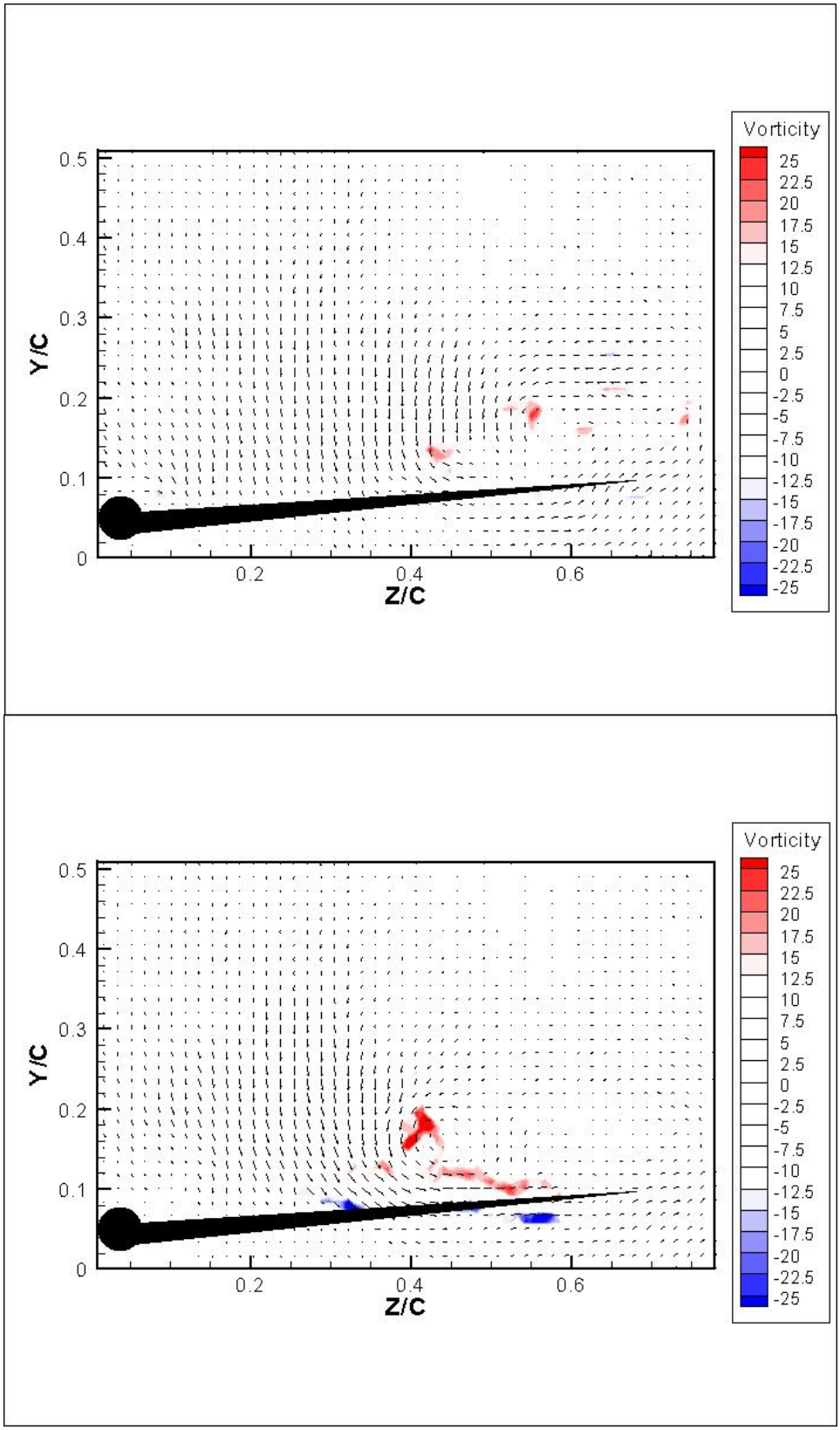

Figure 4-11a: Plane D with control at t=0 & t=1/8T.

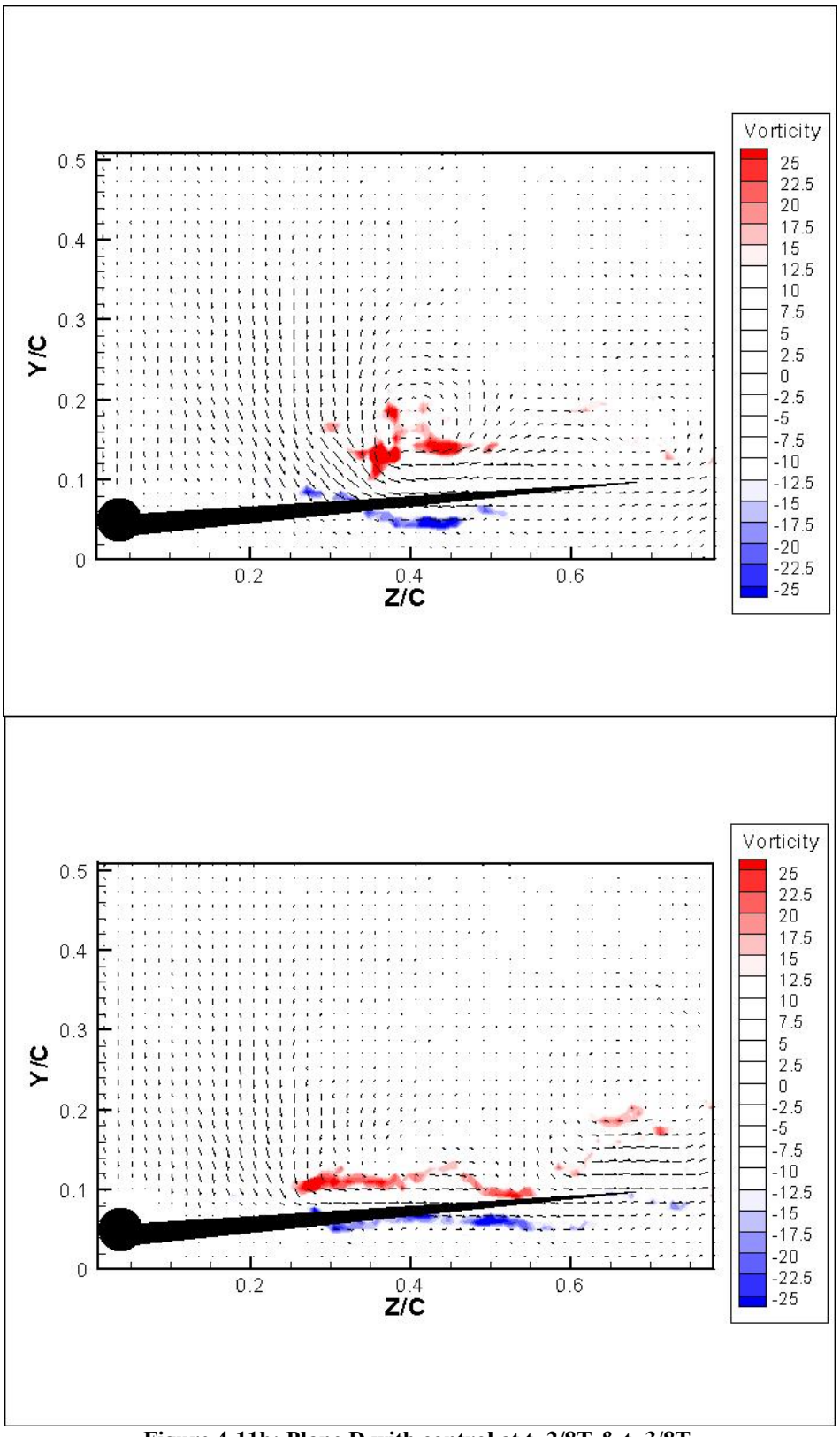

Figure 4-11b: Plane D with control at t=2/8T & t=3/8T.

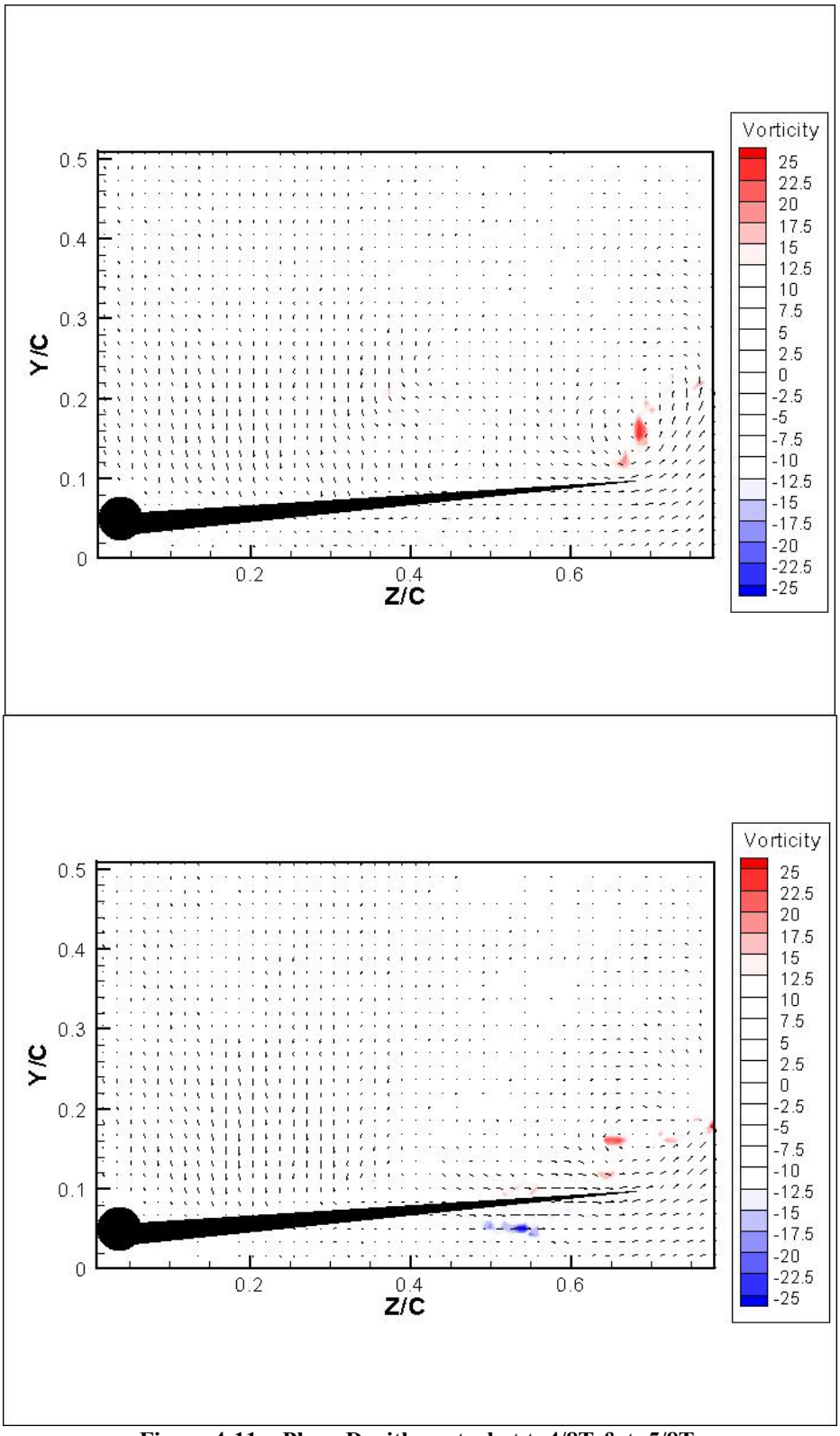

Figure 4-11c: Plane D with control at t=4/8T & t=5/8T.

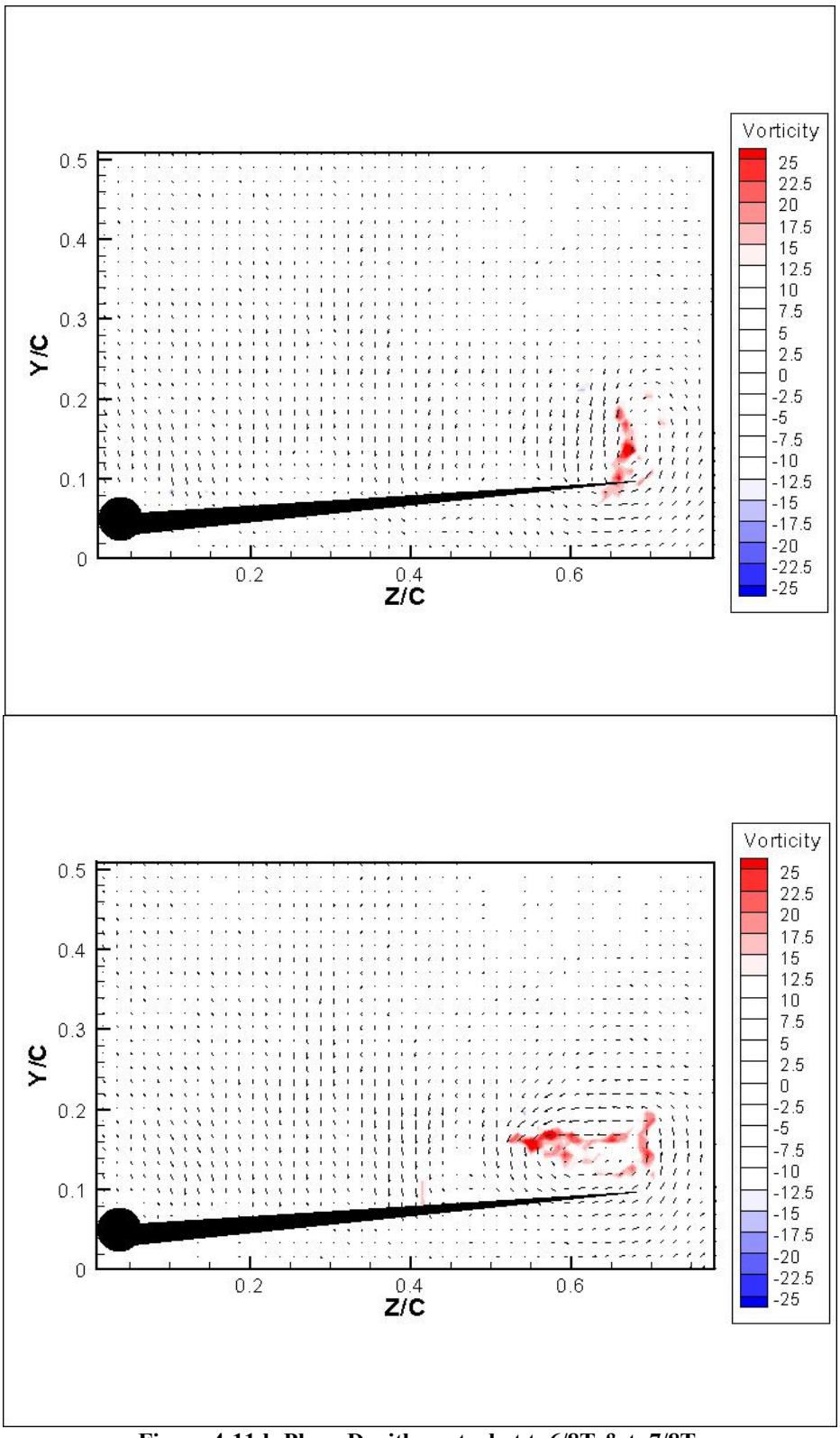

Figure 4-11d: Plane D with control at t=6/8T & t=7/8T.

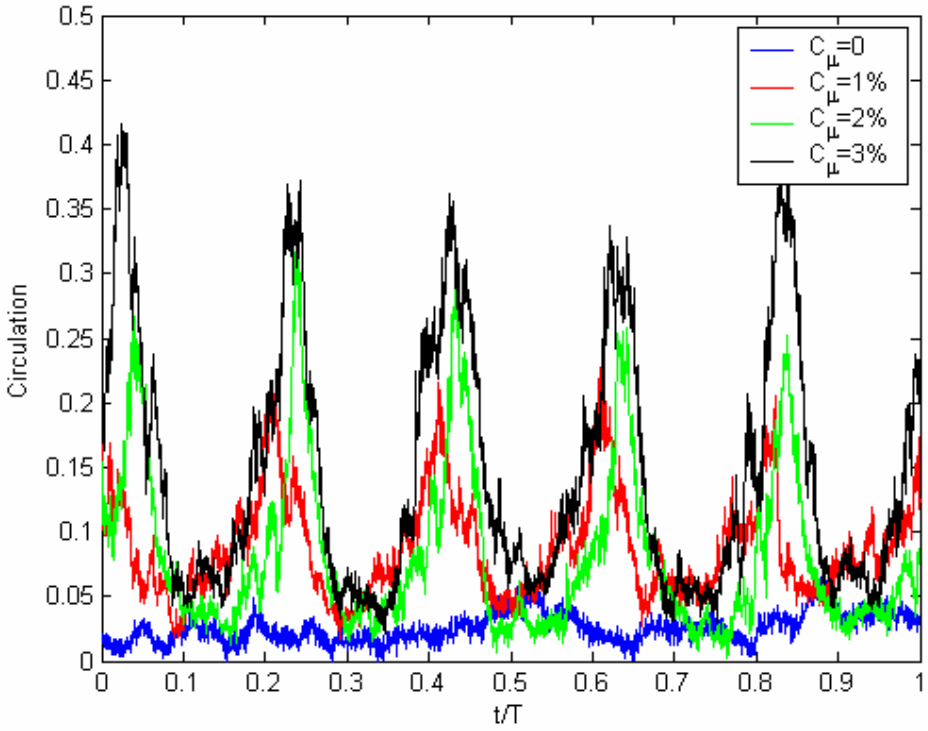

Figure 4-12: Instantaneous circulation over one period for Plane A.

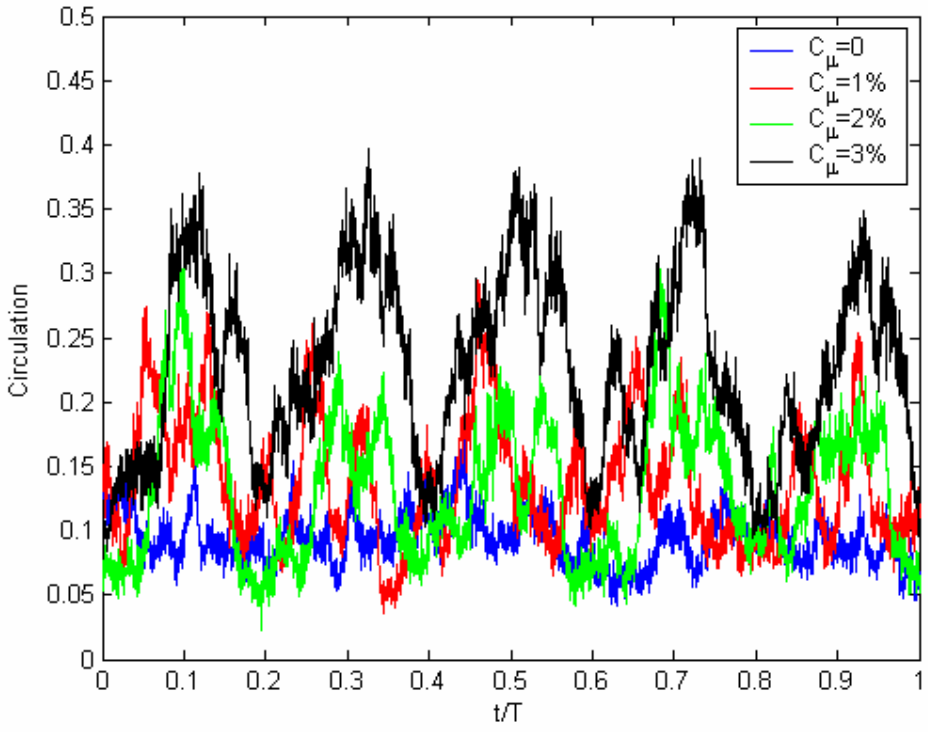

Figure 4-13: Instantaneous circulation over one period for Plane B.

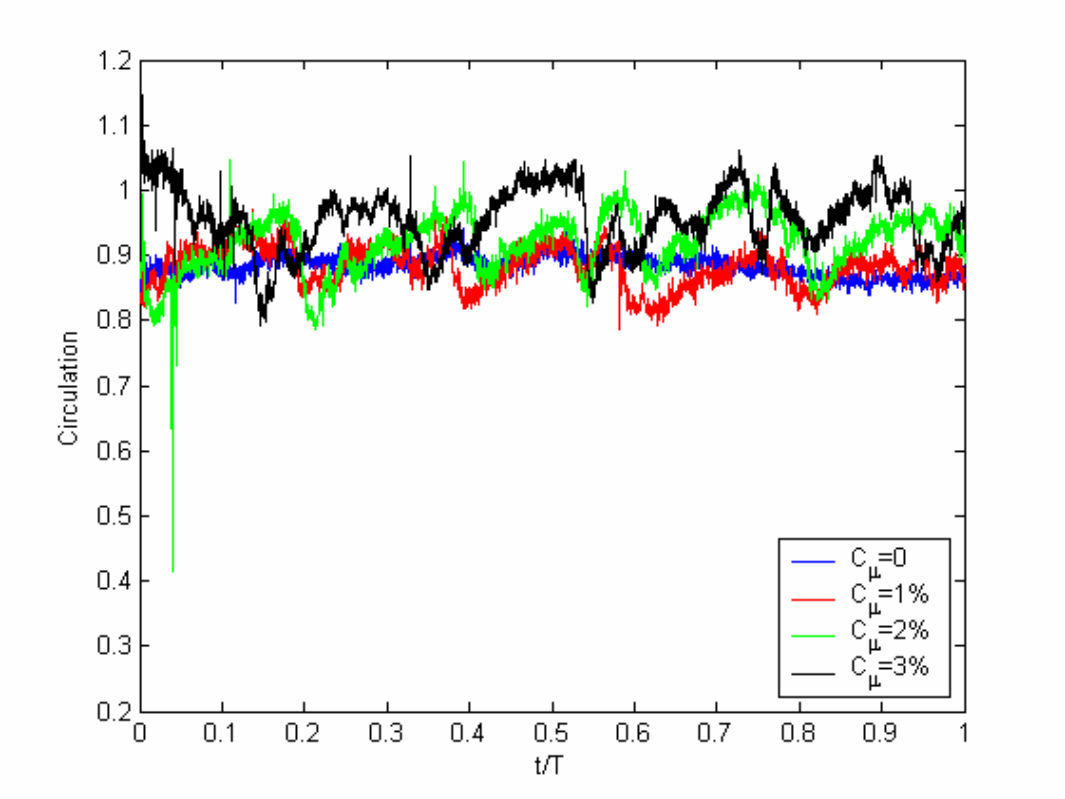

Figure 4-14: Instantaneous circulation over one period for Plane 4.

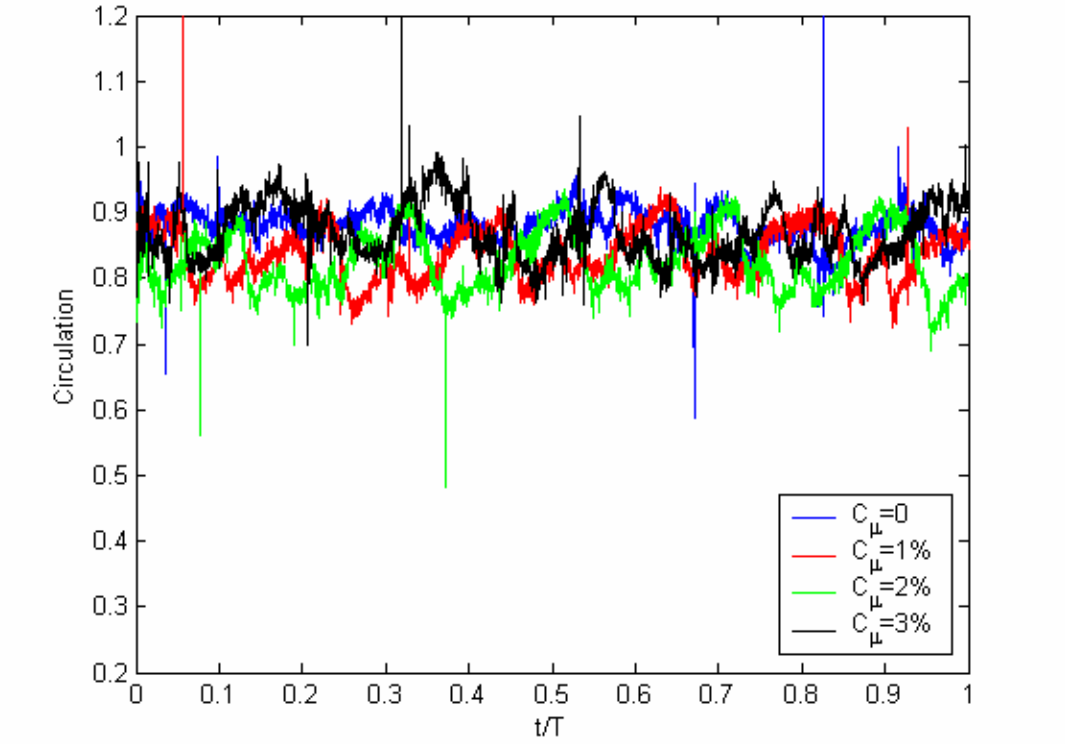

Figure 4-15: Instantaneous circulation over one period for Plane 5.

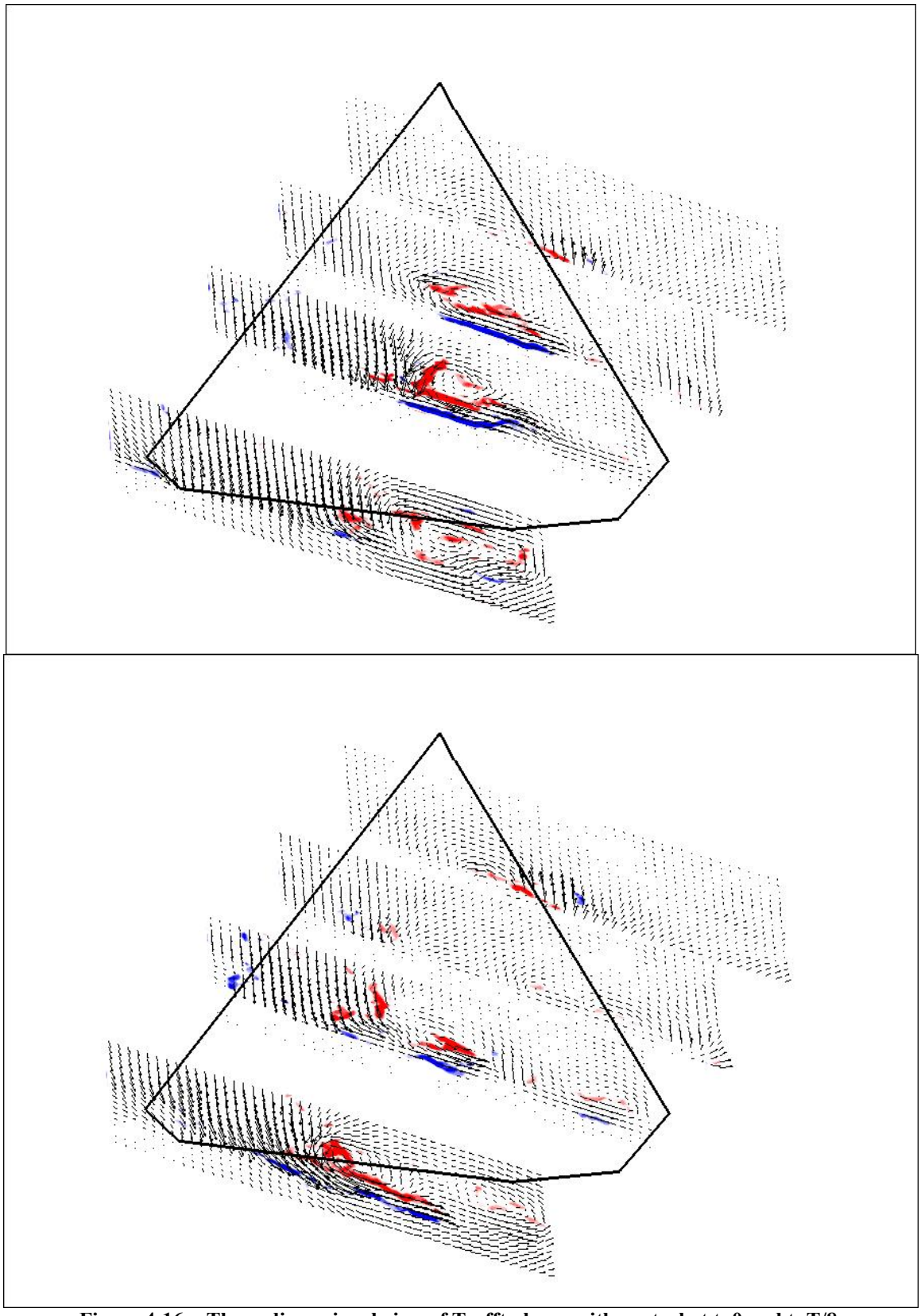

Figure 4-16a: Three-dimensional view of Trefft planes with control at t=0 and t=T/8.

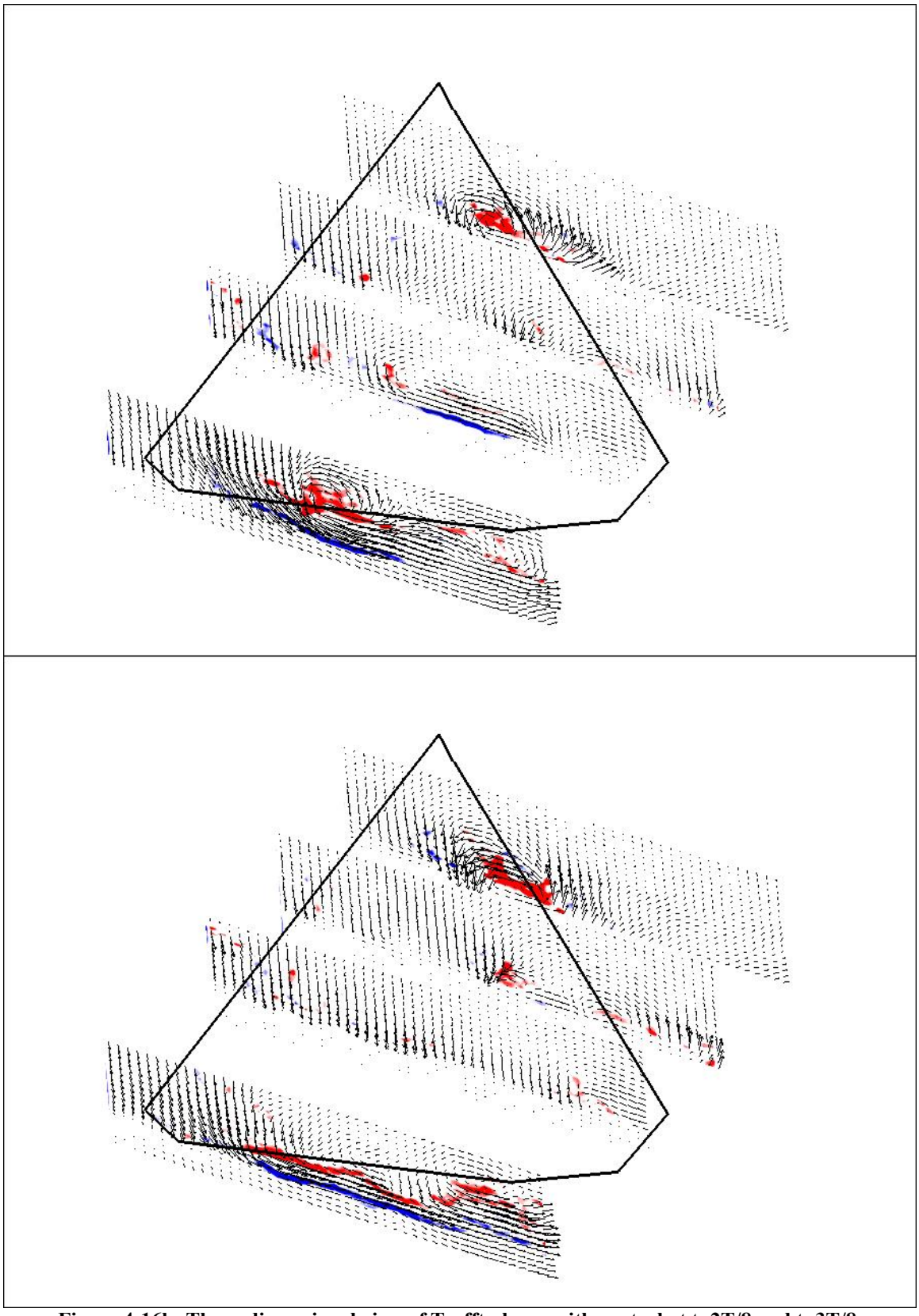

Figure 4-16b: Three-dimensional view of Trefft planes with control at t=2T/8 and t=3T/8.

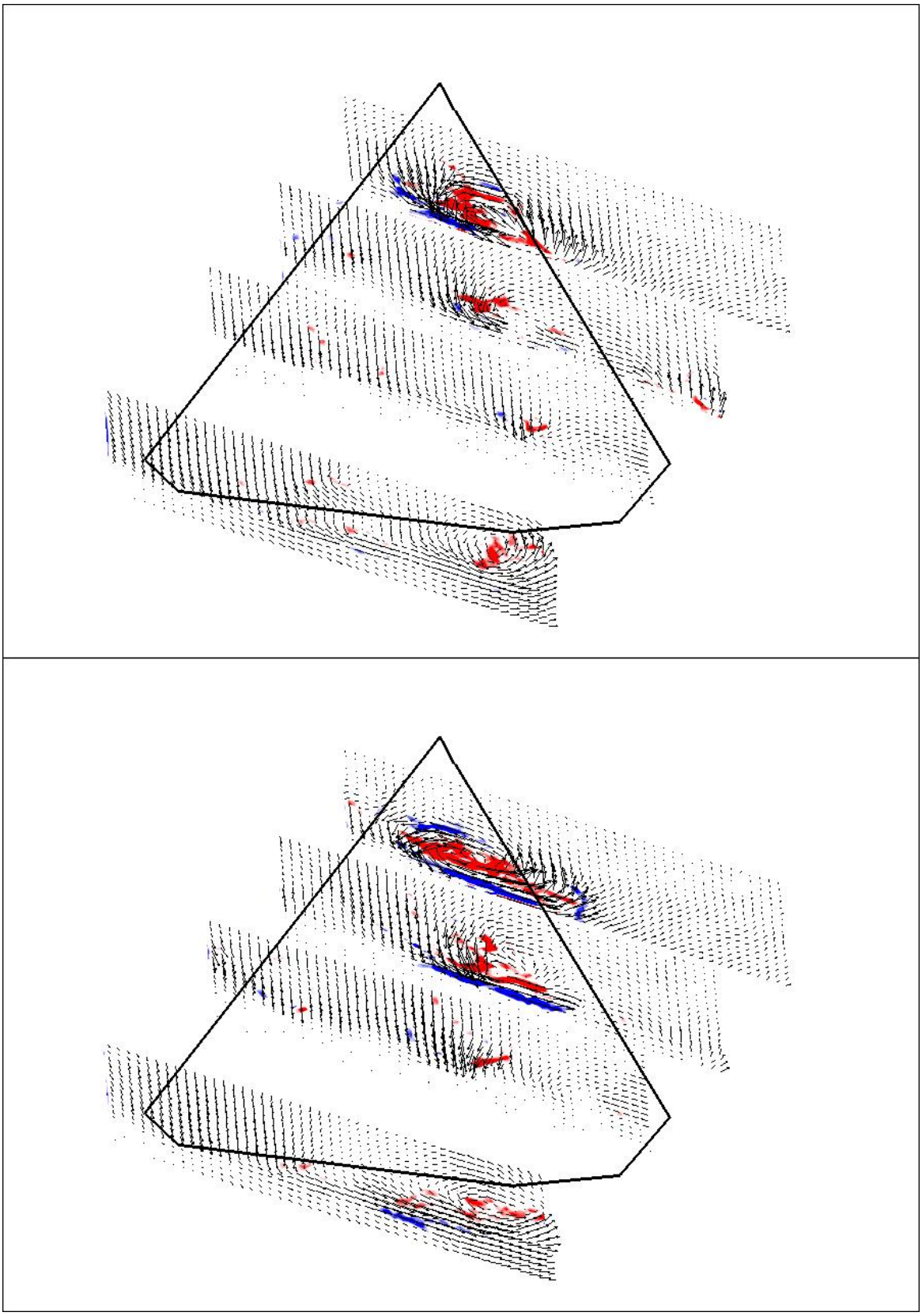

Figure 4-16c: Three-dimensional view of Trefft planes with control at t=4T/8 and t=5T/8.

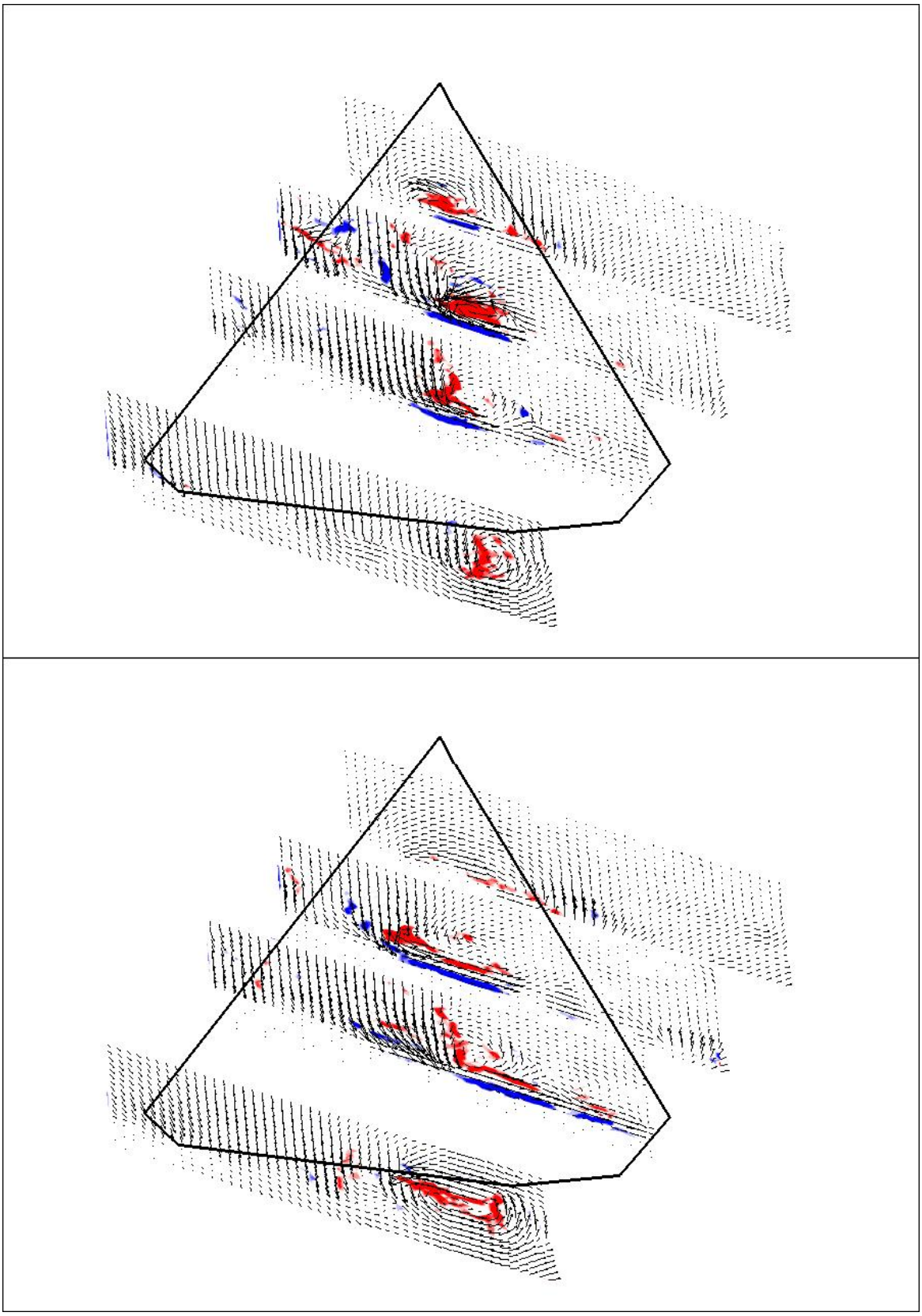

Figure 4-16d: Three-dimensional view of Trefft planes with control at t=6T/8 and t=7T/8.

5. Flow Control over Swept Wings and Wings with Diamond Shaped Planform

Wings swept by 30 to 40 degrees are today very common on fighter aircraft. And yet, there is very little work devoted to the understanding of the aerodynamics of such wings. In this chapter paper we study the aerodynamics and the flow control of two sharp-edged wing models. Two control mechanisms are employed, an oscillating mini-flap and a pulsed jet. Our Model A is a finite wing with parallel leading and trailing edges and a rectangular tip. This wing is swept by 0°, 20°, and 40°. Our Model B is a wing with a diamond-shaped-planform, with a leading edge sweep of 42°. Surface pressure distributions are obtained and the control flow results are contrasted with the no-control cases. Our results indicate flow control is very effective at 20° sweep, but less so at 40° or 42°. It was found that steady spanwise blowing is much more effective at the higher sweep angle.

Nomenclature

α= Angle of attack
b= semi-span
c = root chord
h= slot height
l= slot length
T= period of pulsing jet
x,y,z = coordinate system (see Fig. 3)
U_∞ = Characteristic velocity (free stream)
u_{jet} = Pulsating jet velocity
C_μ =momentum coefficient = $(\rho_{jet} u_{jet}^2 h l) / (\rho_\infty U_\infty^2 2b c \sin\alpha)$
$f_{shedding}=0.21U_\infty /(c \sin\alpha)$
$f_{actuating}$=driving frequency
$F=f_{actuating}/f_{shedding}$

5.1 Introduction

Wings with sharp leading edges are most efficient at supersonic speeds. They also significantly reduce radar signature. But at low speeds, sharp-edged wings have notoriously poor aerodynamic performance, and require large leading-edge flaps for take-off and landing, or for low-speed maneuvering. Flow control can generate extra lift over sharp-edged wings at low speeds, and has proven to have an effect equivalent to the deployment of a large leading-edge flap[1-5].

There is a considerable volume of literature for steady flow over sharp-edged wings swept by over 40°, and the vast majority of these contributions deal with delta wings. But for a wing with sharp leading and trailing edges, at zero sweep angle, the authors were able to find only a NACA report published about fifty years ago[6]. The first authors that reported efforts to control the flow over wings with sharp leading edges are Zhou et al.[1] Since then, the present team has published a sequence of papers[3-5,7,8] on the flow control of sharp-edged wings at low to moderate angles of attack and sweep angles varying between zero and 40°.

Research on delta wing flows for sweep angles as low as 50° indicate that delta wing vortices are present, but break down very close to the leading edge[9-13]. In fact, even before break down, these vortices display wake-like flow where the velocity is very low in the core of the vortex. In some cases[4] it was found that the low-aspect-ratio wing at medium angles of attack does not behave like a delta wing but rather like an unswept wing. A sweep angle of 50° is not low enough to demonstrate the transition from the vortex breakdown stall to the two-dimensional unsteady stall. More recently, Yaniktepe and Rockwell[13] studied the flow over a wing with a sweep angle of 38.7°. They provided evidence that up to an angle of attack of 25°, the flow appears to be dominated by delta wing tip vortices. At the highest angle of attack, the vortices seem to be displaced inboard. But more detailed measurements along planes parallel to the free stream[7] indicate the presence of multiple axial vortices, as well as separated flow patterns similar to those observed over unswept wings. The most common sharp-edged airfoil section studied is the circular-arc airfoil which has been employed both in laboratory studies[6] as well as in aeronautical applications. The flow over airfoils with sharp leading and trailing edges separates at angles of attack as low as 6°.

Zhou et al.[1] and Miranda et al[3] placed a min-flap at the leading edge of the pressure side of sharp-edged wings, and demonstrated that oscillating this mini-flap could lead in the average to lift increases of up to 70%. The present authors designed a pulsed-jet actuator, in order to demonstrate that similar effects with those of oscillating mini-flaps could be achieved pneumatically[4]. But the sections of Zhou et al.[1] and Rullan et al.[5] had a thickness ratio over 10%. As it turned out, the flow over thick sharp-edged airfoils does not separate massively, even at angles of attack as high as 9°.

We should emphasize here that we control fully separated flow. In earlier contributions on airfoil flow control the aim was to delay separation and stall altogether. The control of fully-separated flow has received so far less attention, even though it has a greater potential in defense applications. Such flows are encountered over sharp-edged wings at low to moderate angles of attack or over wings in deep stall. The idea is to accept the fact that in some situations, the flow is fully separated, and periodic shedding of vortices is established. The aim then becomes to control the dynamic development of vortical structures in order to improve the performance of the lifting surface. These are the type of flows that develop over wings moderately swept and the focus of the present research.

The present team has undertaken an exhaustive study of flow control over swept and unswept edges at low and intermediate angles of attack using both oscillating mini-flaps and pulsed jet actuators. Experiments were carried out at Reynolds numbers ranging 10^4 to 10^6. We reported earlier[7] results obtained in a water tunnel for a wing with a leading edge swept by 40°. For this case we presented exhaustive PIV time-averaged and time resolved, data for steady flow. In the present paper we present pressure data obtained over two models, tested in two wind tunnels, at Reynolds numbers of 5×10^4 and 10^6. The first model, Model A is a circular-arc airfoil, with parallel sharp leading and trailing edges. This was mounted at its root, and thus allowed the examination of tip effects, at sweep angles of 0°, 20° and 40°. The second model, Model B, is a trapezoidal wing with a sweep angle of 42°, and a planform typical of modern fighter aircraft. Model A was equipped with the pulsed-jet actuator developed by the present team[4,8]. Model B was equipped with oscillating min-flaps and spanwise blowing nozzles.

5.2 Facilities, Models and Equipment

5.2.1 Facilities and Models

Two wind tunnel facilities were used, the ESM Wind Tunnel and the VA Tech Stability Wind Tunnel. The first is a low-speed tunnel with a 20”x20” test section. Basic ideas and instrumentation are tested there before moving on to the other tunnel.

The second facility, the VA Tech six-foot subsonic wind tunnel (Figure 5-1), originally the NACA Stability Wind Tunnel is classified as a continuous, closed-jet,

single return, subsonic wind tunnel. One of our models mounted on the tunnel sting is shown in Figure 5-2. The tunnel is equipped with 25-foot interchangeable, round and square test sections of six foot cross section. The tunnel is powered by a 600 hp DC motor driving a 14 foot propeller that provides a maximum speed of 230 ft/sec and a Reynolds number per foot up to $1.4X10^6$ in a normal 6'x6' configuration. The settling chamber has a contraction ratio of 9 to 1, and is equipped with seven anti-turbulence screens. This combination provides an extremely smooth flow in the test section. The turbulence levels vary from 0.018% to 0.045% depending on the free-stream velocity. The average velocity fluctuation across the test section is about 0.5%, and flow angularities are limited to 2° maximum. The settling chamber is 9 feet long and the diffuser has an angle of 3°. The ambient temperature and pressure in the test section are nearly equal to the ambient outdoor conditions due to the presence of an air exchanger. During testing, the control room is maintained at the same static pressure as the test section.

Figure 5-1: The VA Tech Stability Tunnel, view from Randolph Hall

Figure 5-2: Diamond planform wing mounted on the Stability Tunnel sting.

We carried out experiments with two basic models. Model A (Figure 5-3) is a rectangular circular-arc wing that can be mounted at different sweep angles, and angles of attack. In the past we have tested two similar wings at low and high Reynolds numbers, with both oscillating mini-flaps and unsteady leading-edge blowing (Miranda et al.[3], Rullan et al.[8]). The present model, Model A has a smaller thickness ratio (10%) and a larger aspect ratio that improves the delivery of pulsed jets. This model was mounted on the floor of the tunnel via a mechanism that allowed the setting of the angle of attack at any desired value and the sweep angle at the values of 0°, 20° and 40°. The model tip reached only close to the middle of the tunnel, and thus the mounting allowed the study of three-dimensional effects with no interference of the opposite wall. This model is equipped with an unsteady jet actuator, which is described later. Pressure taps were placed along four chordwise lines on both the pressure and the suction side, as indicated in Figure 5-3. The spacing of the taps was smaller on the front part of the model. The four stations are labeled with Roman numerals as shown in the Figure.

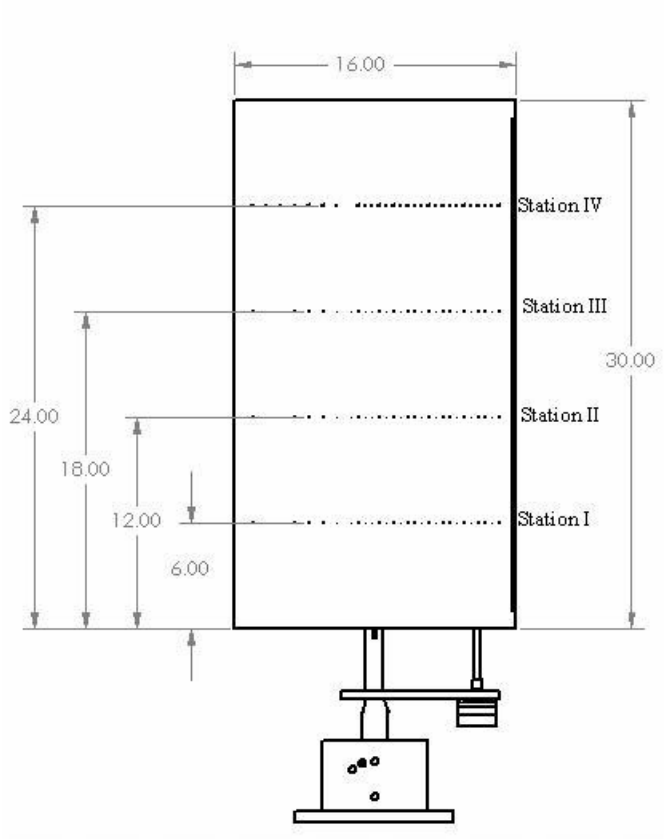

Figure 5-3: Model A showing the pressure tap strips. Also shown is the motor that drives the pulse-jet actuator

Our second model, Model B (Figure 5-4) is a diamond-shaped-planform wing with a leading-edge sweep of 42°. This model is a stainless-steel model on loan by Lockheed Martin, equipped with pressure taps. The flow over this model is controlled by an oscillating mini-flap device, similar to the one already tested on circular-arc wing sections[3]. The spanwise stations are numbered with numerals starting from the root side of the wing. We have also designed, constructed and tested two similar but smaller diamond-shaped-planform wings that were tested in our water tunnel and in our low-speed wind tunnel at low Reynolds numbers.

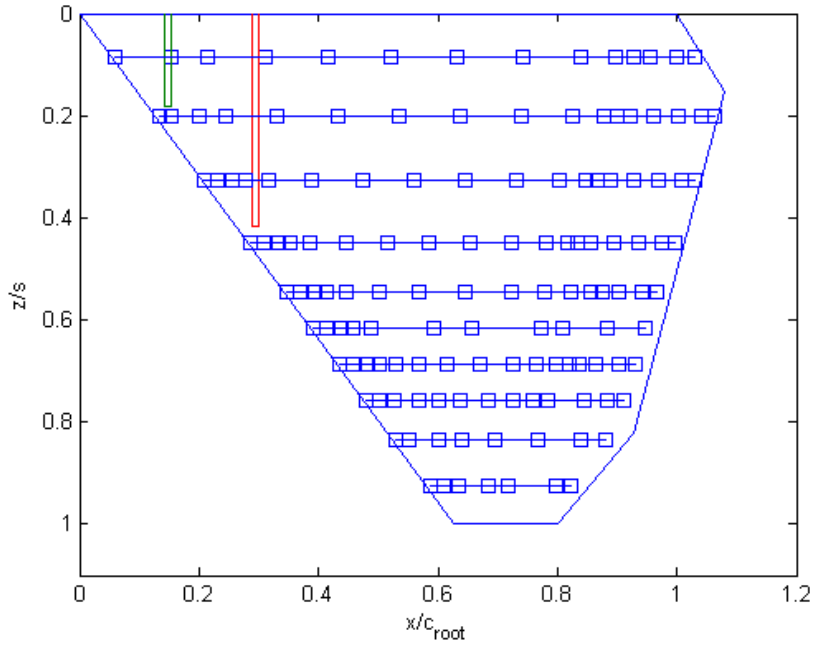

Figure 5-4: Model B, showing pressure tap locations and spanwise blowing nozzles. Ten chordwise stations are shown, Station 1 starting from the root side to the wing tip.

Pressure scanners were employed to monitor the pressure distributions over wind tunnel models. Two 32-channel ESPs by Pressure Systems Inc. monitor the pressure distribution along spanwise stations over both models. Data were obtained along four stations over the span of Model A and along ten stations over the suction side of Model B and seven stations over its pressure side.

5.2.2 Equipment

Pressure scanners by Pressure Systems Inc. have been extensively used in our laboratory. These scanners are small, high-density packages containing multiple differential sensors. ESP packages contain 8, 16, 32 or 64 channels. Each pressure sensor is a miniature piezoresistive pressure transducer, and all of the pressure transducers in a module share a common silicon substrate. The output of each transducer is internally amplified to ±5 V full-scale, and these analog outputs are multiplexed within the scanner. The settling time inherent in the multiplexer corresponds to a maximum sampling rate of 20 kHz. This allows near-simultaneous sampling of the ESP. For instance, thirty-two ports can be sampled in 1.6 ms. However, the pressure port geometry limits the frequency response of the ESP to 50 Hz at the pressure inputs. Since the

transducers are differential, a reference pressure must be chosen. In all cases in the present work, the reference pressure was the tunnel free-stream static pressure. The static accuracy of the ESP's, including nonlinearity, hysteresis and non-repeatability effects, is 0.10% of the full scale at constant temperature after a full calibration.

On many occasions, we have placed miniature ESP scanners inside the wind tunnel models, thus minimizing the length of the Tygon tubing. This allows the monitoring of dynamic phenomena with frequencies up to about 50 Hz, with less than 2% error in the peak values. Data over the 16-inch-chord model (Model A) described in the previous section were obtained with the pressure scanner located at the supporting base. To obtain pressures over Model B, we mounted the pressure scanners near the root of the wing.

5.2.3 Flow Control Mechanisms

The actuation mechanism on Model A consists of a pressurized plenum, essentially the inside of the entire wing, and a valve that allows a jet to issue out of the plenum. This valve consists of two concentric cylinders shown in Figure 5-5. This is essentially the leading sharp edge of the airfoil. The inner cylinder, a 7/16"-inch diameter brass tube has two 1/16" wide slots, which span its length. This cylinder is mounted on five bushings and rotates about a fixed axis inside a fixed outer cylinder created in the machined wedge. The inner cylinder was attached to drive shaft so that it can be driven by a small DC motor as shown in Figure 5-3. The last two bushings are used to stabilize the tube in the machined leading edge but allowing rotation at the same time. All the bushings were press-fit to insure that the inner and outer cylinders are sealed tightly in order to maintain sufficient pressure in the inner cylinder.

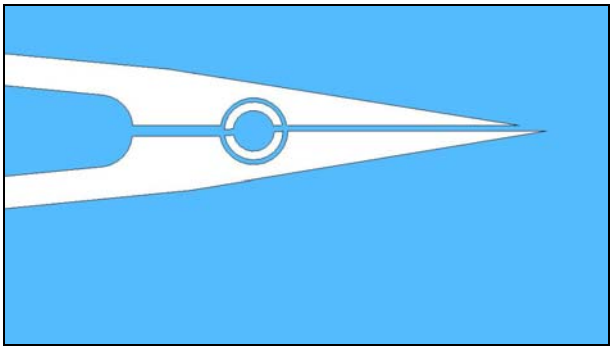

Figure 5-5: The leading edge of Model A showing the pulse-jet actuator.

This device operates as follows. The plenum is continuously supplied with high-pressure air and is driven in rotation at a fixed frequency. When the slots of the inner rotating tube and the fixed outer tube match, as shown in Figure 5-5, the pressurized cavity releases air in the form of a jet. The flow is guided by the 1/16-width duct and released very close to the apex of the wedge. When the slots of the inner and the outer cylinder do not match, the passage is closed but some air leaks between the two cylinders and finds its way through the duct. The jet therefore has a non-zero mean component with an unsteady flow superimposed. Our earlier experimental data[8] indicate that the efficiency of this actuator is practically independent of the driving frequency. In Figure 5-6 we display the jet velocity time record and the corresponding power spectrum for one of the cases tested. This Figure indicates that if the cylinder is not rotating, leaking through the passage between the cylinders generates a steady jet, but when the inner cylinder rotates, a pulsing jet issues, and its wave form is clean, in the sense that most of the energy resides in a narrow frequency band around the driving frequency. The modified design employed in the work discussed here includes a larger plenum and proved that uniform and more powerful pulsing jets could be generated along the span of the airfoil. This means that the device is an excellent candidate for a robust flight actuator, where the required frequency is changing with aircraft speed and the angle of attack.

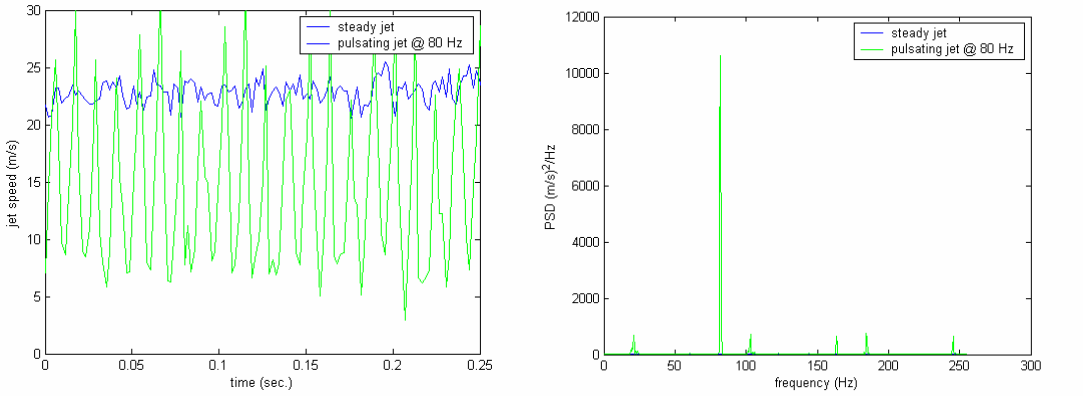

Figure 5-6: Jet velocity time series and power spectrum generated by the pulsed-jet actuator

A pulsed-jet actuation mechanism does not fit near the leading edge of Model B. Instead we employed an oscillating mini-flap that has proven to be equally effective with unsteady blowing[4,7,8]. Miniflaps we employed earlier were hinged downstream of the

leading edge and were flushed with the wing section when not deployed. The flap mounted on Model B was hinged right along the leading edge and thus protruded forward. Two flap configurations were tested; one that spanned half of the length of the wing, starting from the root and another that spanned the entire length of the leading edge. These miniflaps were oscillated by a brushless DC motor connected to a flywheel which is equipped with an eccentric shaft. The flywheel is balanced statically to work with minimum vibrations at speeds in the order of 100 Hertz. The amplitude of oscillation could be adjusted with an accuracy of ±1°.

The DC motor employed for both mechanisms is a Pittman brushless DC servo motor that operates at 24 VDC. It features 3 Hall sensors for feedback control so as to obtain linear torque. It is operated with an Allmotion EZSV23 servo motor controller which in turn is connected to a PC by a serial port. This provides a direct frequency control of the motor. A wire was connected from the output of one of the Hall sensors to obtain a read-out and to record the actual driving frequency.

5.3 Results and Discussion

5.3.1 Model A; Pulsed-Jet Actuation

Experiments were carried out in the VA Tech Stability Wind Tunnel with Model A, at a Reynolds number of one million, for three different angles of sweep, namely 0, 20 and 40 and several angles of attack. The pulsed-jet mechanism was activated at two different momentum coefficients. Data were also obtained with no actuation to provide comparison for the no-control case. The results are presented in Figure 5-7 through Figure 5-11 for a sweep angle of zero, Figure 5-12 through Figure 5-16 for an angle of 20° and Figure 5-17 through Figure 5-21 for an angle of 40°. In all these figures an underline feature of flow control must be observed. Regions of fully separated flow can be recognized by a relatively horizontal and flat pressure distribution. And regions of strong suction that appear like local humps of the pressure distribution may indicate a large vortex that is captured in this area of the wing. It is in these regions that the control mechanism is most effective. It should also be emphasized that for the angles of attack larger than 15°, the flow over sharp-edged leading edges cannot reattach. Our control mechanism therefore is modifying the development of vortices in the separated region. In all the figures of this section, we present pairs of frames, with the left frame

corresponding to Stations I and II, which are close to the root of the wing (see notation in Figure 5-3) and the right frame corresponding to Stations III and IV, which are in the outboard part of the wing.

The case of zero sweep tested here does not correspond to two-dimensional flow, because of the finite span of the wing. The tip effect is therefore significant. We are testing a finite wing, in order to expose the effects of flow control to the aerodynamics of the wing tip. Figure 5-7 indicates that a vortex is captured near the leading edge of the wing. Evidence to this effect was reported earlier by the present authors[8]. Further downstream, the flow in the inboard section is attached. Here actuation has little effect, confined mostly to the leading-edge region.

For higher angles of attach (Figure 5-8 to Figure 5-11), actuation is more effective. It is intriguing to note that actuation results in pressure distributions reminiscent of attached flow over airfoils, namely strong suction on the front that decreases sharply towards the aft region of the wing. What is surprising is that flow control is very effective in the outboard region as well. A possible explanation of this phenomenon is the following. In conventional finite wings with no control, reduction of local circulation and of pressure suction near the tip is due to the tip vortex, which is clearly a three-dimensional effect. Our actuation on the other hand activates and energizes vortices that are normal to the free stream, and thus parallel to the wing axis. It is the pressure imprints of these rolling vortices that when averaged, they produce the increased suction over the wing surface. Apparently the energizing of such vortices allows them to penetrate further in the outboard region and thus suppress that tip effects. This phenomenon is more pronounced at higher angles of attack (Figure 5-10 and Figure 5-11), where we observe that the increase in suction due to flow control is even stronger in the outboard region than in the inboard region. A surprising finding here is that actuation seems to be effective at much higher angles than those we have tested on other models. Working at lower Reynolds numbers and a model with oscillating flaps, we found that actuation effect was barely discernible at angles of attack higher than 15°.

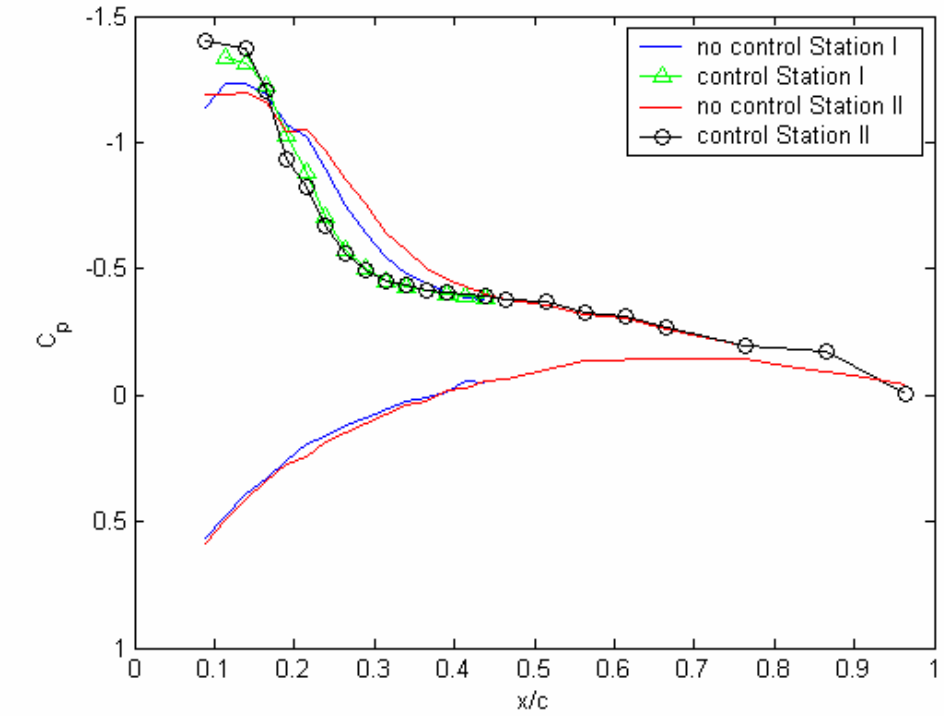

(a)

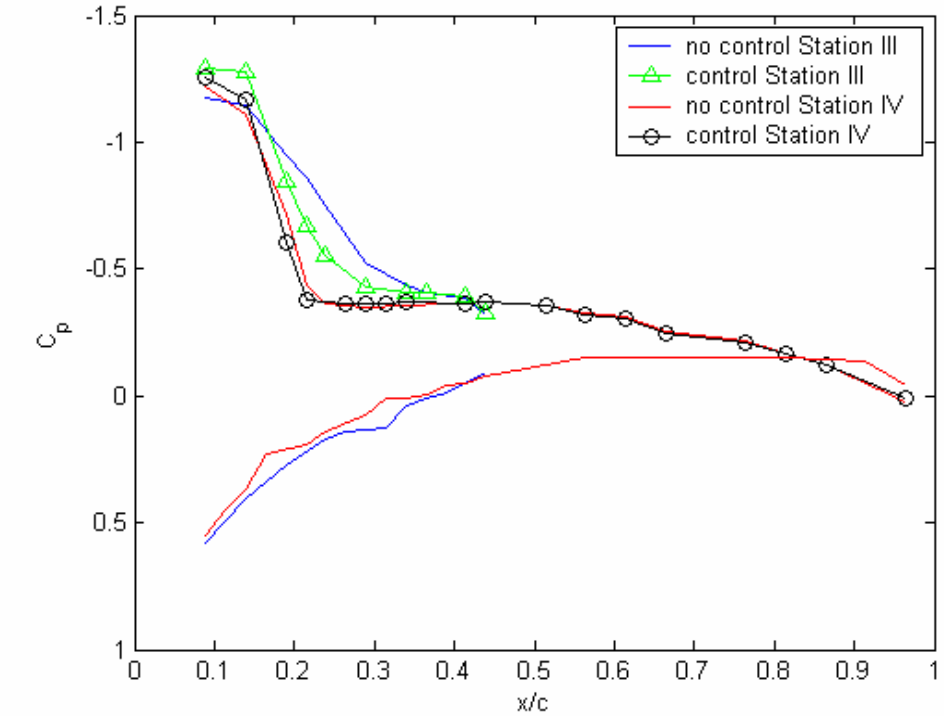

(b)

Figure 5-7: Pressure distributions for zero sweep at α=9°. Stations I and II (a); III and IV (b)

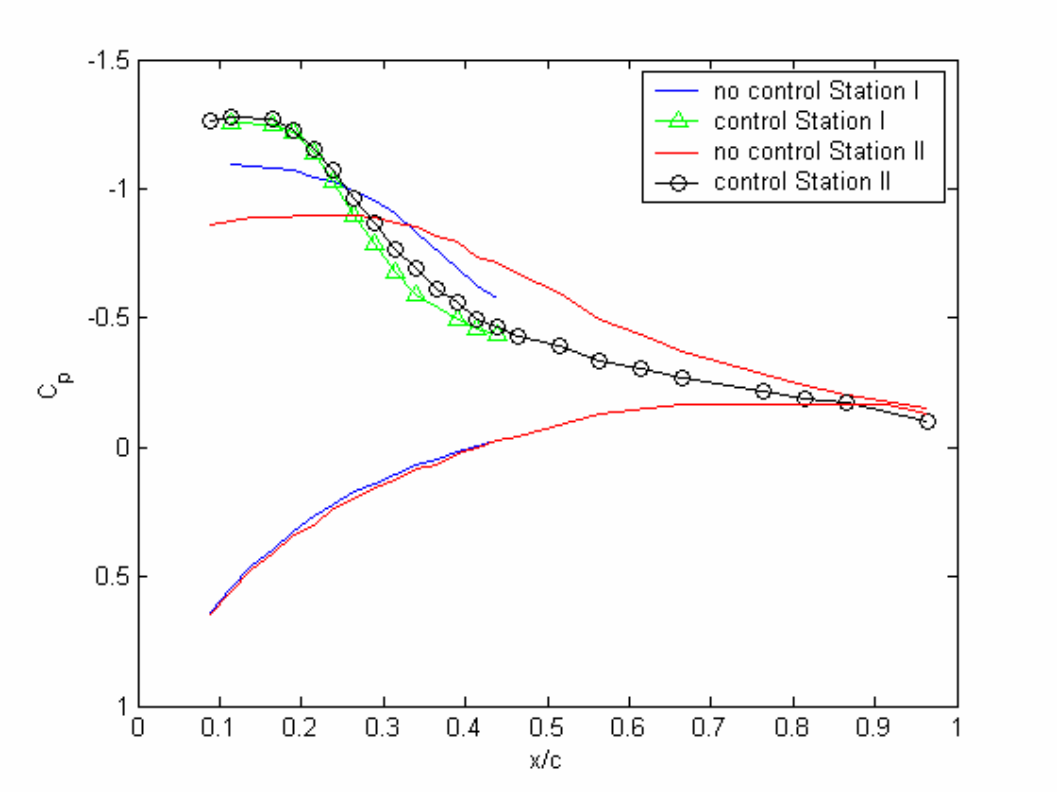

(a)

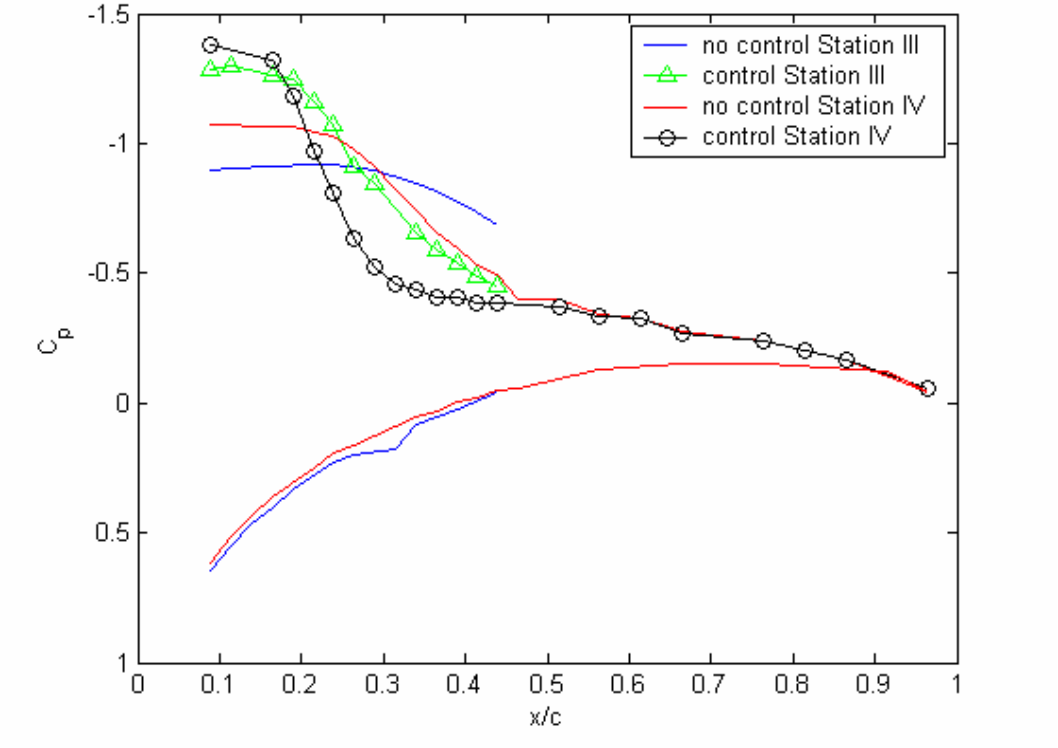

(b)

Figure 5-8: Pressure distributions for zero sweep at α=12°. Stations I and II (a); III and IV (b)

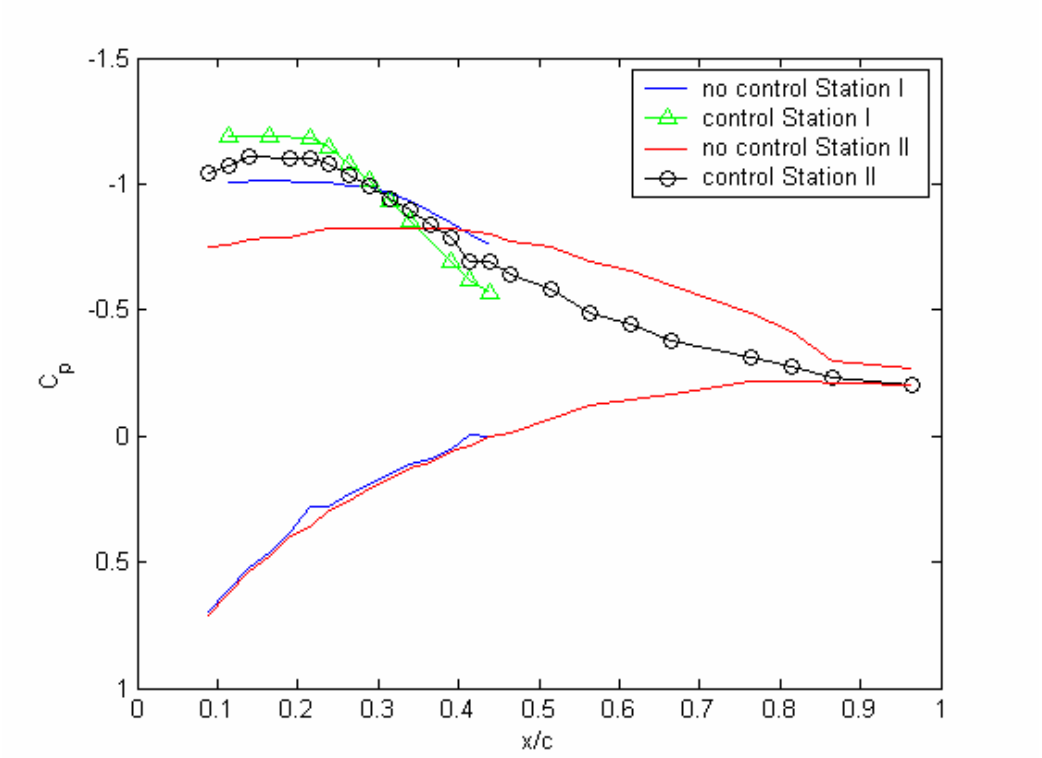

(a)

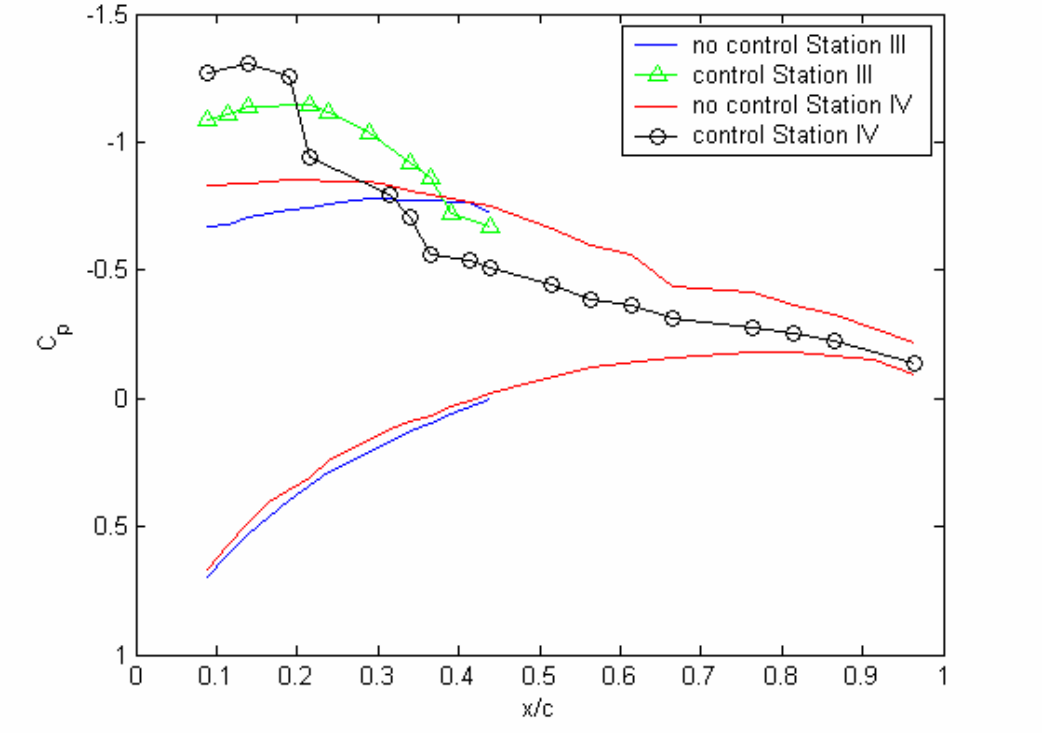

(b)

Figure 5-9: Pressure distributions for zero sweep at α=15°. Stations I and II (a); III and IV (b)

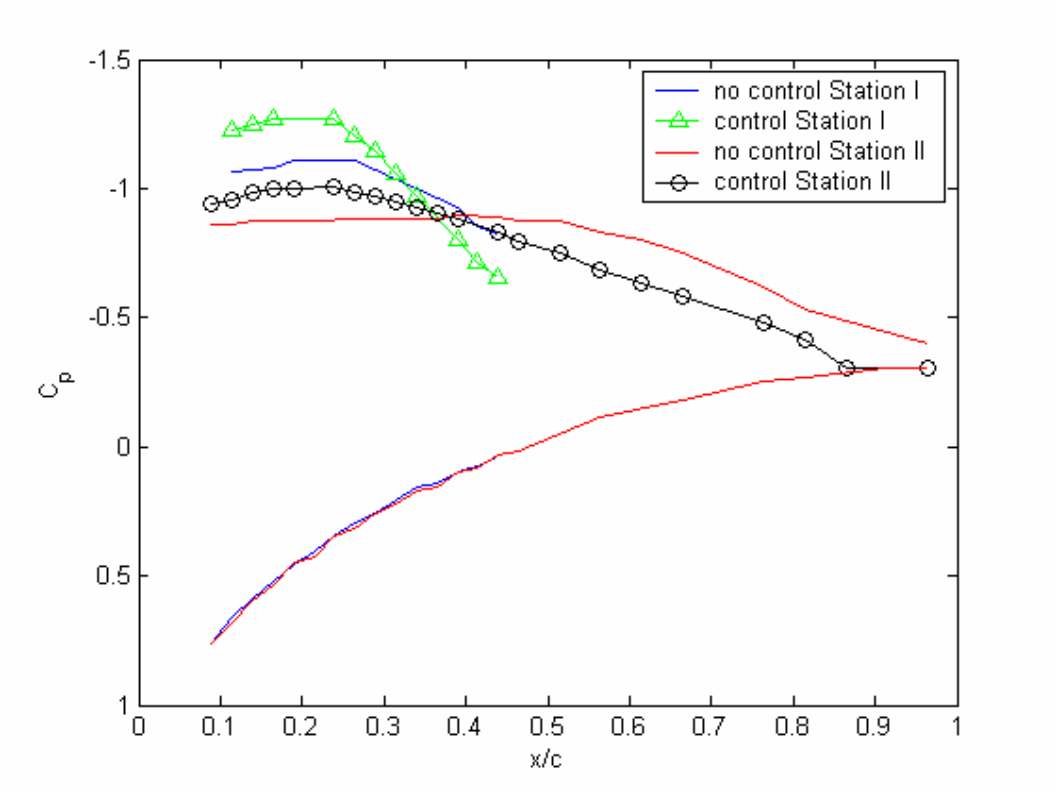

(a)

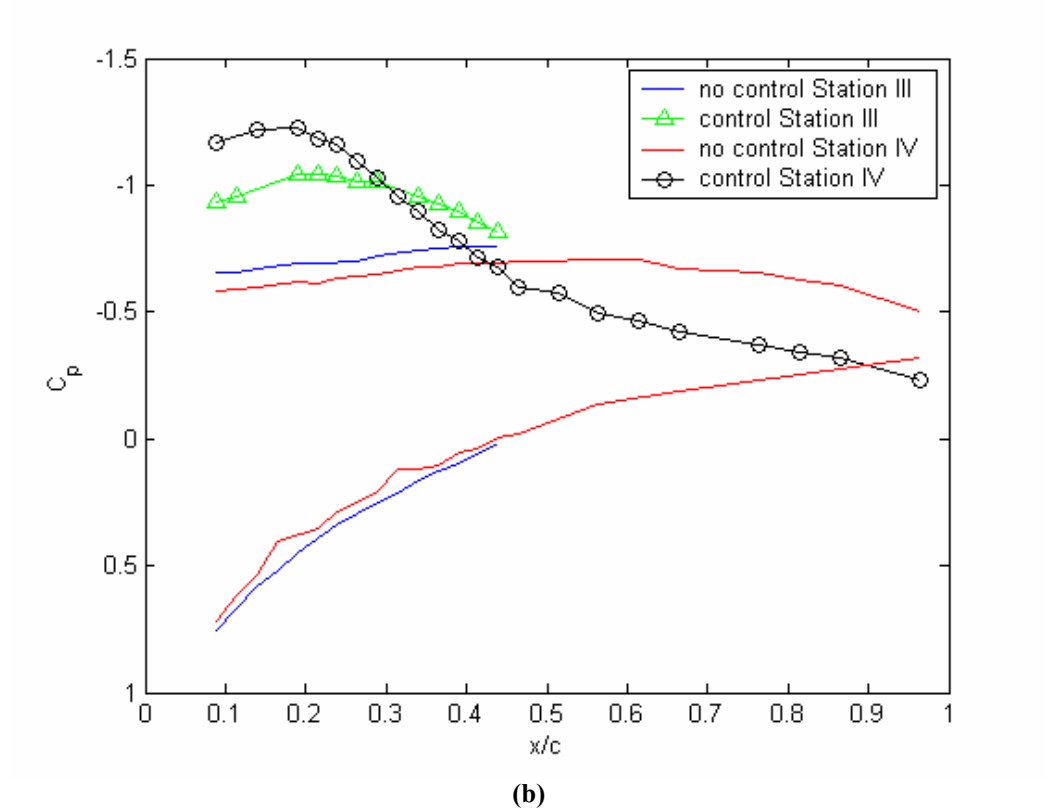

(b)

Figure 5-10: Pressure distributions for zero sweep at α=18°. Stations I and II (a); III and IV (b)

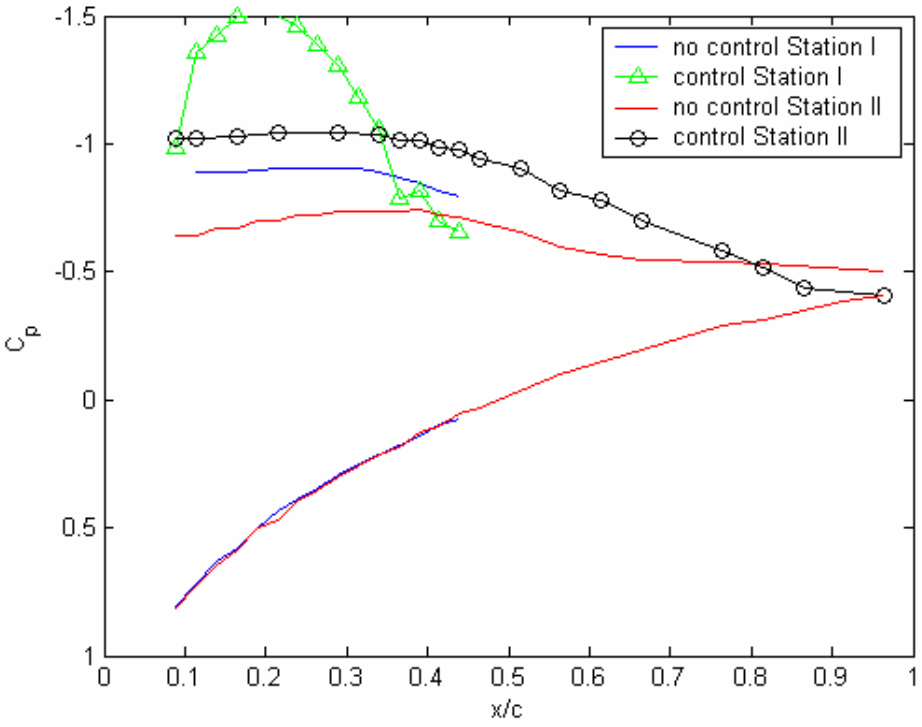

(a)

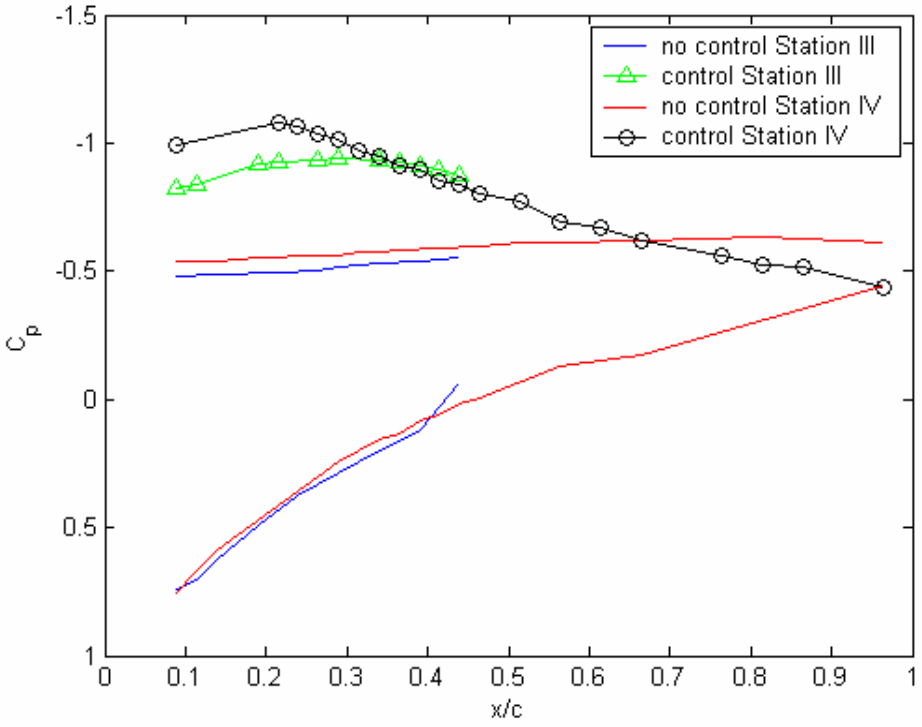

(b)

Figure 5-11: Pressure distributions for zero sweep at α=21°. Stations I and II (a); III and IV (b)

For a sweep angle of 20° (Figs. 12-16) the qualitative behavior is almost the same. We find that the curves are "drawn" to the right, and thus pressure patterns are stretched towards the aft of the wing. But the effect of the control is similar and perhaps even stronger. However, for a sweep angle of 40°, the effect of our flow control mechanism is reduced as shown in Figs. 17 to 21. The phenomenon of reduction in the effectiveness of actuation along the leading edge at high-sweep-angle wings has been observed earlier by the present authors[4] in experiments conducted at lower Reynolds numbers. The results for a sweep angle of 40° (Figs. 17-21) show considerable reduction in the effect of flow control. To achieve the same level of flow control, it may be necessary to increase the momentum coefficient beyond the value of 0.03 that was employed in all the tests discussed here. For angles of attack of 12° and 15° there is some increase in suction in the middle sections of the wing. We did not have the resources to test the case of a sweep angle of 30°.

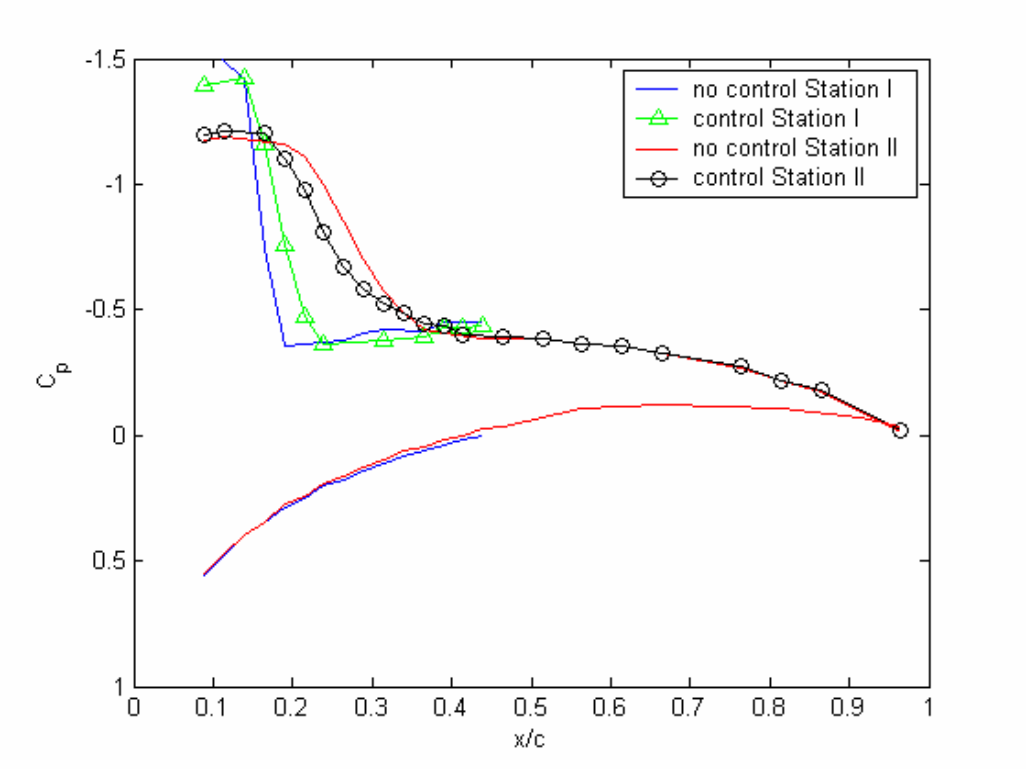

(a)

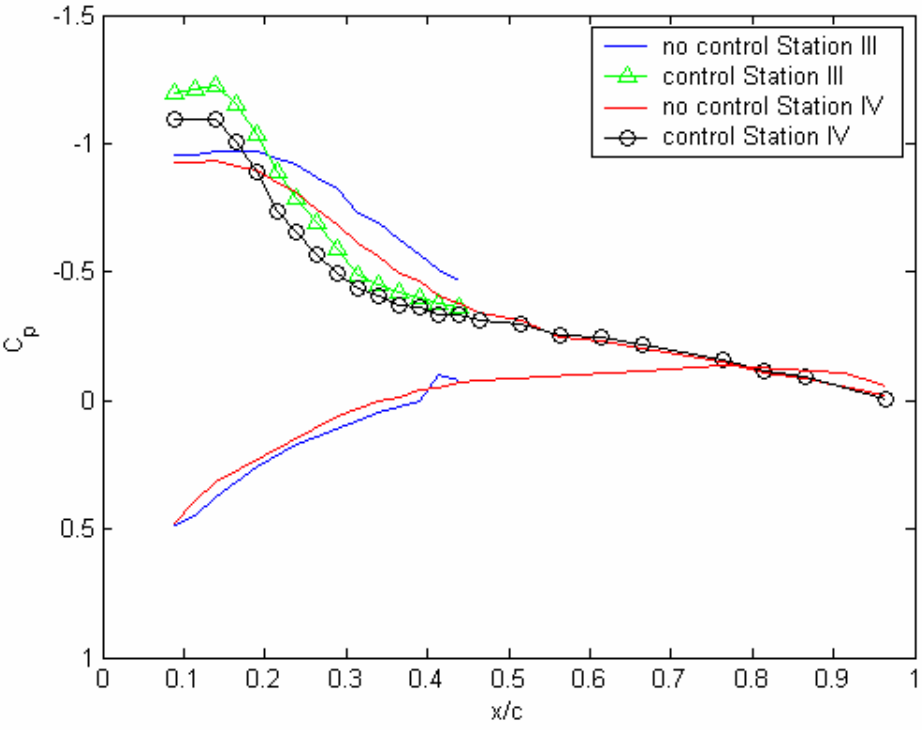

(b)

Figure 5-12: Pressure distributions for 20° sweep at α=9°. Stations I and II (a); III and IV (b)

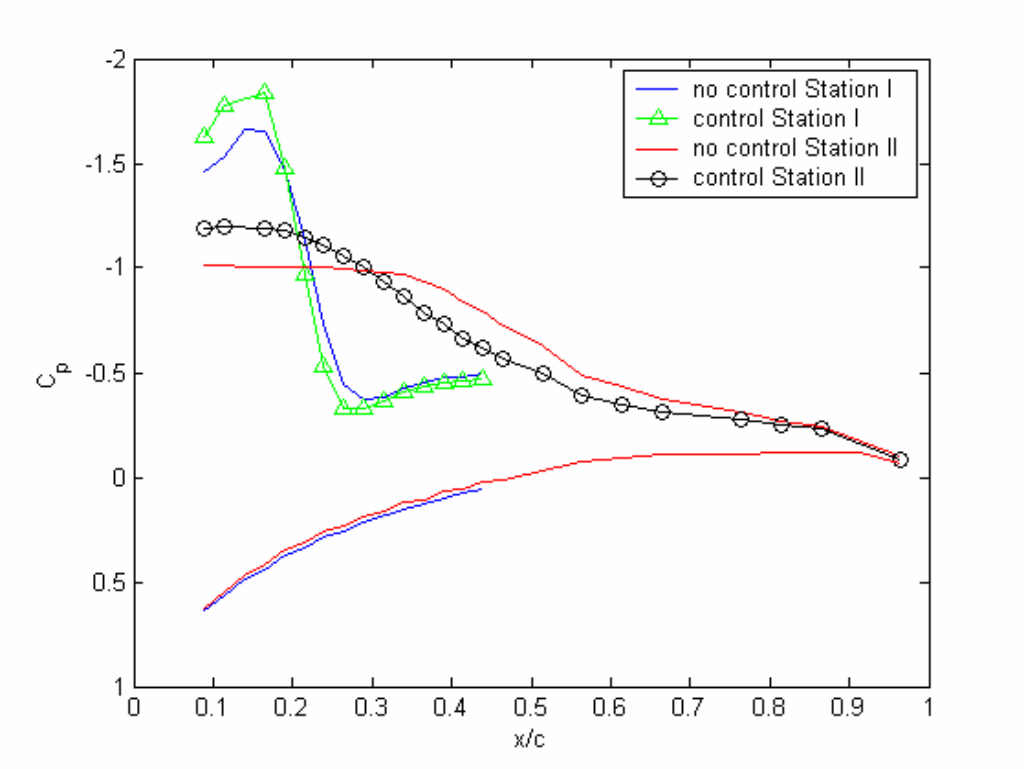

(a)

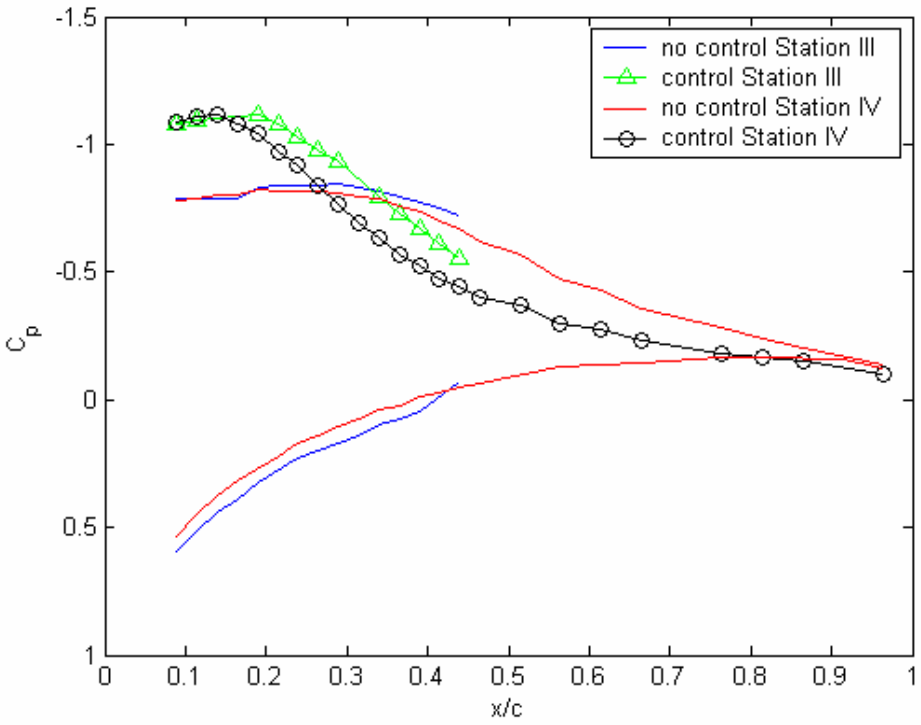

(b)

Figure 5-13: Pressure distributions for 20° sweep at α=12°. Stations I and II (a); III and IV (b)

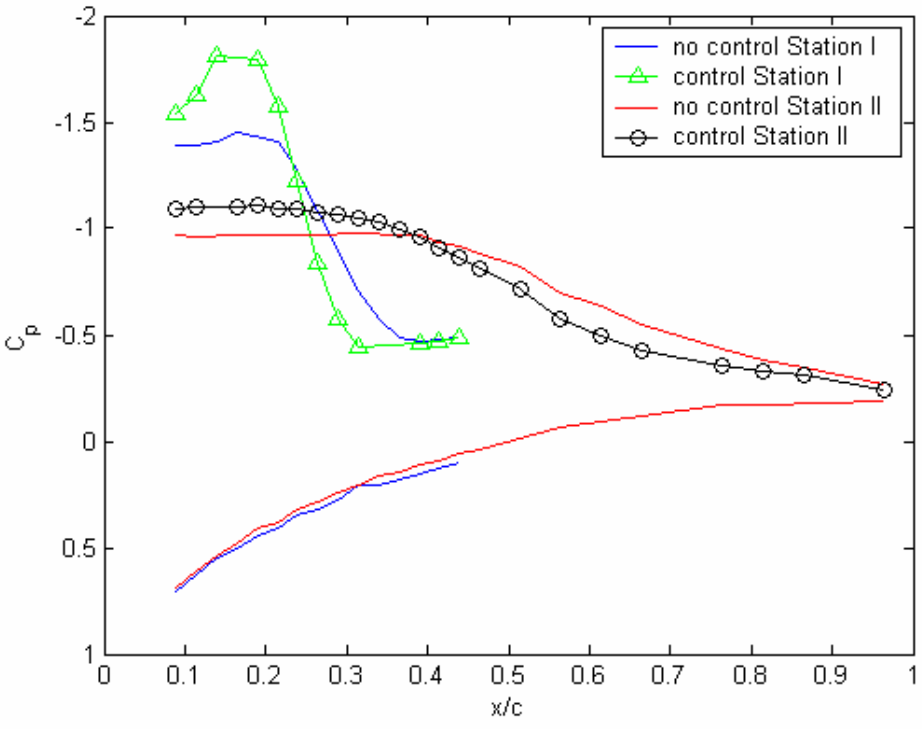

(a)

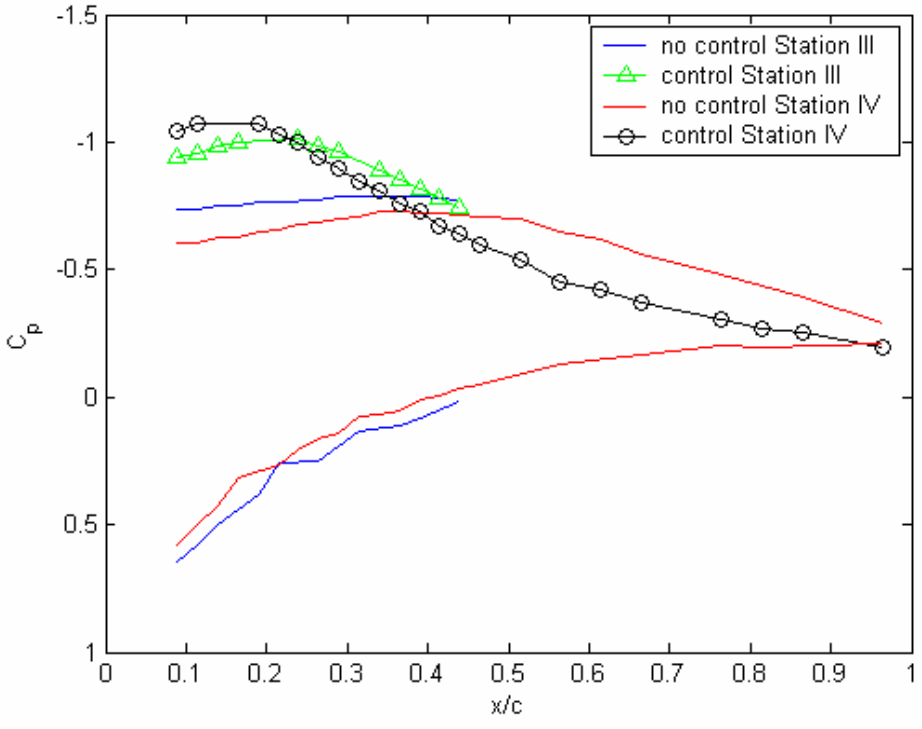

(b)

Figure 5-14: Pressure distributions for 20° sweep at α=15°. Stations I and II (a); III and IV (b)

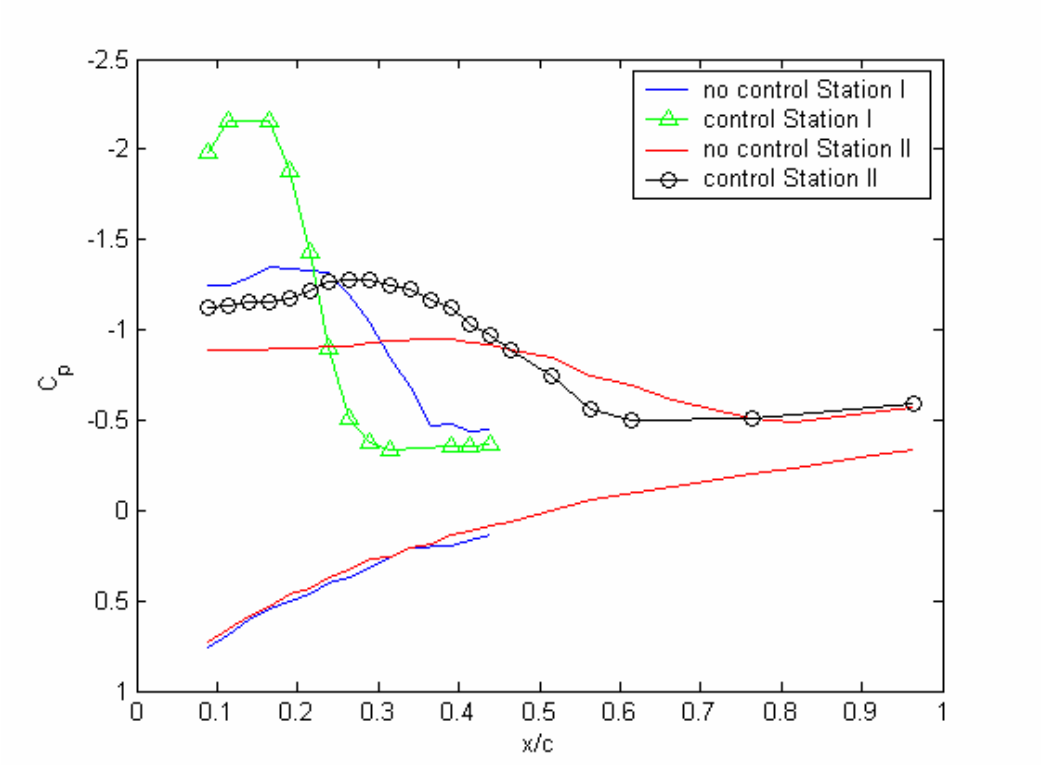

(a)

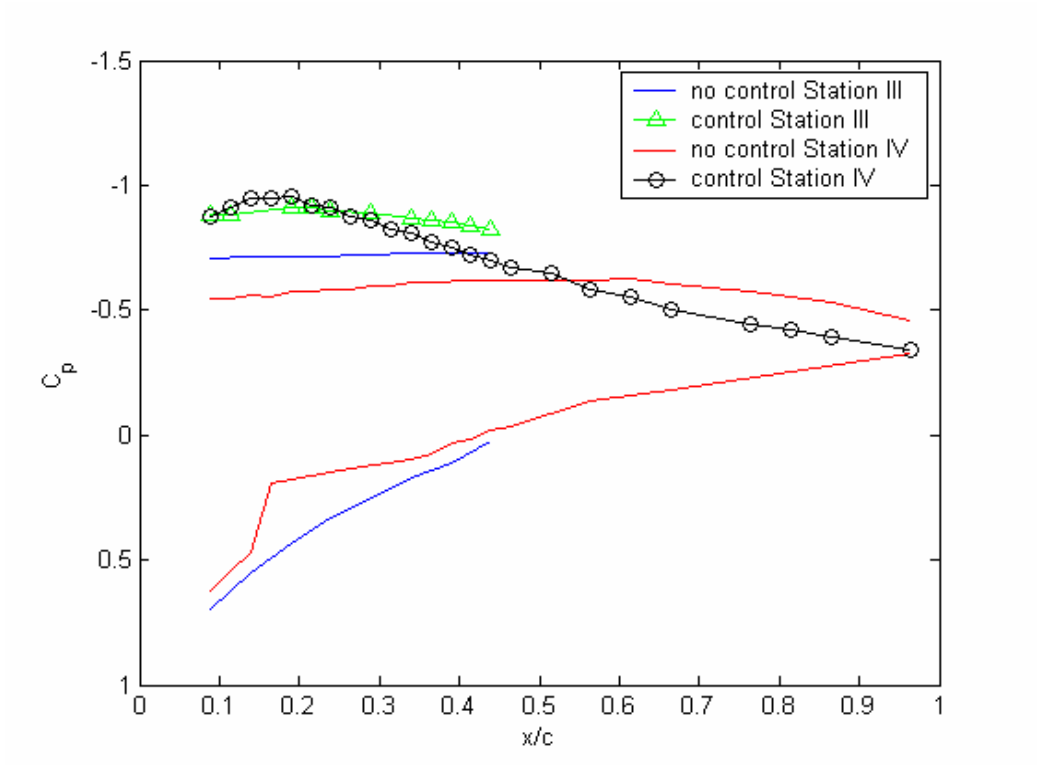

(b)

Figure 5-15: Pressure distributions for 20° sweep at α=18°. Stations I and II (a); III and IV (b)

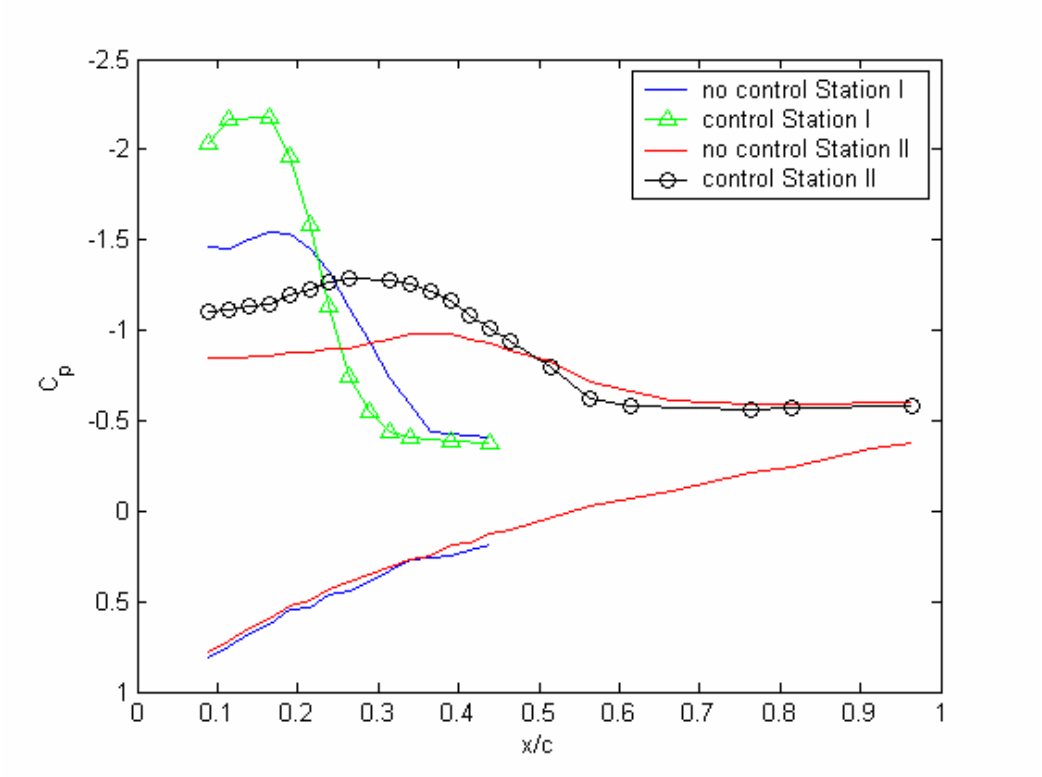

(a)

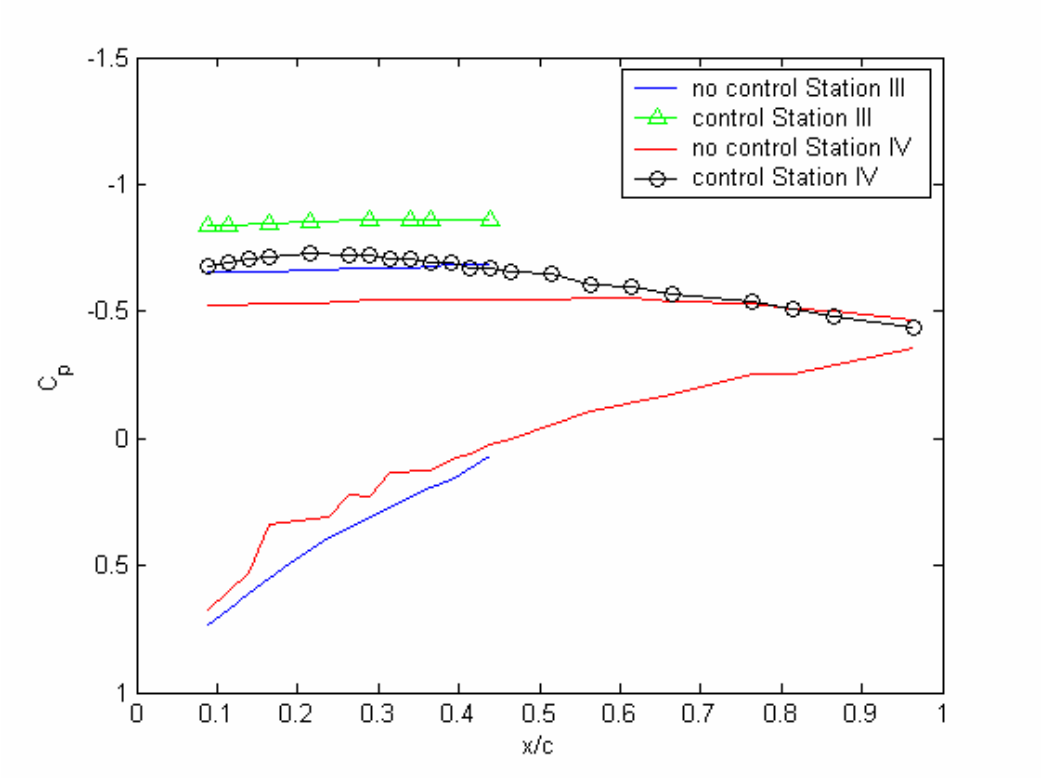

(b)

Figure 5-16: Pressure distributions for 20° sweep at α=21°. Stations I and II (a); III and IV (b)

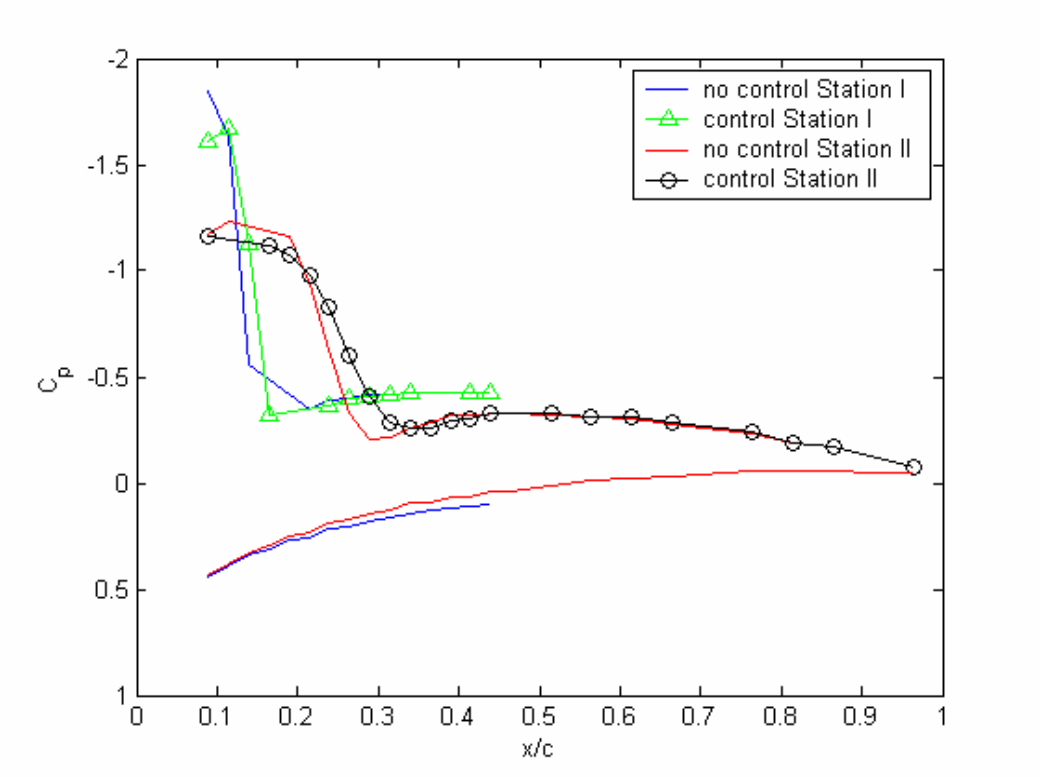

(a)

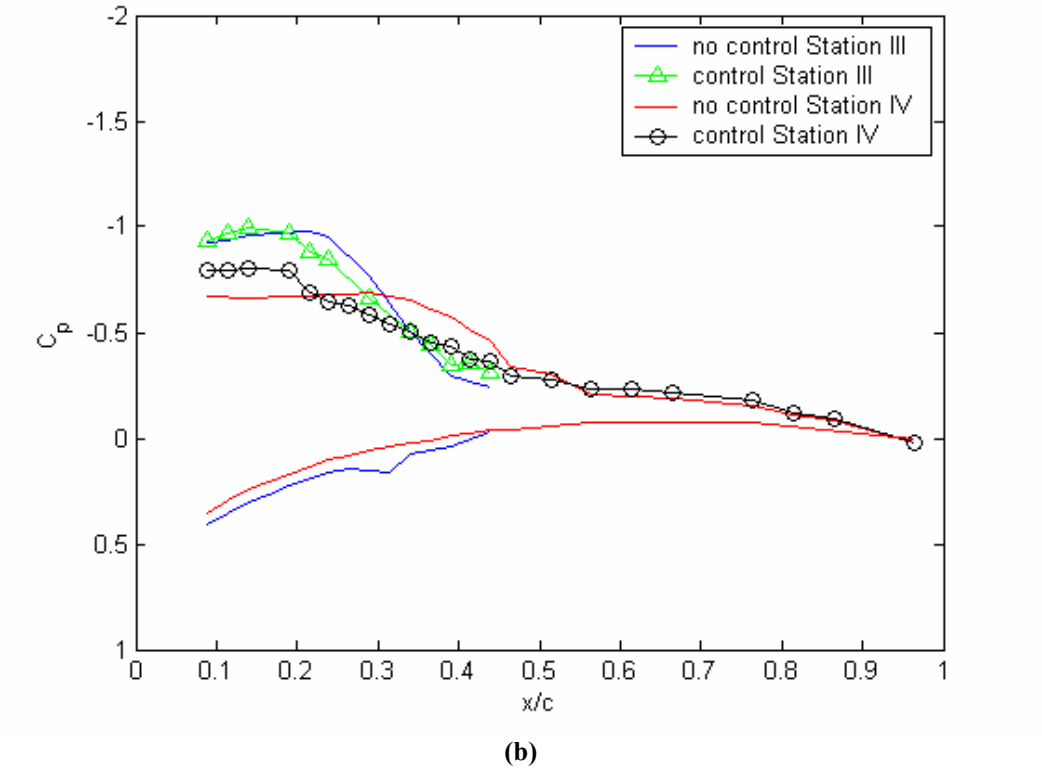

(b)

Figure 5-17: Pressure distributions for 40° sweep at α=9°. Stations I and II (a); III and IV (b)

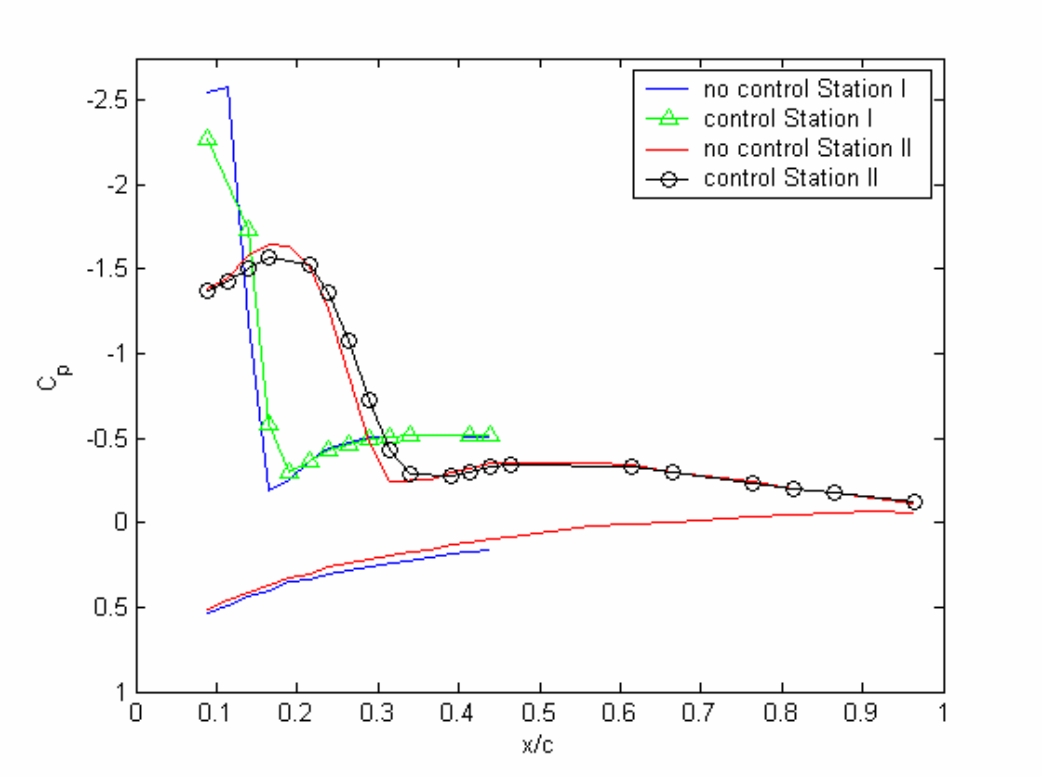

(a)

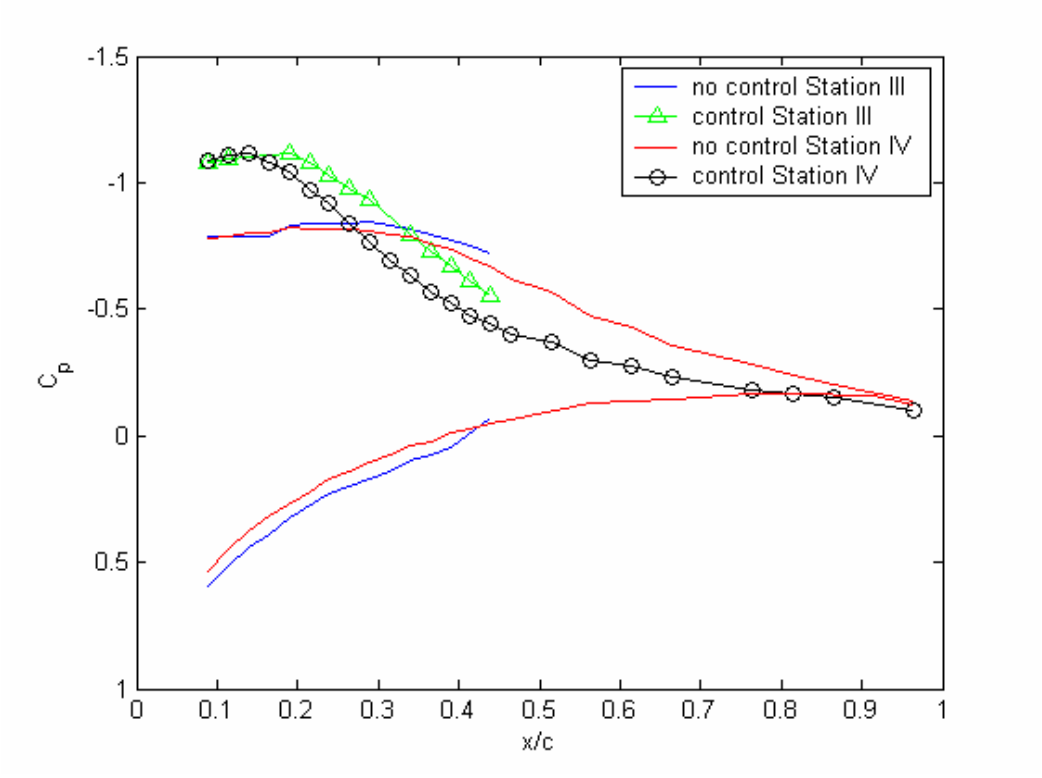

(b)

Figure 5-18: Pressure distributions for 40° sweep at α=12°. Stations I and II (a); III and IV (b)

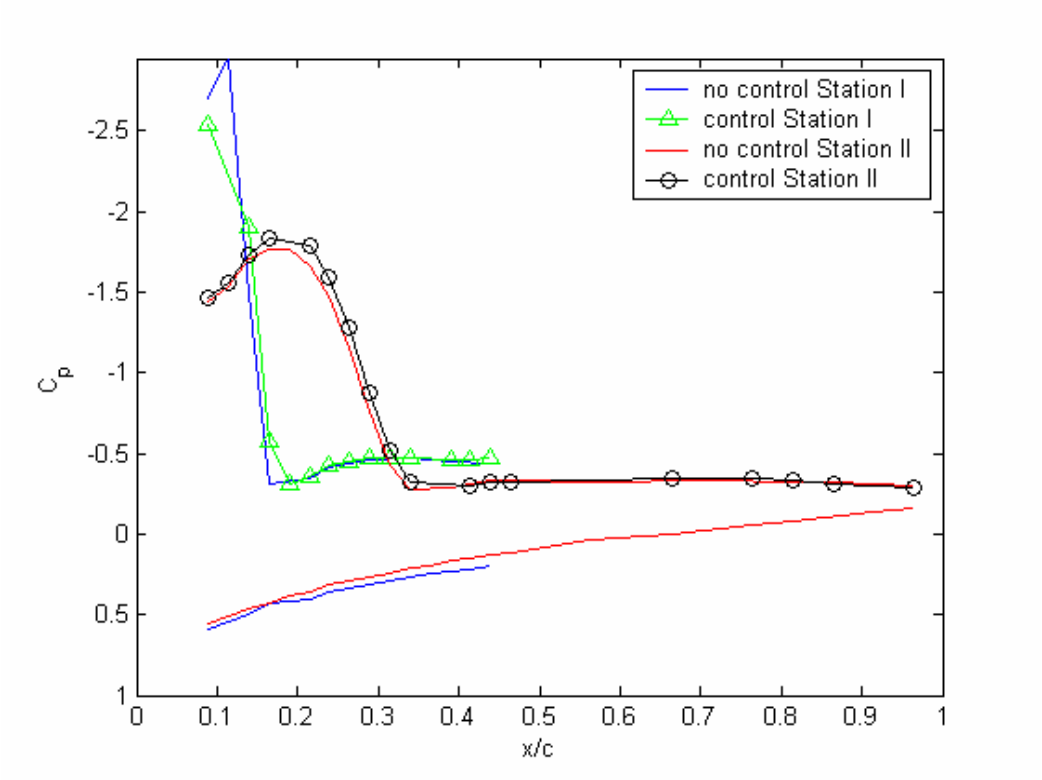

(a)

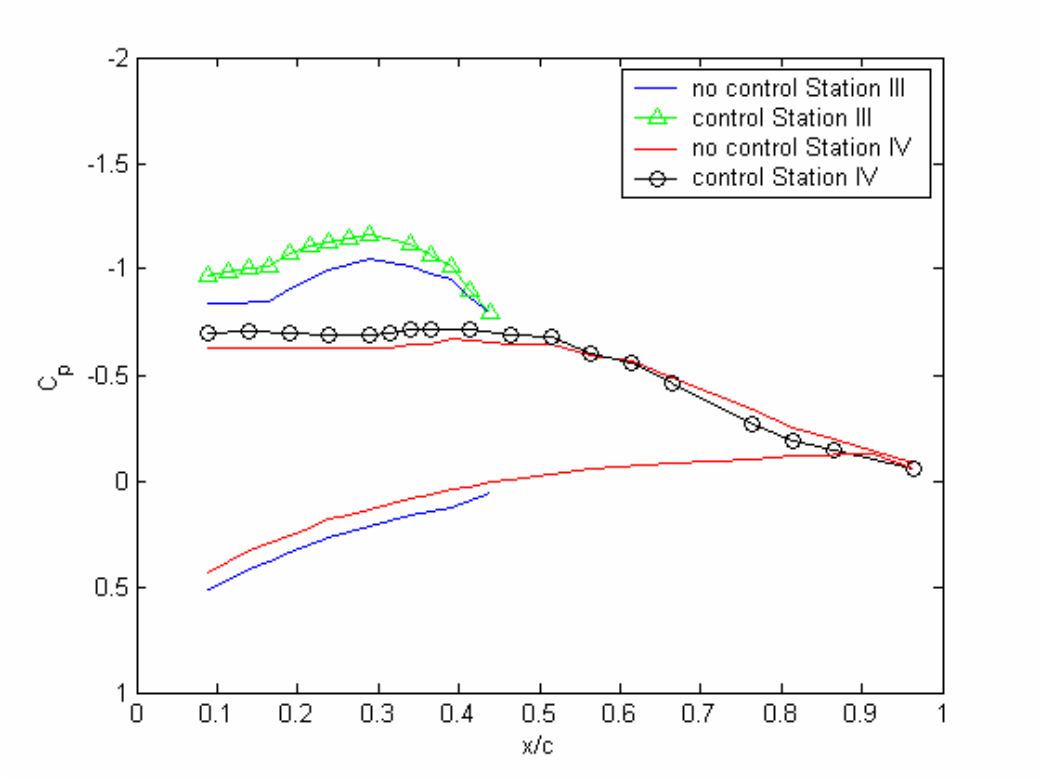

(b)

Figure 5-19: Pressure distributions for 40° sweep at α=15°. Stations I and II (a); III and IV (b)

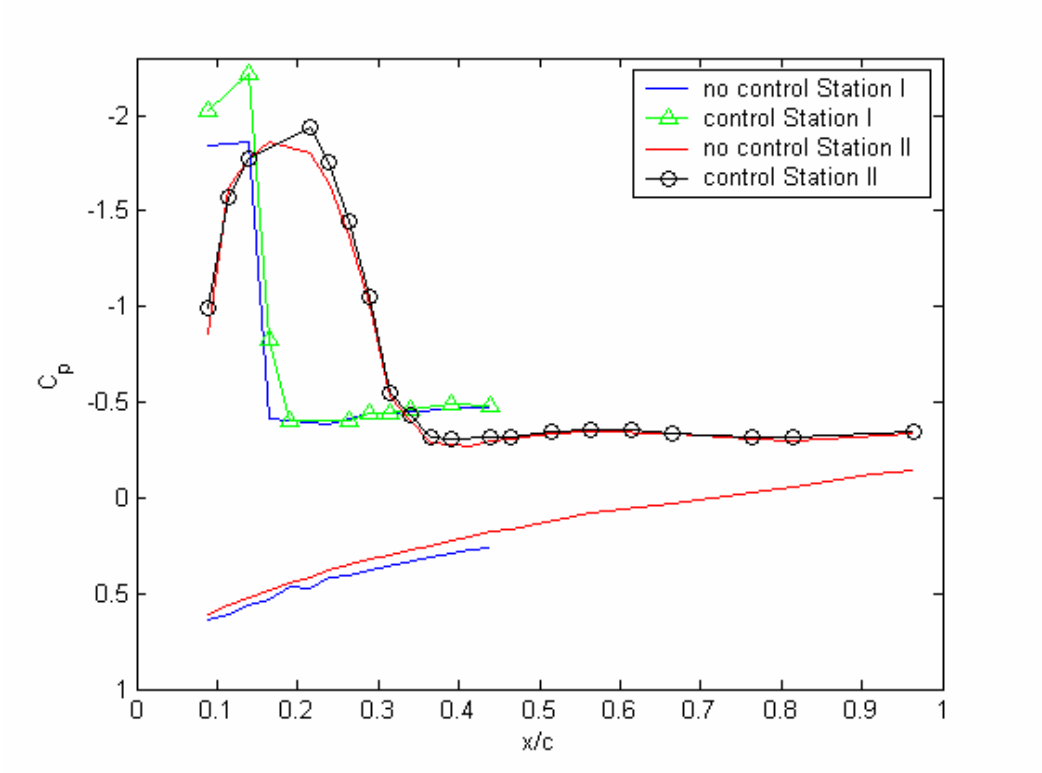

(a)

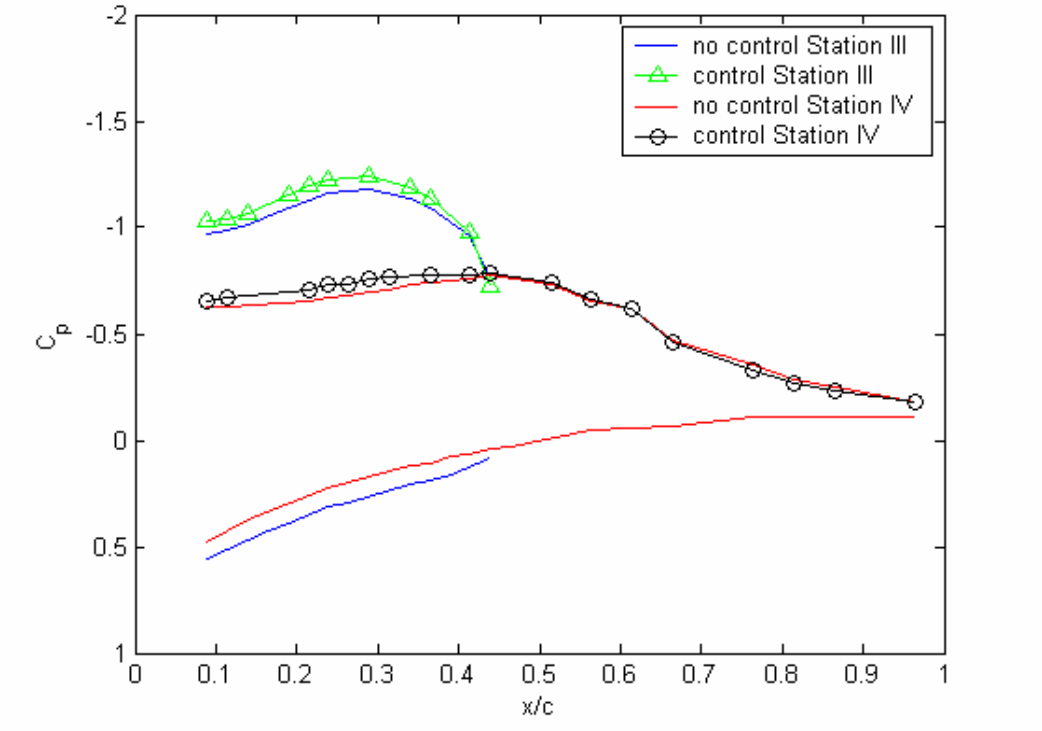

(b)

Figure 5-20: Pressure distributions for 40° sweep at α=18°. Stations I and II (a); III and IV (b)

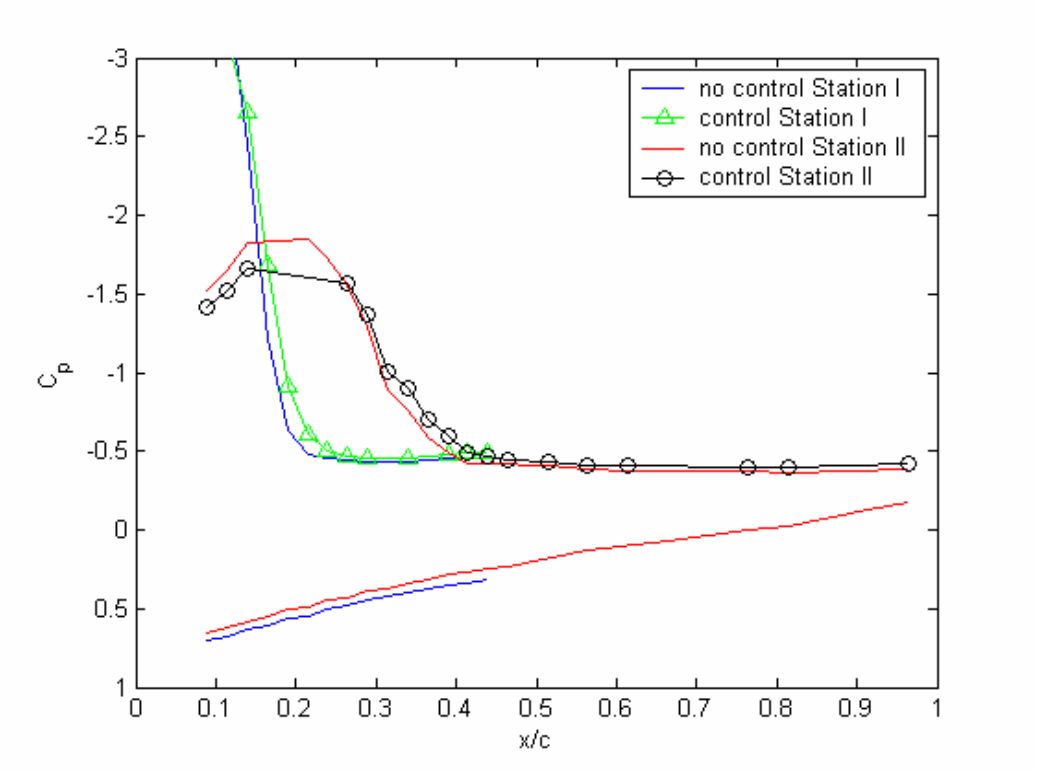

(a)

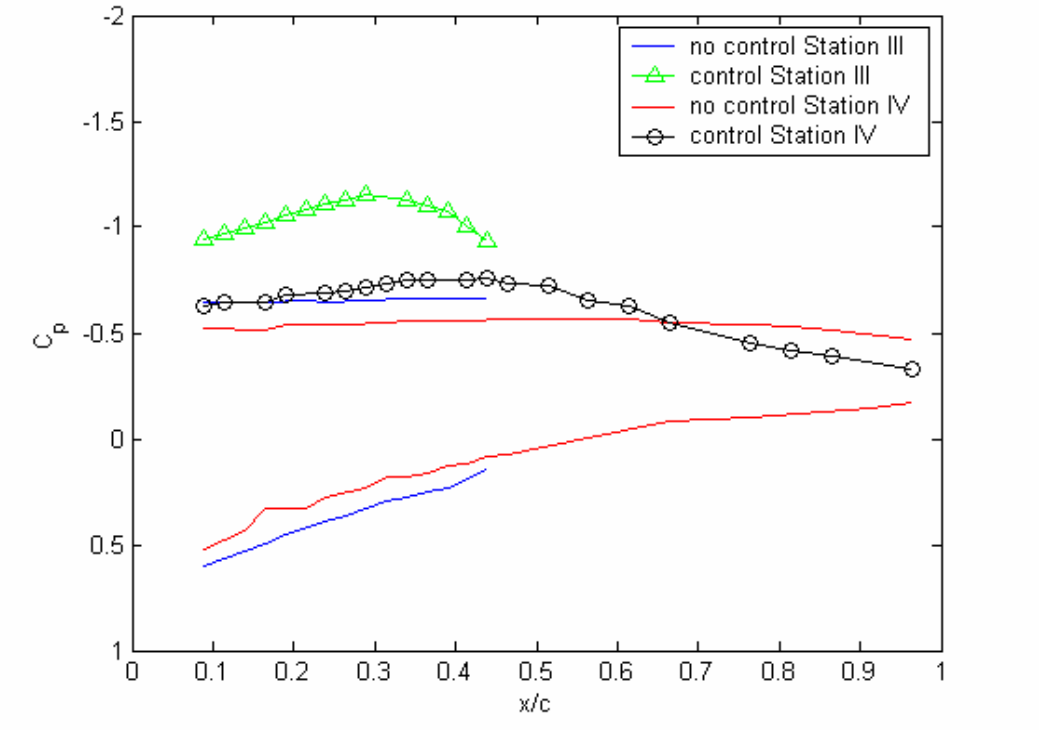

(b)

Figure 5-21: Pressure distributions for 40° sweep at α=21°. Stations I and II (a); III and IV (b)

5.3.2 *Model B; Oscillating-Flap Actuation*

The leading edge of Model B is swept by 42°. It is therefore expected that the distributions would be similar to those obtained with Model A swept by 40°. The differences between the two cases are that the planform of the two wings and the actuation mechanisms are different. Model B has a diamond-shaped planform, and thus its trailing edge may not affect events near the leading edge in the inboard region. Moreover, oscillating flaps probably offer a more robust influence to the flow, unaffected by the local aerodynamic conditions. The results are presented in Figs 22-33 for three angles of attack, namely α=13°, 17° and 21°. Results are displayed for eight of the ten stations, because the data for Stations 5 and 6 were corrupted. As expected and discussed above, the results indicate very small effect of control for low angles of attack (Figs. 22-29), yet somewhat more pronounced than in the case of Model A. The leading edge vortex, appearing as a large localized suction near the front of the wing and mostly in the inboard region indicates some increase in suction with flow control. And further in the outboard region where the flow is separated there is some mild influence of flow control. But for a sweep angle of 21° we observe a considerable influence of flow control resulting in increase of suction by up to about 50%. We can explain this behavior as follows. We know from our previous work[7], that even at angles of attack as high as 20°, the flow is attached in the inboard region. This is a typical behavior for delta wings, for which the vicinity of the apex is where the tip vortices originate, but are very small. In fact for delta wings with leading edges swept by more than 45°, this behavior is sustained at angles of attack as high as 40°, or even 50°. But in the present case, the flow is separated in the inboard region at α=21°. This is indicated by pressure coefficients that take the very low values of -1.6 to -1.8 for α=13° and α=17° at the root of the wing, but this strong suction is decreased to about -1 at α=21°. Here is where the flow control mechanism is most effective. It brings the strength of suction back to the unseparated values, as indicated in Figs. 20 and 21. In fact, for α=21°, flow control is effective further outboard as well, where the flow is fully separated, as detected by a flat horizontal pressure distribution. But as we approach the tip, the influence of flow control is somewhat diminished.

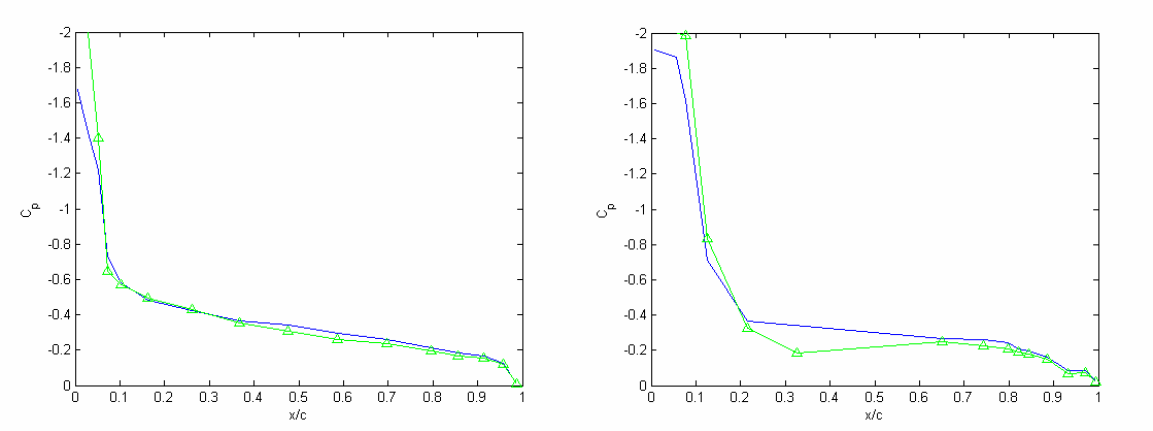

(a) **(b)**

Figure 5-22: Pressure distributions for Model B at α=13°. Stations 1 (a); 2 (b)

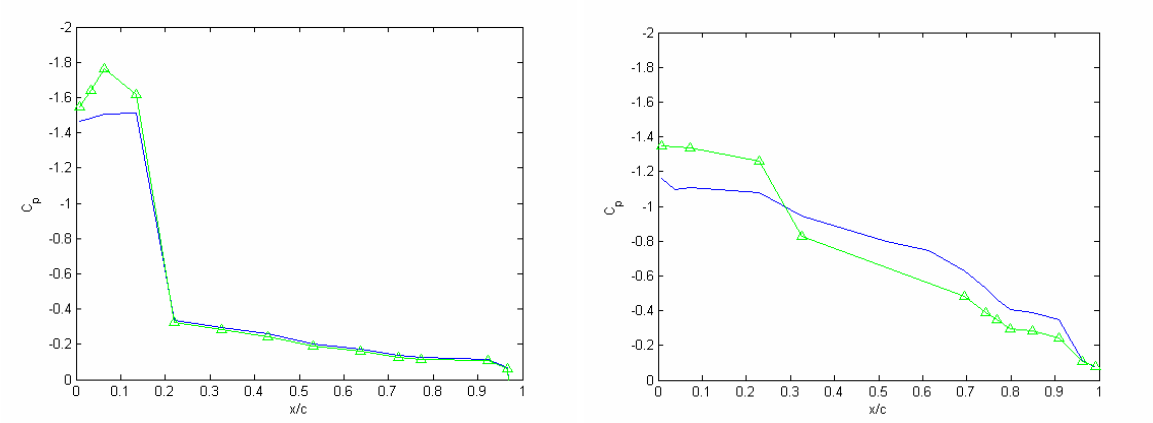

(a) **(b)**

Figure 5-23: Pressure distributions for Model B at α=13°. Stations 3 (a); 4 (b)

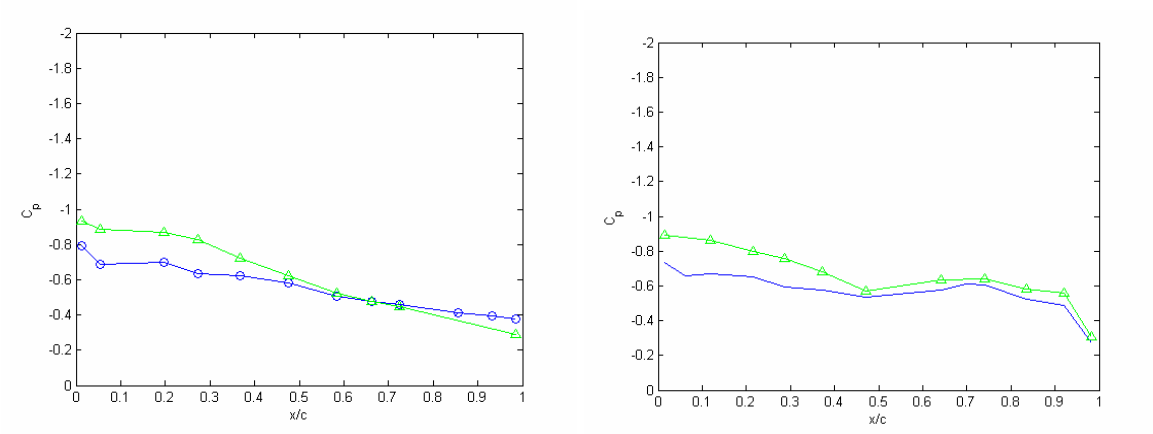

(a) **(b)**

Figure 5-24: Pressure distributions for Model B at α=13°. Stations 7 (a); 8 (b)

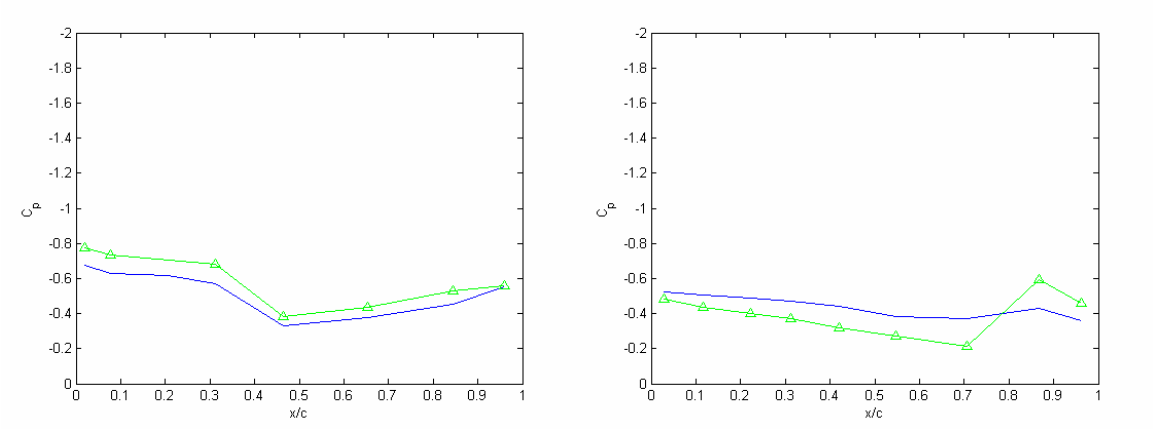

(a) **(b)**

Figure 5-25: Pressure distributions for Model B at α=13°. Stations 9 (a); 10 (b)

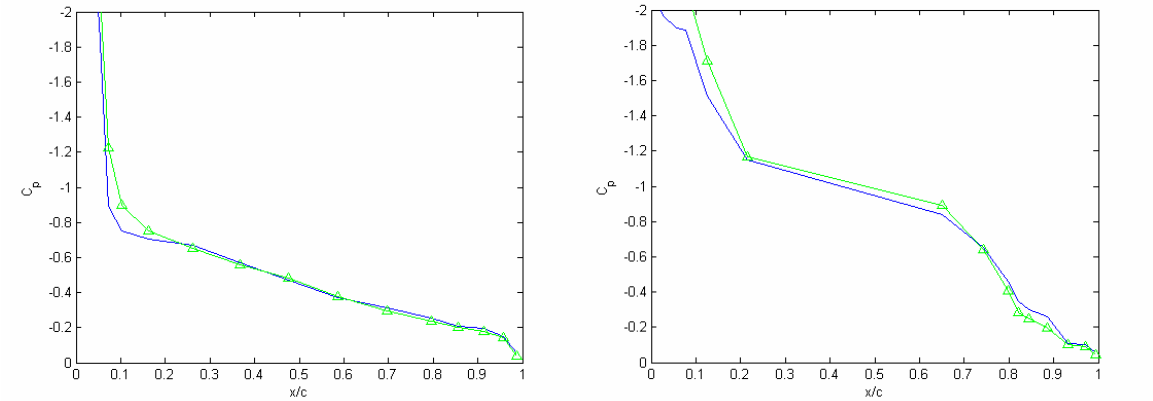

(a) **(b)**

Figure 5-26: Pressure distributions for Model B at α=17°. Stations 1 (a); 2 (b)

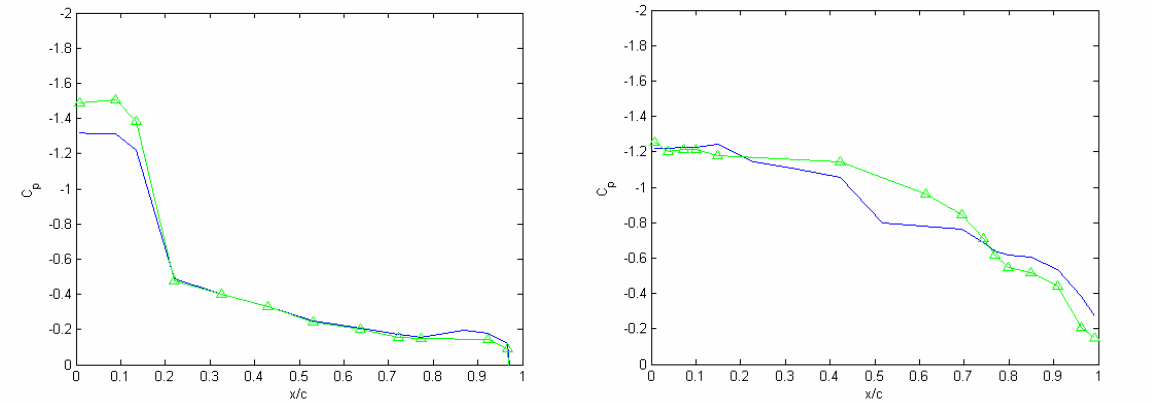

(a) **(b)**

Figure 5-27: Pressure distributions for Model B at α=17°. Stations 3 (a); 4 (b)

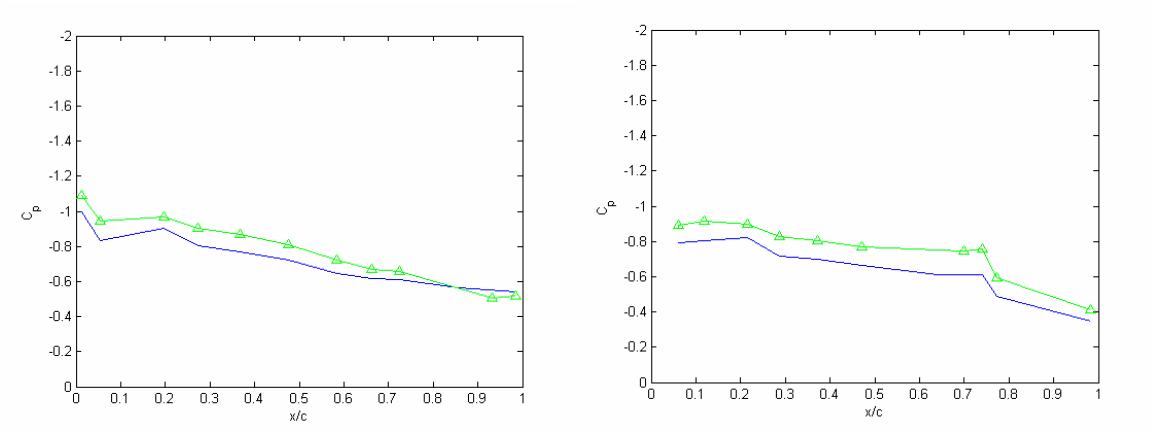

(a) **(b)**

Figure 5-28: Pressure distributions for Model B at α=17°. Stations 7 (a); 8 (b)

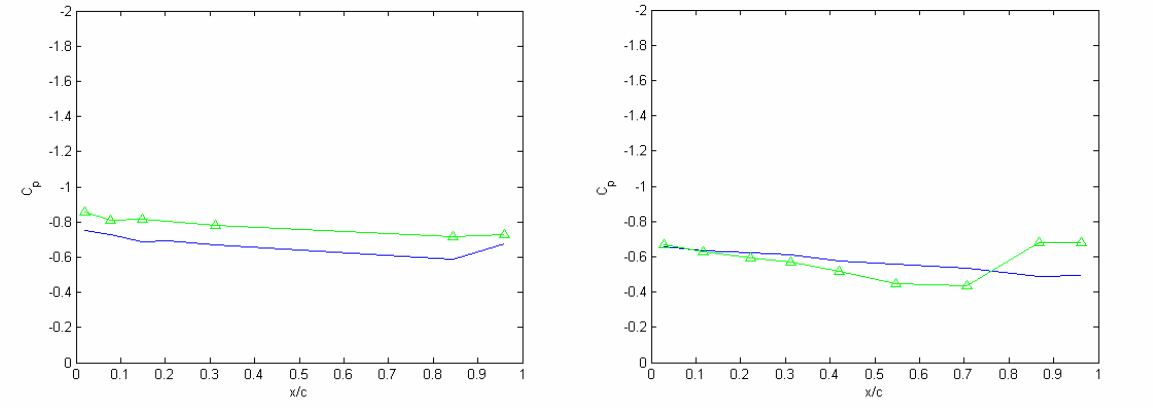

(a) **(b)**

Figure 5-29: Pressure distributions for Model B at α=17°. Stations 9 (a); 10 (b)

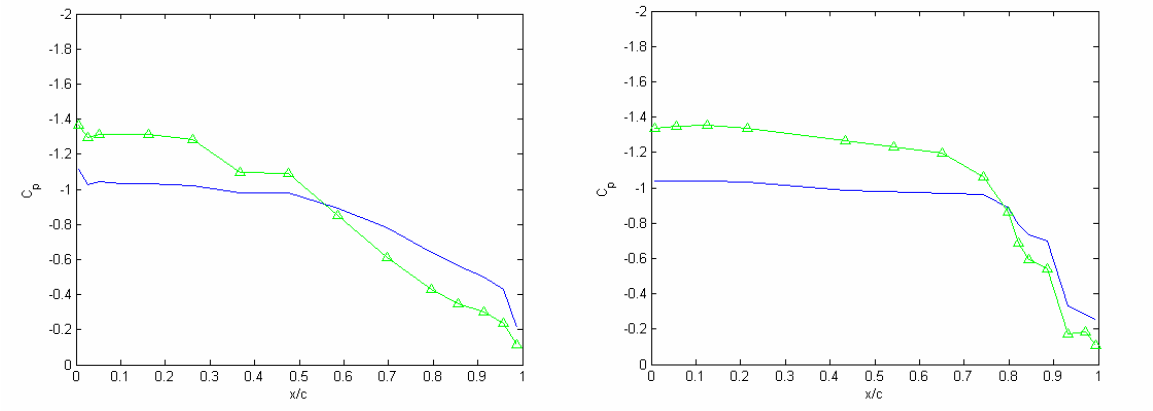

(a) **(b)**

Figure 5-30: Pressure distributions for Model B at α=21°. Stations 1 (a); 2 (b)

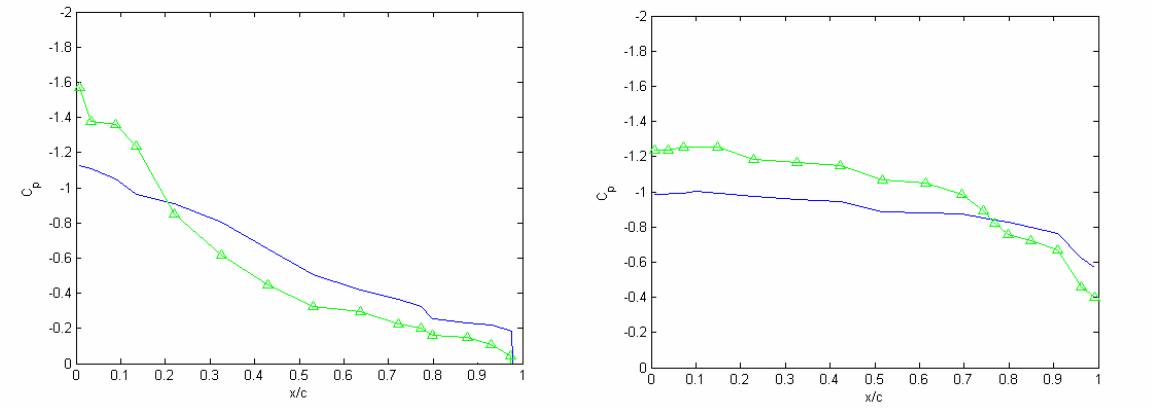

(a) **(b)**

Figure 5-31: Pressure distributions for Model B at α=21°. Stations 3 (a); 4 (b)

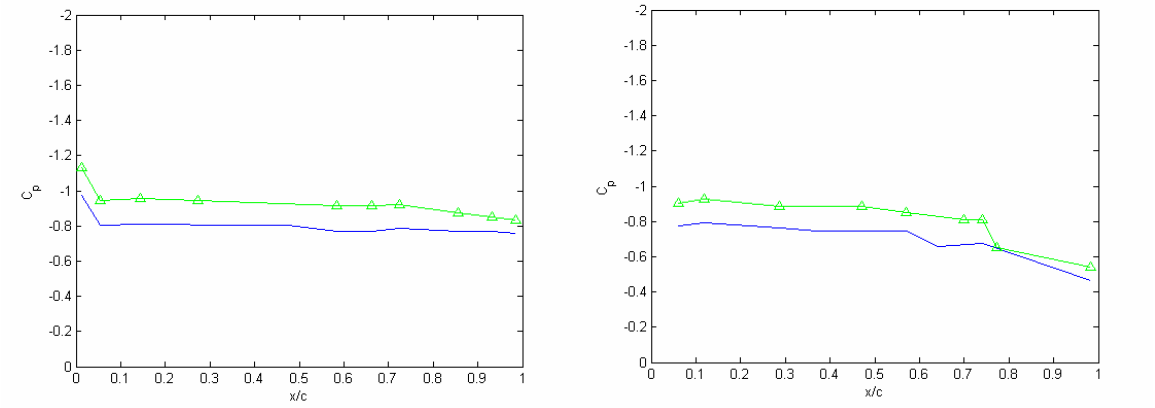

(a) **(b)**

Figure 5-32: Pressure distributions for Model B at α=21°. Stations 7 (a); 8 (b)

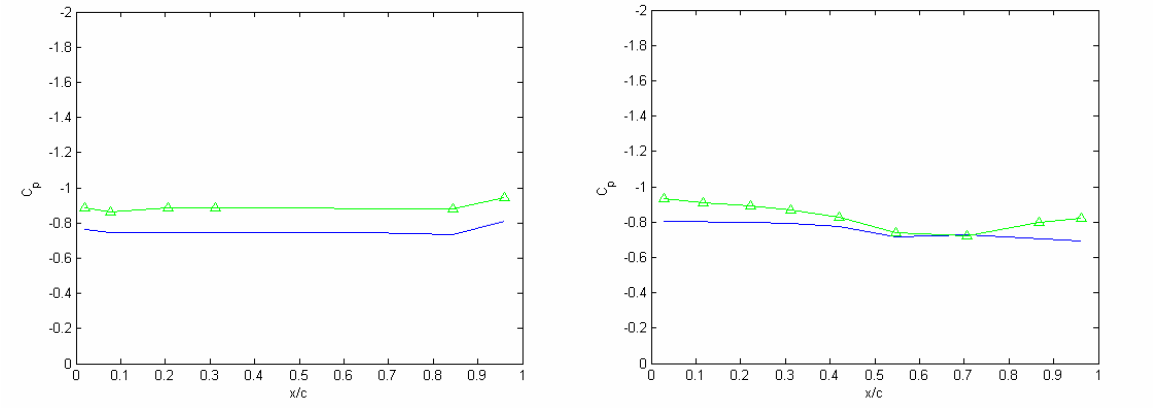

(a) **(b)**

Figure 5-33: Pressure distributions for Model B at α=21°. Stations 7 (a); 8 (b)

In an effort to find ways to increase the effect of flow control at the angles of attack of α=13° and 17°, where the oscillating flap was ineffective, we studied the results of our earlier work. In Ref. 7 we presented PIV evidence that local actuation excites a peculiar underline feature of the flow over mildly swept wings. Axial vortices emerge in the inboard region, with their axis in the streamwise direction and parallel to the tip vortices. To excite such vortices, we decided to blow at a point near the leading edge, but in the spanwise direction. The spanwise nozzle locations are marked in Fig. 4. This method proved to be much more efficient in controlling the flow as shown in Figs. 34 and 35. They show that spanwise blowing produces a strong suction similar to pressure profile induced by attached flow. From previous as well as current data it has been documented that stations 5 through 10 present pressure profiles that belong to separated flow. With the use of steady blowing the effect is very strong up to station 10 even though the two nozzles are located at about 20% and 40% of the span as shown in Fig. 4. It is noticeable that the effect is the strongest for a momentum coefficient of 0.42%. Compare to others this is a very small use of energy. This idea deserves further attention. The data presented are preliminary, but are included here to provide evidence that flow control could be very effective over diamond-shaped-planform wings, even at moderate angles of attack.

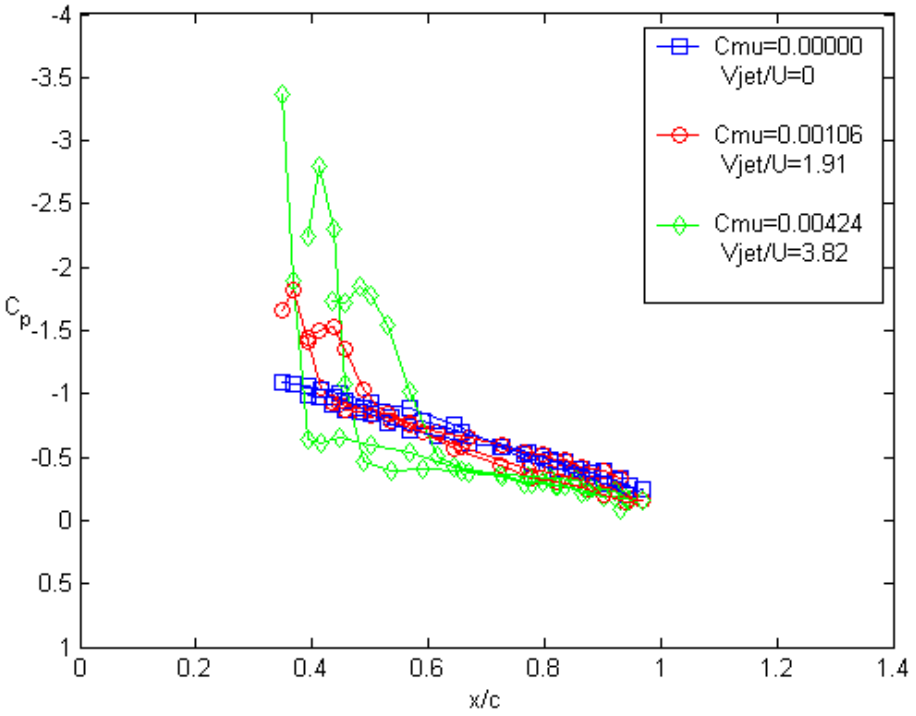

(a)

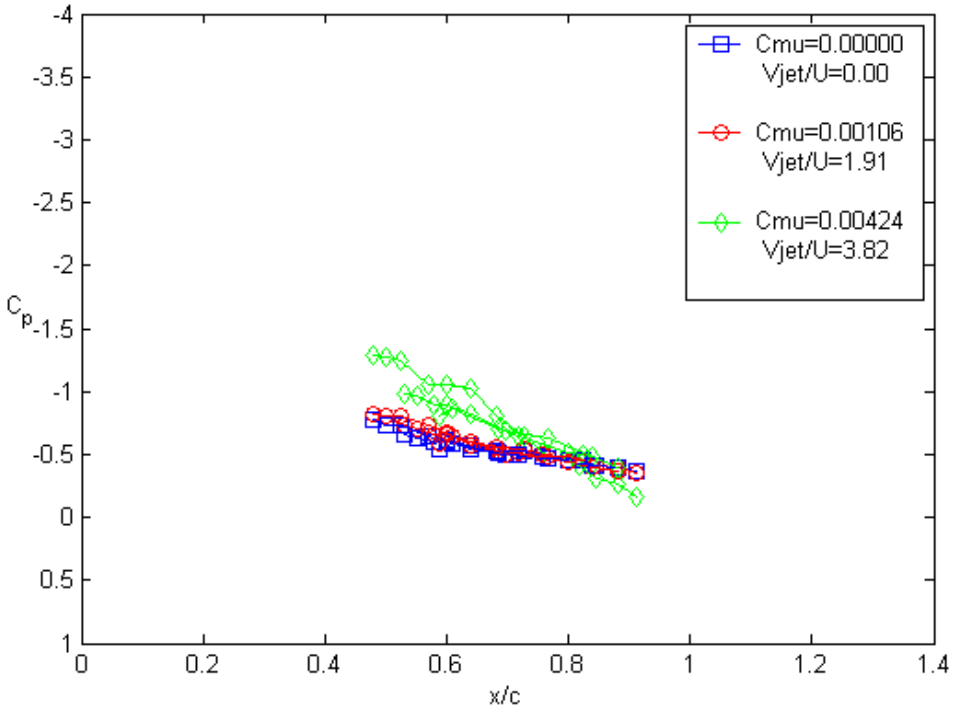

(b)

Figure 5-34: Effect of spanwise blowing on Model B at α=13°. Stations 5-7 (a) and 8-10 (b)

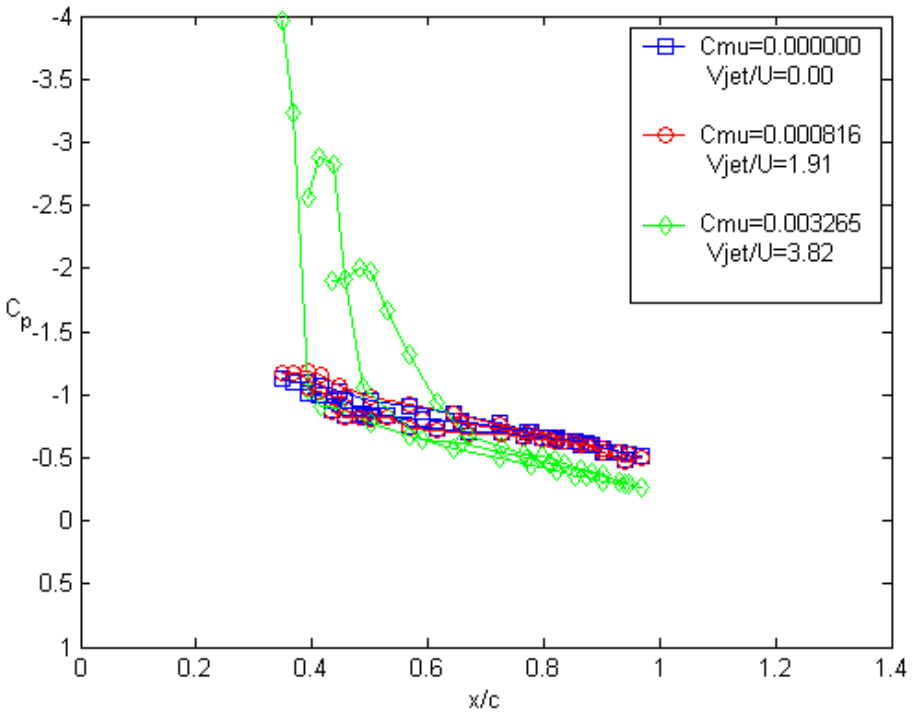

(a)

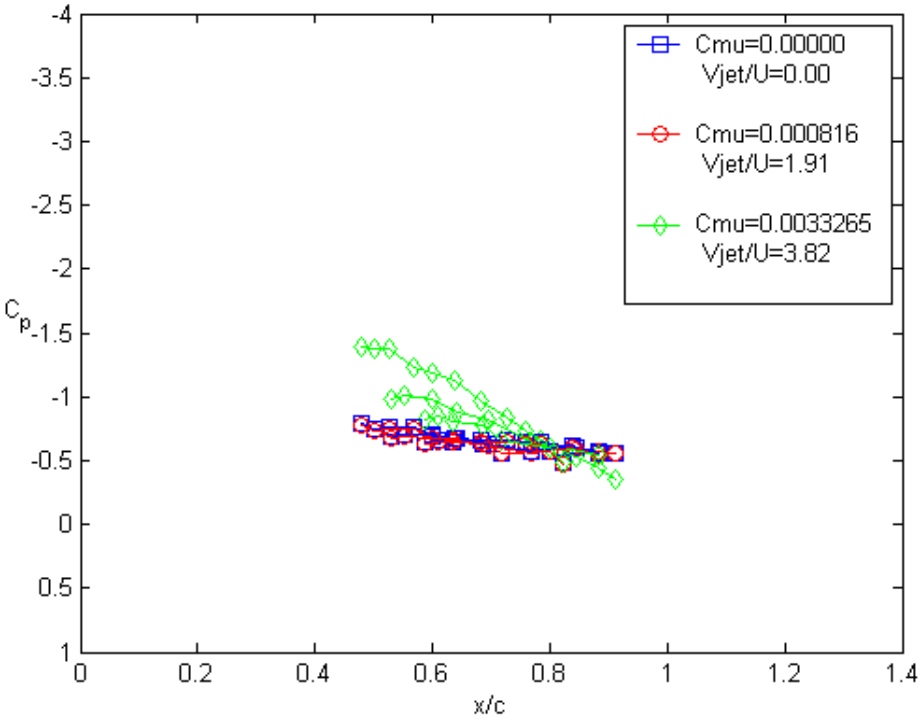

(b)

Figure 5-35: Effect of spanwise blowing on Model B at α=17°. Stations 5-7 (a) and 8-10 (b)

5.4 Conclusions

We tested two models with swept sharp-edged wings employing two actuation mechanisms along the leading edges. We found that when the flow is fully separated, it is still possible for flow control to generate significantly lower suction in the average. This means that the controlled flow is still separated, but the vortical structures in the separated region can be managed so that if averaged over time, they can lead to increases in lift. We experimented with two flow control actuators, a pulsed jet and an oscillating mini-flap, both placed along the entire span of the leading edge. We present evidence that these mechanisms are effective at higher angles of attack than indicated previously, namely up to 21 degrees. Moreover, we demonstrated that the flow over swept edges can also be controlled, but when the leading edge is swept by 40 degrees, the flow control effect is minimal at moderate angles of attack, namely up to 17 degrees. Surprisingly, for an angle of attack of 21 degrees, actuation generates a very strong suction even at a sweep of 42 degrees. We have also tested an alternative actuation mechanism, steady spanwise blowing from two round nozzles. This proved to be very effective in the range of angles that the other methods were inefficient. This was for a sweep of 40 degrees and angles of attack 13 and 17 degrees.

5.5 Acknowledgments

This work was supported by the Air Force Office of Scientific Research, under Grant No FA9550-04-1-0144, Lt Col Rhett W Jefferies, monitor. Dr. Carl Tillman is our point of contact at Air Force Research Labs. We appreciate their interest in our work and their support. Martin Lockheed has made available to us a stainless-steel model of a diamond-shaped-planform pair of wings, instrumented for pressure measurements. We appreciate the Company's support, and in particular, the help of Mr. Charles Wilson who arranged for this loan, and who offered valuable advice on the topic. We acknowledge here the excellent work of the technicians and engineers of LH Corp., especially Mr. Clemens von Claparede who offered great ideas on the design and construction of Model A. We also acknowledge and appreciate the care with which Mr. Aaron Medley worked on

instrumenting this model. Finally we would like to express our appreciation to Mr. David Simonds for his expert machining work in the modifications of Model B.

5.6 References

1. Zhou, M. D., Fernholz, H. H., Ma, H. Y., Wu, J. Z., Wu, J. M., 1993, "Vortex Capture by a Two-Dimensional Airfoil with a Small Oscillating Leading-Edge Flap", AIAA 93-3266.
2. Wu, J. Z., Lu, X. Y., Denny, A. G., Fan, M., Wu, J. M., 1998, "Post-stall flow control on an airfoil by local unsteady forcing", *Journal of Fluid Mechanics* 371, pp. 21-58.
3. Miranda, S., Vlachos, P. P., Telionis, D. P. and Zeiger, M. P., "Flow Control of a Sharp-Edged Airfoil," Paper No. AIAA-2001-0119, 2001, also *AIAA Journal*, vol. 43, pp 716-726, 2005.
4. Rullan, J., Vlachos, P. P., Telionis, D. P. and Zeiger, M. D., "Flow Control of Unswept and Swept, Sharp-Edged Wings via Unsteady Blowing," *42nd Aerospace Sciences Meeting*, Paper No. AIAA-2004-0226, January 2004
5. Rullan, J.G., Vlachos, P.P. and Telionis, D.P., "The Aerodynamics of Low-Sweep Trapezoidal Wings" *43rd Aerospace Sciences Meeting and Exhibit, 10-13 January 2005, Reno, Nevada,* Paper No AIAA-2005-0059.
6. Cahil F, Underwood, W. J., Nuber R. J., and Cheesman G. A., (1953) "Aerodynamics forces on symmetrical circular-arc airfoils with plain leading-edge and plain trailing-edge flaps", NACA Report 1146.
7. Rullan, J.G., Vlachos, P.P. and Telionis, D.P., "Flow Control over Trapezoidal-Wing Planforms with Sharp Edges." *44rth Aerospace Sciences Meeting and Exhibit, 9-12 January 2006*, Reno, Nevada, Paper No AIAA-2006-0857.
8. Rullan, J.G., Vlachos, P.P. and Telionis, D.P., "Post-Stall Flow Control of Sharp-Edged Wings via Unsteady Blowing" *41st Aerospace Sciences Meeting and Exhibit, 6-9 January 2003, Reno, Nevada,* Paper No AIAA-2003-0062, also Journal of Aircraft, Vol. 43, No 6, November 2006, pp. 1738-1746.

9. Ol, M. V. and Gharib, M., "Leading-Edge Vortex Structure of Nonslender Delta Wings at Low Reynolds Number," *AIAA Journal*, Vol. 41, No. 1, January 2003, pp. 16-26.
10. Gursul, I., Taylor, G., and Wooding, C., "Vortex Flows over Fixed-Wing Micro Air Vehicles," *40th AIAA Aerospace Sciences Meeting & Exhibit*, Paper No. 2002-0698, AIAA, January 2003.
11. Taylor, G. S., Schnorbus, T., and Gursul, I., "An Investigation of Vortex Flows over Low Sweep Delta Wings," *AIAA Fluid Dynamics Conference*, Paper No. AIAA-2003-4021, Orlando, FL, June 23-26, 2003.
12. Gordnier, R. E. and Visbal, M. R., "Higher-Order Compact Difference Scheme Applied to the Simulation of a Low Sweep Delta Wing Flow," *41st AIAA Aerospace Sciences Meeting and Exhibit*, Paper No. AIAA-2003-0620, AIAA, Reno, NV, January 6-9, 2003.
13. Yaniktepe, B. and Rockwell, D., "Flow Structure on a Delta Wing of Low Sweep Angle," *AIAA Journal*, Vol. 42, pp. 513-523.

6. Conclusions and Recommendations

6.1 Unique Aspects of Present Contribution

There are three basic elements of the present work that distinguish it from other research in flow control. The first is the effect of sharp leading edges. The second is the effect of sweeping a wing at moderate angles, namely 30° to 40°. The third element is controlling and organizing the resulting separated flow, instead of attempting to mitigate separation. The team of which this author is a member is one of very few to explore each one of these elements independently. And some of the contributions have been made with the present dissertation. The emphasis here has been to investigate the flow physics associated with the combination of all three elements.

Flow control is based on the idea of introducing a small localized disturbance that results in changes in the flow that are orders of magnitude larger in spatial extend over the domain of interest. Flow control is most effective if an underlying feature of the flow is excited. This group has demonstrated that a small disturbance introduced very close to a sharp leading edge leads to the generation of coherent vortices that are nearly parallel to the leading edge. These ideas have been confirmed with the MS thesis of the present author. These vortices form close to the wing surface and induce, in the average, a strong suction that results in lift enhancement. But there is another dominant underlying feature of flows over sharp-edged wings with low sweep angle. This is the inboard development of axial vortices, parallel to the tip vortices. We discovered that such structures are very receptive to localized or three-dimensional actuation. Essentially, vorticity generated parallel to the sharp leading edge is turned in the streamwise direction. This discovery presents us with the opportunity to develop a new paradigm of flow control, namely the localized control of three-dimensional flow structures over three-dimensional wings.

6.2 Summary and Conclusions

We studied in detail the spatial and temporal development of vortical structures in three dimensions and their receptivity to two-dimensional and/or three-dimensional actuation. Experiments were conducted with swept wings and diamond-planform wings, at Reynolds numbers the order of one million in a wind tunnel with a test section of 6’X6’ and at about 20,000 in a water tunnel with a test section of 2’X2’. We employed

new flow diagnostic tools recently developed and/or acquired by our group, namely a Temporally Resolved DPIV (TR-DPIV) system with kHz rate, capable of resolving flows in excess of 150m/s. We have also employed the instrumentation infrastructure of surface pressure and multi-hole velocity measurements.

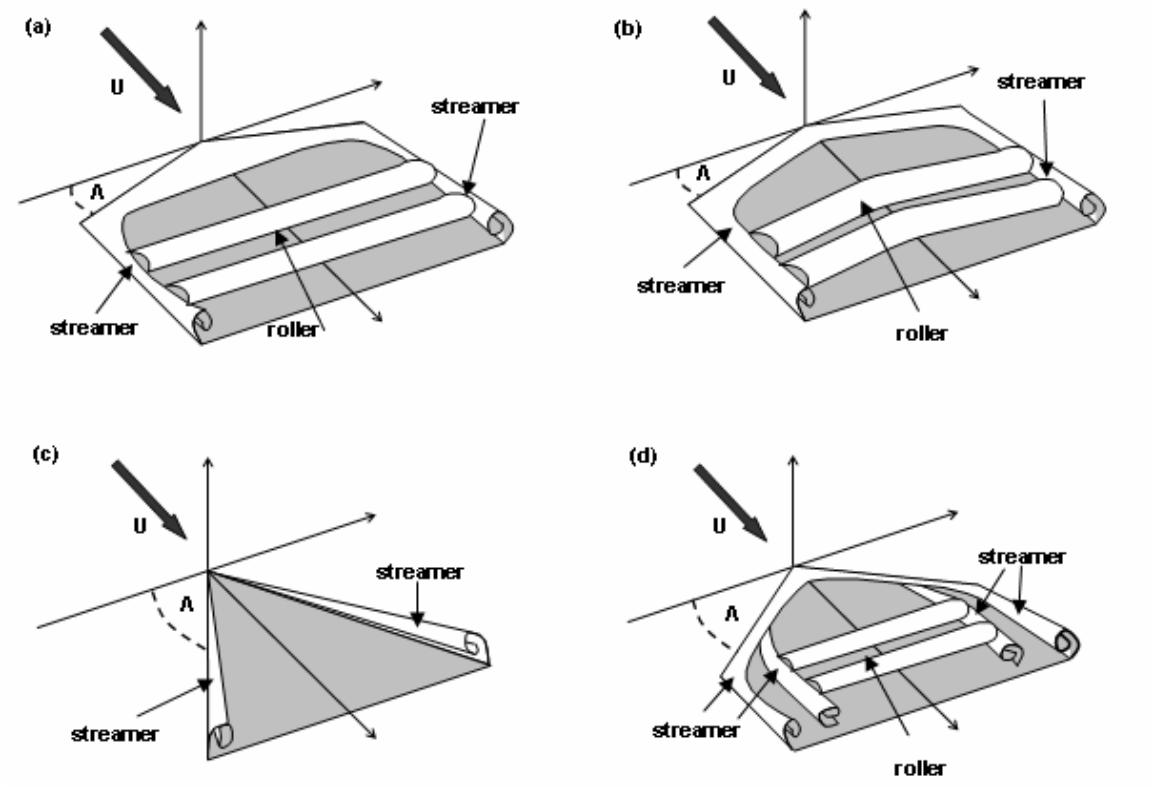

Figure 6-1: Symbolic sketches of vortex roll-up over low-sweep wing (a) and (b), high sweep (c) and moderate- sweep wing (d).

The physics of separated flows over leading edges with no sweep, $\Lambda=0°$, or moderate sweep, $\Lambda<20°$ and leading edges with high sweep angles, $\Lambda> 45°$ have been studied extensively. There is a gap in these investigations for wings with moderate sweeps, namely $30°< \Lambda<40°$. The first class of flows is dominated by vortices with their axis almost normal to the oncoming stream, i.e. parallel to the leading edge, as shown schematically in Fig. 6-1a and 6-1b. Such vortices roll over the wing and are shed periodically in time and are called here rollers. The second class of flows, namely for $\Lambda> 45°$, displays the character of the flow over delta wings. The flow is essentially conical,

dominated by leading-edge vortices (Fig. 6-1c). Vorticity is now nearly aligned with the stream or the leading edge. Such vortices are called here streamers.

We discovered that leading-edge sweeps of 30° to 40° give rise to hybrid modes of vorticity shedding (Fig. 6-1d), and that different modes of vortex shedding can be activated by proper flow control strategies. Rollers may be generated along the entire leading edge and sent rolling over the suction surface, or streamers could be excited where they dominate some areas over the wing. Vorticity generated over the leading edge of all wings is turned in the streamwise direction at their tip. We found that with proper actuation, and only at medium sweep angles, leading-edge vorticity can be turned streamwise, in midspan to form streamers as shown in Fig. 6-1d.

The aerodynamics of wings swept by moderate angles, namely 30° to 40°, and moderate to high angles of attack is very little understood. We found that in this range of sweep angles, the flow may stall like the flow over an unswept wing, shedding large rollers in an unsteady fashion, or it could stall like a delta wing, sustaining leading-edge vortices that break down. The significant difference between the two modes is that delta wing vortices, or streamers, shed vorticity by directing it in the core of the vortex and then telescoping it downstream, whereas rollers grow, and then shed by rolling over the wing and detaching from its surface. The second mode is essentially the phenomenon of unsteady stall.

Flow control was achieved by introducing a small disturbance along the leading edge. We employed both pulsing jets, as well as oscillating mini-flaps, and proved that these two techniques are similarly effective. Actuation along the entire leading edge can be considered two-dimensional actuation of a three-dimensional problem. And as discussed later, it generates quasi-two-D motions. We attempted true three-dimensional actuation by activating only the inboard portion of the leading edge.

The vorticity shed along the leading edge has two components, one in the streamwise direction and another in the spanwise direction. And vortex sheets thus generated have the tendency to roll either in the spanwise direction, generating rollers, or in the streamwise direction, generating streamers. Activating the entire length of the leading edge tends to generate rollers. In fact, even in the presence of the tip, as shown with our model A, the quasi-two dimensional character of the rollers is sustained almost to the tip,

suppressing the tendency of uncontrolled wings to turn their vorticity in the streamwise direction in the neighborhood of the tip. This was detected by observing pressure profiles that are similar and very little affected by the presence of the tip.

Three-dimensional activation promotes the rolling of the shear layer into a streamwise direction. Rollers are thus generated that form in the inboard region of the wing, and emerge downstream of the trailing edge. We captured the temporal development of such rollers that are activated by the pulsed jet actuation, and we measured their effect on the pressure distribution. Another interesting but preliminary finding, which is beyond the scope of the present work is that steady spanwise blowing along a point at the leading edge could lead into significant changes of the pressure distribution. This indicates that streamers can be excited by blowing at a single point rather than the entire leading edge of the wing.

6.3 Recommendations

We employed uniform actuation along the entire leading edge of the wing. This worked quite well. But the fact remains that this actuation is a two-dimensional actuation of a three-dimensional flow. We call this a two-dimensional actuation in the sense that it does not vary with the span of the wing. A first attempt at three-dimensional actuation was carried out. But this was somewhat limited, because we actuated just the first inboard half of the wing. It will be useful to explore other modes of true three-dimensional actuation. But first it will be necessary to study in detail the spatial and temporal development of vortical structures in three dimensions. This can be followed by investigations of their receptivity to two-dimensional and/or three-dimensional actuation and the management of forces and moments that develop.

It is also suggested that we explore the effect and effectiveness of three-dimensional forcing of the flow along the leading edge of the wing. It will be necessary to develop the actuation mechanisms that will dictate the orientation and origin of the vortical structures over the wing. Here is where point blowing instead of blowing along a portion of the leading edge could prove a more efficient control mechanism. In fact we recommend that a pulsating jet at point blowing be tested. Pulsing has always produced more significant results than steady blowing. Finally, it will be important to design the necessary control mechanisms that will result in controlling independently forces and moments over the

wing. This would allow flight control by flow control, instead of aerodynamic control using hinged control surfaces.